CXCR4 as a target for preclinical Positron Emission Tomography of cancer

Elizabeth Stevens

Supervised by Prof. Eric Aboagye

Imperial College London

Department of Surgery and Cancer

A thesis submitted for the degree of Doctor of Philosophy at Imperial College London

Declaration

I declare that the following report is my own work, and that the work of others is not included except where appropriately referenced. Other contributors to the work presented include Dr. Ola Åberg, Guillaume George, Dr. Federica Pisaneschi and Dr. Diana Brickute. Their precise contributions are specified within chapter two of this thesis.

Abstract

The chemoattractive interactions of the chemokine stromal derived factor-1 (SDF1) and its receptor CXCR4 play a key role in tumour metastasis, with CXCR4 expression found to be significantly higher in cancers with aggressive phenotypes. There is therefore an impetus for non-invasive means to sensitively identify tumours prone to progression. As such, the aim of this work was to develop a number of novel CXCR4 antagonists to assess their suitability as imaging radiotracers for positron emission tomography (PET).

In this study, novel 14-mer peptide, pentapeptide and small molecular antagonists were designed, assessed for *in vitro* potency using radioligand binding and migration assays, and validated *in vivo* through imaging and biodistribution experiments.

Several novel pentapeptide antagonists (CCIC7, CCIC15 and CCIC30) were found to inhibit CXCR4 function with moderate potency, although the radiolabelled tracers unfortunately showed poor localisation *in vivo*, due to rapid clearance or metabolism. Additionally, fluorophenylated derivatives of the small molecular antagonists It1t and AMD3465 were found to antagonise SDF1 binding and function at low concentrations, suggesting potential as CXCR4-targeting molecules. Finally, it was shown that a cation-chelated NO2A-conjugate derivative of the 14mer peptide TN14003 could antagonise CXCR4 at low concentrations, and furthermore that CXCR4-expressing tumours could

be identified from non-expressing tumours by PET imaging with the use of a ^{68}Ga-labelled derivative in CXCR4-dependent manner. The tracer accumulated in CXCR4-expressing tumours with a favourable signal-to-muscle ratio of 2.9, and was also found to show metabolic stability in plasma appropriate for PET imaging at 60 minutes.

In conclusion, this study documents the successful validation of [^{68}Ga]-CCIC16 for the identification of CXCR4-expressing tumours *in vivo*, and highlights several potential small molecular antagonist derivatives suitable for further investigation as PET tracers. While functionalisation of pentapeptide antagonists was generally unsuccessful, the report proposes further analysis and modifications that may potentially be used in future developments.

“I am so smart! S-M-R-T!”

Homer Simpson (1993)

Acknowledgements

I dedicate this thesis to myself, because I wrote it. However, lots of people helped me with this so I'll mention them here:

First I'd like to thank Prof. Eric Aboagye for giving me the opportunity to work on this project, and to benefit from his advice. As this was an interdisciplinary project, I really wouldn't have got anywhere without the chemists Guillaume George, Dr. Federica Pisaneschi and Dr. Ola Åberg, who synthesised the novel compounds and radiotracers that I worked with, took part in the metabolism experiments, and helped me understand more chemistry than I really wanted to. I'd also like to thank the whole CCIC group for their help and for putting up with me for the last few years, and feeding me cake. Cancer Research UK also has my thanks for providing the funding for my project. Thanks very much to the RIA lab for letting me use their facilities, and eat cake.

Last but not least, the developers of fluoxetine hydrochloride have my eternal gratitude for their significant contribution to my mental wellbeing. This thesis would certainly not have existed without them.

Table of Contents

Table of Figures

Table of Tables

List of Abbreviations

14mer	Polypeptide with 14 amino residues
17AAG	17-N-Allylamino-17-demethoxygeldanamycin
17DMAG	17-dimethylaminoethylamino-17-demethoxygeldanamycin
µCi	Microcurie
µg	Microgram
µl	Microlitre
µM	Micromolar
AC	Adenylyl cyclase
AKT	Protein kinase B
ALI	Acute lung injury
ALK	Anaplastic lymphoma kinase
ANOVA	Analysis of variance
Arg	Arginine
Asp	Aspartic acid
ATCC	American Type Culture Collection
ATP	Adenosine triphosphate
AUC	Area under curve
BAD	B-cell lymphoma-2 associated death promoter
BCA	Bicinchoninic acid
BMSC	Bone marrow mesenchymal stem cell
Bn	Benzene
bp	base pair(s)
BSA	Bovine serum albumen
C	Carbon
CAF	Cancer-associated fibroblast
cAMP	Cyclic adenosine monophosphate

CAM	Cell adhesion molecule
CCIC	Comprehensive Cancer Imaging Centre, Imperial College London
CD4	Cluster of differentiation 4
CDK4	Cyclin-dependent kinase 4
cDNA	Complementary deoxyribonucleic acid
CHIP	C-terminus of HSP70-interacting protein
Cit	Citrulline
CPM	Counts per minute (decay-corrected)
CT	Computed tomography
Cu	Copper
CXCL	CXC ligand e.g. CXCL12
CXCL12	Stromal-derived factor 1 (see SDF1)
CXCR	CXC receptor e.g. CXCR4
CXCR4	CXC receptor 4
Cys	Cysteine
DDI	Drug-drug interaction
DMEM	Dulbecco's modified Eagle's medium
DMSO	Dimethyl sulfoxide
DNA	Deoxyribonucleic acid
dNTP	Deoxyribonucleotide triphosphate
DOTA	1,4,7,10-tetraazacyclododecane-1,4,7,10-tetraacetic acid
e-	Electron
e+	Positron
EAG	Electron-accepting group
E.coli	*Escherichia coli*
ECL	Electrochemiluminescence
EDG	Electron-donating group
EDTA	Ethylenediaminetetraacetic acid

EGFR	Epidermal growth factor receptor
ELR	Glumate-Leucine-Arginine domain
ERK	Extracellular signal-regulated kinases
F	Fluorine
FACS	Fluorescence-activated cell sorting
FB	Fluorobenzyl
FBA	Fluorobenzaldehyde
FBS/FCS	Foetal bovine/calf serum
FBP	Filtered back-projection
FDA	Food and Drug Administration
FDG	Fluorodeoxyglucose
FLT	3’-fluoro-3’-deoxy-L-thymidine
FPh	Fluorophenyl
FSC	Forward scatter
FTA	Fluorotriazole
Ga	Gallium
GAPDH	Glyceraldehyde 3-phosphate dehydrogenase
GBq	Gigabecquerel
GCSF	granulocyte colony-stimulating factor
GDP	Guanosine diphosphate
Ge	Germanium
Glu	Glutamate
gp	Envelope glycoprotein
GPCR	G protein-coupled receptor
HEPES	4-(2-hydroxyethyl)-1-piperazineethanesulfonic acid
HER2	Human epidermal growth factor receptor 2
HIF	Hypoxia-inducible factor
His	Histidine

HIV	Human immunodeficiency virus
Hop	HSP70-HSP90 organising protein
HPV	Human papilloma virus
HRP	Horseradish peroxidise
HSF	Heat shock factor
HSP	Heat shock protein
I	Iodine
IC_{50}	Half-maximal inhibitory concentration
ICAM-1	Intercellular cell adhesion molecule-1
ID	Injected dose
ID	Inhibitor-of-differentiation
Ig	Immunoglobin
IgG	Immunoglobin G
In	Indium
i.p.	Intraperitoneal
IP_3	Inositol triphosphate
ITF	Immunoglobin transcription factor
i.v.	Intravenous
JAK	Janus kinase
Kb	Kilobase
KDa	Kilodalton
LB	Luria broth
LDS	Lithium dodecyl sulphate
LogD	Distribution constant
LogP	Partition coefficient
LOR	Line-of-response
Lys	Lysine
MAP	Maximum *a posteriori*
MAPK	Mitogen-activated protein kinase

MBq	Megabecquerel
MEM	Minimum essential media
mEV	Milli-electron volt
mg	Milligram
MIF1	Macrophage migration inhibitory factor 1
MIP	Macrophage inflammatory protein
ml	Millilitre
mM	Millimolar
MMP	Matrix metalloproteinase
MRI	Magnetic resonance imaging
mRNA	Messenger RNA
MS	Multiple sclerosis
MSC	Mesenchymal stem cell
N	Nitrogen
N (unit)	Normality; Equivalent molarity per litre
Nal	2-naphthylalanine
NFκB	Nuclear factor kappa-light-chain-enhancer of activated B cells
ng	Nanogram
NIH	National Institute of Health
NK	Natural killer
nM	Nanomolar
NO2A/NODA	1,4,7-triazacyclononane-diacetic acid
NOTA	1,4,7-triazaacyclononane-triacetic acid
O	Oxygen
OCT	Organic cation transporter
OSEM	Ordered-subset expectation maximisation
PAGE	Polyacrylamide gel electrophoresis
PBS	Phosphate buffered saline
PCR	Polymerase chain reaction

PE	Phycoerythrin
PE-A	Fluorescence intensity
PEG	Polyethylene glycol
pERK	phosphor-extracellular signal-regulated kinase
PET	Positron emission tomography
PGC	Primordial germ cell
PGK1	Phosphoglycerate kinase 1
P_i	Inorganic phosphate
Pi3K	Phosphoinositide 3-kinase
PIP_2	Phosphatidylinositol 4,5-bisphosphate
PKC	Protein kinase C
PLC	Phospholipase C
pM	Picomolar
Prg	Proparylglycine
Pro	Proline
qRT-PCR	Quantitative polymerase chain reaction
RA	Rheumatoid arthritis
RBA	Radioligand binding assay
RBC	Red blood cell
RIPA	Radioimmunoprecipitation assay
RNA	Ribonucleic acid
RNAi	RNA interference
ROI	Region of interest
rpm	Revolutions per minute
RPMI	Roswell Park Memorial Institute medium
RT-PCR	Reverse transcriptase polymerase chain reaction
SAR	Structure-activity relationship
SDF1	Stromal-derived factor 1 (also known as CXCL12)

SDS	Sodium dodecyl sulphate
SEM	Standard error from the mean
SOB	Super optimal broth
SPECT	Single photon emission computer tomography
Src	proto-oncogene tyrosine kinase Src
SSC	Side scatter
STAT	Signal transducers and activators of transcription
SUV	Standardised uptake value
TAC	Time-against concentration
TBE	Tris borate EDTA buffer
TBST	Tris-buffered saline with 0.1% tween
Tc	Technetium
TEM	Trans-endothelial migration
TFF2	Trefoil family factor 2
TGF	Tumour growth factor
Thr	Threonine
TNM	Tumour-node-metastasis
Tris	Tris(hydroxymethyl)aminomethane
Trp	Tryptophan
Tyr	Tyrosine
Ub	Ubiquitin
US	Ultrasound imaging
Val	Valine
VCAM	Vascular cell adhesion molecule
VEGF	Vascular endothelial growth factor
WHIM	Warts, hypogammaglobulinemia, infections and myelokathexis

Chapter One - Introduction

1.1 - Preamble

Despite decades of intensive research, cancer is still one the most common causes of death in developed nations, responsible for an estimated 25% of mortality in Britain (Office for National Statistics, 2008). With decades of fervent research from countless institutions, significant advances have been made in our understanding of the complex and diverse molecular biology of myriad cancer types (Cianfrocca and Gradishar, 2009, Curtis *et al.*, 2012, Leary and Olson, 2012, Sjodahl *et al.*, 2012), and the many successive steps that must take place before the cancer phenotype arises (Hanahan and Weinberg, 2011). As a result of this huge complexity, it has become clear that the much-hoped-for 'magic bullet' for cancer will likely never be found, thus directing a shift in recent years towards personalised medicine, where therapies are tailored to the individual requirements of patients and are therefore hoped to enable better-informed decisions regarding the potential fates of cancer sufferers (De Palma and Hanahan, 2012).

This transition towards individualisation of cancer therapy involves research on many fronts, beginning with the identification of biomarkers that can be used to determine the aggressiveness of the cancer or to predict response to therapy, reducing the reliance on the anatomical tumour-node-metastasis (TNM) staging criteria. Biomarkers may take many forms, including gene expression within the tumour, circulating blood or urine, and abnormal phenotypes identified by

immunohistochemistry (Ludwig and Weinstein, 2005). A continual challenge faced in the personalised medicine approach is the currently limited ability of oncologists to interpret biomarker profiles correctly and give accurate advice or treatment to patients. Despite the identification of a number of potential biomarkers in research, few have been translated to the clinic as a result of unreliability of the conclusions drawn, and high costs of biomarker tests (Thariani *et al.*, 2012).

A promising approach to enable the further development of novel biomarkers pertains to the field of molecular imaging, whereby molecular targets associated with cancer are utilised through contrast agents or radiotracers to visualise tumours *in vivo* (Mankoff, 2008). An advantage of molecular imaging approaches over commonly used biopsy tests is the non-invasive nature of imaging, which can allow repeated assessments over time, potentially allowing response to therapy to be determined. Furthermore, molecular imaging methods would allow oncologists the ability to determine the heterogeneity of biomarker expression within the tumour, which may influence therapeutic decisions. This introduction outlines the role of CXCR4, a chemokine receptor and emerging biomarker in cancer. In addition, the recent research developing potent antagonists to CXCR4 for their potential as therapeutic or imaging agents is also described, followed by the synopsis for this project in the development and validation of CXCR4-targeting radiotracers for positron emission tomography of tumours.

1.2 - Chemokines, chemokine receptors and CXCR4

Chemokines are a family of secreted protein cytokines that are characterised by their ability to induce directed migration known as chemotaxis in responsive cells as a result of their recognition at cell surface receptors. CXCR4 is just one of over twenty known different chemokine receptors (Murphy, 2002), a class of G-protein coupled receptors (GPCRs). These chemokines are categorised according to the positioning of conserved cysteine residues of the amino terminus, and are so designated C, CC, CXC, and CX_3C ligands (Zlotnik and Yoshie, 2000). The CXC class of chemokines that contains CXCR4, the subject of this project, are split into two groups, ELR+ and ELR- depending on the presence or absence of a glutamate-leucine-arginine domain. A chemokine's possession of the ELR domain is biologically relevant, as its presence denotes the angiogenic properties of the chemokine's signalling pathways, whereas its absence indicates its role in homeostasis (Strieter *et al.*, 1995). Stromal cell-derived factor 1 (SDF1, also known as CXCL12), the ligand to CXCR4, is unusual among the CXC-class chemokines in that it is angiogenic, yet it does not possess the characteristic ELR domain of most angiogenic CXC chemokines (Liang *et al.*, 2007a).

The downstream physiological effects of chemokine receptor binding are numerous as a result of influence by many different cell signalling pathways. Many chemokines are considered to be 'promiscuous', as they usually bind with

more than one receptor, and, likewise, most chemokine receptors induce signal transduction in response to binding by a number of different ligands. This functional redundancy is considered a strategy to maintain normal cellular processes if a particular chemokine is defective, although the cellular responses to ligand binding can also be fine-tuned to exert minor differences in biological activity (Devalaraja and Richmond, 1999). In contrast, CXCR4 is notable for its near-monogamous relationship with its primary ligand, SDF1. Despite this, in recent years SDF1 has been shown to also bind with the CXCR7 receptor (Balabanian *et al.*, 2005a). In addition, the ligands macrophage migration inhibitory factor (MIF1) and trefoil factor family 2 (TFF2), are capable of inducing CXCR4-dependent responses in cells (Bernhagen *et al.*, 2007, Schwartz *et al.*, 2009, Dubeykovskaya *et al.*, 2009).

Signal transduction in the CXCR4-CXCL12 pathway is complex, and is largely dependent on homodimerisation with other CXCR4 receptors for signal transduction processes, including the Gαi-mediated JAK/STAT pathway (Vila-Coro *et al.*, 1999). Liberated Gβγ subunits may then activate other pathways involving phospholipase C (PLC) or phosphatidylinositide 3-kinase (PI3K), whilst the interaction of β-arrestin with the CXCR4 receptor (a key step in desensitisation by receptor internalisation) has been found to influence chemotaxis via p38 mitogen-activated protein kinase (MAPK) pathways (Sotsios *et al.*, 1999, Sun *et al.*, 2002). These pathways appear to be regulated by the process of receptor heterodimerisation, which can inhibit downstream

signalling. For example, dimerisation with CXCR7, the alternative CXCL12-binding receptor, has been found to impair CXCR4-mediated signalling mechanisms. It is thought that the coexpression of these receptors on cells may provide a mechanism for the regulation of chemotaxis (Levoye *et al.*, 2009). A simplified diagram of CXCR4 dependent cell signalling pathways and biological processes is shown in figure 1.

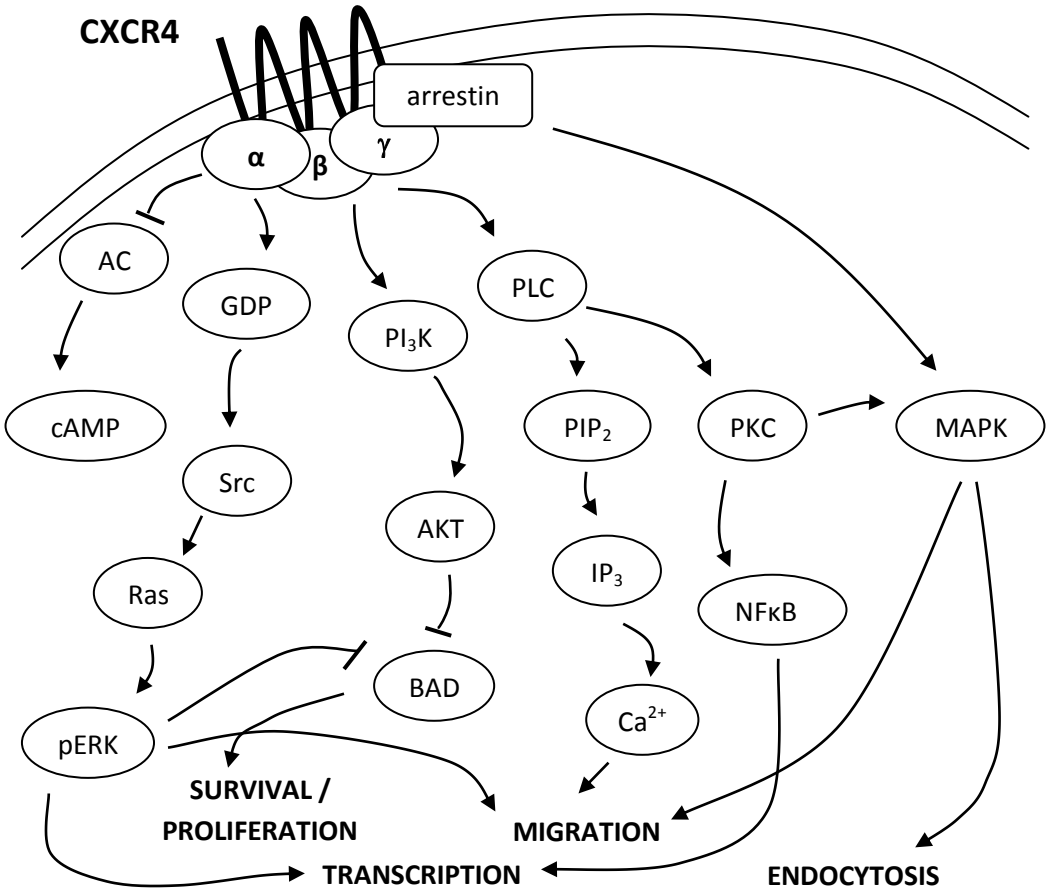

Figure 1. Signalling pathways of CXCR4. Adapted from (Wong and Korz, 2008)

AC (adenylyl cyclase); AKT (protein kinase B);BAD (B-cell lymphoma-2 associated death promoter); cAMP (cyclic adenosine monophosphate); GDP (guanosine diphosphate); IP_3 (inositol triphosphate); MAPK (mitogen-activated protein kinase); NFκB (nuclear factor kappa-light-chain-enhancer of activated B cells); pERK (phospho-extracellular signal-regulated kinase); PI_3K (phosphatidylinositide-3 kinase); PIP_2 (phosphatidylinositol 4,5-bisphosphate); PKC (protein kinase C); PLC (phospholipase C); Src (proto-oncogene tyrosine protein kinase Src)

1.3 - CXCR4 in health and disease

The importance of CXCR4 signalling is apparent at the earliest possible stage of life - conception. Recent research has demonstrated that the activation of CXCR4 receptors present in the head of spermatozoa by SDF1 results in intracellular calcium increases and increased motility, which are suggested to enable sperm chemotaxis towards SDF1-expressing oocytes (Zuccarello *et al.*, 2011). Furthermore, conceptus expression of both SDF1 and CXCR4 has been shown to be increased in the early pregnancies of ewes, with higher endometrial expression of CXCR4 at day 15 of pregnancy as compared to day 15 of the oestrus cycle. It is suggested that the upregulation of CXCR4 and SDF1 in early pregnancy may be related to an adhesive role in implantation (Ashley *et al.*, 2011).

The role of CXCR4 signalling is also of critical importance during embryogenesis in mice, as knockout of either the receptor or its ligand results in a lethal phenotype by E18.5, with vascular, gastrointestinal or cerebellar irregularities (Tachibana *et al.*, 1998, Zou *et al.*, 1998). Furthermore, CXCR4 signalling appears to direct the migration of primordial germ cells (PGCs) in embryogenesis, as they follow a trail of SDF1 production from the production site towards the gonads, with a marked reduction in PGCs present in the gonads of CXCR4 null zebrafish and mice (Doitsidou *et al.*, 2002, Ara *et al.*, 2003). The severe effects of knockout upon embryonic development are likely due to the relatively monogamous

nature of SDF1-CXCR4 signalling - the lack of alternative ligands that may signal through CXCR4 prevent other chemokines from fulfilling the role during embryogenesis.

In adults, CXCR4 expression is most noted for its role in the regulation of inflammation in various cells of the immune system. CXCR4 signalling plays both a homeostatic and an inflammatory role, as it is capable of reducing blood counts of immunocytes as well as directing their migration towards sites of injury. For example, neutrophils, natural killer lymphocytes and monocytes are retained within bone marrow until required by the presence of a chemokine gradient of SDF1, which is recognised by CXCR4 receptors expressed on the cell surface. This interaction promotes a strong chemotactic response towards the site of the SDF1 release at bone marrow stromal cells, ensuring retention (Beider *et al.*, 2003, Wang *et al.*, 2009, Eash *et al.*, 2009).

However, in order for the various haematopoietic cells to form an inflammatory response, the cells must be released from the bone marrow microenvironment; this is achieved through the antagonistic effects of the signalling of another chemokine receptor, CXCR2. This assertion is supported by the finding that the mobilisation of neutrophils by ligands to CXCR2 could be increased in a synergistic fashion by incubation with low concentrations of CXCR4 antagonist (Suratt *et al.*, 2004). Furthermore, CXCR2 null neutrophils do not show the

normal mobilisation response expected upon application of CXCR4 inhibitors, whilst CXCR4 and CXCR2 double knockout neutrophils are constitutively mobilised (Eash *et al.*, 2010). This CXCR2 expression reduces as neutrophils mature, providing a mechanism for the sequestration of senescent circulating neutrophils back in the bone marrow (Martin *et al.*, 2003). The CXCR2-directed mobilisation response appears to be mediated by p38 MAPK as inhibitors to p38 were able to prevent CXCR2-mediated mobilisation (Burdon *et al.*, 2008).

Signalling by CXCR2 is not the only mechanism by which CXCR4-induced neutrophil retention is overcome, as granulocyte colony-stimulating factor (GCSF) is also a major mediator of neutrophil mobilisation. It has been shown that GCSF (whose receptor, GCSFR, is expressed on neutrophils) can reduce SDF1 expression by bone marrow stromal cells as well as CXCR4 expression on neutrophils, indirectly causing neutrophil mobilisation (Kim *et al.*, 2006). Furthermore, the presence of GCSF has also been shown to promote the expression of the serine proteases capthepsin G and neutrophil elastase, as well as matrix metalloprotease-9 (MMP9) which together cause the degradation of SDF1 and other molecules with adhesive qualities, such as vascular cell adhesion protein-1 (VCAM1) (Levesque *et al.*, 2004). This antagonism of CXCR4 action by CXCR2 and GCSFR signalling is an effective mechanism for the regulation of neutrophilia.

Once mobilised, chemotactic signalling on neutrophils and other immunocytes enables their migration towards the site of injury and disease to take part in the inflammatory response. This inflammation response to injury can become severe and uncontrolled, as is the case for acute lung injury (ALI), resulting in morbidity and death. As ALI progresses, there is an increase both in SDF1 expression at the lung epithelium, as well as in CXCR4 expression of neutrophils, whereas late-stage neutrophilia in ALI can also be abrogated by SDF1 inhibition (Petty *et al.*, 2007). CXCR4 has also been indicated in the disease mechanism of the autoimmune disorder rheumatoid arthritis (RA), as SDF1 expression has been documented at the synovium of RA patients, and is considered responsible for the accumulation of CD4+ T cells that are associated with the disorder (Nanki *et al.*, 2000). Accordingly, inhibition of CXCR4 signalling by antagonists was capable of reducing both hypersensitivity and inflammation in mouse models of RA (Tamamura *et al.*, 2004). CXCR4 has also been linked to the activation of basophils and subsequent histamine release, suggesting a role in the allergic inflammatory response (Jinquan *et al.*, 2000).

Allergic response as a result of CXCR4 signalling appears to arise on several fronts, as CXCR4-mediated chemotaxis has been shown to direct the migration of antigen-presenting dendritic cells to the lymph nodes, with CXCR4 inhibition reducing in vivo contact hypersensitivity (Kabashima *et al.*, 2007). CXCR4-directed chemotaxis has likewise been determined to contribute to a number of autoimmune disorders, including ulcerative colitis, multiple sclerosis (MS) and

autoimmune encephalomyelitis (Kohler *et al.*, 2008, McCandless *et al.*, 2008, Xia *et al.*, 2011).

The overactivity of the CXCR4/SDF1 signalling axis in immune disorders may also have a genetic basis, as is the case of Warts, Hypogammaglobulinemia, Infections and Myelokathexis (WHIM) syndrome (Hernandez *et al.*, 2003). As the name implies, sufferers show a range of clinical symptoms including a reduction in gamma globulins such as antibodies (hypogammaglobulinemia), increased susceptibility to a range of infections (particularly wart-causing human papillomavirus infections; HPV), and a reduction in circulating leukocyte and neutrophil numbers as a result of increased retention at the bone marrow (myelokathexis). The most common WHIM-associated autosomal dominant mutations result in truncation of the C-terminus of CXCR4, resulting in increased chemoattraction between SDF1 and CXCR4 and thus increased leukocyte retention (Gulino *et al.*, 2004, Hernandez et al., 2003, Balabanian *et al.*, 2005b, Kawai and Malech, 2009). Knowledge of the regulation mechanisms of CXCR4 have been instrumental in the treatment of WHIM, as therapy options include treatment with GCSF (Hord *et al.*, 1997), increases neutrophil counts through the antagonism of CXCR4 signalling mechanisms as previously described. Antagonists to CXCR4 have also been shown to reduce myelokathexis in clinical experiments (McDermott *et al.*, 2011, Dale *et al.*, 2011).

Whilst CXCR4 is notable for role in immunocyte retention and inflammation responses, the receptor itself was discovered in relation to its role in human immunodeficiency virus (HIV) infection of cluster of differentiation 4-positive (CD4+) immunocytes (Feng *et al.*, 1996). Binding of the HIV virus to CD4 upon the cell surface is achieved via the HIV envelope proteins gp120 and gp41, although the virus is not able to fuse with the membrane until the envelope proteins are bound to a co-receptor, which allows a conformational change in gp41 to bring the viral and cellular membranes in closer proximity (Salzwedel and Berger, 2000). There are two main co-receptors which lead to this outcome: CCR5 and CXCR4, the identity of which determines the type of cell that is infected. CCR5-mediated HIV infects macrophages (M-tropic), whilst CXCR4 results in T cell infection (T-tropic). It is theorised that a shift in later stages of the disease may involve a shift from M-tropic to T-tropic infection (Rosen *et al.*, 2006), so CXCR4 antagonism is a prime target for therapies attempting to halt progression of the disease. Concordantly, treatment with antagonists to CXCR4 has been found to inhibit infection of T cells *in vitro* and with *in vivo* models of the disease (Pettersson *et al.*, 2010, Murakami *et al.*, 2009b).

Despite appearances, the physiological role of CXCR4 is not limited to the chemotaxis of immunocytes, as other cell types can migrate towards SDF1 expressing tissue in the process of injury repair. For example, CXCR4 expression on bone marrow mesenchymal stem cells (BMSCs) has been linked to differentiation to endothelial cell phenotypes which could migrate to the site of

vascular lesions to promote neovascularisation and hence wound repair (Li *et al.*, 2010b). Furthermore, both SDF1 and CXCR4 expression have been shown to become increased in hypoxic conditions, through downstream signalling effects of hypoxia-inducible factor 1 (HIF1) (Schioppa *et al.*, 2003), enabling increased expression at sites of ischaemia and subsequent recruitment of progenitor cells for tissue regeneration (Ceradini *et al.*, 2004).

CXCR4 now represents an intriguing target for ischaemia research as transplantation of mesenchymal stem cells (MSCs) bearing increased CXCR4 expression show superior migratory, angiogenic and neuroprotective qualities in animal models of stroke (Yu *et al.*, 2012). The multipotent natures of MSCs enables differentiation into multiple cell types and so are implicated in wound healing of multiple tissues. For example, the formation of new bone by MSCs in models of skeletal fracture could be inhibited by CXCR4 antagonists or in models expressing lower levels of SDF1 or CXCR4 (Kitaori *et al.*, 2009). Furthermore, the involvement of the SDF1/CXCR4 signalling axis in stem cell populations is not limited to MSCs, as CXCR4 expression has been positively identified on a number of committed progenitor populations in the bone marrow, including those destined for neural, hepatic and muscle progenitor fates, and could migrate towards SDF1 by chemotaxis (Ratajczak *et al.*, 2004).

As has been described, CXCR4 signalling plays a significant role in inflammation and wound healing, and is implicated in the disease mechanism of a variety of disorders. However, the role of CXCR4 in one disease has been conspicuously absent from this literature review - cancer, which will now be described in detail.

1.4 - CXCR4 and cancer

Whilst CXCR4 has been known for its role as a coreceptor in HIV virus entry to CD4+ cells since 1996 (Feng *et al*., 1996), its potential role in cancer was not discovered until 1998, when CXCR4 was found to be overexpressed in a number of glioblastoma cell lines and tissues (Sehgal *et al.*, 1998). Since this discovery, CXCR4 overexpression has been positively identified in numerous cancer types, including breast, ovarian, prostate, melanoma, oesophageal, lung, bladder, colorectal cancers, as well as osteosarcomas, leukaemias and neuroblastomas, with expression often correlated with metastatic spread and the worst prognoses (Schmid *et al.*, 2004, Jiang *et al.*, 2006, Sun *et al.*, 2003, Scala *et al.*, 2006, Sasaki *et al.*, 2008, Phillips *et al.*, 2003, Eisenhardt *et al.*, 2005, Kim *et al.*, 2005, Laverdiere *et al.*, 2005, Barretina *et al.*, 2003, Russell *et al.*, 2004).

In addition, SDF1 is highly expressed in common sites of breast cancer and melanoma metastasis, suggesting a role of the chemokine in cancer progression (Muller *et al.*, 2001). Malignant tumour cells can respond to this chemokine gradient to home in on and infiltrate distant ligand-secreting organs in much the

same manner as normal leukocyte migration to injured tissues. This mechanism is supported by numerous studies investigating the ability of cancer cell lines to migrate through matrigel-type barriers and adhere to epithelial cells, with the effect blocked by administration of CXCR4 antagonists (Libura *et al.*, 2002, Scotton *et al.*, 2002).

In addition, it has been found that cells isolated from metastatic tumours express higher quantities of CXCR4 than cells derived from primary tumours (Marchesi *et al.*, 2004, Nimmagadda *et al.*, 2010). Furthermore, the inhibition of CXCR4 action by RNA interference (RNAi) knockdown, antibodies or antagonists were able to significantly reduce the number of lung metastases in animal models (Ma *et al.*, 2009, Liang *et al.*, 2007b, Liang *et al.*, 2005, Smith *et al.*, 2004, Liang *et al.*, 2004, Yoon *et al.*, 2007, Darash-Yahana *et al.*, 2004), whereas overexpression of the receptor is able to increase metastasis burden (Bartolome *et al.*, 2009). Thus the role of CXCR4 in metastasis and disease progression is well-characterised.

Interestingly, SDF1-induced transendothelial migration (TEM) could also be almost completely abolished by the administration of an antibody to the matrix metalloprotease MMP9 to cultured leukaemia cells, suggesting the role of the enzyme in invasion processes of CXCR4. It was found that MMP9 expression was upregulated in these cells according to the activation of the ERK pathway by

SDF1/CXCR4 signalling, and that inhibition of MMP9 could significantly impair SDF1 mediated migration (Redondo-Munoz *et al.*, 2006, Tang *et al.*, 2008a). The expression of CXCR4 has been found to be linked to the expression of a number of MMP enzymes including MMP2 and MMP13 (Pan *et al.*, 2013, Yu *et al.*, 2011), with their expression playing a role in SDF1-induced migration and invasion. Proteolytic enzymes such as MMPs are vital to the invasive activity of cancer as they are required to degrade the vascular basement membrane and extracellular matrix of tissues. This role for MMP enzymes following SDF1-CXCR4 signalling is supported by a study which showed that membrane-bound MMP was required for dissemination of tumour cells into metastatic sites, following initial homing by CXCR4-mediated pathways (Bartolome *et al.*, 2009).

Aside from CXCR4's clear role in metastatic spread, a number of other key findings indicate that CXCR4 signalling is integral to maintaining a pro-tumour environment. Firstly, increased CXCR4 expression has been linked to enhanced vascularisation of tumours (Darash-Yahana *et al.*, 2004). A number of mechanisms have been suggested for this effect, notably the CXCR4-mediated release of vascular endothelial growth factor (VEGF), an angiogenic growth factor, which itself induces CXCR4 expression in a positive feedback loop that serves to ensure the tumour is well-supplied with oxygen and other nutrients, as well as to promote invasion of the surrounding tissues (Bachelder *et al.*, 2002). In addition to this, there is evidence for VEGF-independent means of angiogenesis promotion (Guleng *et al.*, 2005), such as the downregulation of the

glycolytic enzyme phosphoglycerate kinase 1 (PGK1), which ordinarily cleaves extracellular plasminogen to produce the angiogenesis inhibitor protein, angiostatin. A reduction in PGK1 expression therefore allows angiogenesis to occur, supporting the growth of the metastatic tumour (Wang *et al.*, 2007).

CXCR4 has also been found to promote the cell proliferation in some cancers when cultured in suboptimal serum-free conditions (Scotton *et al*., 2002, Scala *et al*., 2006, Sun *et al*., 2003). The mechanism of this is largely unknown, but the effect is thought to promote tumour survival and metastasis to less favourable sites. CXCR4 expression can also be induced in conditions of hypoxia, which is common to tumours as a result of the inability of angiogenic tumour perfusion to keep up with the rate of tumour growth. CXCR4 expression is induced by signalling mechanisms of hypoxia-inducible factor-1α (HIF1α), which is upregulated in response to hypoxia; HIF1α has been found to bind at the hypoxia response element in the CXCR4 promoter (Schioppa *et al*., 2003). This may help to promote tumour survival in large tumours through the induction of angiogenic processes, or to promote the development of a cancer cell phenotype that is better able to escape to more favourable sites by metastasis (Hongo *et al.*, 2013).

One major factor in the effects of CXCR4 downstream signalling is the function of nuclear factor kappa-light-chain-enhancer-of-activated-B-cells (NFκB), a

transcription factor that ordinarily binds at DNA to promote the expression of genes involved in cell survival, proliferation and differentiation, but which can also enable the exploitation of these processes when misregulated in cancer cells (Zubair and Frieri, 2013). There is evidence to suggest that the signalling processes between SDF1 and CXCR4 can result in the activation of NFκB, resulting in the expression of genes associated with cancer and its progression (Singh *et al.*, 2012, Rehman and Wang, 2009). Furthermore, there are also suggestions that NFκB activation itself induces increases in CXCR4 expression (Maroni *et al.*, 2007, Miyanishi *et al.*, 2010), giving cause to believe that the NFκB/CXCR4 signalling axis could potentially use positive feedback to generate a conducive environment to cancer cell survival.

Another mechanism through which CXCR4-dependent signalling pathways maintain a cancer-promoting microenvironment is through the induction of immunoglobulin transcription factor 2 (ITF2) expression (Appaiah *et al.*, 2010). ITF2 has been shown to promote the transformation of neoplasms (Kolligs *et al.*, 2002), and its expression is thereby correlated with poor diagnoses (Appaiah *et al.*, 2010). Furthermore, ITF2 acted in tandem with CXCR4 to reduce the expression levels of ID2, a member of the inhibitor-of-differentiation (ID) family of transcription factors which is not favourably associated with positive patient outcomes. It was found that ITF2 expression in CXCR4-expressing tumours significantly increased the tumour growth rate, and that inhibition of ITF2-mediated signalling could reduce the invasiveness of CXCR4-expressing cancer

cells. This evidence points to the role of ITF2 as an important downstream target of CXCR4 that promotes tumour survival and progression.

An alternative mechanism for the upregulation of CXCR4 in metastatic disease involves the presence of additional cell types within the tumour, which promote transition of the cancer cells to a more metastatic phenotype through the upregulation of CXCR4. There is evidence to suggest that these cells may arise either from the infiltration of bone marrow-derived mesenchymal stem cells (MSCs) or from fibroblasts residing nearby to secrete factors including SDF1, tumour-growth factor β (TGFβ) and SDF1 to promote progression of the fibroblasts into the tumour-promoting cancer-associated fibroblast (CAF) phenotype. The tumour-promoting ability of CAFs is brought about by their expression of high levels of SDF1, which both promotes survival of the tumour cells and induces CXCR4 expression in tumour cells to give rise to the more metastatic mesenchymal phenotype (Kojima *et al.*, 2010, Jung *et al.*, 2013).

There is evidence to suggest that the induction of CXCR4 expression in tumour cells can occur as a result of a process known as cell fusion - where over-ploid hybrid cells are created that stably bear the characteristics of co-cultured stem cells (Terada *et al.*, 2002). Compelling evidence comes from the observation that tumour cells could undergo cell fusion with infiltrating haematopoietic cells to give rise to hybrid lines that expressed haematopoietic markers including CXCR4.

Furthermore, this fused population was more responsive to the presence of an SDF1 concentration gradient in migration assays (Ramakrishnan *et al.*, 2013), The induction of CXCR4 signalling processes in the progression of the disease can therefore occur through variety of different mechanisms (summarised in figure 2), highlighting the complexity of the challenge faced by researchers.

One particularly interesting and clinically relevant effect of CXCR4 signalling is its proposed role in resistance to therapy; a number of published studies have noted that SDF1 and/or CXCR4 expression can be increased following treatment with radiotherapy, chemotherapy or anti-angiogenic therapy (Shaked *et al.*, 2008, Ebos *et al.*, 2007, Arora *et al.*, 2013), with evidence that this increase in expression is linked to poor prognosis in clinical settings (Xu *et al.*, 2009, Zhu *et al.*, 2009, Li *et al.*, 2013). Furthermore, blockade of the SDF1-CXCR4 signalling axis can overcome resistance, often in a synergistic manner with conventional treatment (Singh *et al.*, 2010, Murakami *et al.*, 2009a, Kioi *et al.*, 2010). The mechanisms involved in CXCR4-mediated resistance appear to be a combination of increased expression of survival proteins (such as nuclear factor kappa-light-chain-enhancer of activated B cells (NFκB) and β-catenin), and the induction of metastatic and angiogenic processes. As a result, it has been suggested that anti-CXCR4 therapy could be used in combination as a sensitizer to treatment, increasing the effectiveness of the chemotherapy (Duda *et al.*, 2011). As a result of these collective findings regarding both the function of CXCR4 signalling in

cancer and its role in therapy resistance, CXCR4 is now an attractive emerging therapeutic target.

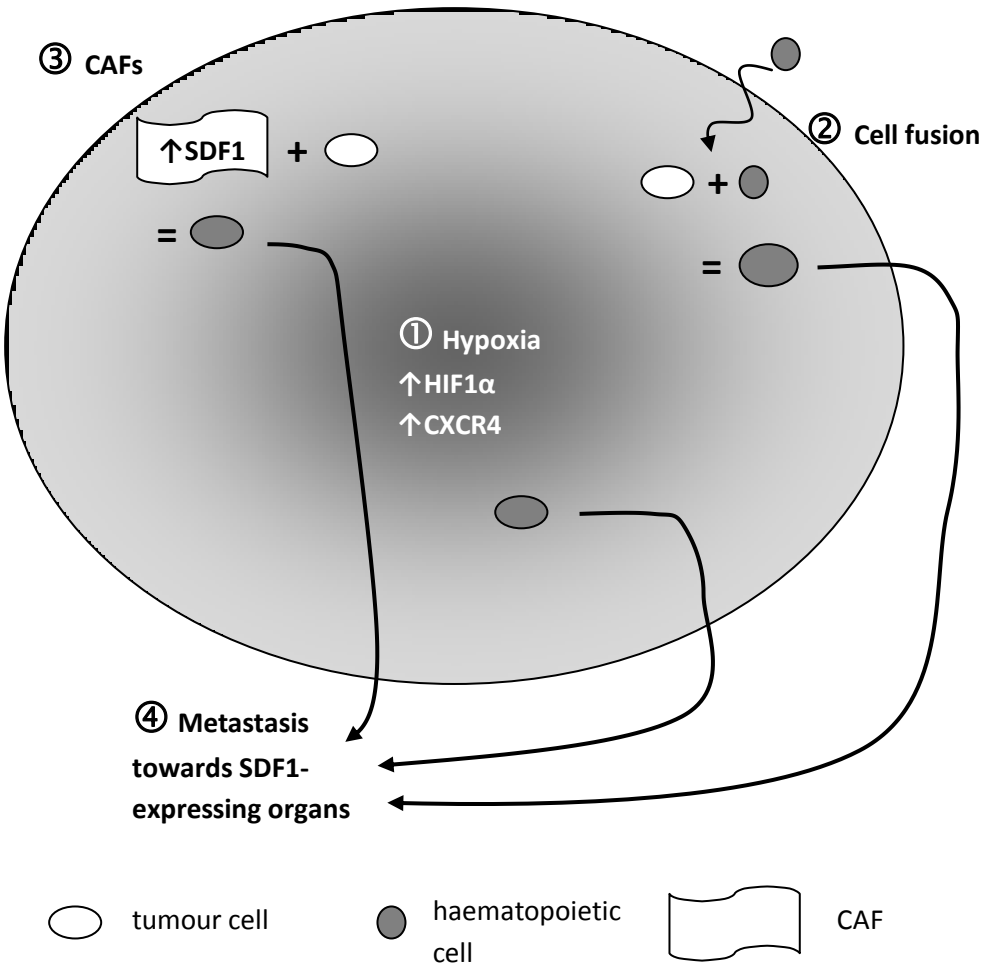

Figure 2. Roles of CXCR4 expression in disease progression.

① Hypoxia in tumour promotes expression of HIF1α, which in turn upregulates CXCR4.
② The tumour is infiltrated by haematopoietic cells, which undergo cell fusion with the resident tumour cells to give rise to hybrid cells bearing characteristics of both cell types - including CXCR4 expression.
③ Fibroblasts near tumours overexpress SDF1 which acts in a paracrine manner upon tumour cells to promote increased CXCR4 expression.
④ Tumour cells bearing increased CXCR4 expression show greater metastatic potential, due to their ability to migrate towards SDF1-secreting organs.

1.5 - Approaches to CXCR4 antagonism

In recent years there has been considerable interest in the use of antagonist molecules against CXCR4 activity as therapeutic strategies. The antagonists so far described chiefly fall into one of two broad groups: the peptide antagonists and small molecular antagonists. Peptide antagonists are derived from the horseshoe crab self-defence proteins tachyplesin and polyphemusin, first identified by screening for peptides active against HIV (Nakashima *et al.*, 1992). Of the synthesised peptides originating from this screening, peptide T140 (figure 3A) was the most active against CXCR4, and is commonly used as a template to design more active and stable derivatives (Tamamura *et al.*, 1998). For example, amidation at the C-terminus of T140 has yielded analogues such as TN14003, which bears markedly increased stability in serum *in vivo*. However, this increased stability came at the price of cytotoxicity as a result of increased net charge of the compound, which is less desirable for certain applications (e.g. as an inhibitor of HIV entry). It was found that substitution of charged amino residues such as arginine or lysine for neutral L-citrulline could temper this cytotoxicity to yield antagonists of high potency and stability, with reduced cytotoxiciy, such as the derivative TC14012 (Tamamura *et al.*, 2001).

In a study exploring the substitution of the individual amino acid residues that comprise T140, it was found that the L-3-(2-Naphthyl)alanine at position 3 is indispensible to receptor function, whilst the residues Arginine-2, Tyrosine-5 and

Arginine-14 are vital to conserve the structure-activity relationship (SAR) of the antagonist (Tamamura *et al.*, 2002). The identification of this 4-residue pharmacophore has led to the development of T140-derived tetra- and penta-peptide antagonists, which show potencies to CXCR4 comparable to that of T140, at a much reduced size, and a reduction in undesirable peptide-specific effects, such as reduced bioavailability due to systemic metabolism (Tamamura *et al.*, 2005a).

The same group also conducted an extensive investigation of the structure-activity relationships of pentapeptide antagonists through sequential modification of the amino side chains and chirality (Fujii *et al.*, 2003, Tanaka *et al.*, 2009, Tamamura *et al.*, 2005b, Ueda *et al.*, 2007). Optimisation of the pentapeptide FC131 (cyclo[D-Tyr^{1}-Arg^{2}-Arg^{3}-Nal^{4}-Gly^{5}], figure 3B) in this way enabled the identification of the residues that are most necessary to retain CXCR4 antagonism. For example, Arginine-^{3} must not be substituted for any residue that is not basic, whereas modification of Arginine-^{2} to include aromatic or methyl groups was well-tolerated. This process led to the development of the more potent pentapeptide compound FC122. Other modifications to the FC131 structure included substitution of the carbonyl (C=O) group of the peptide bond with an imino (C=NH) group, resulting in a much improved bioactivity of the pentapeptide analogues (Inokuchi *et al.*, 2011).

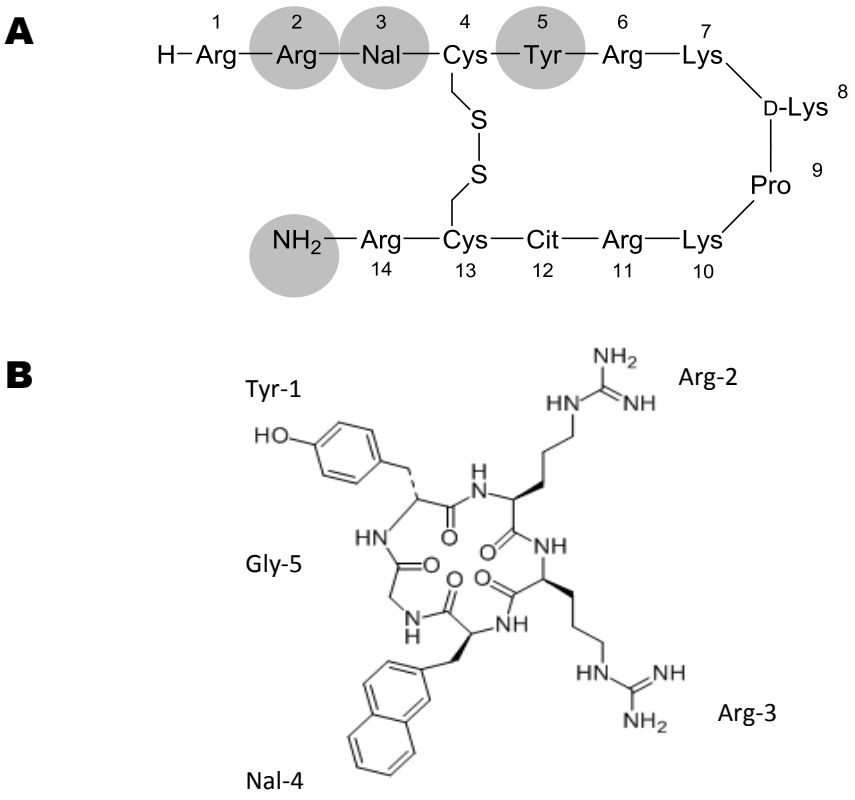

Figure 3. T140, the identification of the pharmacophore, and the pentapeptide FC131.

A Simplified structure of T140 14-mer peptide, grey circles denote pharmacophore amino acids. **B** Structure of cyclic pentapeptide FC131. Arg (Arginine); Nal (2-Naphthyl)alanine; Cys (Cysteine); Tyr (Tyrosine); Lys (Lysine); Pro (Proline); Cit (Citrulline).

Whilst the peptide antagonists described above show a great potency for CXCR4 (in terms of affinity and/or antagonism of downstream signalling), peptides are disadvantageously marked by the fact that they tend to show a poor bioavailability as a result of their vulnerability to enzymatic digestion, and therefore need special drug delivery systems in place (Craik *et al.*, 2013). The structure-activity relationship studies described above yielded some useful information - that the potency of the pentapeptide for CXCR4 was derived primarily from three of its residues: An aromatic ring at position 4, an arginine-like group at position 3 and either a phenol or an arginine-like group at position 1

(Ueda *et al.*, 2007, Tamamura *et al.*, 2005b). The Tamamura group theorised that an alternative non-peptidic backbone that preserved the positions of the side-chains might result in a small-molecular antagonist that retained the potency of FC131 for CXCR4 whilst not suffering from the drawbacks associated with peptidic drugs. They identified 5-aminoindole-2-carboxylic acid as a core structure that met the spatial requirements of the proposed design, as well as the potential for bioavailability (figure 4). As such they developed a library of indole-derived CXCR4 antagonists, however, none came close to the potency of FC131 for CXCR4 antagonism (Ueda *et al.*, 2008).

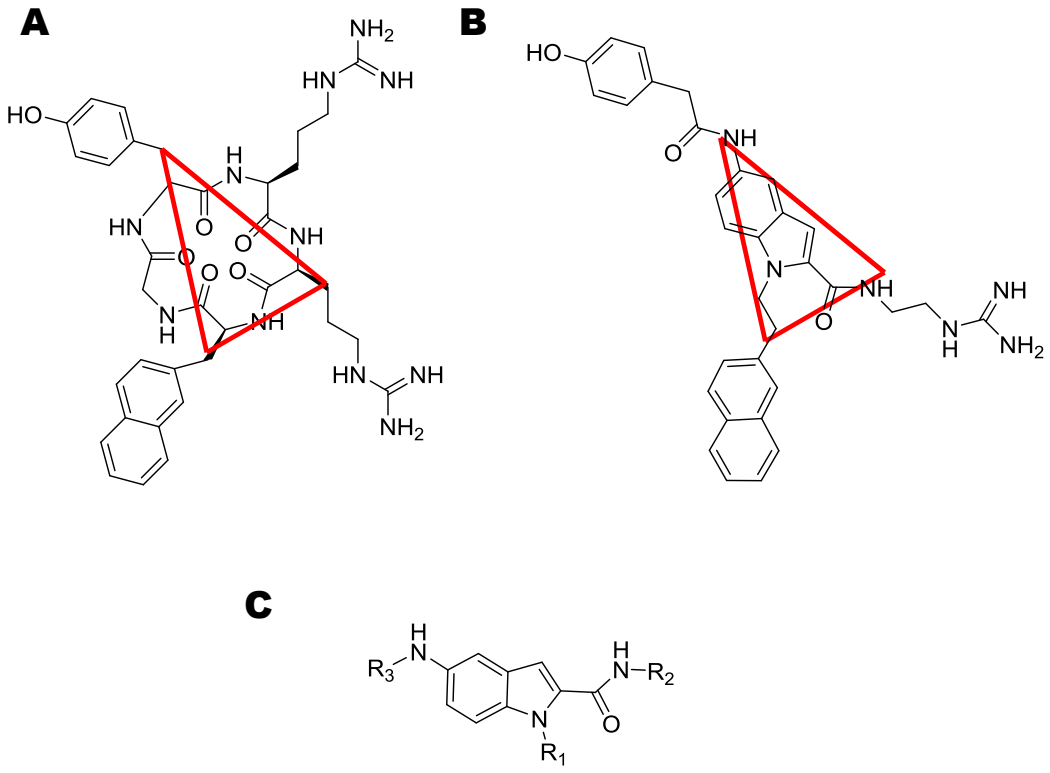

Figure 4. Evolution of the indole class of CXCR4 antagonist from cyclic pentapeptides

A FC131 with a triangle superimposed above the carbon atoms joining the amino side-chains to the cyclopentapeptide backbone. **B** An example of a similar indole-derived antagonist with the same triangle superimposed upon the equivalent atoms. Note the relatively close fit of the triangle over the indole backbone. **C** Core structure of indole CXCR4 antagonists. R_n designates the presence of an amino acid R-group. Adapted from (Ueda *et al.*, 2008).

Aside from the T140-derived peptide antagonists, the other major class of CXCR4 antagonists are the small-molecule antagonist class, which includes the bicyclam compound AMD3100 (figure 5A). AMD3100 is the the only CXCR4 antagonist to have been approved for use in humans albeit for stem cell mobilisation in non-Hodgkin's lymphoma and multiple myeloma, (US Food and Drug Administration (FDA), 2008, Genzyme, 2008). The compound's mechanism of action appears to be related to its bi-protonated nature at physiological pH, enabling hydrogen bonding with carboxylic groups of the CXCR4 receptor, at Asp171 and Asp262 (Hatse *et al.*, 2002). It has been reported that AMD3100 exerts its antagonistic effect by acting as a partial agonist (Zhang *et al.*, 2002), however other experimental data contradicts this finding (Hatse et al., 2002, Fricker *et al.*, 2006). AMD3100 was initially developed for its potential anti-HIV activity; further research in this area has largely been abandoned as a result of cardiac irregularities, a lack of oral availability and limited therapeutic efficacy (Hendrix *et al.*, 2004). Aside from its well-documented use as a stem cell mobiliser in haematological malignancies (Tekgunduz *et al.*, 2012), AMD3100 is currently under investigation in a phase I clinical to determine its ability to treat recurrent glioblastomas (www.clinicaltrials.gov, 2013).

The structure of AMD3100 clearly requires optimisation to overcome its limitations; the molecule was therefore sequentially deconstructed in order to ascertain the minimum necessary composition whilst still retaining CXCR4 antagonism. It was found that one of the cyclam rings of AM3100 could be

substituted for a pyridinylmethylene group that allowed for higher efficacy CXCR4 antagonism as a result of more potent interactions at a greater number of sites on CXCR4 (Rosenkilde *et al.*, 2007). This diamine compound, designated AMD3465 (figure 5B), was also found to show excellent bioavailability in dogs (Bodart *et al.*, 2009) and an ability to inhibit tumour invasion and metastasis *in vivo* (Ling *et al.*, 2013), suggesting considerable potential for further development. As such the substitution of the remaining cyclam group for similar 14-member azamacrocyclic moieties resulted in the identification of two AMD3465 analogues bearing increased inhibition of CXCR4 (Bridger *et al.*, 2010).

The success of substituting the AMD3100 cyclam groups led researchers to consider whether any cyclam or macrocyclic moiety at all was necessary for CXCR4 inhibition. A structure-activity relationship study deconstructing AMD3100 led to the discovery that the central aromatic ring was vital to its potency as an antagonist, and that phenol groups on either end must be separated by a single carbon spacer and amine group in order to retain CXCR4 antagonism (Zhan *et al.*, 2007). Further optimisation of this lead compound structure led to the development of the CXCR4 antagonist class known as dipyrimidines, which showed more potent CXCR4 antagonism than the previous lead compound (Zhu *et al.*, 2010). A potent member of this group, MSX-122 (figure 5C), was found to be able to inhibit CXCR4-mediated invasion *in vitro* through matrigel, as well as to diminish the severity of several models of inflammation, and of tumour metastasis to the lung *in vivo* (Liang *et al.*, 2012).

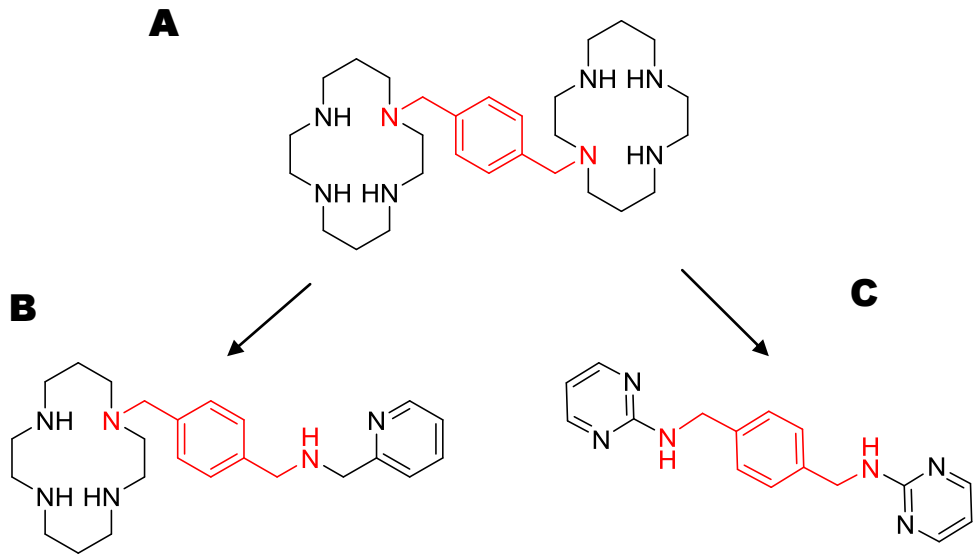

Figure 5. Common structural features of AMD3100 and diamine CXCR4 antagonists

A Bicyclam AMD3100 **B** Monocyclam AMD3465 **C** Dipyrmidine MSX-122. Adapted from (Zhan *et al.*, 2007).

Intriguingly, it was found that this class of compounds could inhibit the $G\alpha_i$-associated cAMP modulation of CXCR4 whilst harbouring no effect upon $G\alpha_q$-mediated calcium flux, and showing an inability to inhibit SDF1α binding to CXCR4. This was rationalised to result from the smaller size of cyclic groups, which might therefore interact with less sites on CXCR4 and result in a less complete antagonism.

An additional class of small molecular CXCR4 antagonists are the tetraquinolines, comprised of a core structure of benzimidazol and tetrahydroquinoline connected by a methylamine alkyl linking group. One notable example is

AMD070 (also known as AMD11070; figure 6A), found to be a potent inhibitor of ligand binding to CXCR4, orally available, relatively non-cytotoxic and with promising pharmacokinetics (Skerlj *et al.*, 2010). In the face of these positive indications, AMD070 has been tested for its ability to inhibit SDF1-mediated invasion in melanoma cells *in vitro*, and found to be more effective for CXCR4 inhibition than AMD3100 (O'Boyle *et al.*, 2013). Furthermore, AMD070 was found to be successful in increasing the lifespan of mouse models of acute lymphoblastic leukaemic when administered in combination therapy (Parameswaran *et al.*, 2011). As a result of these findings AMD070 was assessed in phase I clinical trials to determine the safety and pharmacokinetics of the drug in healthy human subjects, and found to be slowly eliminated and well-tolerated, with mostly grade 1 and grade 2 side-effects, with the exception of a single grade 3 result of lipase increase (Stone *et al.*, 2007). AMD070 therefore shows considerable potential as a cancer therapeutic and CXCR4 antagonist.

A final class of small molecular CXCR4 antagonists to be discussed is isothioureas, an isolated group of compounds developed by Novartis that does not share much structural similarity to either the peptide or small molecular antagonists so far described. The lead compound of this group is known as It1t (figure 6B), which was found to show extremely potent antagonism for CXCR4, oral availability in rats, as well as low non-specific binding to plasma samples (Thoma *et al.*, 2008). This class is less developed than others published in that very few compounds have been synthesised, and very little research has been

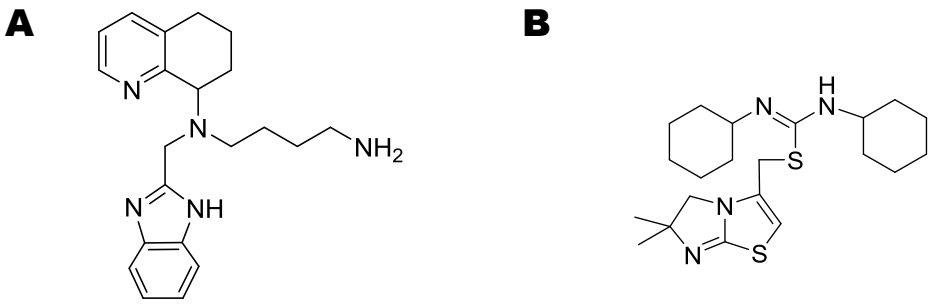

Figure 6. Examples of CXCR4 antagonist classes

A Tetraquinoline AMD070 **B** Isothiourea It1t

done by way of determining their efficacy as CXCR4 antagonists in disease models *in vivo*. Despite this, the compound class holds considerable potential as budding CXCR4 antagonists given that the compound bears several qualities that suggest suitability for further development: very high potency, acceptable bioavailability even through the oral route, and high aqueous solubility.

In summary, there are a variety of approaches to designing CXCR4 antagonists, each with their own advantages and drawbacks. The peptide classes of antagonists are potent, yet vulnerable to enzymatic digestion and cannot be administered orally, however advances have been made in reducing the size of the peptide through identification of a pharmacophore for use in cyclic pentapeptides. Attempts to capitalise on the potency of pentapeptide structure whilst replacing its cyclic pentapeptide ring with an indole backbone unfortunately resulted in considerably less potent CXCR4 antagonists. The cyclam molecules AMD3100 and AMD3465 resulted in high potency CXCR4

inhibition yet show poor oral bioavailability and so are restricted to parenteral routes of administration. AMD070 exhibited high potency and oral bioavailability and also displays promising signs from phase I clinical trials. Isothioureas likewise show high potency and oral bioavailability yet are currently underdeveloped and in need of further assessment.

1.6 - Molecular imaging and Positron Emission Tomography

A large variety of imaging techniques are available for the detection of cancer, with many of them suitable for specific molecular targets, each with their own advantages and drawbacks. Information on the imaging modalities used in molecular imaging will be briefly mentioned here, and is summarised in table 1. Of the major imaging modalities, Computerised Tomography (CT) scanning is the least developed towards utilisation in molecular imaging; even though progress has recently been made in the use of targeted heavy metal nanoparticle contrast agents (Li *et al.*, 2010a), CT scanning is almost exclusively anatomical in nature. Contrast in CT images is generated by the variable densities of tissues, with high-density heavy metal compounds exacerbating the absorption of X-rays emitted from the X-ray tube. Contrast in Ultrasound (US) imaging is similarly induced by changes in the density of tissues, although in this case it is at the interface between tissues of different densities, creating altered echogenicity of the ultrasound waves. This quality can be induced by the introduction of

microbubbles which can be targeted to a particular cancer biomarker (Bzyl *et al.*, 2013). The last of the major anatomical imaging techniques is Magnetic Resonance Imaging (MRI), which detects tissues structures in a very different manner, through the electromagnetically induced disruption of nuclear spin properties. Contrast agents bearing paramagnetic and superparamagnetic properties can be targeted towards tumour tissues through conjugation to biomarker-specific molecules, allowing alteration of the recovery rate of nuclei from disruption, generating contrast in tumour tissues (Geraldes and Laurent, 2009).

Whilst CT, US and MRI can be considered anatomical imaging techniques that are able to be applied towards the molecular imaging of biomarker targets, other imaging modalities do not provide anatomical data at all, with images solely consisting of the location of the injected tracer molecule. Such imaging methods are uniquely suitable for molecular imaging purposes as the use of tracer molecules that are targeted to cancer biomarkers can therefore theoretically generate contrast almost exclusively within the tissue of interest (aside from the organs of excretion), if a sufficiently specific tracer is used. One such imaging modality is optical imaging, whereby a biomarker-targeting molecule is conjugated to a fluorescent or bioluminescent dye that emits light within the optical light frequencies (including those of near-infrared frequencies; NIR) (Adams *et al.*, 2007). Alternative molecular imaging approaches include nuclear imaging techniques such as Single-Photon Emission Computed

Tomography (SPECT) and Positron Emission Tomography (PET). These require the administration of tracers incorporating atoms emitting ionising radiation - gamma ray-emitting radionuclides in the case of SPECT, and positron-emitting radionuclides in the case of PET. These radionuclides are integrated into the design of the molecule targeting the cancer biomarker and therefore primarily localise within the tissues that express that biomarker (Oh *et al.*, 2011).

The purpose of this project is to develop novel radiotracers for use with PET to target the expression of the CXCR4 cancer biomarker. While all the imaging modalities described have applications in molecular imaging, PET scans bear a number of advantages over the others. The use of CT scanning as a method of molecular imaging is within its infancy and not well-characterised in clinical studies, whereas numerous PET radiotracers are approved for use or testing in humans. Both ultrasound and optical imaging have issues with low tissue penetration, which makes the modalities unsuitable for the imaging of deep tissues, whereas PET is not affected in this way (Higgins and Pomper, 2011). MRI gives images of extremely high resolution, however the method is inherently insensitive and therefore requires the administration of large quantities of contrast agents (Skotland, 2012). In contrast to SPECT, PET bears a much higher sensitivity which in turn allows an improvement of image quality as a result of the increased signal-to-noise ratio. The use of short-lived isotopes in PET imaging also enables greater quantities of radioactivity to be administered to patients without additional risk, as scans can be considerably shorter and more

convenient to the patient and hospital department. This feature also enables greater temporal resolution which is of particular importance for dynamic scanning (Rahmim and Zaidi, 2008).

PET imaging therefore possesses a number of qualities that make it a sound choice for molecular imaging purposes, and the mechanism of its operation will now be discussed in detail. Positron emission tomography (PET) is a nuclear imaging technique that detects radioisotopes emitting ionising radiation in the form of B^+ decay (positron emission). Decay of the radiotracer is detected indirectly, as collision of the antimatter positrons with their matter counterparts, the electrons, results in annihilation of both subatomic particles within the surrounding tissue, producing 2 bursts of γ radiation travelling in approximately opposite directions, which are detected by a detector ring within the scanner (figure 7). The distance that the positron travels from the site of emission before the annihilation event occurs depends upon the energy of the emitted positron. This is in turn dependent upon the radioisotope source of the positron - for example, positron emission from gallium-68 occurs with a maximum energy of 3.8 MeV, whereas positron emission from copper-64 possesses 0.58 MeV of energy. As annihilation between the positron and electron may only occur once the kinetic energy of the positron has dropped to 0.551 MeV (as will occur spontaneously as a result of collisions), the spatial resolution of the PET image generated is both dependent upon the energy

Table 1. Comparative table of pre-clinical imaging modality qualities.

Modality	Spatial resolution	Molecular probe types	Advantages	Limitations
Ultrasound	50-500 µm	Microbubbles.	Portable. Cheap. Widely available. No major safety concerns. Sensitivity can be high, depending on the structure of microbubble used.	Low tissue penetration.
Optical	2-5 mm	Fluorescent or bioluminescent compounds.	Ability to detect multiple probes in single imaging session.	No major safety concerns. Limited tissue penetrance.
CT	50-200 µm	Heavy metal nanoparticles.	Relatively cheap. High resolution. Widely available.	Requires exposure to ionising radiation. Anatomical imaging method, generally not used for molecular imaging. Large quantities of contrast agent required. Low temporal resolution.
MRI	25-100 µm	Paramagnetic or superparamagnetic compounds.	High resolution.	Expensive. Low sensitivity. Requires exposure to powerful magnetic fields. Large quantities of contrast agent required. Low temporal resolution.
SPECT	1-2 mm	Gamma ray-emitting radionuclides e.g. ^{99m}Tc, ^{125}I and ^{111}In.	High sensitivity.	Requires exposure to ionising radiation. Poor spatial and temporal resolution.
PET	1-2 mm	Positron-emitting radionuclides e.g. ^{11}C, ^{18}F, ^{68}Ga and ^{64}Cu.	High sensitivity. Use of ^{11}C, ^{15}O and ^{13}N enables radiolabelling of biologically relevant molecules with no further modification.	Low resolution. Requires exposure to ionising radiation. Must be located near a cyclotron or radioisotope generator. Expensive.

Summarised from (Alberti, 2012, Skotland, 2012, Higgins and Pomper, 2011)

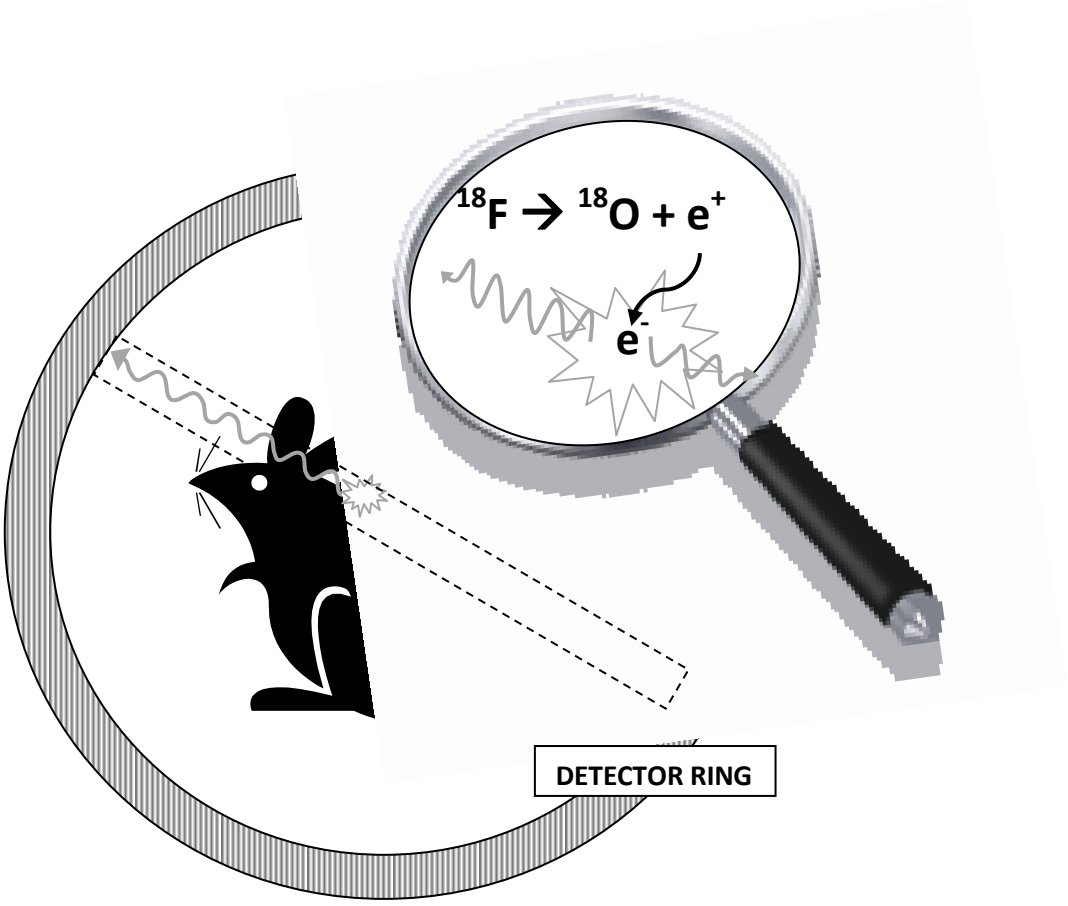

Figure 7. Diagram of positron emission and subsequent gamma ray detection by PET scanner

A radiotracer accumulates in the tissue of interest (e.g. tumour). B+ decay of the radioisotope (in this case ^{18}F) results in the emission of a positron (e^+) which is annihilated upon collision with a nearby electron (e^-), causing the projection of 2 γ ray bursts in opposite directions. These are detected at the detector ring of the PET scanner.

possessed by the positron upon emission and the density of the tissue surrounding it (Sanchez-Crespo *et al.*, 2004, Zanzonico, 2004). The localisation of the radiotracer within the test subject is determined by the measurement of so-called 'coincidence events' - the detection of a pair of γ ray bursts at approximately opposite sides of the detector ring (at ~180 ° apart) that are detected within 6-12 ns of each other. These events are designated 'true' events, and any detected paired or single events that fall outside these criteria

are discarded by the reconstruction as noise. The region of space that falls between the two detectors is known as the line of response (LOR), and designates the possible source of the positron emitter. The detectors themselves are comprised of a scintillator, which luminesces upon contact with ionising radiation, allowing detection by a photomultiplier tube (Zanzonico, 2004, Tomasi and Aboagye, 2013). Considerable computational reconstruction is required to convert this raw coincidence event data into a quantitative PET image, and may include algorithms for attenuation correction and reconstruction, including filtered back projection and iterative reconstructions (Tarantola *et al.*, 2003). Despite the advanced image processing required, PET imaging is ideally suited to the molecular imaging of cancer biomarkers as the positron-emitting radioactive isotopes such as ^{18}F and ^{11}C that it detects can be incorporated into biological molecules that are taken up or bound by cancerous cells.

1.7 - CXCR4 as a molecular imaging target

The molecular imaging of cancer by targeting CXCR4 expression is an emerging field, and has great potential for the identification of patients that may respond well to CXCR4 antagonists as therapeutic agents. Given that biopsy data are available for most primary tumours (with the exception of inoperable tumours), the most clinically relevant application of CXCR4-targeted molecular imaging would be in further assessment of patients who had already begun therapeutic

treatment, rather than for the initial analysis of primary tumours. For example, a patient bearing an excised primary tumour that had been tested positive for CXCR4 might benefit from non-invasive assessment, either to ensure that all lesions had been removed, or as a re-staging procedure to detect progression of the malignancy, given that CXCR4 expression in primary tumours is a risk factor for metastasis (Cabioglu *et al.*, 2005). This utilisation of CXCR4-targeted imaging shows great potential, as a personalised approach to patient care may increase the sensitivity of the modality to tumour detection.

Furthermore, CXCR4-targeted imaging methods could potentially detect whether a tumour that is currently unresponsive to alternative therapies might be sensitised by targeted CXCR4 antagonism. Given that AMD3100 has been shown to be well-tolerated in patients with only grade 1 toxicity reported (Devine *et al.*, 2004), allowing oncologists to make a more informed choice on the best therapeutic regimen for a given patient would hopefully reduce unnecessary adverse effects or delays in effective treatment for the patients. It is also possible that the higher expression of CXCR4 in invasive and recurrent tumours might enable the use of CXCR4-targeted imaging methods as a tool for the prediction of disease outcome. The molecular imaging of CXCR4 therefore has considerable potential in clinical medicine, and the current status of the development of radioisotope probes for the nuclear molecular imaging of CXCR4 will now be described in detail.

There has been substantial progress in the development of radiotracers targeting CXCR4 in recent years, beginning with a publication in 2006 regarding an ^{111}In-labelled Ac-TZ14011 CXCR4 antagonist for use as a SPECT tracer (Hanaoka *et al.*, 2006). A significant difference in tracer accumulation was found in the tumour-to-muscle and tumour-to-blood ratios of nude mice bearing pancreatic tumours, as compared with mice that had received blocking doses of 10 mg/kg unlabelled Tz14011. However, accumulation within the tumours was still very low, with a maximum measurement of 0.51 %ID/g at 1 hour post-injection. Nevertheless, the paper proved that the concept of a CXCR4-targeted radiotracer was possible, and subsequent publications have developed tracers with improved biodistribution data.

In 2008, a ^{99m}Tc radiolabelled SDF1α was developed for use as a SPECT tracer for the identification of increases in CXCR4 as a result of myocardial infarction (Misra *et al.*, 2008). Whilst accumulation in the infarcted tissue was low, at 0.57 %ID/g at 2 hours post-injection, this reflected a 5-fold increase compared to non-infarcted tissue, as well as the biodistribution in other organs (excluding the kidneys). ^{99m}Tc was also utilised as radioisotope in disclosed findings in a communication to Chinese Chemical Letters regarding the uptake of a ^{99m}Tc-labelled AMD3100 CXCR4 antagonist into liver tumour animal models, although precise values (such as %ID/g and tumour to muscle ratios) were not divulged (Zhang *et al.*, 2010). However, an identical ^{99m}Tc-labelled AMD3100 was found to be taken up in PC-3 prostate cancer tumours to a maximum of ~1.7 %ID/g which

was significantly higher than in the tumours of mice that had been injected with a blocking dose of 20 mg/kg AMD3100. However it is important to note that this peak uptake occurred within the first 5 minutes following injection, and very rapidly washed out over the duration of the 60 minute scan. This extremely fast pharmacokinetics is not ideal for a radiotracer as it is not practical for either clinical or preclinical use. In addition, there was high uptake at 60 minutes in a number of non-target tissues, including the liver, lungs, thymus, intestine, spleen and bone, however the authors rationalised that this may be due to the presence of CXCR4-expressing cells, as many of the sites are known to express SDF1, and the uptake could be partially blocked by the AM3100 blocking dose, implying specific uptake (Hartimath *et al.*, 2013). This uptake profile in additional tissues besides the tumour may further limit the usefulness of the tracer in identifying tumours in these localities.

The first reported study to investigate the uptake of a radiolabelled probe in tumour models of both high and low CXCR4 expression was in the form of an ^{125}I-labelled monoclonal antibody, which showed a significant difference in tracer accumulation in comparison to the radiolabelled control antibody (~6 %ID/g and ~3 %ID/g, respectively) (Nimmagadda *et al.*, 2009). However, considerable uptake of the control antibody was also seen, suggesting some probe uptake in the tumour did not arise as a result of receptor-mediated binding, but instead by the enhanced nonspecific permeability and retention of large macromolecules such as antibodies (Maeda *et al.*, 2000). Furthermore, no

significant difference in control and CXCR4 antibody binding was seen in smaller tumours (<200 mm^3), and further analysis led the group to conclude that the greater visibility of CXCR4 antibody in larger tumours was due to an increase in CXCR4 expression as a result of the hypoxic tumour microenvironment, rather that the endogenous difference in CXCR4 expression.

In recent years SPECT tracers being developed that target CXCR4 have explored bimodality with optical imaging fluorophores as a way to increase the practical applications of the tracers. The first of these was an ^{111}In- and Cy5.5-like fluorophore-labelled derivative of the T140 CXCR4 antagonist, which was found to accumulate specifically in CXCR4-expressing tumours at a 3.8-fold higher level than in CXCR4-negative tumours, although there was also high uptake of the tracer in the liver, kidneys, spleen and intestines (Kuil *et al.*, 2011b). However, as the affinity of the tracer for CXCR4 was adversely affected by 20-fold following the conjugation of the bimodal label, the same group attempted multimodal labelling of a dendrimeric version of the Ac-TZ14011 antagonist, which was found to bear an increased affinity for CXCR4. While the tracer had low uptake in the CXCR4-expressing tumour (0.42 %ID/g for the tetrameric tracer), the use of this dendrimeric tracer reduced the background uptake in muscle by 3.6-fold, therefore increasing the tumour-muscle ratio. Unfortunately the background uptake in almost all other tissues measured was higher than in the tumour, suggesting that the signal-noise ratio is poor (Kuil *et al.*, 2011a). While the use of an optical imaging label within the bimodal tracer also allows some additional

functions including *in vitro* labelling of CXCR4 expression for confocal microscopy and flow cytometry (Buckle *et al.*, 2013) it also comes with some disadvantages. For example, it is important to consider that the conjugation of both a metal ion-chelating group and a fluorophore to the already-macromolecular T140 CXCR4 antagonist results in an extremely bulky radiotracer, particularly in the case of the dendrimerised antagonist tracer. It is therefore perhaps unsurprising that the imaging of tumours with these tracers took place a full 24 hours post-injection, which is not practical for clinical use.

Despite the announcement of several of the SPECT tracers described above, there was no published PET radiotracer targeting CXCR4 before 2009. In the years since, there has been an upsurge in interest in such developments (summarised in table 3), which began with the chelation of ^{64}Cu within a cyclam ring of the small molecular antagonist AMD3100 (Jacobson *et al.*, 2009). This same tracer was utilised by the Nimmagadda group in various tumour models to show that the tracer accumulated significantly more in tumours of high CXCR4 expression versus tumours of lower expression using both transfected glioblastoma cellular models (35 %ID/g and 9 %ID/g, respectively) and cancer cell lines exhibiting endogenous high or low CXCR4 expression. Furthermore, they showed that it was possible to use this tracer to image lung metastases, which showed an increased CXCR4 expression profile in comparison to lungs without metastases (Nimmagadda *et al*., 2010). However, high uptake was

observed in many tissues, including the lungs, liver, spleen and kidneys, and there was evidence of considerable binding of AMD3100 to blood proteins, suggesting non-specific binding, with similar findings also reported by the group who first developed the ^{64}Cu-AMD3100 tracer (Weiss *et al.*, 2011).

A significant advance was the development of a ^{64}Cu-labelled monocyclam antagonist AMD3465 (De Silva *et al.*, 2011), which has shown 102 %ID/g of tracer uptake in CXCR4-overexpressing tumour tissue versus 3 %ID/g in the control tumour. Furthermore, the maximum tracer uptake showed a tumour-to-muscle ratio of 361 (versus 18 for the non-CXCR4-transfected tumour), with the differences in uptake vividly apparent upon PET images. The uptake of tracer in CXCR4-expressing tissues could also be blocked by the administration of unlabelled Cu-AMD3465, providing compelling evidence of CXCR4-specificity *in vivo*. This level of specific uptake is far superior to previously reported data for CXCR4-targeting compounds; however, for all its strengths, there was considerable uptake of non-targeted [^{64}Cu]$CuCl_2$ at the tumour. Furthermore, the tracer is limited by the undesirability of ^{64}Cu as a PET radionuclide, which will now be described.

As table 2 shows, the half-life of ^{64}Cu is long, relative to the other commonly used PET radioisotopes. This is exacerbated by the fact that only 19% of the total radioactivity emitted occurs by positron emission - the rest occurs primarily by

beta decay and electron capture. This means that a higher dose of ionising radiation would be required to be administered to the patient in order to receive the same quality of data. PET imaging can be conducted with even longer-lived radioisotopes such as ^{89}Zr and ^{124}I (with half lives of 3.3d and 4.2d, respectively), although this is most suited to immunoPET applications, where the labelled antibody takes considerably longer to penetrate the tumour than the far smaller antagonists (Verel *et al.*, 2003). For these reasons, it would be better to choose a radionuclide with both a short half-life, and a high proportion of positron emission for the development of antagonist-based radiotracers. While the radionuclides ^{15}O, ^{13}N and ^{11}C would appear to fulfil these requirements, the half-lives are so short as to be very impractical for many applications unless the clinical department or preclinical laboratory is located extremely close to a cyclotron. Thus ^{18}F is considered to be an excellent compromise - its decay is 97% positron emission and the half-life is a very manageable 109.8 minutes, which enables delivery of radiotracers to users within a limited distance (Zanzonico, 2004). Furthermore, the positrons emitted are very low-energy, and

Table 2. Properties of commonly used radionuclides for positron emission tomography

Radionuclide	Half-life	% e+ emission	Maximum e+ energy (MeV)	Produced by
Oxygen-15	2.1 min	100	1.7	Cyclotron
Nitrogen-13	10.0 min	100	1.2	Cyclotron
Carbon-11	20.4 min	99	1	Cyclotron
Gallium-68	1.1 h	88	1.9	Generator
Fluorine-18	1.83 h	97	0.6	Cyclotron
Copper-64	12.7 h	19	0.6	Cyclotron
Yttrium-86	14.7 h	32	1.4	Cyclotron

Summarised from Zanzonico (2004).

so there is a short linear range within tissues and thus high resolution comparative to many other radionuclides.

The first implementation of an ^{18}F label into a CXCR4-targeting radiotracer was in 2010 [when this project had already commenced], and involved an ^{18}F-fluorobenzoate derivative of the T140-derived antagonist TN14003 (Jacobson *et al.*, 2010). This tracer accumulated in CXCR4-expressing, but not in CXCR4-negative tumours at a tumour-to-muscle ratio of 21.6. However, the ability of the tracer to discern tumours of varying CXCR4 expression was only possible following coinjection of a blocking dose of the cold antagonist; it was proposed that the tracer would otherwise bind in a non-specific manner on red blood cells (RBCs) to such a degree that there was insufficient radiotracer left for specific binding at the tumour. The requirement to coinject subjects with additional compound would be extremely inconvenient in a clinical setting, and would drive up the costs of the procedure. In an attempt to address these concerns, the group modified the T140-derived peptide tracer by instead introducing the radionuclide through chelation at a conjugate NOTA or DOTA group (Jacobson *et al.*, 2012), resulting in a tumour-to-muscle ratio of ~5. Whilst radiolabelling the tracer in this way considerably improved the specificity of the tracer for CXCR4, as it was no longer subject to unintended binding to red blood cells, it came notionally with the caveat of ^{64}Cu as the radionuclide, rather than the more preferable ^{18}F. Nonetheless, this approach was considerably more effective than conjugation of the peptide with ^{64}Cu-DOTA at lysine residues 7 and 8, which

again resulted in the requirement for a cold peptide coinjection to prevent unspecific tracer uptake within the blood before CXCR4 expression within tumours could be elucidated (Jacobson *et al.*, 2011).

The situation regarding ^{18}F imaging of CXCR4 was not improved until 2013, when the T140 derivative Ac-TC14012 was conjugated to ^{18}F via either a fluorobenzoate or fluoroproprionate group at Lys-7, which were found to accumulate in CXCR4-expressing tumours at levels of around 4 or 5-fold higher than in CXCR4-negative tumours (Zhang *et al.*, 2013). Unlike previous efforts, there was minimal binding to red blood cells, leading the authors to conclude that the C-terminal placement of fluorobenzoate must have been responsible for this effect in the ^{18}F- and ^{64}Cu- labelled versions of this T140-derived peptide antagonist (Jacobson *et al*., 2010, Jacobson *et al*., 2011). However, the authors also purported evidence for some specific binding of the tracer at the liver, as the coinjection of a small quantity of cold compound resulted in reduced liver uptake, and increased uptake of the tracer in CXCR4-expressing tumours, presumably as a result of the increased circulation of the tracer. However, it seems plausible that this may instead have been due to reduced clearance of the tracer by the liver when excess unlabelled is present in competition. This suggestion is supported by the observation that the blocking dose did not have the effect of increasing contrast at the tumour, as binding within the CXCR4-negative tumour increased at the same proportion as in the CXCR4-expressing tumour. Despite the improvement, tracer uptake within CXCR4-expressing

tumours was still low, at a maximum of 4.81 %ID/g with cold peptide coinjection, or 2.4 %ID/g without. Thus there is still some way to go in the development of ^{18}F-labelled PET tracers targeting CXCR4 expression, and further optimisation of tracer design may well be possible.

Despite all the advantages of ^{18}F as a PET radionuclide described previously, there are situations where its use is not practical. As mentioned in table 2, ^{18}F, along with most other commonly used PET radionuclides, is generated within a cyclotron. The expense of running such machinery, along with the short half-life of fluorine puts limits upon the feasibility of using such tracers at locations more distant from cyclotrons, or where higher costs are prohibitive. In contrast, ^{68}Ga is produced by the decay of ^{68}Ge with the aid of a generator, which extracts the clinically useful ^{68}Ga product from the parent isotope. ^{68}Ge also has a long half-life of 271 days, enabling cost-effective production of ^{68}Ga from a generator for a year or more, even where cyclotron facilities are unavailable (Breeman and Verbruggen, 2007). The half-life of ^{68}Ga is also a relatively convenient 68 minutes, with 88% of radioactive decay occurring by positron emission. These desirable qualities counteract the potentially negative aspect of a high positron energy level (which may reduce maximum image resolution); thus ^{68}Ga may be considered a very desirable radionuclide to use in PET imaging.

As such, progress has recently been made in the development of a ^{68}Ga-labelled cyclic pentapeptide ligand to CXCR4 known as CPCR4-2. It was found that this tracer accumulated in the tumour at a concentration higher than in any other organ, to a maximum of 6.2 %ID/g (Gourni *et al.*, 2011). Furthermore, the same group developed a dimeric pentapeptide moiety that could be labelled with ^{68}Ga-DOTA (Demmer *et al.*, 2011) although the maximum tumour uptake with this tracer was considerably lower, at 2.1 %ID/g, and there was high uptake measured in non-target tissues. In neither of these investigations was there were a CXCR4-negative tumour model used; given non-specific binding characteristics with previous radiotracers have affected the ability to discern CXCR4-positive and CXCR4-negative tumours without the coinjection of competing cold compound, the omission of this control condition is starkly apparent. Some progress has been made in the ^{68}Ga-DOTA labelling of a TN14003 derivative at lys-7, which showed a significant difference in uptake in cell lines of differing CXCR4 expression *in vitro*, although no *in vivo* data have yet been reported for this compound (Hennrich *et al.*, 2012). Given that the radiotracer contains the same fluorobenzoyl group blamed for the nonspecific binding of other tracers, it is likely that similar difficulties would be seen. There is therefore considerable scope for further investigation of the use and development of ^{68}Ga-labelled PET probes targeting CXCR4 in cancer, as there has been only very limited research into this area thus far.

Table 3. Comparative table of recent attempts to develop CXCR4-targeting PET tracers for cancer detection *in vivo*

Radioisotope	Probe	CXCR4+ tumour uptake (%ID/g)	CXCR4+/CXCR4- tumour uptake	Tumour/ muscle	Notes	Reference
^{18}F	T140	4*	4*	21.6*	High uptake of tracer in blood and spleen. High blood retention of tracer prevented identification of CXCR4+ tumour without additional pre-administration of cold peptide.	(Jacobson *et al*., 2010)
^{64}Cu	AMD3100	33	6	47	Tracer could also be used to identify lung metastases and tumours endogenously expressing CXCR4. Highest tracer uptake in liver, spleen and kidneys.	(Nimmagadda *et al*., 2010)
^{64}Cu	T140-2D	4.1*	2*	3.8*	High tracer uptake in blood, liver, spleen, kidneys and bone marrow. High blood retention of tracer prevented visualisation of CXCR4+ tumour without pre-administration of cold peptide.	(Jacobson *et al*., 2011)
^{64}Cu	AMD3100	12.3	8	59	Highest tracer uptake seen at 6 hours. High tracer uptake in liver and kidneys. High uptake also seen in CXCR4+ lung and liver tumours.	(Weiss *et al.*, 2011)
^{64}Cu	4F-benzoyl-TN14003	4.4	9	39.3	Highest tracer uptake in liver and kidneys. Minimal blood retention.	(Jacobson *et al*., 2012)
^{64}Cu	AMD3465	102.7	17	362.5	Higher tracer uptake in tumour than in liver or kidneys. Some specific uptake evident in bone marrow.	(De Silva *et al*., 2011)
^{68}Ga	CPCR4-2	6.1	-	18.5	Higher tracer uptake in tumour than in any other tissue, however no CXCR4- tumour was used in the study.	(Gourni *et al.*, 2011)
^{68}Ga	Dimer-7	2.1	-	6.0	High tracer uptake in liver, spleen and kidneys. No CXCR4- tumour used in this study.	(Demmer *et al.*, 2011)
^{18}F	Ac-TC14012	4.8*	3	Not stated	Minimal blood retention. Low dose cold peptide increased uptake in CXCR4 tumour, but also in CXCR4 negative tumour. High tracer uptake in liver, kidneys and spleen. Low maximum uptake within CXCR4-expressing tumours.	(Zhang *et al.*, 2013)

* denotes that the maximum uptake was achieved following injection of a blocking dose of unlabelled compound.

1.8 – Considerations for the synthesis of novel CXCR4-targeting radiotracers

The literature described indicates the high potential of radiolabelled antagonists to CXCR4 as radiotracers for PET imaging, particularly where ^{18}F and ^{68}Ga-radionuclides are incorporated. However, when designing novel radiotracers, the common characteristics of successful radiotracers should be taken into account.

Chief amongst all concerns, it is vital that any novel CXCR4-targeting radiotracer should bind selectively to the target, enabling high target-to-background ratios. There are three facets to this issue: Firstly, the tracer should bind *selectively* to CXCR4, with minimal interactions to other related structures (such as other chemokine receptors). Secondly, the tracer should bind with high *affinity*, so binding can be achieved at low physiological concentrations. For consideration, other successful radiotracers targeting cell surface proteins typically bind their target protein with affinities between 10 pM-1 nM (Laruelle *et al.*, 2003), although lower affinity tracers have been shown to be acceptable for targets that are highly expressed (Dean *et al.*, 1997). Lastly, non-*specific* binding should be avoided, where uptake of the tracer occurs independently of site-specific interactions. Non-specific binding is most commonly observed in tracers and compounds bearing high lipophilicity, which encourages binding at plasma proteins (Ermondi *et al.*, 2004). As a result, highly lipophilic compounds are

generally avoided in pharmaceuticals (Leeson, 2012), and novel radiotracers assessed for specificity in the presence of an excess of a competitor, which saturates site-specific binding. These characteristics all contribute to the ability of a tracer to accumulate in tissues expressing the target protein, with low uptake elsewhere (known as a high target-to-background ratio).

However, the binding characteristics of the tracer is only part of the story, as *in vivo* processes also frequently have a significant effect upon the distribution of the tracer, such as the metabolic and excretory pathways. Metabolism refers to enzyme-catalysed reactions of the tracer that are employed physiologically (primarily by the liver) as a means to reduce toxicity of a given compound, or to increase the ability to excrete it (Meyer, 1996). Potential radiopharmaceuticals should remain relatively metabolically stable for the duration of imaging to maximise specific tracer uptake at the tissue of interest, as metabolites may gain undesirable non-specific binding characteristics that will reduce the target-to-background ratio (Pike, 2009). The excretion of a tracer is primarily performed by the kidneys and liver, through a variety of transporter mechanisms that drugs and drug metabolites are frequently substrates for (Mizuno *et al.*, 2003). It is preferable for radiotracer metabolites to be cleared quickly and for the radiotracer itself to be more slowly cleared, in order maximising radiotracer circulation to allow specific tissue uptake.

There are also considerations for the physical properties of a radiotracer, as radiopharmaceutical preparations for PET must also conform to high levels of "specific activity". This is defined as the radioactivity present per unit of mass (such as μmol or mg) of a labelled compound. This is especially important for tracers targeting cell-surface receptors such as CXCR4, as even very small concentrations of ligand can saturate receptors. The lower the specific activity, the lower the signal received from the target, which may contribute to a low target-to-background signal ratio. Thus the most successful PET radiotracers targeting cell receptors so far have therefore been those produced with the highest specific activities (Mankoff *et al.*, 2008), highlighting the importance of this characteristic in any future PET tracer development.

Central to all of the above concerns is the structure of a given radiotracer; ideally, a radiotracer would differ very little in structure to the antagonist it is derived from, so as to fulfil the conditions outlined above and therefore maximise specific tracer uptake. However, fluoride and gallium atoms do not typically reside within the CXCR4 antagonists described in chapter 1.5, and so derivatives must be designed to include functional groups that contain them. These designs may be dictated by the available radiolabelling techniques, which will influence where and how a radionuclide is to be incorporated. Furthermore, the radiolabelling protocol used to synthesise them must be rapid enough that the decay of the short-lived positron-emitting radioisotopes used in PET is kept to a minimum. There are three general methods of incorporating radionuclides

into molecules to be used as targeted radiotracers: direct labelling, indirect labelling via a linker group, or indirect labelling via chelation (Sugiura *et al.*, 2014). A number of mechanisms commonly used to covalently label compounds with the radionuclides ^{18}F and ^{68}Ga will now be described.

Direct labelling with the ^{18}F radionuclide is possible due to its highly nucleophilic nature, and so is capable of replacing leaving groups such as halide, nitro or tetramethylammonium groups upon aromatic and aliphatic groups by nucleophilic substitution reactions (Ding *et al.*, 1990, Machulla *et al.*, 2000, Becaud *et al.*, 2009). Direct labelling methods such as these frequently require harsh conditions to react which are unsuitable for precursor molecules that may react in that environment, and are also generally limited in variety. As a result, ^{18}F is more frequently introduced via prosthetic groups incorporated into the target molecule alongside the radionuclide. Methods of achieving this include fluoroamidation such as with [^{18}F]fluoroethylamine (Jelinski *et al.*, 2002), fluoroacylation such as with *N*-succinimidyl [^{18}F]fluorobenzoate ([^{18}F]SFB)(Tang *et al.*, 2008b), and fluoroalkylation such as with fluoromethyl bromide or fluoroethyl tosylate (Tsukada *et al.*, 2006). Despite the many benefits of ^{18}F-labelling with prosthetic linkers, the methods are sometimes associated with nonselectivity for the intended molecular site, time-consuming preparation of the prosthetic precursor, and instability of the prosthetic group in biological systems. [^{18}F]fluorobenzaldehyde, however, can be formed in a single step, and reacts by reductive amination with aminooxy groups to create a radiotracer

containing an [^{18}F]fluorophenyl group attached to an oxime linkage, and has been found to be highly chemoselective, and stable *in vivo* (Poethko *et al.*, 2004a, Poethko *et al*., 2004b), and is therefore widely used in ^{18}F radiolabelling. Similarly popular is the "click" reaction between alkyne-containing precursors and an ^{18}F-labelled azide, which forms a radiotracer containing a [^{18}F]1,2,3-triazole group (Glaser and Arstad, 2007); This reaction is capable of achieving high yields under mild conditions, with the labelled azide prosthetic produced efficiently in a one-step reaction.

While the methods described above are frequently used in ^{18}F radiosynthetic chemistry, the formation of radiotracers via prosthetic groups is, by definition, a multi-step reaction, which therefore takes time to produce, reducing the specific activity of the finished tracer. The use of radiometal chelation chemistry is a simple, fast single-step alternative, used for the incorporation of cationic radionuclides such as ^{68}Ga (Anderson and Welch, 1999, Burke *et al.*, 2014), although chelation of the ^{18}F radionuclide has recently been achieved in the form of $[Al^{18}F]^{2+}$ (McBride *et al.*, 2012). The most commonly used chelating agent for radiopharmaceuticals was until recently 1,4,7,10-tetraazacyclododecane-1,4,7,10-tetraacetic acid (DOTA), which complexes ^{68}Ga through hexadentate interactions with amine and carboxylate groups. However, incorporation of the ^{68}Ga radionuclide into DOTA is generally slow unless heated to temperatures that are impractical for many pharmaceutical compounds

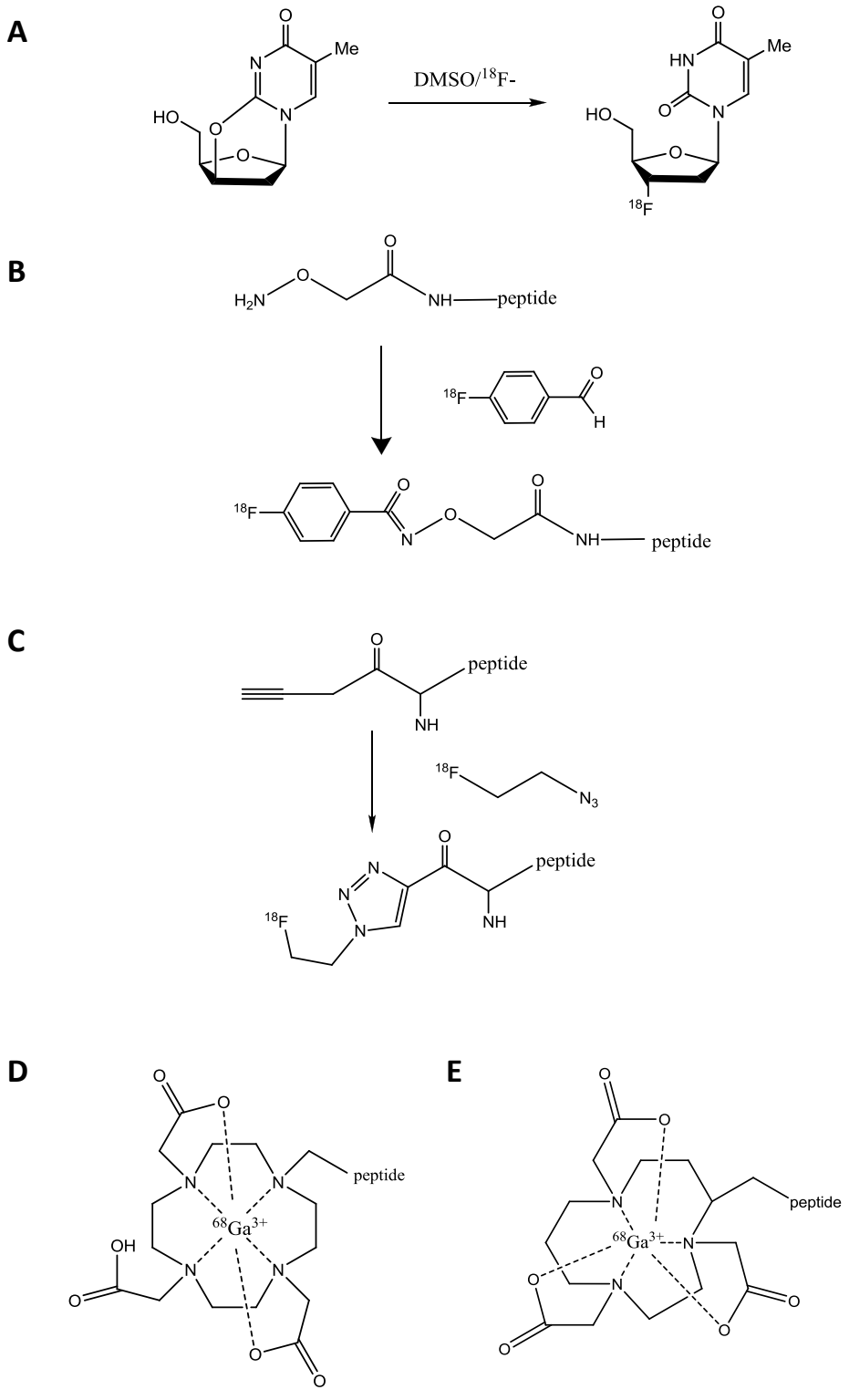

Figure 8. Summary of commonly used ^{18}F and ^{68}Ga radiolabelling methods.

A Direct labelling by nucleophilic substitution with ^{18}F- for the synthesis of [^{18}F]fluorodeoxythymidine (Machulla *et al.*, 2000). Indirect labelling via a prosthetic group by **B** benzaldehyde nucleophilic substitution or **C** "click" chemistry reactions. Indirect radiometal labelling via chelation to **D** DOTA and **E** NOTA macrocycles.

stable interactions with Ga(III) ions as a result of the small size of the triazanonane ring and the favourable steric orientation of the donor groups (Clarke and Martell, 1991). NOTA is therefore an especially favourable chelating agent for the rapid ^{68}Ga radiolabelling of PET radiopharmaceuticals sensitive to harsh conditions. Another frequently used chelating moiety is the cyclam group, which is present in some CXCR4 antagonists (including the well-characterised AMD3100) and strongly complex copper(II) ions, as well as a number of other transition metals. While most frequently complexed with the SPECT radioisotopes ^{64}Cu, ^{67}Cu and ^{99m}Tc (Engelhardt *et al.*, 2002), beta-emitting radioisotopes such as ^{94m}Tc and ^{60}Cu may also be possible (Laforest and Liu, 2008), although these are non-standard PET radionuclides, and beyond the scope of this report.

The mechanisms described above outline several radiolabelling methods that may be suitable for ^{18}F or ^{68}Ga labelling of CXCR4 antagonists, and are outlined in figure 8. This enables the comprehensive investigation of a variety of functionalised antagonists to determine which antagonist structures are most capable of retaining features appropriate for the use of PET radiotracers, such as high affinity for the CXCR4 target and *in vivo* stability.

1.9 – Potential of CXCR4-targeting tracers to noninvasively determine response to HSP90 inhibiting cancer therapeutics

An advantage of PET as an imaging modality is the ability to noninvasively determine the expression of clinically relevant biomarkers. As has been discussed in section 1.3, CXCR4 is clinically relevant to cancer in its own right, with its expression correlated with various diagnostic measures, and is therefore a target for PET imaging probes. However, PET imaging tracers targeting CXCR4 expression could also be used to detect changes in CXCR4 expression that are indirectly elicited by other triggers, such as treatments targeting a particular oncogenic pathway. One such pathway that affects CXCR4 expression is the regulation of chaperone protein heat shock protein 90 (HSP90), which plays a role in signalling protein function, protein folding and stabilisation, and protein trafficking throughout the cell. HSP90 is responsible for the stabilisation of a number of oncogenic proteins, including CXCR4 (Mandawat *et al.*, 2010), but also the cell cycle-associated protein CDK4 (Fu *et al.*, 2013), the epidermal growth factor receptor (EGFR) family of proteins (Ahsan *et al.*, 2012), as well as mutant versions of the tumour suppressor protein p53 (Li *et al.*, 2011) that are associated with cancer phenotypes.

The mechanism of HSP90 substrate stabilisation is most well-characterised in steroid hormone receptors and must be considered in tandem with HSP70, a

chaperone that interacts with HSP90 in the substrate-chaperone complex. Unchaperoned proteins may partially unfold to a conformation that exposes a binding domain that HSP70 binds to, in conjunction with HSP40 which modulates the ATPase function of HSP70 and hence its substrate binding ability (Kanelakis *et al.*, 2002). The HSP70-HSP90 organising protein (Hop) possesses binding domains for both HSP70 and HSP90 and helps to assemble the chaperone complex around the substrate (Johnson *et al.*, 1998). Upon recruitment of the cochaperone p23, the Hop-HSP70 dissociates from the complex, leaving HSP90 and the remaining cochaperones to stabilise the substrate until the complex dissociates (Morishima *et al.*, 2003). A model has been proposed whereby the stabilisation of proteins is subject to a triage decision; HSP70 is associated with the ubiquitination of the substrate while subsequent HSP90 binding prevents its ubiquitination (Chen *et al.*, 2012, Stankiewicz *et al.*, 2010). As long as HSP90 is present and can interact with the binding domain, the protein is protected from HSP70-mediated proteasomal degradation (Pratt *et al.*, 2010). A simplified mechanism of HSP90 stabilisation of proteins is summarised in figure 9.

Given HSP90's role as the 'cancer chaperone', it is unsurprising that its inhibition has been investigated as a therapeutic target. As such, a number of inhibitors have been developed (Neckers and Workman, 2012), which have chiefly been based upon the natural products radicicol and geldanamycin (see figure 9). These inhibitors exert their action *via* blockade of the nucleotide-binding pocket

of HSP90, preventing binding and subsequent hydrolysis of adenosine triphosphate (ATP) and so inactivating the chaperone (Roe *et al.*, 1999). Substrate-binding by HSP90 is dependent upon its ATPase activity although the mechanism is so far not completely understood; when HSP90 is not bound to ATP, the dimeric chaperone possesses high affinity for the substrate and promotes binding. The binding and subsequent hydrolysis of ATP promotes the dissociation of the chaperone-substrate complex, enhanced by the presence of the cochaperone p23, releasing newly reduced adenosine diphosphate (ADP) and inorganic phosphate (P_i) (Young and Hartl, 2000). This ATP-dependent substrate release mechanism may allow rapid cycling, enabling HSP90 to stabilise a greater number of proteins, as even transient HSP90-binding is sufficient to prevent proteasomal degradation (Peng *et al.*, 2009). As such, the inhibition of HSP90 results in the proteasomal degradation of numerous proteins normally stabilised by HSP90 through HSP70-dependent ubiquitination.

While radicicol showed promise as a cancer therapeutic *in vitro* (Schulte *et al.*, 1998), the compound was found to be inactive *in vivo* (Yang *et al.*, 2004), and the toxicity profile of geldamycin was found to be unacceptable (Supko *et al.*, 1995). Development of HSP90 inhibitors has therefore primarily focused upon the development of more suitable derivatives such as the geldanamycin family of inhibitors, which include the drug candidates 17AAG and 17DMAG (see figure 10) that show reduced toxicity compared to geldanamycin. The relative hepatotoxicities of geladanamycin and its derivatives has been linked to their

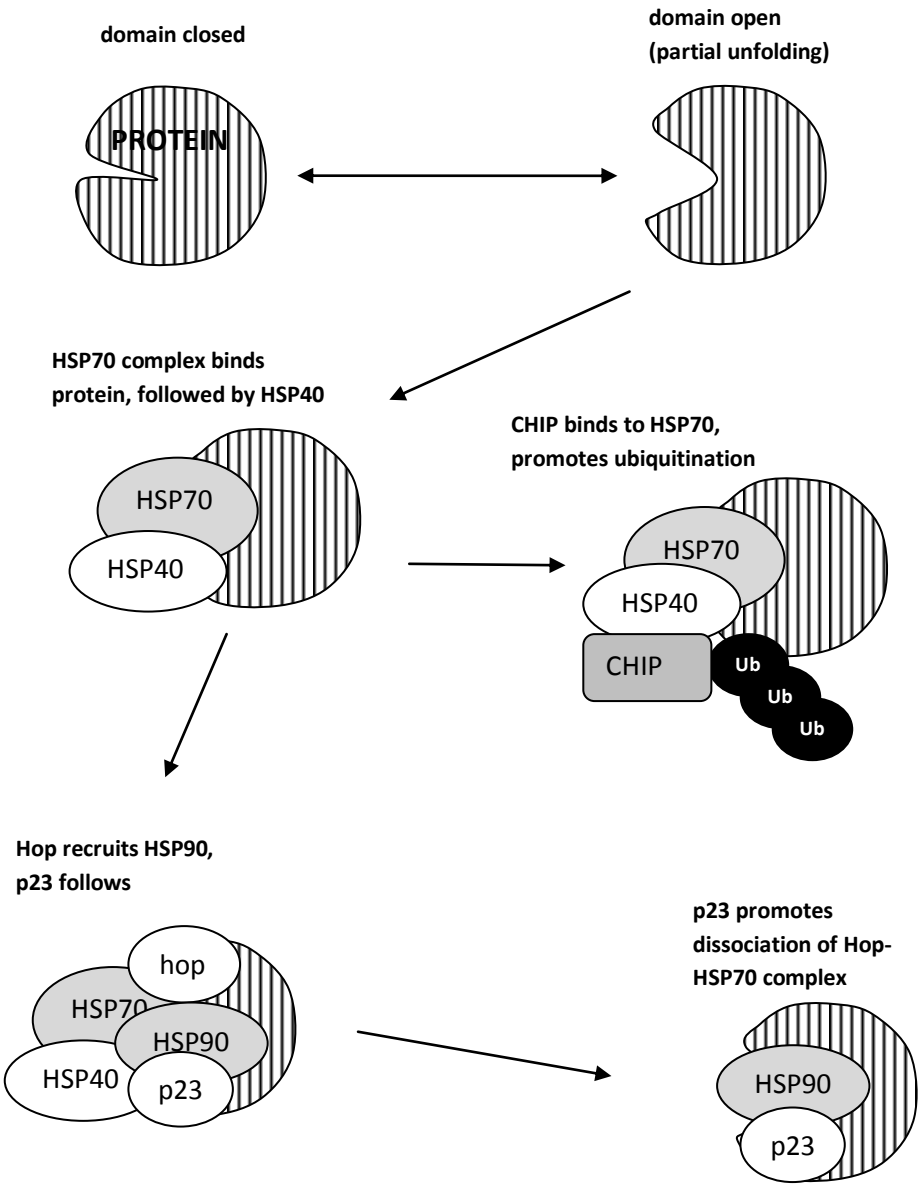

Figure 9. Diagram of mechanism of protein stabilisation by HSP90

Partial unfolding of client proteins results in binding by HSP70 complex. Subsequent binding of CHIP promotes ubiquitination, whereas binding by Hop allows recruitment of HSP90, and thus stabilisation of the protein. Heat shock protein 70 (HSP70); Heat shock protein 40 (HSP40); C-terminus of HSP70-interacting protein (CHIP); Ubiquitin (Ub); HSP90-HSP70 organising protein (Hop); Heat shock protein 90 (HSP90); Proteolytically resistant 23 kDa (p23). Adapted from (Pratt *et al*., 2010).

redox properties and reactivity with thiols; both 17AAG and 17DMAG showed more favourable properties in this regard (Samuni and Goldstein, 2012, Guo *et*

al., 2008). 17AAG has been particularly effective in combination with Trastuzumab in clinical trials in breast cancer patients expressing human epidermal growth factor receptor 2 (HER2), a sensitive HSP90 client protein (Modi *et al.*, 2007, Modi *et al.*, 2011), highlighting the promise of HSP90 inhibitors as therapy options.

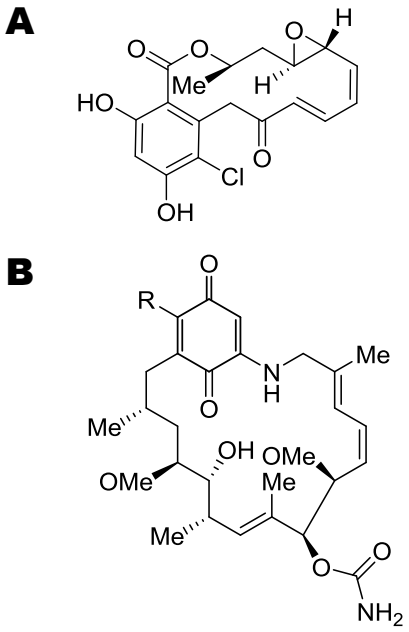

Figure 10. Structures of HSP90 inhibitors

A Radicicol B Geldanamycin-derived structures.

The degradation of many HSP90 substrate proteins following HSP90 inhibition offers an opportunity for therapy monitoring and as such many client proteins and downstream targets have been researched as biomarkers of response to treatment, such as HSP70 (Dakappagari *et al.*, 2010), AKT (Yamazaki *et al.*, 2011) and HER2 (Smith-Jones *et al.*, 2006). Molecular imaging techniques are ideally suited to development as noninvasive means of assessing biomarker expression and patient response to therapy. As CXCR4 has been shown to be degraded in

response to HSP90 inhibition (Mandawat *et al*., 2010), it may also be possible to use novel radiotracers targeting CXCR4 as tools of response to therapy. The possibilities of similar methods have been explored in a number of studies, summarised in table 4. However, of the PET imaging studies described, many target their biomarker using large macromolecular antibodies (Niu *et al.*, 2009, Nagengast *et al.*, 2010, Oude Munnink *et al.*, 2012), which are prone to suffer from issues with poor penetrance in tumours as a result of their large size, resulting in lengthy intervals between tracer injection and imaging. Alternatively, the tracers may be non-specific (Li *et al.*, 2012) or else use undesirable PET radionuclides. Thus the PET tracers currently in development to detect biomarkers of HSP90 inhibition leave a lot to be desired, creating an opportunity for smaller ^{18}F and ^{68}Ga-labelled PET tracers targeted to an alternative biomarker of HSP90 inhibition, CXCR4.

Table 4. Comparative table documenting recent attempts to image changes in HSP90 activation with positron emission tomography.

HSP90 target	Inhibitor	Probe	Notes	Reference
HER2	17AAG	[^{68}Ga]-DOTA-F(ab')$_2$-trastuzumab	Response detected after 24 hours. More sensitive than [^{18}F]fluorodeoxyglucose (FDG).	(Smith-Jones *et al*., 2006)
EGFR	17AAG	[^{64}Cu]-DOTA-cetuximab	Response detected after 24 hours. High accumulation of tracer in blood and liver.	(Niu *et al.*, 2008)
HER2	17DMAG	[^{64}Cu]-DOTA-trastuzumab	Response detected after 24 hours. More sensitive than [^{18}F]FDG. High accumulation of tracer in blood.	(Niu *et al*., 2009)
VEGF	NVP-AUY922	[^{89}Zr]-Bevacizumab	Response detected after 2 weeks. High accumulation of tracer in blood and liver. Images obtained 144 hours after tracer injection.	(Nagengast *et al*., 2010)
HER2	17AAG	[^{89}Zr]-Trastuzumab-F(ab')$_2$	Response detected after 24 hours. High accumulation of tracer in kidneys. Images obtained 6 hours after tracer injection.	(Oude Munnink *et al*., 2012)
ALK	NVP-AUY922	[^{18}F]-3'-fluoro-3'-deoxy-L-thymidine(FLT)	Reponse detected after 5 days. More sensitive than [^{18}F]FDG. Not truly targeted to ALK expression.	(Li *et al.,* 2012)

1.10 – Rationale for Project

The aim for this project was to develop cellular models appropriate for the study of CXCR4 to subsequently enable validation of the test compounds. It was planned to assess the potential of a range of novel compounds from within 4 classes of currently described CXCR4 antagonists - the T140-related oligopeptides, FC131-derived pentapeptides, It1t-related isothioureas and AM3100-related cyclam compounds. The analogues were designed to allow incorporation of chemical groups amenable to radiolabelling and with the following desirable characteristics:

- Potent antagonism of CXCR4 receptor binding and CXCR4-dependent cellular processes
- Preferential use of ^{68}Ga and ^{18}F radionuclides
- Rapid radiolabelling procedures to maximise the potential of short-lived radioisotopes

In order to establish the potential of the newly synthesised compounds as PET imaging agents, the compounds needed to be assessed for the potency of their antagonism for CXCR4 (in terms of affinity and efficacy), to ensure that the tracer would bear specificity for the receptor. This was achieved with the following methods:

- Competitive CXCR4 radioligand binding, to determine the relative affinities of the compounds for CXCR4
- Inhibition of CXCR4-directed migration, to ascertain the effect of antagonist binding upon CXCR4-dependent biological processes

Following this initial characterisation, promising candidate compounds were selected for radiolabelling and assessed for their suitability as CXCR4-targeting PET imaging agents in the following ways:

- Uptake into CXCR4 cell lines *in vitro*, to determine the tracer's specificity for CXCR4
- *In vivo* imaging experiments, to confirm accumulation of radiotracer in CXCR4-expressing tumours, and a sufficiently high target-to-background ratio (contrast) to clearly visualise lesions against background uptake
- *In vivo* biodistribution experiments to confirm precise organ-by-organ uptake of the tracer, and to suggest likely routes of excretion.
- *In vivo* metabolite studies to determine the metabolic stability of circulating and excreted radioactivity

In order to aid the above experiments, appropriate cellular models were to be characterised, beginning with the identification of cell lines that express CXCR4

endogenously, followed by modification by transfection with CXCR4 expression vectors to create parallel sublines that differ only in their expression of CXCR4, which was verified by qRT-PCR, western blot and flow cytometry. Ideally the developed radiotracers would display the ability to accumulate in tissues according to CXCR4 expression, minimal 'noise' in background tissues such as blood or muscle, and a pharmacokinetic profile that favours the circulation of unmetabolised radiotracer for the duration of the experiment before clearance through excretory routes.

A further evaluation of CXCR4-targeting was to examine CXCR4 expression as a biomarker for response to therapy, such as the inhibition of HSP90.

- To evaluate the potential of radiolabelled probes to detect degradation of CXCR4 as a result of HSP90 inhibition by 17AAG through differential radiotracer uptake in cell lines and tumours.

1.10 - Hypotheses

- The antagonists developed will exert an inhibitory effect upon CXCR4-dependent *in vitro* biological processes, including radioligand binding and ligand-directed migration, enabling the determination of the IC_{50} values for the compounds.

- The radiolabelled antagonist tracer will accumulate in CXCR4-overexpressing cell lines at a significantly higher level than in non-expressing lines *in vitro*. Any uptake seen will be significantly reduced by preincubation with unlabelled tracer.

- The radiolabelled antagonist will accumulate in CXCR4-expressing tumours at a significantly higher level than in non-CXCR4 expressing tumours *in vivo*, which can be significantly reduced by coinjection with unlabelled tracer.

- The radiolabelled antagonist will accumulate in the tumours of 17AAG-treated mice at a significantly lower level than in the tumours of untreated mice.

Chapter Two - Materials and Methods

2.1 - Reagents

AMD3100 was purchased from Sigma-Aldrich (Missouri, USA), whereas the compounds AMD3465, TC14012 and It1t were purchased from Tocris Bioscience (R&D Systems, Minneapolis, USA).

2.2 - Cell lines and culture

The human cell lines Jurkat clone E6-1 (T cell lymphocyte), MDA-MB-231 (breast cancer), MDA-MB-435S (disputed origin – potentially breast cancer or melanoma) and HCT116 (colon carcinoma) were purchased from the American Type Culture Collection (ATCC, Virginia, USA) and maintained in Roswell Park Memorial Institute 1640 (RPMI) medium (Invitrogen, California, USA). The human non-small cell lung cancer A549 cell line was purchased from ATCC, and maintained in low glucose Dulbecco's Minimum Essential Medium (DMEM) (Invitrogen, California, USA). The stably transfected human glioblastoma cell lines U87.MG, U87.CD4 and U87.CD4.CXCR4 were gifts from Dr. Erman Mandaci at the NIH-AIDS Research and Reference Reagent Programme (Maryland, USA), and were maintained in low glucose DMEM medium. The medium for U87.CD4 was supplemented with 300 µg/ml G418 (Sigma, Missouri, USA), whilst U87.CD4.CXCR4 was cultured in medium containing 300 µg/ml G418 and 1 µg/ml puromycin (Sigma, Missouri, USA). All cell lines were cultured in the presence of 10% Foetal Bovine Serum (FBS) (Sigma-Aldrich, Missouri, USA), 2mM

L-glutamine (Invitrogen, California, USA) and 100 U/ml penicillin-streptomycin (Invitrogen, California, USA) in a humidified atmosphere of 5% CO_2 at 37 °C.

2.3 - qRT-PCR

i) RNA extraction

Cells were seeded at 60-80% confluency in 60 mm dishes (MDA-MB-231: 1×10^6 cells, MDA-MB-435S: 1×10^6 cells, HCT116: 1.4×10^6 cells, A549: 4×10^5 cells, U87.MG: 1×10^6 cells, U87.CD4: 1×10^6 cells, U87.CD4.CXCR4: 1×10^6 cells Jurkat: 3×10^6 cells) in 5 ml complete medium (as specified in section 2.2) 48 hours before RNA extraction using the QIAGEN RNeasy RNA purification kit (QIAGEN, Germany) as follows: Medium from the 60 mm dishes was aspirated and replaced with 600 µl buffer RLT, scraped, and collected in RNA-free microcentrifuge tubes. Lysates were homogenised by vortexing for 1 minute, before dilution in an equal volume of 70% ethanol. 700 µl of the solution was then loaded into an RNeasy spin column placed inside a 2 ml collection tube, and centrifuged at >10,000 g for 15 seconds. The flow-through was discarded, and the process repeated with any remaining lysate from the sample. The spin column was then washed with 700 µl buffer RW1 by centrifugation at >10,000 g for 15 seconds, and flow-through discarded. The spin column was then additionally washed by 2 centrifugation steps with 500 µl buffer RPE at >10,000 g, first for 15 seconds, then for 2 minutes. The spin column filter was then dried by centrifugation into a fresh collection tube at >16,000 g for 1 minute. The spin column was then placed into an RNAse free microcentrifuge tube and the RNA eluted with 2 × 50 µl RNAse-free water. The RNA

concentration of 2 µl of the resulting samples were analysed for concentration and quality by a Nanodrop 1000 (Thermo Scientific Fisher, Massachusetts, USA).

ii) Reverse transcription

RNA samples were transcribed to complementary deoxyribonucleic acid (cDNA) using the QuantiTect Reverse Transcription kit (QIAGEN, Germany) as follows: Genomic DNA contaminants in 1000 ng of the RNA samples were eliminated by incubation for 2 minutes at 42 °C in the presence of 1X gDNA Wipeout Buffer in a total sample volume of 20 µl. 14 µl of this RNA sample mixture was then mixed with 1 µl Quantiscript Reverse Transcriptase, 4 µl Quantiscript RT buffer and 1 µl of the supplied RT primer mix. This reaction mixture was incubated at 42 °C for 15 minutes to form the cDNA, and then incubated at 95 °C for 3 minutes to inactivate the reverse transcriptase.

iii) Polymerase chain reaction

Polymerase chain reaction (PCR) was performed with a Taqman system (Invitrogen, California, USA) as follows: 45 ng cDNA was mixed with 1X Taqman universal mastermix II, 1X Taqman assay mixture for CXCR4 or glyceraldehyde 3-phosphate dehydrogenase (GAPDH) and water to give a total volume of 20 µl. The samples were then loaded into duplicate wells of a 96-well reaction plate and loaded into a 7900HT Fast Real-Time PCR System (Applied Biosystems, California, USA), which conducted the amplification reaction (1 cycle of 95 °C for 20 seconds, followed by 40 cycles of 95 °C for 1 second followed by 60 °C for 20

seconds) and derived the cycle number threshold (C_T) value for each sample. This C_T value was averaged over the duplicate samples, and converted to a $\Delta\Delta C_T$ value of expression by two successive antilog steps, which were expressed relative to the values of a control sample (Jurkat cells), according to the following equations:

$\Delta C_T = 2^{-(\text{average Ct})}$

Relative expression = ΔC_T CXCR4/ΔC_T GAPDH

$\Delta\Delta C_T = 2^{-(\text{relative } \Delta\text{CTsample} - \text{relative } \Delta\text{CTcontrol})}$

The graphical images shown were representative of 3 independent experiments.

2.4 - Immunoblotting

i) Preparation of lysates from cell culture

Cells were cultured in 6 well plates at 60-80% confluency [MDA-MB-231: 5×10^5 cells, MDA-MB-435S: 7×10^5 cells, HCT116: 7×10^5 cells, A549: 2×10^5 cells, Jurkat: 1.5×10^6 cells, U87-derived lines: 5×10^5 cells] in 2 ml complete medium at 48 hours before lysis with 200 µl radioimmunoprecipitation assay (RIPA) buffer (Sigma-Aldrich, Missouri, USA) supplemented with 1/100 Halt™ protease and phosphatase inhibitor cocktail (Thermo Fisher Scientific, Massachusetts, USA) on ice using cell scrapers. All lysates were sonicated to homogenise, and centrifuged at 17,800 rpm for 5 minutes to remove precipitates, and protein concentration of the supernatants determined by mixing of 25 µl of lysates with 200 µl bicinchoninic acid (BCA) assay kit reagents (Thermo Fisher Scientific,

Massachusetts, USA) prepared to a 1:50 ratio mixture of reagent A to reagent B. The samples were incubated for 30 minutes at 37 °C in the dark, and then analysed using a spectrophotomer for absorbance at 560 nm. Protein concentration of the samples was calculated by comparison to a standard curve of known protein concentrations.

ii) Preparation of lysates from snap-frozen tumour samples

Tumour lysates were prepared by addition of 500 µl RIPA buffer containing 1/100 Halt™ protease and phosphatase inhibitor cocktail (Thermo Fisher Scientific, Massachusetts, USA) the frozen tumours within Precellys® CK14 lysing kit tubes (Berlin Technologies, France). These tubes were homogenised at 6500 rpm for 2×25 seconds using Precellys®24 lysis equipment (Berlin Technologies, France), and the tubes centrifuged at 17,800 rpm for 5 minutes to settle the liquid supernatant. The protein concentrations of these supernatants were determined with a BCA kit (Thermo Fisher Scientific, Massachussetts, USA) and spectrophotometer analysis as described in chapter 2.4i.

iii) Immunoblotting

120 µl of the lysate samples were mixed with 50 µl NuPage® lithium dodecyl sulphate (LDS) loading buffer and 20 µl NuPage® reducing agent (Invitrogen, California, USA) within microcentrifuge tubes and heated at 70 °C for 10 minutes to denature. Sample volumes corresponding to a fixed quantity (15-30 ug) of cell lysate mixtures were loaded into Mini-PROTEAN® TGX™ 4-15 % pre-cast gels (Bio-Rad, California, USA), and separated by gel electrophoresis at 250 V for 20

minutes in a Tris-Glycine running buffer [25 mM Tris, 192 mM glycine, 0.1% SDS]. The size-separated samples were then removed from the gel cassette and placed within a Trans-Blot® Turbo™ System loaded with a Trans-Blot® Turbo™ PVDF transfer pack (Bio-Rad, California, USA) for the transfer of the protein samples to the supplied membrane by application of a 2.5 A current for 7 minutes. Following transfer, the membranes were blocked for 30 minutes by agitation in the presence of 5% milk in tris-buffered saline with TWEEN 20 (TBST), and then incubated with primary antibodies in 5% milk-TBST overnight at 4 °C. Following three 5 minute washes in TBST, secondary antibodies were incubated for 45 minutes in 5% milk-TBST at room temperature. The membranes were washed 3 more times in TBST, and incubated with 3 ml of reagent mixture (1:1) from the Amersham enhanced chemiluminescence (ECL) Plus Western Blotting Detection Kit (GE Healthcare Life Sciences, UK). The following primary antibodies were used: rabbit anti-human CXCR4 (clone UMB2, Epitomics, California, USA) at a concentration of 1/2000, rabbit anti-human CD4 (Epitomics, California, USA) at a concentration of 1/1000, mouse anti-human CDK4 (New England Biolabs, Massachusetts, USA) at a concentration of 1/1000, mouse anti-human α-tubulin (Santa Cruz Biotechnology, California, USA) at a concentration of 1/500, rabbit anti-human β-actin (Sigma-Aldrich, Missouri, USA) at a concentration of 1/5000, and rabbit anti-human GAPDH (New England Biolabs, Massachussetts, USA) at a concentration of 1/1000. Secondary antibodies used were goat anti-mouse Immunoglobin G-horseradish peroxidise (IgG-HRP) and goat anti-rabbit IgG-HRP (Santa Cruz Biotechnology, California, USA), all at a

concentration of 1/2000. Protein expression was quantified by densitometric analysis using a GS-800 Imaging Densitometer (Bio-Rad, California, USA), with bands selected using Quantity One® software (Bio-Rad, California, USA), and the CXCR4 expression of each sample lane expressed relative to the loading control within the same lane.

2.5 - Flow cytometry

Cells were cultured in T75 flasks and detached while at 60-80% confluence with 4 ml 0.5mM ethylenediaminetetraacetic acid in Dulbecco's phosphate-buffered saline (EDTA-DPBS) buffer (Sigma-Aldrich, Missouri, USA). 1.4×10^{6} cells were washed three times in 3 ml 0.1% bovine serum albumin in phosphate-buffered saline (BSA-PBS) by centrifugation at 600 g for 3 minutes, and then resuspended at a density of 4×10^{-6} cells/ml in 1% BSA-PBS for 30 minutes to block non-specific binding. 100 μl aliquots of the cellular suspensions were incubated with 20 μl either phycoerythrin (PE)-conjugated anti-human CXCR4 monoclonal antibody (clone IgG5) or PE-conjugated mouse Ig2B isotype control antibody (R&D Systems, Minnesota, USA) for 45 minutes on ice. Unbound antibody was separated from the cells by two washes with 0.1% BSA-PBS using centrifugation at 600 g for 3 minutes. Cells were strained and placed in 5 ml flow cytometry tubes (BD Bioscience, New Jersey, USA) on ice prior to analysis by flow cytometry using the FACS Canto (BD Biosciences, New Jersey, USA). The photomultiplier voltage gains were set so that the cells stained with the isotype control antibody appeared in the first quantile of the output scatterplot [Jurkat FSC:5 SSC:400 ; MDA-MB-231 FSC:5, SSC:320 ; MDA-MB-435S FSC:5, SSC:320;

HCT116 FSC:5, SSC:330 ; A549 FSC:5, SSC:330; U87 FSC: 5, SSC:330]. Fluorescence emissions were detected by 488 nm argon laser excitation with emissions filtered to 585/42 nm. The cell populations were gated for viability using FlowJo7.6.4 software (Treestar, Oregon, USA), and CXCR4 expression described in terms of median fluorescence intensity (PE-A). Histogram representations of anti-CXCR4 PE staining for each cell line were compared against the isotype control PE staining for the positive control cell line (Jurkat cells or stable 3).

2.6 - Vector cloning

i) Cloning

Vectors used were as follows: pcDNA™3.1 empty vector control (Invitrogen, California, USA), pcDNA™3.1-CXCR4 and pcDNA3.1™-3xHA-CXCR4 (Missouri cDNA S&T Resource Center, Missouri, USA). *E. coli* transformation was achieved by incubation of 50 µl Subcloning Efficiency™ DH5α™ Competent *E. coli* with 10 ng of the appropriate vector on ice for 30 minutes, followed by heat shock for 20 seconds at 42 °C, and then incubation on ice for a further 2 minutes. The transformed cell were cultured in 950 µl super optimal broth with catabolite repression (SOC) medium (Invitrogen, California, USA) at 37 °C for 1 hour before being spread onto agar plates containing 100 µg/ml ampicillin (Sigma-Aldrich, Missouri, USA) and cultured at 37 °C overnight. Individual colonies were selected and amplified in 3 ml lysogeny broth (LB) medium (Sigma-Aldrich, Missouri, USA) containing 100 µg/ml ampicillin for 8 hours, before inoculation of a larger 100 ml culture medium for further expansion overnight. The cloned vectors were

purified using a QIAGEN plasmid midi kit (QIAGEN, Germany) as follows: The cells were collected by centrifugation at 15 minutes at 6000 g at 4 °C and resuspended in 4 ml buffer P1. Lysis was achieved by addition of 4 ml buffer P2 followed by vigorous shaking and incubation at room temperature for 5 minutes. The addition of 4 ml buffer P3 precipitated genomic DNA, proteins and debris, enabling their separation from the vector-containing supernatant by two centrifugations at 20,000 g for 30 minutes at 4 °C. This supernatant was added to a QIAGEN-tip 100 (primed with 4 ml buffer QBT) and allowed to empty by gravity. The tip was washed twice with 20 ml buffer QC, and the vector eluted with 5 ml buffer QF. Finally, the vector was precipitated by the addition of 3 ml isopropanol and collected by centrifugation at 15,000 g for 30 minutes at 4 °C. The pellet was washed in 70% ethanol, dried, and re-dissolved in 250-500 µl Tris-EDTA buffer [10 mM Tris, 1 mM EDTA, pH 8.0] and stored at -20 °C until required.

ii) Analysis

DNA concentration and quality of the vector samples were determined by analysis of 2 µl samples with the Nanodrop 1000 (Thermo Scientific Fisher, Massachusetts, USA) at 260, 280 and 230 nm wavelengths, with samples bearing 260/280 nm below 1.8, and 260/230 nm values below 2.0 discarded. Presence of the transgene-coding insert region within the plasmid samples was confirmed by analysis of sample aliquots following restriction digest. In the digestion reaction 2ng of DNA samples were incubated with 2 µg acetylated BSA (Promega, Wisconsin, USA), 2 µl 10X restriction enzyme buffer D (Promega, Wisconsin,

USA), and 0.5 μl of the appropriate restriction enzyme [12 u/μl EcoRI and 10 u/μl XhoI for the pcDNA3.1™-CXCR4 vector, 10 u/μl HindIII and 10 u/μl XhoI for the pcDNA3.1™-3xHA-CXCR4 vector (all enzymes obtained from Promega, Wisconsin, USA)] were incubated at 37 °C for 4 hours. 15 μl of the digested samples were then loaded directly into an 0.8% eGel (Invitrogen, California, USA) system, separated by gel electrophoresis for 10 minutes with the eGel iBase power system (Invitrogen, California, USA), and then visualised using a UV transilluminator.

2.7 - Transfections and maintenance of cloned cell lines

4×10^5 HCT116 cells were seeded per well of a 6 well plates in 2 ml antibiotic-free RPMI medium 24 hour prior to transfection. The following day, 2.5 μg of sample vector was mixed with 150 μl opti-MEM medium (GIBCO, California, USA) and 2.5 μl Lipofectamine Plus reagent (Invitrogen, California, USA) added. This mixture is added to 9 μl of Lipofectamine LTX reagent (Invitrogen, California, USA) diluted in 150 μl opti-MEM medium, and incubated at room temperature for 5 minutes, before being added dropwise to cells cultured in 1.5 ml opti-MEM medium. At 48 hours post-transfection the cells were detached with 1 ml 0.05% trypsin-EDTA (Invitrogen, California, USA) and passaged at 1:10 dilution in 100 mm dishes in complete medium supplemented with 1000 μg/ml G418 (Sigma-Aldrich, Missouri, USA). Once colonies had formed (7-10 days later), geographically isolated colonies were selected by local detachment with 50 μl 0.05% trypsin-EDTA (Invitrogen, California, USA) in cloning cylinders (Millipore,

Massachusetts, USA), and remaining clones pooled together by detachment with 3 ml 0.05% trypsin-EDTA. All clonal populations were maintained in medium supplemented with 1000 µg/ml G418 for 3-4 weeks before a reduction in G418 concentration to 500 µg/ml thereafter.

2.8 - Doubling time assay

U87.MG, U87.CD4 and U87.CD4.CXCR4 cells were detached and counted by Cell Scepter 2.0 Automated Cell Counter with 60 µm Scepter Sensors (Millipore, Massachusetts, USA), then seeded into triplicate wells of five 6-well plates at a density of 1×10^4 cells per well in 2 ml complete DMEM medium. After each 48 hour time-point, one triplicate wells of each cell line was aspirated with 1 ml 0.05% trypsin-EDTA (Invitrogen, California, USA), diluted in 4 ml complete DMEM medium and the cells in sample counted by haemacytometer. Medium within the wells was replenished with complete medium every 48 hours. The cell counts for each cell line over the 10-day period was used to calculate doubling time according to the following exponential growth calculation:

$$\text{Cell number at time t} = \text{cell number at time 0} \times e^{(\text{doubling time} \times \text{time})}$$

2.9 - Scratch wound assay

U87.CD4 and U87.CD4.CXCR4 cells were detached and seeded at a density of 2×10^5/well in 12 well plates 24 hours before commencement of the experiment in 1 ml complete DMEM medium. At the beginning of the experiment the medium was removed from the wells to allow thin tracks of cells to be scraped

away with a p10 pipette tip (forming a scratch wound) and then washed with 500 μl PBS to remove debris. The well plates were then incubated with 1 ml serum-free DMEM media containing either no additives, 400 ng/ml SDF1, or both 400 ng/ml SDF1 and 20 μM AMD3100. An Axiovert 100 (Zeiss, New York, USA) time-lapse microscope was used to photograph scratch wounds at fields of view for three separate scratches at two time points, 12 hours apart. The cells were incubated at 37 °C in the presence of 5% CO_2 for the duration of the time-lapse experiment. The sizes of the scratches photographed at t=0 and t=12 for each sample were quantified using ImageJ software (NIH, Maryland, USA) by outlining the scratch wound by hand, and expressing the scratch area in terms of pixel quantity. Closure of the scratch wound was calculated according to the following equation below.

$$\textbf{\% change} = \textbf{(}(\text{area}_{\text{scratch t0}} - \text{area}_{\text{scratch t12}})/\text{area}_{\text{field of view}} \textbf{)} \times 100$$

2.10 – Synthetic chemistry and radiosynthesis

i) CCIC7/[^{18}F]CCIC7

CCIC7 was synthesised at Imperial College London by Dr. Ola Åberg (illustrated in figure 12) using a purchased aminoxyfunctionalised precursor, Cyclo-[D-Tyr-Arg(PEG_2-O-NH2)-Arg-2-Nal-Gly] (Cambridge Research Biochemicals, UK). This precursor was reacted with 4-fluorobenzaldehyde dissolved in methanol and 10 mM ammonium formate (pH 2.5) to give CCIC7 at a 74% yield, and a distribution coefficient at pH 7.4 ($\log D_{\text{pH 7.}}4$) of 1.09. The compound was formulated at a concentration of 10 mM in 100% DMSO and frozen at -20°C in

aliquots. [^{18}F]CCIC7 was radiosynthesised at Imperial College London by Dr. Ola Åberg by the reaction of [^{18}F]fluorobenzaldehyde in methanol with a freshly prepared suspension of the aminooxy functionalised peptide precursor, cyclo-[D-Tyr-Arg(PEG$_2$-O-NH2)-Arg-2-Nal-Gly], in 100 mM ammonium formate buffer (pH 2.0), before venting and dilution in ammonium formate buffer (pH 3.5). The high performance liquid chromatography (HPLC) purified fraction was immobilised upon a Waters SepPak tC18 cartridge (Waters, Massachusetts, USA) before elution with 5 mM hydrochloric acid in ethanol. The resultant [^{18}F]-CCIC7 possessed a mean specific activity of 31 GBq/µmol, a radiochemical yield of 22%, and a radiochemical purity of >99%.

ii) CCIC16

CCIC16 (illustrated in figure 26) was custom-synthesised by Peptide Protein Research Ltd (Fareham, UK), whereas Ga^{3+}, $[AlF]^{2+}$, In^{3+} and Cu^{3+} cation chelates were synthesised at Imperial College London by Guillaume George. The chelates Ga-CCIC16, AlF-CCIC16, In-CCIC16 and Cu-CCIC16 were synthesised according to a general protocol as follows: A solution comprising CCIC16 in buffer [0.1M sodium acetate pH 4.0 for Ga^{3+} and $[AlF]^{2+}$ chelates, 65 mM ammonium acetate pH 6.0 for In^{3+} and Cu^{3+} chelates] was reacted with a solution of the metal salt [$GaCl_3$, $AlCl_3$, $InCl_3$ and $CuCl_2.H_2O$] before purification by semi-preparative HPLC using a Luna C18(2) column (Phenomenex, California, USA) and elution in ethanol-PBS (7:3). The compound was then freeze-dried to derive the solid compound with a measured $\log D_{pH\ 7.4}$ of -3.58. [^{68}Ga]-CCIC16 was radiosynthesised at Imperial College London by Guillaume George using the

custom-synthesised CCIC16 (Peptide Protein Research Ltd, UK) as the peptide precursor. [^{68}Ga]GaCl^{3} was directly eluted from an Eckert & Ziegler Isotope Products IGG100-10M Gallium-68 Generator (Eckert & Ziegler Strahlen-Medizintechnik, Germany) into a solution of CCIC16 in 0.5 M acetate buffer (pH 5.8) and allowed to react for 5 minutes at 90 °C. The reaction mixture was purified by HPLC with a Light C18 cartridge (Waters, UK) and the tracer eluted in ethanol-PBS (7:3). [^{68}Ga]-CCIC16 showed a radiochemical yield of 90%, a radiochemical purity of 98%, and a specific activity of 2.76 GBq/µmol.

iii) Cyclopentapeptide synthesis/[^{18}F]CCIC15/[^{18}F]CCIC30

CCIC15, CCIC29, CCIC30 and CCIC36 were synthesised at Imperial College London by Guillaume George (illustrated in table 10). The general procedure for the synthesis of these compounds involved reaction between protected amino acids, N,N-diisopropylethylamine, hydroxybenzotriazole, HBTU peptide-coupling reagent, and H-Glycine-chlorotrityl resin in a solution of dimethylformamide to form a resin-bound pentapeptide. The resin was later cleaved by treatment with 1:1:3 mixture of acetic acid, trifluoroethylene and dichloromethane to form a linear pentapeptide. Cyclisation was achieved by treatment with sodium carbonate in dimethylformamide and 2,2-diphenylphosphoroazide, followed by filtration of the suspended products in methanol-chloroform. The peptide product was precipitated with ethanol and then dissolved in a 190:5:5 mixture of trifluoroacetic acid (TFA), triisopropylsilene and water to give a TFA salt of the cyclised pentapeptide precursor. Finally, the alkyne groups of the cyclopentapeptide precursors underwent click chemistry reactions in copper

sulphate, sodium ascorbate, 2-fluroethylazide and sodium acetate buffer. The triazole-containing cyclopentapeptide final products were produced in quantitative yields of 89-99%. The measured log$D_{pH\ 7.4}$ for CCIC15 and CCIC30 was -0.11 and -2.30, respectively. Radiosynthesis of [^{18}F]CCIC15 and [^{18}F]CCIC30 perfomed by Dr. Federica Pisaneschi at Imperial College London by successive addition of 238 mM CuSO4 in water, 262 mM sodium ascorbate in 250 mM acetate buffer (pH 5), 298 mM bathophenanthrolinedisulfonic acid disodium salt in water, 2-[^{18}F]fluoroethylazide in acetonitrile, and 15 mM of the alkyne-containing cyclopeptide precursor [cyclo(D-Tyr-Prg-Arg-2-Nal-Gly) for [^{18}F]CCIC15 and cyclo(D-Prg-Gly-Arg-2-Nal-Gly) for [^{18}F]CCIC30] in dimethylformamide. The reaction was continued in the presence of benzylazide in methanol, and the reaction product purified by reverse phase semi-preparative HPLC using a Luna $C18_2$ column (Phenomenex, California, USA). [^{18}F]CCIC15 was eluted in 25 mM HCl in ethanol, and showed a decay-corrected radiochemical yield of 63%, a radiochemical purity of >98%, and a mean specific activity of 19.4 GBq/µmol. [^{18}F]CCIC30 was eluted in 25 mM HCl in ethanol, and showed a decay-corrected radiochemical yield of 55%, a radiochemical purity of >98%, and a mean specific activity of 6.7 GBq/µmol.

iv) GG343, CCIC8, GG345, CCIC27, GG337 and GG338

GG343, CCIC8, GG345, GG337 and GG338 were synthesised at Imperial College London by Guillaume George (illustrated in table 14) according to a common procedure, by the reaction of 0.5 mmol 3-(chloromethyl)-6,6-dimethyl-5H,6H-imidazo[2,1-b][1,3]thiazol with 0.5 mmol thiourea precursor [3-cyclohexyl-1-(2-

fluorophenyl)thiourea for GG343, 3-cyclohexyl-1-(1-fluorophenyl)thiourea for CCIC8, 3-cyclohexyl-1-(4-fluorophenyl)thiourea for GG345, 1-cyclohexyl-3-{1-[4-fluorophenyl)methyl]piperidin-4-yl}thiourea for CCIC27, 3-cyclohexyl-1-{1-[2[fluoroethyl)-1H-1,2,3-triazol-4-yl]cyclohexyl}thiourea for GG337, 1-cyclohexyl-2-{2-[1-(2-fluoroethyl)-1H-1,2,3-triazol-4-yl]propan-2-yl}thiourea for GG338] in anhydrous acetonitrile and ethanol. The reaction mixture for the synthesis of CCIC27 was further treated by purification by flash column chromatography, and the acidification of the product with 2 N hyrdrochloric acid in diethyl ether, and centrifugation to give the finished CCIC27 product. All compounds were also purified by preparative HPLC.

v) GG366

GG366 was synthesised at Imperial College London by Guillaume George (illustrated in table 14) by reaction of 0.05 mmol of the isothioureapiperidine precursor [N'-cyclohexyl-N-(piperidine-4-yl)[({6,6-dimethyl-5H,6H-imidazo[2,1-b][1,3]thiozol-3-yl}methyl]methanimidamide] in anhydrous acetonitrile with 0.255 mmol potassium carbonate. 0.05 mmol fluoroethyltosylate was added to the reaction mixture to produce GG366 in an alkylation reaction before quenching with 2 N aqueous hydrochloric acid and purification by preparative HPLC.

vi) GG248

GG366 was synthesised at Imperial College London by Guillaume George (illustrated in table 14) by reaction of a 1:5 solution of the alkyne precursor N-

[(cyclohexylimino)[({6,6-dimethyl-5H,6H-imidazo[2,1-b][1,3]thiazol-3-yl}methylsulfanyl]methyl]-2-[2[(prop-2-yn-1-yloxy)ethoxy]ethan-1mine in dimethylfluoride, with 250 mM sodium acetate buffer (pH 5), 0.038 mmol copper sulphate and 0.95 mM sodium ascorbate. The reaction product was purified using flash column chromatography and preparative HPLC.

vii) DB011

DB011 was synthesised by Dr. Diana Brickute (DB011, illustrated in figure 43) in a multi-step process. The cyclam was coupled with ethyl trifluoroacetate to yield a protected cyclam [4,8,11-tris(trifluoroacetyl)-1,4,8,11-tetra-azacyclotetradecane], which was alkylated by α,α'-dibromo-p-xylene in the presence of potassium carbonate and acetonitrile to form a protected bromoxylene cyclam, enabling a further reaction in acetonitrile to substitute the halide group for ethylenediamine. A reductive amination reaction of the reaction products with fluorobenzaldehyde in the presence of sodium triacetoxyborohydride provided 4, followed by deprotection of the cyclam group with 5 M sodium hydroxide in methanol. The reaction product was then converted into a hydrochloride salt with hydrochloric acid in the presence of ether, giving rise to DB011, which was then purified using preparative HPLC.

2.11 - ^{125}I-SDF1α radioligand binding assays

i) Method A

The experiment was conducted using siliconised 1.5 ml microcentrifuge tubes (Sigma, Missouri, USA) to prevent non-specific binding of radioactivity. A 100 µl suspension of 2×10^5 Jurkat cells assay buffer [PBS containing 50 mM 4-(2-hydroxyethyl)-1-piperazineethanesulfonic acid (HEPES), 1 mM $CaCl_2$, 5 mM $MgCl_2$, 0.3 mM NaN_3, 0.5% BSA; pH 7.4] was placed in the tube, followed by 50 µl of the indicated antagonist to give a variable final concentration [may include 0 nM, 1 mM, 200 µM, 100 µM, 10 µM, 1 µM, 100 nM, 10 nM, 1 nM, 100 pM, and 10 pM], along with 50 µl of ^{125}I-SDF1α radioligand (PerkinElmer, Massachusetts, USA) to give a final concentration of 0.1 nM. The tubes were then incubated at room temperature for 90 minutes. Following incubation, the bound and unbound radioactivity within the sample was separated by filtration using a 96-well MultiScreen HTS GV filter plate system (Millipore, Massachusetts, USA) with a vacuum manifold, followed by 3 washes of 200 µl assay buffer. The filters were then punched out and counted in an NE1600 gamma counter (Thorn-EMI/Nuclear Enterprises, UK) for 240 s. The bound radioactivity was expressed as a percentage of the IC_{max} using GraphPad Prism 5 (GraphPad Software, CA, USA).

ii) Method B

2.5×10^6 U87.CD4.CXCR4 cells were detached with 0.05% Trypsin-EDTA (Invitrogen, California, USA) and incubated at 37 °C in 5 ml complete DMEM

medium for 2 hours to recover from trypsinisation, then resuspended in binding buffer [PBS containing 2 mg/ml BSA] at a concentration of 1.5×10^6/ml. To each 1.5 ml siliconised microcentrifuge tube (Sigma-Aldrich, Missouri, USA), 1.5×10^5 cells were added in 50 μl binding buffer, followed by 25 μl of the indicated antagonist in binding buffer [variable concentration; may include final concentrations of 0 nM, 1 mM, 500 μM, 200 μM, 100 μM, 50 μM, 10 μM, 1 μM, 100 nM, 10 nM, 1 nM, 100 pM, and 10 pM], and 25 μl ^{125}I-SDF1α radioligand (PerkinElmer, Massachusetts, USA) in binding buffer to give a final concentration of 0.1 nM. The tubes were then incubated on ice for 90 minutes under agitation. Following incubation the bound and unbound radioactivity within the samples were separated by filtration using a 96-well MultiScreen HTS GV filter plate system (Millipore, Massachusetts, USA) with a vacuum manifold, followed by 3 200 μl washes in assay buffer. The filters were then punched out and counted in an NE1600 gamma counter (Thorn-EMI/Nuclear Enterprises, UK) for 240 s. The bound radioactivity was expressed as a percentage of the IC_{max} using GraphPad Prism 5 (GraphPad Software, CA, USA).

2.12 - Migration assays

4×10^6 Jurkat cells were serum-starved in 1% FBS-RPMI media for 24 hours prior to the commencement of the experiment. The transwell plates contained 2 chambers separated by a polycarbonate membrane of 8 μm pore diameter (BD Biosciences, New Jersey, USA). The lower chamber was filled with 1 ml medium (1% FBS) containing either no additives or 100 ng/ml SDF1 (R&D Systems,

Minneapolis, USA). The upper chambers were filled with a 300 μl suspension of 1×10^5 Jurkat cells, which had either been untreated or pre-treated with the indicated concentration of antagonist for 30 minutes (suspended in 1% FBS medium). The plates were then incubated for 3 hours in a humidified atmosphere at 37 °C and 5% CO_2. Following incubation the upper wells and their contents were discarded, and the medium from the lower wells collected, the numbers of cells in each well counted, and expressed as a percentage of the number of cells seeded into each well. All conditions were repeated in triplicate.

2.13 - In vitro uptake assay

Cells were seeded in triplicate wells of 6 well plates to be 60-80% confluent at 24 hours [HCT116: 7×10^5 cells per well, A549: 2×10^5 cells per well, U87.CD4: 5×10^5 cells per well, U87.CD4.CXCR4: 5×10^5 cells per well]. On the day of the experiment, the wells were treated with 1 ml of either the indicated concentration of competitive inhibitor-containing complete media [variable; included 10 μM AMD3100, 10 μM Ga-CCIC16, or 20 μM FC131] or inhibitor-naive media, and incubated for 15 minutes at 37 °C 5% CO_2. The wells were then incubated with the indicated radiotracer [variable; included 0.37 MBq [^{18}F]CCIC7, 0.74 MBq ^{68}Ga-CCIC16, 0.37 MBq [^{18}F]CCIC15, or 0.37 MBq [^{18}F]CCIC30] in 1 ml complete medium for a further 60 minutes. Following incubation the medium was aspirated on ice and washed two times with 1 ml ice-cold PBS. The cells were scraped in 1 ml PBS and collected in microcentrifuge tubes and centrifuged at 5000 rpm for 5 minutes. The supernatant was removed and replaced with 350 μl RIPA buffer (Thermo Fisher Scientific, Massachusetts,

USA) and the lysates transferred to counting tubes. Bound radioactivity was immediately counted using an LKB Wallac 1282 Compugamma laboratory gamma counter (PerkinElmer, Massachusetts, USA). The protein concentration of the lysates was determined by BCA assay (Thermo Fisher Scientific, Massachusetts, USA) as previously described. The radioactivity counts per minute (CPM) of each sample was divided by the total quantity of protein in the sample (in μg) in order to calculate the CPM normalised to the protein concentration of the sample (CPM/μg protein).

2.14 - Xenotransplantation

All animal work was carried out in accordance with the United Kingdom's *Guidance on the Operation of Animals (Scientific Procedures) Act 1986* and within guidelines set out by the United Kingdom National Cancer Research Institute Committee on Welfare of Animals in Cancer Research (Workman *et al.*, 2010). Female BALB/c nu/nu athymic nude mice aged between 6-8 weeks were obtained from Charles River (Massachusetts, USA). Anaesthesia was induced in the animals at 3-4% isoflurane in a 1:4 mixture of nitrogen and oxygen at a flow rate of 1 L/minute, and then reduced to 2% isoflurane for anaesthesia maintenance. Xenotransplants were performed by injection of a 100 μl suspension of 4.5 x 10^6 cells [HCT116, A549, U87.CD4 or U87.CD4.CXCR4 cells] in PBS subcutaneously to the nape of the neck using a 25 mm 25 gauge needle. Animals were allowed to recover from anaesthesia for 5-10 minutes at 37 °C before being returned to their cages. Tumour size was measured every 2-3 days

using callipers, and tumour volume calculated according to the equation π*length*width*depth/6 (to give volume in mm^3) in order to determine when further *in vivo* experiments would commence.

2.15 - In vivo imaging and biodistribution

Imaging and biodistribution experiments began once the tumours had reached at least 80 mm^3 (2-4 weeks post-transplant, depending on the cellular model).

i) *In vivo* imaging experiments with Inveon CT/PET scanner

Anaesthesia was induced in the animals at 3-4% isoflurane in a 1:4 mixture of nitrogen and oxygen at a flow rate of 1 L/minute, and then reduced to 2% isoflurane for anaesthesia maintenance during imaging. A cannula was inserted into the lateral tail vein of the animal and fixed in position with tape. The animals were then placed in a thermostatically controlled rig at 37 °C in a dedicated small animal CT/PET scanner (Siemens Multimodality Inveon, Siemens Molecular Imaging Inc., Knoxville, USA). A low-dose CT orientation scan was performed (80 kVp, 0.5 mA, 220° rotation, 600 ms per degree exposure time, 80 µm reconstruction pixel size) to use as an anatomical reference and as a reference for attenuation correction of PET data. 3.7 MBq of the indicated radiotracer [[^{18}F]CCIC7, or ^{68}Ga-CCIC16] in 100 µl 100 units/ml heparin-PBS was injected via the lateral tail vein at commencement of a dynamic PET scan, which was acquired over 60 minutes in a list-mode format to give decay-corrected values of radioactivity accumulation in tissues. The collected data were then

ordered into 0.5 mm sonogram bins and 19 time frames (4 × 15, 4 × 60, 11 × 300 seconds) and reconstructed by filtered back-projection (FBP), ordered subset in 2 dimensions (OSEM2D), and ordered subset in 3 dimensions with maximum *a posteriori* (OSEM3D-MAP ; 2 OSEM 3D iterations and 18 MAP iterations) algorithms. The OSEM3D-MAP reconstruction was used for the visual representation of PET images only, whereas the OSEM2D-FBP was used to derive dynamic data from the regions of interest (ROIs). These ROIs (tumour, thigh muscle) were selected using Siemens Inveon Research Workplace software (Siemens Molecular Imaging Inc., Knoxville, USA) by hand, and the count densities (counts/ml) of these ROIs were averaged for each of the 19 time points to obtain time against radiactivity concentration curves (TACs) for each ROI. The radioactive counts for each tissue at any given time-point was divided by the total injected dose to the animal in order to obtain the standardised uptake value (SUV), expressed as %ID/ml. At the end of the experiment the animals were sacrificed and tissues collected under terminal anaesthesia as described in section 2.15iii. Certain subsets of mice were treated with competing nonradioactive compound to block CXCR4 receptors as follows: For *in vivo* [^{18}F]CCIC7 studies, CXCR4 receptors in mice were blockaded by administration of a single 5 mg/kg AMD3100 dose in 50 μl 100 units/ml heparin-PBS via the lateral tail vein at 30 minutes prior to [^{18}F]CCIC7 injection via the same route. For *in vivo* [^{68}Ga]-CCIC16 studies, CXCR4 blockade was induced by coinjection of 50 μg Ga-CCIC16 together with the competing [^{68}Ga]-CCIC16 in 100 μl 100 units/ml heparin-PBS via the lateral tail vein at commencement of the scan.

ii) *In vivo* imaging experiments with Genisys^4 PET scanner

Anaesthesia was induced in the animals at 3-4% isoflurane in a 1:4 mixture of nitrogen and oxygen at a flow rate of 1 L/minute, and then reduced to 2% isoflurane for anaesthesia maintenance during imaging. A cannula was inserted into the lateral tail vein of the animal and fixed in position with tape. Animals were then placed in a thermostatically controlled rig at 37 °C in a dedicated small animal Genisys^4 PET scanner (SOFIEBIOSCIENCES, CA, USA). 1.1 MBq of the [^{18}F]CCIC30 in 100 μl 100 units/ml heparin-PBS was injected via the lateral tail vein at commencement of the dynamic PET scan, acquired over 60 minutes in a list-mode format to give decay-corrected values of radioactivity accumulation in tissues. The collected data were then ordered into 0.5 mm sonogram bins and 19 time frames (4 × 15, 4 × 60, 11 × 300 seconds) and reconstructed according to ordered subset in 3 dimensions with maximum *a posteriori* (OSEM3D-MAP ; 2 OSEM 3D iterations and 8 MAP iterations) algorithms. The ROIs (tumour, thigh muscle) were selecteded using Siemens Inveon Research Workplace software (Siemens Molecular Imaging Inc., Knoxville, USA) by hand, and the count densities (counts/ml) of these ROIs averaged for each of the 19 time points to obtain time against time-activity curves (TACs) for each ROI. The radioactive counts for each tissue at any given time-point was divided by the total injected dose to the animal in order to obtain the standardised uptake value (SUV), expressed as %ID/ml. At the end of the experiment the animals were sacrificed and tissues collected under terminal anaesthesia as described in section 2.15iii.

iii) Biodistribution experiments

Biodistribution experiments were either conducted immediately after imaging experiments had finished, or by themselves as standalone experiments (anaesthesia non-recovery to mimic imaging studies) at the indicated time (various; includes 2, 5, 15, 30 or 60 minutes) post-radiotracer injection (3.7 MBq in 100 µl 100 units/ml heparin-PBS). Whilst under anaesthesia (2.5% isoflurane) the animals were exsanguinated by cardiac puncture using a 25 gauge 25 mm needle and syringe pre-coated in 10,000 units/ml heparin, and the collected blood separated into plasma and cellular blood fractions by centrifugation at 14,000 rpm. The remaining tissues of interest (heart, lung, liver, gall bladder, spleen, kidney, stomach, duodednum, jejunum, caecum, colon, muscle, brain) were harvested and collected in pre-weighed counting tubes. Urine samples were collected by immersion on pre-weighed filter paper. Radioactivity within all tissue samples was counted for in the LKB Wallac 1282 Compugamma laboratory gamma counter (PerkinElmer, Massachusetts, USA), and then weighed to determine the mass of the tissue. The counts per minute for each sample was normalised to the total injected dose of radioactivity to the animal to give the % injected dose (%ID), and then normalised to the weight of the counted tissue to give the radioactivity uptake of the tissue as %ID/g.

2.16 - Metabolism experiments

i) Preparation of animals and tissues

Female BALB/c mice aged between 6-8 weeks were obtained from Charles River (Massachusetts, USA). Anaesthesia was induced in the animals at 3-4%

isoflurane in a 1:4 mixture of nitrogen and oxygen at a flow rate of 1 L/minute, and then reduced to 2% isoflurane for anaesthesia maintenance during imaging. A cannula was inserted into the lateral tail vein of the animal and fixed in position with tape. The radiotracer [3.7 MBq [^{18}F]CCIC7, 7.4-11.1 MBq [^{68}Ga]-CCIC16, or 7.4-11.1 MBq [^{18}F]CCIC30] in 100 µl 100 units/ml heparin-PBS was injected via the cannula at commencement of the experiment. At the indicated time post-injection [various; includes 2 minutes, 5 minutes, 15 minutes or 60 minutes], the animal was sacrificed by cardiac puncture using a 25 gauge 25 mm needle and syringe pre-coated in 10,000 units/ml heparin, and the collected blood separated into plasma and cellular blood fractions by centrifugation at 14,000 rpm. The remaining tissues of interest (liver and urine) were also collected. Samples of plasma, urine and liver were stored in microcentrifuge tubes on ice prior to processing as described in the following steps.

ii) Liquid samples

This protocol was used for processing of the collected samples of urine and plasma, and was performed jointly with Dr. Ola Åberg (for ^{18}F-CCIC7), Guillaume George (for ^{68}Ga-CCIC16) and Dr. Federica Pisaneschi (for ^{18}F-CCIC30). To each sample was added 100 µL of an aqueous solution saturated with urea at 37 ^{o}C and this mixture was added dropwise to an equivalent volume of ice-cold methanol. The mixture was vortexed for 30 seconds and centrifuged (15 rpm, 5 minutes, 4 ^{o}C). The supernatant was added to an equivalent volume of ice-cold methanol, and the mixture was vortexed and centrifuged as earlier. The radioactivity recovery of plasma samples treated in this was 81%, defined as the

radioactivity remaining in the liquid supernatant following methanol-induced protein precipitation, expressed as a percentage of the total sample radioactivity (supernatant + pellet). The supernatant was added to 3 mL of ice-cold H_2O–trifluoroacetic acid (TFA; 999:1). This mixture was filtered through a 0.20 µm Millipore Millex-LG 0.20 µm × 13 mm polytetrafluoroethylene (PTFE) syringe-driven filter unit (Millipore, Massachusetts, USA) and injected into the high performance liquid chromatography (HPLC) machine.

iii) Liver samples

This protocol was performed jointly with Dr. Ola Åberg (for ^{18}F-CCIC7), Guillaume George (for ^{68}Ga-CCIC16) and Dr. Federica Pisaneschi (for ^{18}F-CCIC30). To each liver sample was added 100 µL of an aqueous solution saturated with urea at 37 ^{o}C and 1 mL of ice-cold methanol and was homogenised with an IKA Ultra-Turrax T25 basic homogeniser (IKA, Germany) at 25,000 rpm/min. The resulting suspension was centrifuged (15 rpm, 5 minutes, 4 ^{o}C). The supernatant was added to 3 mL of ice-cold H_2O – TFA (999:1). This mixture was filtered through a 0.20 µm Millipore Millex-LG 0.20 µm × 13 mm PTFE syringe-driven filter unit (Millipore, Massachusetts, USA) and injected into the HPLC.

iv) High performance liquid chromatography (HPLC)

The HPLC procedures were carried out using a Agilent 1100 Series G1312A pump and Lablogic Laura 3 software equipped with a linear Agilent 1100 Series G1314A UV detector (λ = 254 nm), a IN/US Systems γ-RAM model 3 detector and a Waters µBondapak C18 125 Å 10 µ 7.8 × 300 mm HPLC column, and a 5 ml

injection loop. Following injection of the prepared sample, a 5-65% solvent gradient was set up over 15 minutes was at a flow rate of 5 ml/min between mobile phase solution A (water, 0.1% trifluoroacetic acid; TFA) and solution B (acetonitrile ; MECN, 0.1% TFA). The data was analysed by reference to the area under curve (AUC) measurements of the peaks on the HPLC trace. The percentage of unmetabolised (parent) compound within each sample was calculated according to the following equation:

$$\% \text{ parent} = \frac{AUC^{parent}}{AUC^{total}} \times 100$$

2.17 – 17AAG treatment in vitro and in vivo

i) *In vitro* treatment of cells with 17AAG

U87.CD4 and U87.CD4.CXCR4 cells were seeded into the wells of a 6-well plate 48 hours before commencement of the experiment (5×10^5). The cells were cultured in 2 ml complete DMEM medium in the presence of either 100 nM 17AAG, 500 nM 17AAG or no additives (control condition). Following either 24 or 48 hours' treatment in the above conditions, the cells were either lysed and analysed for protein expression as described in sections 2.4i and 2.4iii, or else used to assess *in vitro* uptake of [^{68}Ga]-CCIC16 as described in section 2.13.

ii) *In vivo* treatment of tumour-bearing mice with 17AAG

U87.CD4 and U87.CD4.CXCR4 cells were introduced into BALB/c nu/nu mice by xenotransplantation, and tumour growth progress tracked as described in

section 2.14. Once the tumours reached 80 mm^3 in size, the mice were treated intraperitoneally (*i.p*) with either 80 mg/kg 17AAG or the vehicle solution (DMSO) daily for 48 hours. 24 hours after the final treatment had been given, the accumulation of [^{68}Ga]-CCIC16 within the tumours and other tissues was assessed in biodistribution experiments as described in 2.15iii. Tumour samples were excised and snap-frozen in liquid nitrogen for use as samples for western blots as described in section 2.4ii and 2.4iii.

2.18 - Statistical Analysis

Where specified, data were statistically analysed using either two-tailed independent t-tests where only 2 sets of data were compared, or analysis of variance (ANOVA) tests with Bonferroni post-tests in comparisons of three or more datasets. These tests were conducted using GraphPad Prism v5.01 (GraphPad Software, CA, USA). Results were considered statistically significant when P values < 0.05 had been obtained.

Chapter Three - Results

3.1- Development of [^{18}F]CCIC7 and tumour model characterisation

3.11 - Use of A549, HCT116 and Jurkat cells as cellular models of CXCR4 expression

In order to assess the affinity of novel antagonists for CXCR4, it was first necessary to determine the most appropriate cellular models to use to investigate CXCR4. The relative CXCR4 expression of a number of cell lines was compared, including a small panel of cancer cell lines that was available in the department and were known to express CXCR4 at varying levels. These cell lines were the human breast cancer cell line MDA-MB-231 (Siciliano *et al.*, 1979), the MDA-MB-435S line of disputed source (there is evidence to suggest either human breast or melanocytic origin (Ellison *et al.*, 2002, Chambers, 2009), the human colon colorectal cancer HCT116 line (Brattain *et al.*, 1981), and human lung epithelial adenocarcinoma line A549 (Lieber *et al.*, 1976). The CXCR4 expression in these cell lines were compared (according to the protocol described in section 2.4) against Jurkat cells, an immortalised human T-lymphocyte line of known high CXCR4 expression (Hesselgesser *et al.*, 1998), which served as a positive control. As shown in figure 11, the quantity of CXCR4 protein expressed varied between cell lines, with the positive control Jurkat cell line expressing the most CXCR4, followed by A549 cells, which expressed 77% of the CXCR4 expressed by Jurkat cells. This was closely followed by the MDA-MB-231 line (57% of Jurkat cell expression), and trailed by the HCT116 and MDA-MB-435S lines (32% and 28% of Jurkat cell expression, respectively).

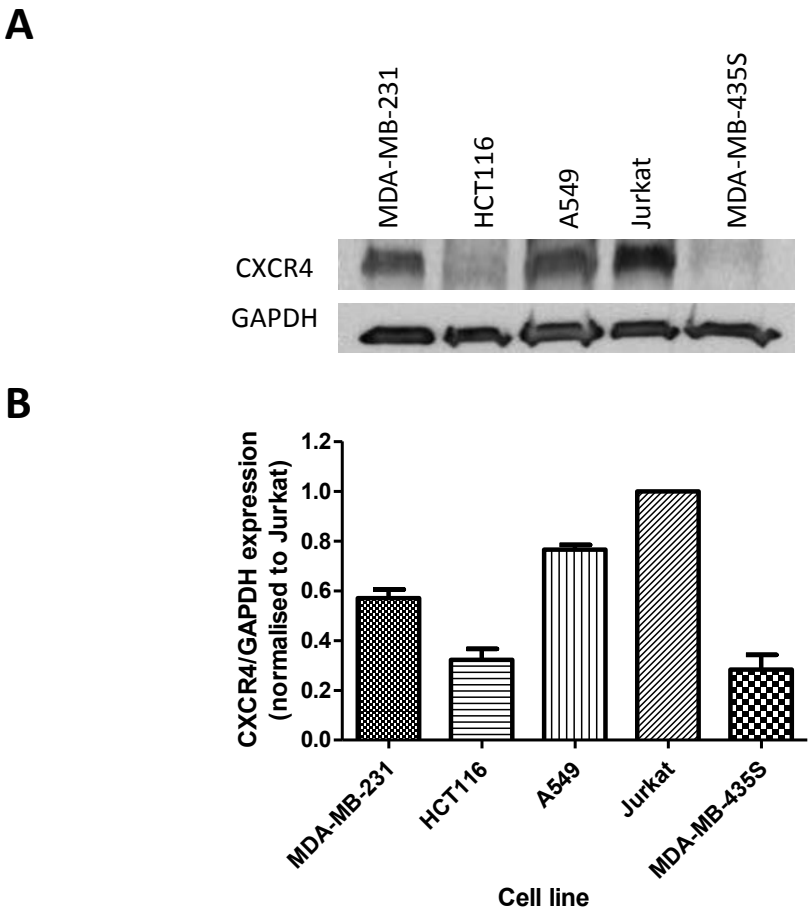

Figure 11. Analysis of endogenous CXCR4 protein expression in a small panel of cell lines.

A Western blot of CXCR4 protein expression, an example of 3 independent experiments
B Mean densitometric analysis of CXCR4 expression, normalised to GAPDH expression and expressed as relative values to CXCR4 expression in Jurkat cells (n=3).

Any novel radiotracer that aims to target CXCR4 should be capable of distinguishing between cell lines of differing CXCR4 expression. Thus a pair of cell lines of high and low CXCR4 expression would be the most appropriate cellular models to determine whether a novel radiotracer bound to cells in a CXCR4-dependent manner. Whilst the Jurkat cell line clearly expressed CXCR4 protein the most, it was not deemed to be suitable for many of the intended

applications due to its lack of tumorigenicity *in vivo* (Deguchi and Kehrl, 1993), as well as its status as a suspension, rather than adherent, line which made it considerably less practical for much of the planned *in vitro* work. The A549 and HCT116 cell lines were chosen as models of high and low CXCR4 expression for use in investigations as a result of their 2.4-fold difference in expression and tumourigenicity *in vivo*. While impractical for uptake assay (refer to section 2.13) or *in vivo* tumour growth (section 2.14), the Jurkat cell line was considered ideal as a model of CXCR4-directed migration, as their expression of high levels of CXCR4 and their status as a suspension cell line enables SDF1-induced migration assays to be conducted rapidly at comparatively low ligand concentrations, with minimal processing before quantification, unlike adherent cell lines. The Jurkat cell line was therefore utilised for the testing of novel antagonist compounds in migration assay.

3.12 - Development of CCIC7 and *in vitro* characterisation of [^{18}F]CCIC7

CCIC7, a novel CXCR4 antagonist that was synthesised by Dr. Ola Åberg, is based on the structure of the potent cyclopentapeptide antagonist FC131. As described in the introduction, it has previously been noted that modifications to the arginine-^{2} of FC131 can be well-tolerated (Ueda *et al*., 2007), and so it was theorised that this would be the pentapeptide residue with the greatest potential for incorporation of a radionuclide-containing chemical group. Thus, a fluorobenzyl (FB) chemical group that is amenable to radiolabelling with ^{18}F was attached to the pentapeptide structure via a hydroxy-imino linker (see figure

12). When migration of Jurkat cells towards 100 ng/ml SDF1 was assessed (according to the protocol in section 2.12) significantly fewer Jurkat cells migrated when incubated with 10 µM CCIC7, in comparison to untreated cells, with a mean 42.4% reduction in the number of migrated cells after 3 hours. This appeared to confirm the antagonistic activity of CCIC7 towards CXCR4, albeit not as potently as the commercially available bicyclam antagonist

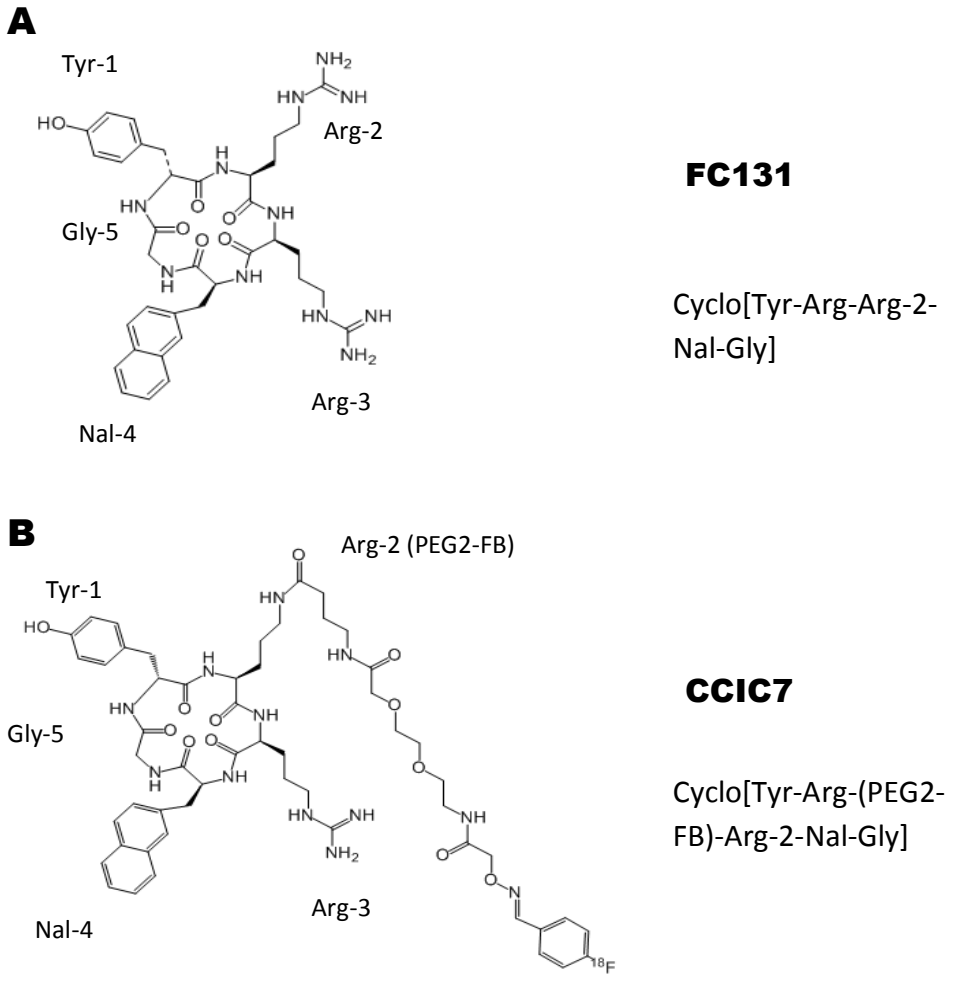

Figure 12. Structure of lead pentapeptide FC131 and novel peptide CCIC7

A Candidate pentapeptide FC131 **B** Novel pentapeptide CCIC7. CCIC7 bears a PEGylated FBA group on arg-2, for the purposes of radiolabelling with ^{18}F. Tyr (Tyrosine); Arg (Arginine); PEG2 (poly[ethylene glycol]); FB (fluorobenzyl); Nal (2-Naphthylalanine); Gly (Glycine)

AMD3100, which at the same concentration inhibited Jurkat cell migration by a mean of 80.3%. While disappointing in comparison to AMD3100, the moderate potency of CCIC7 was considered encouraging enough to attempt to further characterise the potential of CCIC7 as a PET tracer by assessing the radiolabelled compound's ability to accumulate in CXCR4-expressing cancer cells *in vitro*. Uptake assays confirmed that following a 60 minute incubation with 0.37 MBq radioactivity (refer to section 2.13), significantly more [^{18}F]CCIC7 remained bound to A549 cells compared HCT116 cells, with a difference of approximately 1.6-fold, a difference that is comparable to the fold-difference in protein expression of CXCR4 shown in figure 13. Furthermore, blockade of the CXCR4

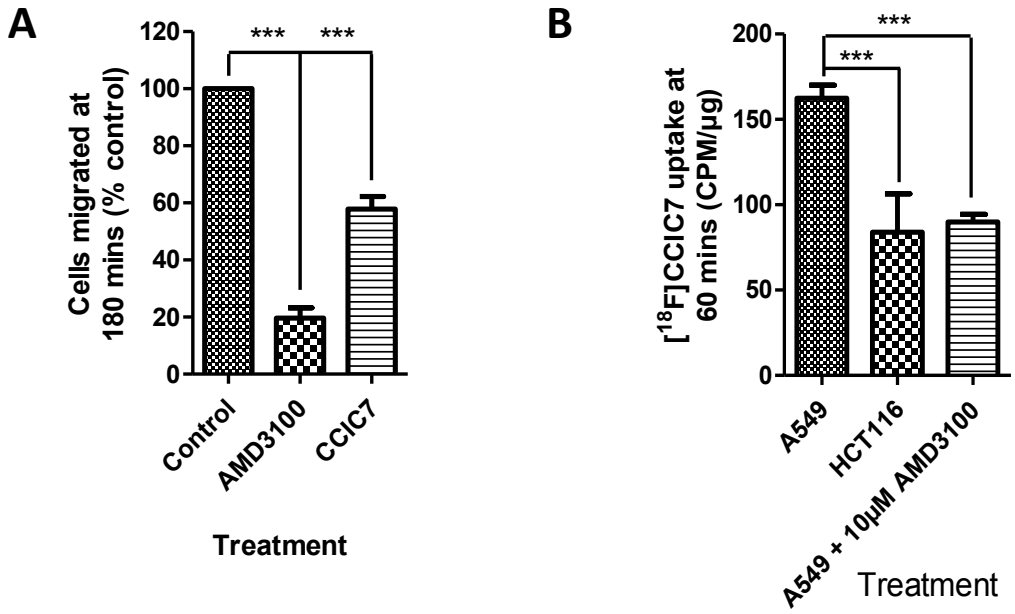

Figure 13. *In vitro* characterisation of CCIC7

A Mean inhibition of SDF1-mediated Jurkat cell migration in the presence of 10 µM CCIC7 or AMD3100, relative to the control (n=3; refer to section 2.12). **B** *In vitro* uptake of 0.37MBq [^{18}F]CCIC7 in A549 and HCT116 cells at 60 minutes (refer to section 2.13). Values are normalised to protein concentration of the wells. Figure shown is an example of 3 independent experiments with triplicate samples. Error bars represent SEM (***, p=0.001).

receptor by pre-incubation with 10 μM AMD3100 (chosen over the more analogous FC131 due to the commercial availability of AMD3100 at the time the experiment took place) prevented the high radioactivity uptake within A549 cells, suggesting specificity of [^{18}F]CCIC7 for the CXCR4 receptor. These findings suggest that despite the low potency of CXCR4 antagonism that CCIC7 exerts, there was still ample promise in its utilisation as a radiotracer that can differentiate between varying levels of CXCR4 expression.

3.13 - *In vivo* assessment of [^{18}F]CCIC7

As a result of this potential, [^{18}F]CCIC7 was further assessed by *in vivo* imaging of HCT116 and A549 tumour xenografts following an injection of 3.7 MBq [^{18}F]CCIC7 (n=4 and 7 respectively; protocol as described in section 2.15i). As the PET images in figure 14 show, there was little discernible difference in tracer accumulation between HCT116- and A549-derived tumours. While the dynamic uptake of radioactivity in the tumour regions of interest yielded time-against-concentration (TAC) curves suggesting potential modest increases in levels of tracer uptake in the higher-expressing A549 tumours than in the lower-expressing HCT116 tumours, there was no significant difference in the standardised uptake values of the two tumours at 60 minutes (SUV_{60}), or indeed at any time-point measured (figure 15A). Furthermore, uptake of [^{18}F]CCIC7 in A549 tumours was not found to be significantly different following pre-injection of 5 mg/kg AMD3100 (a quantity >1000-fold higher than the mean

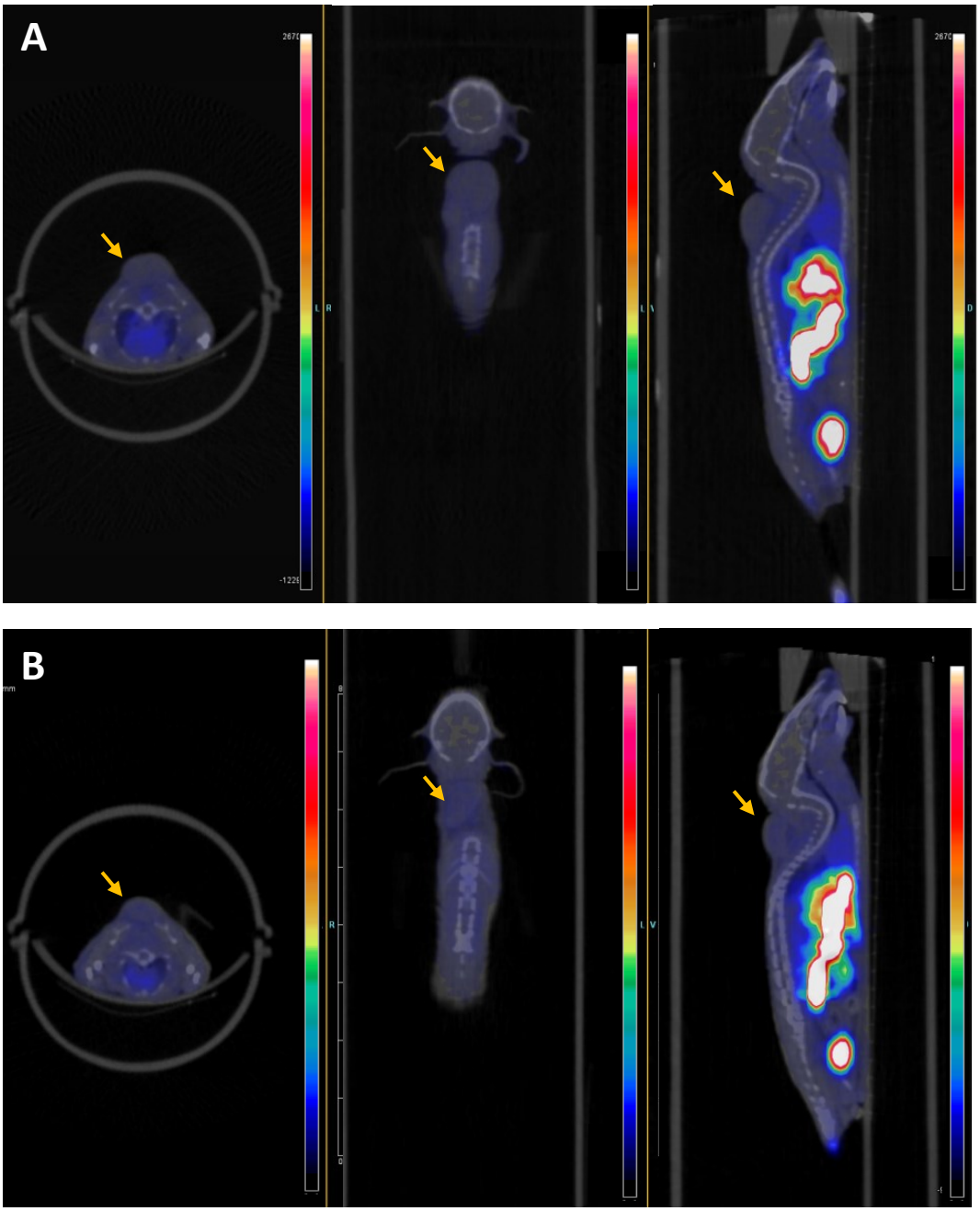

Figure 14. PET/CT images of HCT116 or A549 tumour-bearing BALB/c nu/nu mice following injection of 3.7 MBq [^{18}F]CCIC7

Representative transverse (left), coronal (middle) and sagittal (right) merged PET/CT images from **A** HCT116 and **B** A549 tumour-bearing mice, 60 minutes after lateral tail-vein injection of [^{18}F]CCIC7 (refer to section 2.15i). Arrow identifies location of tumour.

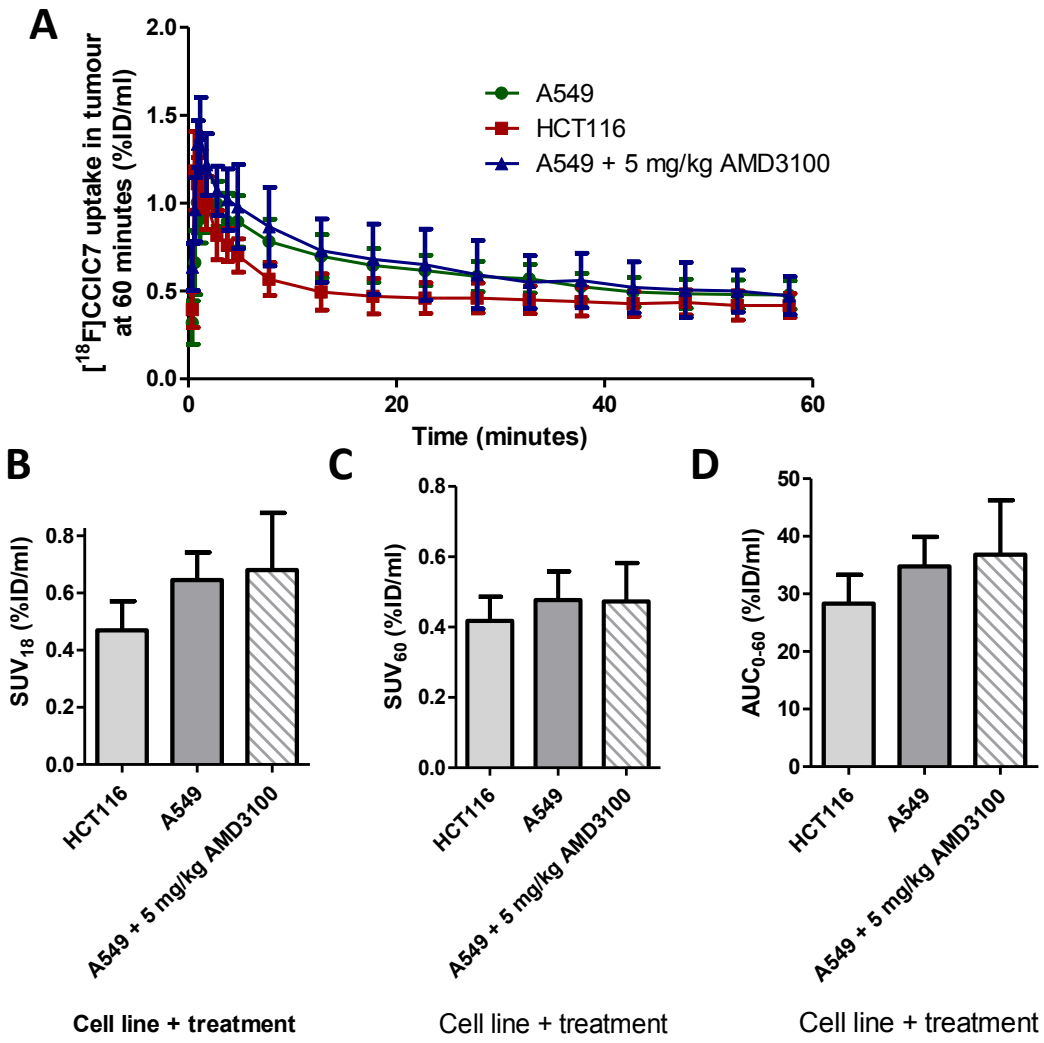

Figure 15. PET imaging of HCT116 or A549 tumour-bearing BALB/c nu/nu mice following injection of 3.7 Mq [^{18}F]CCIC7.

Cohorts of mice bearing HCT116 or A549 tumours (n= 4 and 7, respectively) were imaged using dynamic PET/CT immediately post-injection (refer to section 2.15i). A separate cohort of A549 tumour-bearing mice (n=3) were pre-treated with an *i.v.* blocking dose of 5 mg/kg AMD3100 30 minutes prior to imaging with [^{18}F]CCIC7. **A** Dynamic time-activity curves for the tumour ROIs over the 60 minute scan with [^{18}F]CCIC7. Mean standardised uptake value (SUV) of tumour ROIs at **B** 18 and **C** 60 minutes. **D** Mean area-under-curve values for tumour ROI between 0-60 minutes.

injected quantity of [^{18}F]CCIC7) 30 minutes prior to radiotracer injection (n=3; figure 15). In addition, the overall shape of the time-activity curves show initial delivery of [^{18}F]CCIC7 into the tumour immediately followed by a relatively rapid and sustained reduction of tracer localisation in the tumour ROIs in all cases.

The biodistribution profile of [^{18}F]CCIC7 at 60 minutes (figure 16; refer to section 2.15iii) was in keeping with the imaging data, as in addition to the lack of increased uptake within A549 tumours in comparison to HCT116 tumours (n=4, 3, respectively) there was also no notable tracer uptake in many tissues of reported high CXCR4 expression, such as the lung, bone, and spleen (Rimland *et al.*, 1991, Federsppiel *et al.*, 1993, Shao *et al.*, 2011). Indeed, the most prominent sites of [^{18}F]CCIC7 uptake were the gallbladder, liver, stomach, duodenum, jejunum, kidneys and urine of the mice, which indicate that radiotracer accumulation was primarily associated within organs of excretion. Whilst CXCR4 expression has been reported in the liver (Rimland et al., 1991), the lack of blockade in liver tissues following pre-injection with 5 mg/kg AMD3100 (n=3) appears to preclude CXCR4-specific uptake of [^{18}F]CCIC7 in this situation.

To elucidate the reasons for the poor uptake a time-course metabolite and biodistribution study was conducted (as described in section 2.16), in order to determine the role that metabolism of [^{18}F]CCIC7 might have played in the eventual biodistribution of the radiotracer. It was found that within even 5 minutes (n=3) the majority of circulating [^{18}F]CCIC7 in the plasma had been metabolised to a smaller fragment (with 44 ± 12% tracer remaining), and that by 15 minutes (n=3) the unmetabolised [^{18}F]CCIC7 was almost entirely absent from the plasma (6 ± 2% remaining) (figure 16 and table 5). This provides a possible explanation for the disappointing findings of the *in vivo* imaging experiments, as

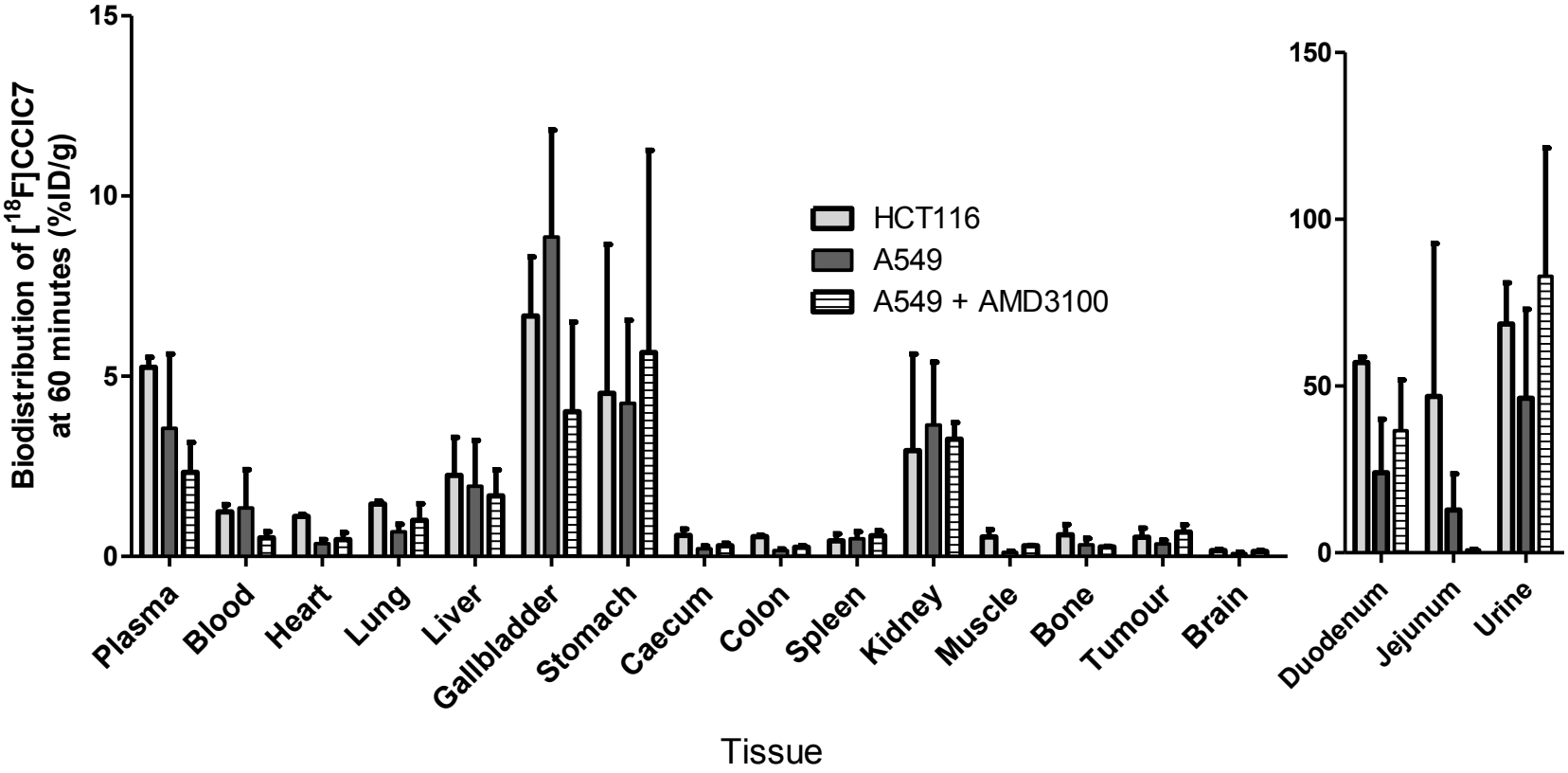

Figure 16. Biodistribution of 3.7 MBq [^{18}F]CCIC7 at 60 minutes post-injection in tissues of HCT116 or A549 tumour-bearing BALB/c nu/nu mice, or A549 tumour bearing mice treated with 5 mg/kg AMD3100 30 minutes prior to radioactivity injection (n=3, 4, and 3, respectively).

Mice were sacrificed immediately following the 60-minute scan by exsanguinations and tissues harvested as described in section 2.15iii. The radioactivity present in the tissue was then counted and normalised to the weight of the tissue, and to the injected dose.

it suggests that a high degree of metabolism within a short period of time may be responsible for the lack of CXCR4-dependent [^{18}F]CCIC7 accumulation within A549 tumours.

In contrast, [^{18}F]CCIC7 appeared to be less rapidly metabolised at the liver, where a considerable majority (88 ± 10%) of [^{18}F]CCIC7 remained unmetabolised at 5 minutes post-injection (n=3), although this proportion decreased steadily over the remaining hour to 44 ± 3% (see table 5 and figure 16; n=3). At least two radioactive fragments were present in liver homogenates, with the proportion of the largest of these gradually diminishing over time, possibly reflecting successive stages of metabolism of [^{18}F]CCIC7. The role of the liver in the course of [^{18}F]CCIC7 *in vivo* processing and elimination was supported by time-course biodistribution study data (n=3) as shown in figure 18; the rapid accumulation of radioactivity within the liver precedes the passage of radioactivity from the liver to the duodenum and jejunum of the gastrointestinal (GI) tract, confirming the rapid clearance of [^{18}F]CCIC7 through the hepatic excretory pathway. Rapid clearance of [^{18}F]CCIC7 was also observed through the urinary route of excretion, as peak radioactivity levels at the kidneys occurred at 5 minutes following injection, and within the urine at 15 minutes post-injection. The fast action of both the hepatic and urinary routes of excretion for [^{18}F]CCIC7 are likely to be a key reason for the poor performance of the radiotracer in differentiating CXCR4 expression in tumours.

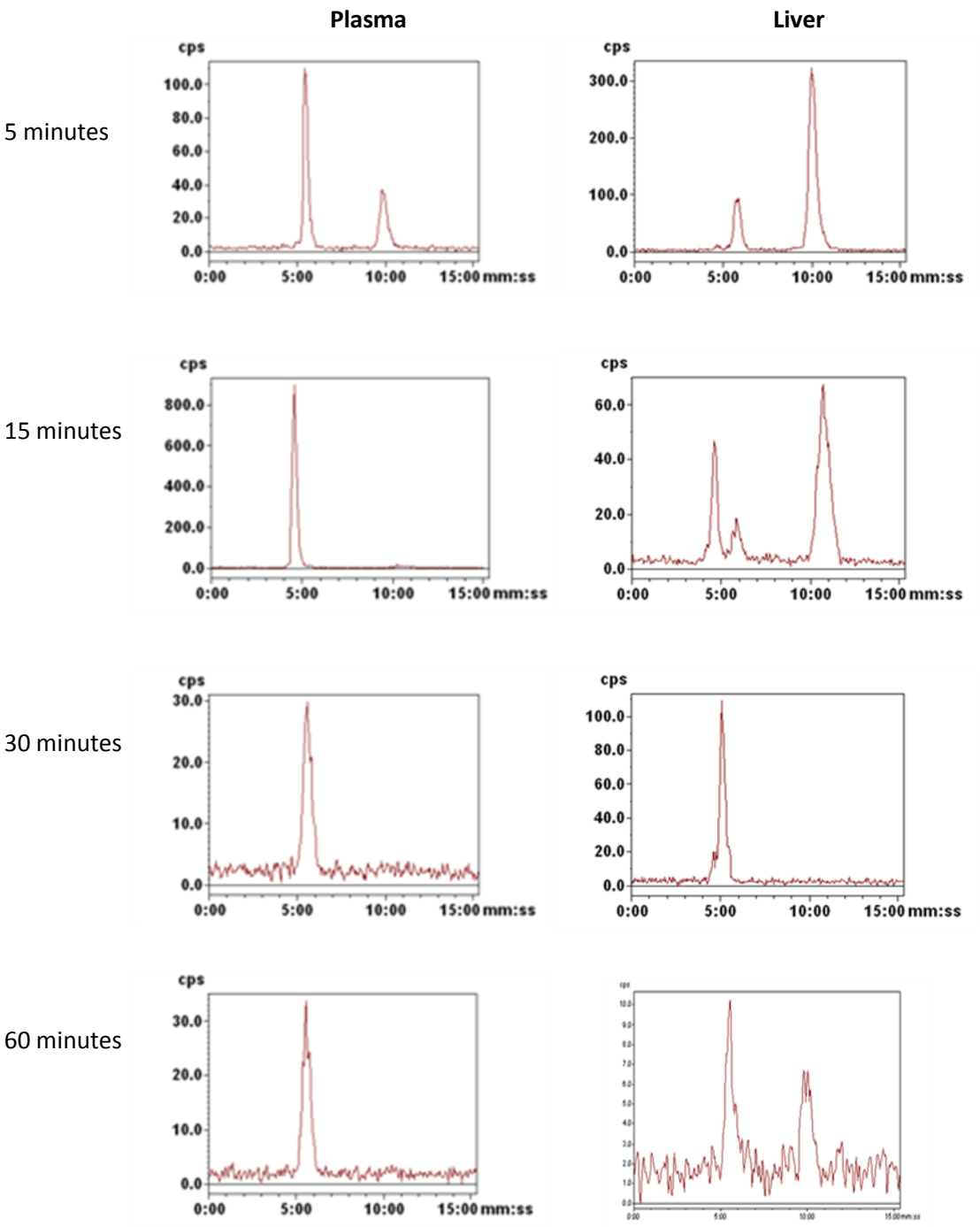

Figure 17. HPLC traces showing parent compound and metabolite peaks in liver and plasma extracts of BALB/c mice following 5, 15, 30 and 60 minute inoculation of 3.7 MBq [^{18}F]CCIC7. Representative example radiochromatograms (n=3) from acetonitrile extracts from mouse plasma and homogenised liver samples at the indicated time points. The parent tracer [^{18}F]CCIC7 has a retention time of 10m50s, whereas metabolite peaks 1 and 2 arise at 4m30s and 5m50s, respectively. Refer to protocol described in section 2.16.

Table 5. *In vivo* metabolism of compound [^{18}F]CCIC7 at selected time points, showing the percentage of [^{18}F]CCIC7 present in plasma, liver and urine extracts (n=3)

Time (min)	Plasma	Liver	Urine
5	44 ± 12	88 ± 10	33
15	6 ± 2	64 ± 10	71
30	4 ± 7	38 ± 34	0
60	0 ± 0	47 ± 3	0

The values shown for plasma and liver samples are the mean of three test subjects (± the SEM), the urine samples are n=1. Refer to section 2.16.

3.14 - *Changes to CXCR4 expression analysis methology and transfection of HCT116 colon carcinoma cells*

Following the failure of [^{18}F]CCIC7 to identify A549 from HCT116, alternative methods to were considered. While the outcome of *in vivo* validation of [^{18}F]CCIC7 was perhaps doomed to fail from the outset as a result of the poor pharmacokinetics of the tracer, doubts had also begun to arise regarding the specificity of the antibody used to detect CXCR4 by immunoblotting (ab2074)(Smith et al., 2004, Dubrovska *et al.*, 2012a), as the presence of numerous bands upon the anti-CXCR4 immunoblot was a considerable cause for concern. However, the band sized at ~43kDa was the predicted size of the CXCR4 protein, and appeared to show data in line with observations from literature (Wendt *et al.*, 2008, Tang *et al*., 2008a), and so had previously been the only data taken into consideration when quantifying relative protein expression. As figure 19 shows, the blots yielded with this antibody (using the protocol described in section 2.4) were cluttered with additional bands, which

were presumed at the time to be non-specific and not relevant to the investigation.

This conclusion was re-evaluated once subsequent qRT-PCR findings (refer to section 2.3) showed mRNA expression of CXCR4 within the cell lines to be considerably different to the protein expression levels reported using antibody ab2074 shown in figure 19; in this case Jurkat cells expressed by far the most CXCR4 mRNA, followed by MDA-MB-231, HCT116, A549 and finally MDA-MB-435S (with mean relative expression levels of 972.0, 58.6, 1.6, 1 and 0, respectively; see figure 20A and 20B). A departure from the mRNA expression levels of cell lines might be explained by differences in the processing of mRNA before protein synthesis in each cell line, such as in the regulation of post-transcriptional, translational and degradation processes (Vogel and Marcotte, 2012). However, the apparent presence of CXCR4 protein within cell lines that did not express CXCR4 mRNA cannot be explained, except to conclude that the antibody used was inappropriate for the detection of CXCR4 or reduced coverage of the PCR primers. The result of the qRT-PCR data, which suggested approximately equal low-level CXCR4 expression within the HCT116 and A549 lines, further explains why [^{18}F]CCIC7 could not differentiate between the cell lines MDA-MB-435S and A549, as there was indeed almost no difference in CXCR4 expression between them. It was therefore decided that an alternative, more specific antibody should be found, and that it should be used to identify CXCR4 expression stably induced within a given cell line through transfection,

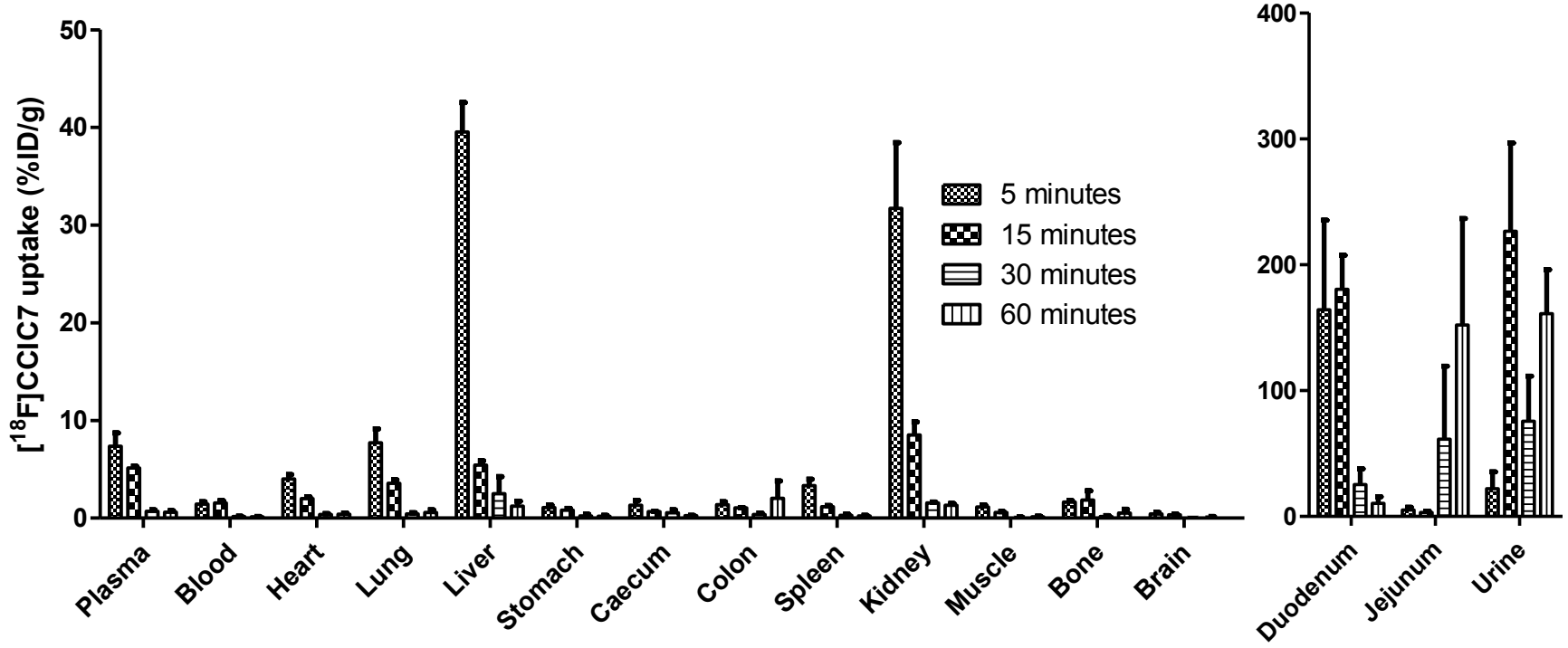

Figure 18. Biodistribution of [^{18}F]CCIC7 at 5, 15, 30 and 60 minutes following injection of 3.7 MBq [^{18}F]CCIC7 in healthy BALB/c mice (n=3).

Mice were exsanguinated by cardiac puncture and tissues harvested. The radioactivity present in the tissue was then counted and normalised to the weight of the tissue, and to the injected dose. Refer to section 2.15iii.

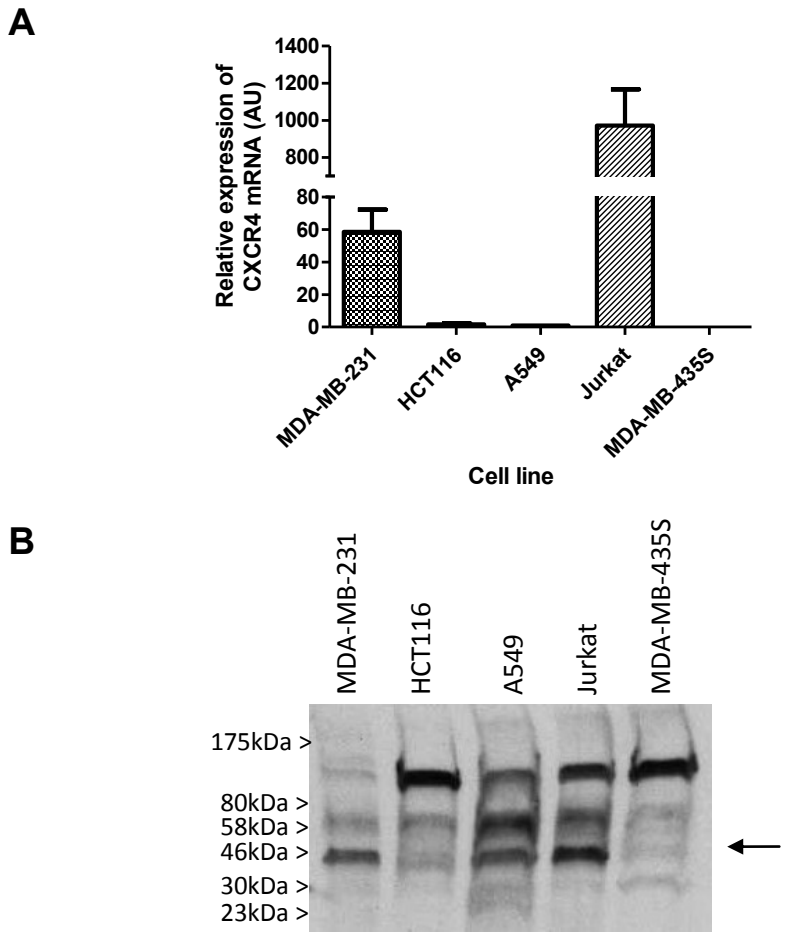

Figure 19. Evidence of poor specificity of ab2074 anti-CXCR4 antibody for CXCR4 protein.

A CXCR4 mRNA expression in vitro, normalised to GAPDH mRNA expression, and expressed as a factor of CXCR4/GAPDH mRNA expression (n=3; error bars denote SEM). Refer to section 2.4. **B** Example whole-view image of immunoblot using ab2074 anti-CXCR4 antibody. Note the numerous bands, and non-conformity with mRNA expression reported in **A**. Band previously presumed to represent CXCR4 shown adjacent to arrow.

allowing the utility of pairs of isogenic cell lines differing only in their CXCR4 expression.

To this end, the UMB2 clone CXCR4 antibody was used (according to the protocol described in section 2.4) as a result of reports of its high specificity for

CXCR4 in comparison to other commercially available antibodies (Fischer *et al.*, 2008). This antibody identified Jurkat cell lysates (used in this regard as a positive control, due to their high reported CXCR4 expression) with a strongly stained broad smear, chiefly above 50 kDa in size. In contrast, the cell lines MDA-MB-231, MDA-MB-435S, HCT116 and A549 showed very little staining (figure 20A and 20B), corroborating the qRT-PCR findings. The cell lines were further assayed by flow cytometry (described in section 2.5) using a different CXCR4 antibody (clone G5) to validate the findings of the UMB2 clone CXCR4 antibody used in immunoblotting, and in particular to give an indication of the surface expression of CXCR4 receptors, which would naturally be of utmost importance to the development of novel radiotracers for CXCR4 expression. The flow cytometry data were in agreement with the results of the new immunoblotting experiments - both HCT116 and A549 expressed similarly low quantities of CXCR4 protein which was not detectable above background levels. The Jurkat cells, in contrast, exhibited strong CXCR4 expression as expected (Hesselgesser *et al*., 1998).

With two antibodies for detecting CXCR4 now validated, it became clear that the A549 and HCT116 cell lines were unsuitable as models of differential CXCR4 expression. However, it remained to be ascertained why the *in vitro* uptake assays had previously appeared to confirm a difference in CXCR4 expression between the two cell lines (figure 13). It was suspected that the difference in

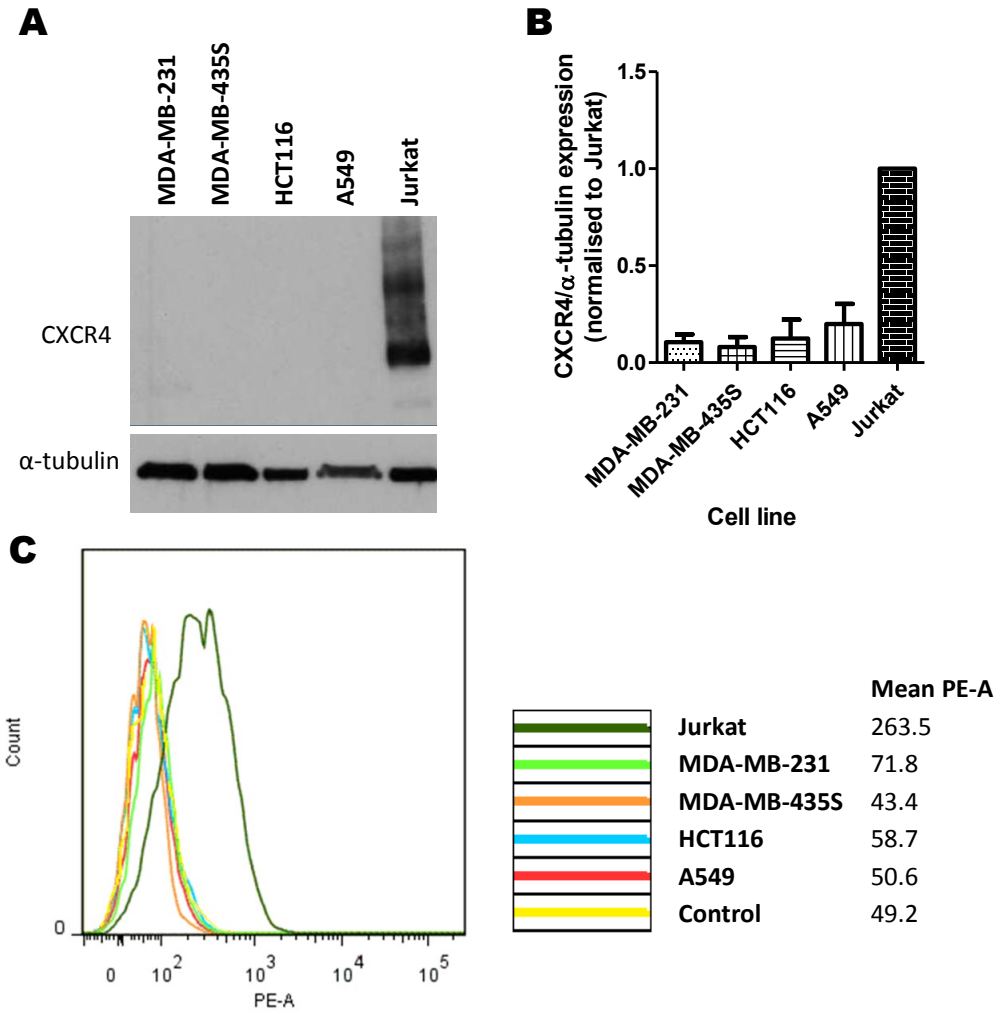

Figure 20. Reanalysis of endogenous CXCR4 expression in a panel of cell lines using alternative antibodies and techniques.

A Representative western blot (see section 2.4) with UMB-2 clone rabbit anti-CXCR4 antibody. Primary band is visible at ~50 kDa, faint band observed ~25 kDa. **B** Mean densitometric analysis of immunoblots with clone UMB2 anti-CXCR4 antibody. CXCR4 expression is normalised to α-tubulin expression, and represented relative to expression in Jurkat cells (n=3). **C** Flow cytometry of same cell lines using PE-conjugated anti-CXCR4 clone 47717, with mean PE-A values included (n=3). 'Control' refers to Jurkat cells stained with isotype control antibody. See section 2.5.

uptake may have related to differences in size of the cells assayed, as A549 cells covered a considerably larger surface area than HCT116 cells. No difference in [^{18}F]CCIC7 uptake *in vitro* was seen between HCT116 and A549 cells before

normalisation to the protein content of the lysate sample, yet significance was obtained following normalisation (figure 21). The normalisation of radiotracer uptake to the protein content of the cells would ordinarily be an appropriate control to take into account slight differences in confluency of the cell lines. However, in this circumstance it appears that false significance may have been achieved through equivalent binding at the cell surface, with the large differences in the size of A549 and HCT116 cell lines (and hence overall cellular protein expression data) skewing the normalised result towards significance. It was unfortunate in this circumstance that the false positive result appeared to confirm the expected difference predicted from the findings of immunoblots that are now known to be inaccurate.

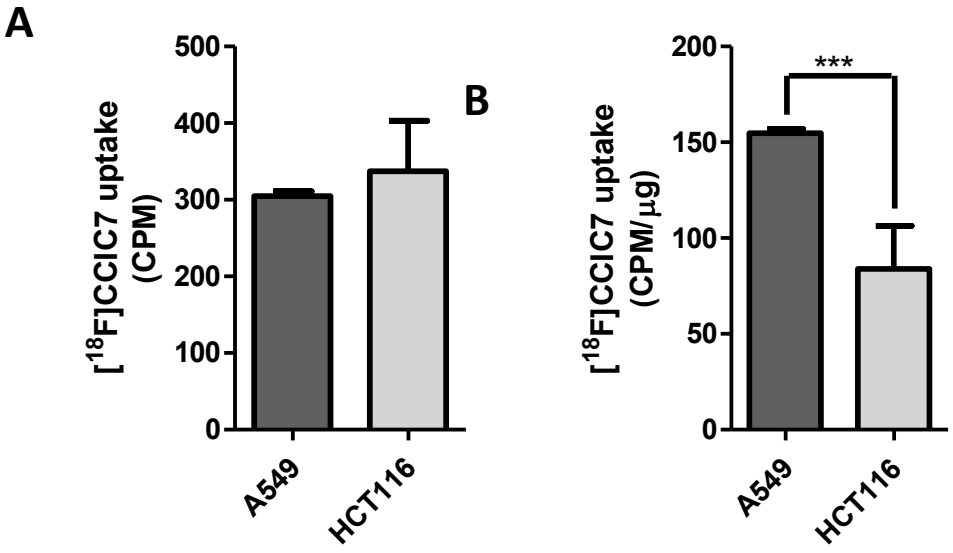

Figure 21. Effect of protein normalisation upon perceived *in vitro* [^{18}F]CCIC7 uptake at 60 mins.

A Representative example of *in vitro* [^{18}F]CCIC7 uptake in HCT116 and A549 cells prior to protein normalisation. Perceived uptake in HCT116 and A549 cells approximately the same. **B** Same assay data as A, but instead normalised to protein content of wells. Perceived uptake in HCT116 cells significantly lower than in A549 cells. A549 an HCT116 cells were seeded to give equivalent confluency of 70% surface area coverage. Counts per minute (CPM).

The results of the investigation into the effectiveness of [^{18}F]CCIC7 as a CXCR4-targeting tracer therefore highlighted a number of issues with the methodology used up to this point. Firstly, the anti-CXCR4 antibody used in the characterisation of the protein expression of CXCR4 in the various cell lines was determined to be insufficiently specific for CXCR4; the UMB-2 and 12G5 antibodies for western were postulated as suitable replacements. Secondly, the results of radiotracer uptake assays may be prone to give false suggestions of differential uptake in cells of markedly different sizes. The use of isogenic pairs of cell lines in future investigations would restore faith in the method, as the similarity between the cell lines would ensure that any difference in uptake would occur as a result of differences in CXCR4 expression, rather than other physiological characteristics. These two errors combined led to the utilisation of cellular models of CXCR4 expression that were unsuitable for the purpose of the investigation.

To correct this issue it was decided to introduce CXCR4 expression into the HCT116 colon carcinoma cell line by transfection, thereby obtaining a syngeneic pair of cell lines appropriate for the development of new CXCR4-targeting radiotracers. However, despite many attempts to derive clones of stable CXCR4 transgene expression with a pcDNA3.1 vector (described in section 2.7), very few of the clones derived showed any substantial level of CXCR4 expression as judged by western blot or flow cytometry (figure 22; refer to sections 2.4 and 2.5). For example, the most encouraging clone, Stable 3, was found to stably

express only twice as much CXCR4 as the untransfected HCT116 cells, and approximately half as much CXCR4 as Jurkat cells. In contrast, other clones survived under G418 selection with no additional expression of CXCR4 protein at all.

3.15 - *Characterisation of CXCR4 transfected cancer cell lines*

Given the previous concerns regarding the use of appropriate cellular models it was decided that more reliable data could be obtained by acquiring a pair of CXCR4-transfected lines from the National Institute of Health (NIH) AIDS Research and Reference Reagent Program derived from the U87.MG human glioblastoma cell line, called U87.CD4 and U87.CD4.CXCR4. The U87.CD4.CXCR4 cell line had been shown to express far higher CXCR4 than its parent cell line U87.CD4 (Endres *et al.*, 1996, Bjorndal *et al.*, 1997), much more so than the HC116 transfectants described in figure 22. As such, the acquired U87.CD4.CXCR4 cell line showed markedly higher CXCR4 expression than the parent U87.CD4 line in our own investigations, which did not express CXCR4 at all, as judged by qRT-PCR, western blotting and flow cytometry (figure 23). The cell line even proved to express more CXCR4 protein than the Jurkat cell line, used as a positive control for CXCR4. The high degree of agreement between the three methods of assessing CXCR4 expression strongly indicated the veracity of these findings, putting any remaining concerns regarding the specificity of the antibodies currently in use firmly in the past.

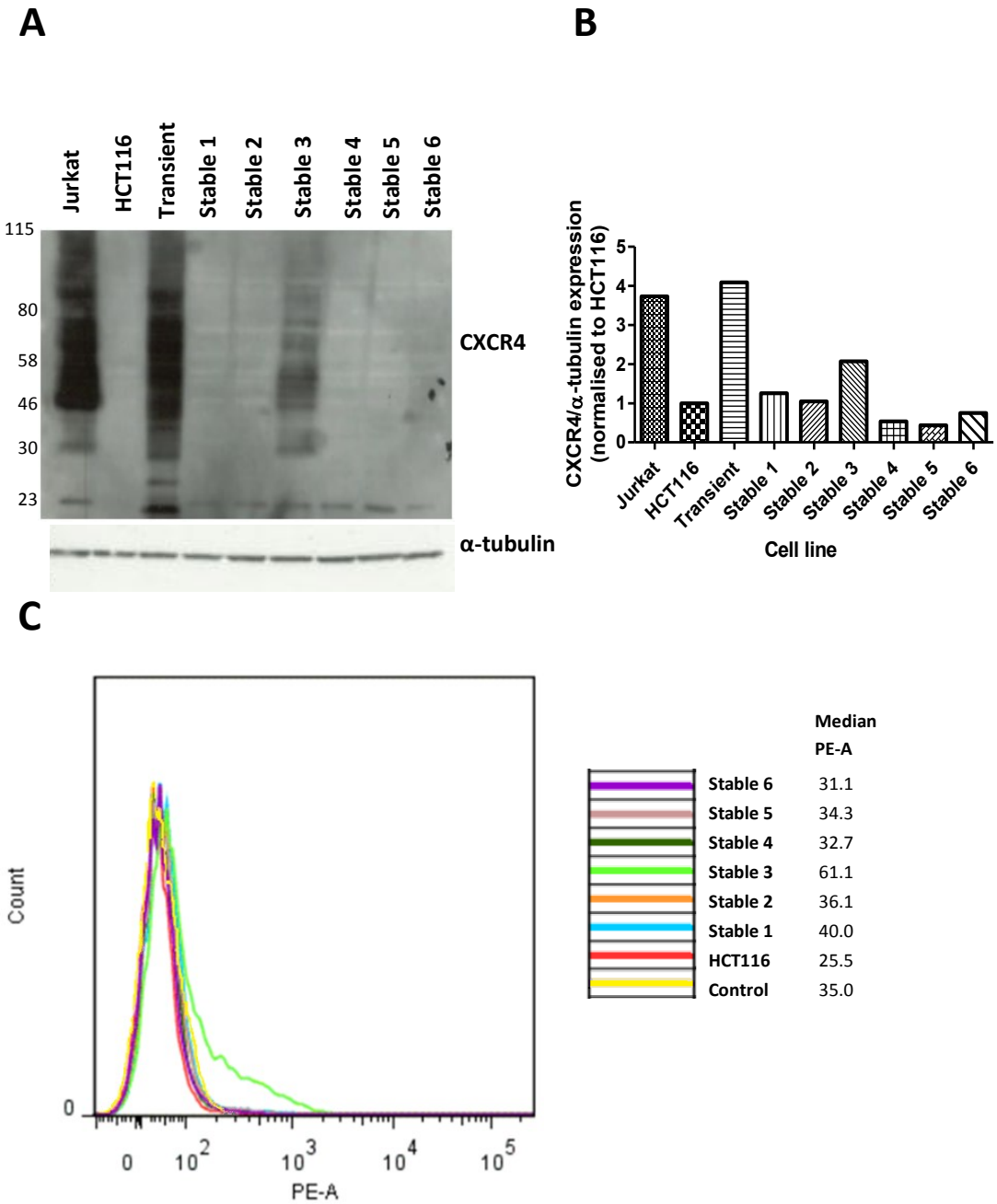

Figure 22. Transfection of HCT116 colorectal line with pcDNA.CXCR4 vector

A Representative example of CXCR4 protein expression in stably transfected HCT116 clones by western blot using the UMB2 clone anti-CXCR4 antibody. **B** Densitometric analysis of CXCR4 expression normalised to α-tubulin and expressed relative to HCT116 cell expression (n=1). Refer to section 2.4. **C** Flow cytometric analysis of CXCR4 expression in CXCR4-transfected stable HCT116 transfectants, showing median PE-A values (n=1). 'Control' refers to the 'stable 3' cell line stained with isotype control antibody. Refer to section 2.5.

With these considerations addressed, it remained to consider the effect of the CXCR4 overexpression upon downstream cellular processes, such as proliferation and SDF1-directed migration. In order to check that the difference in motility in wound closure was not mediated by alternative CXCR4-dependent process, such as increased proliferation, a doubling time assay was conducted as described in section 2.8, which confirmed no significant difference in the proliferation rate of U87.CD4 and U87.CD4.CXCR4 cells (figure 24A). A scratch wound motility assay was then conducted as described in section 2.9, and it was found that significantly greater wound closure occurred in cells overexpressing CXCR4, and that this difference in motility could be blocked by the presence of AMD3100 (figure 24B). A difference in CXCR4 expression between U87.CD4 and U87.CD4.CXCR4 was maintained *in vivo* (protocol described in section 2.4ii), albeit at a mean 2.6-fold difference (figure 25), considerably lower than the 10-fold difference in CXCR4 expression in the same cell lines *in vitro* (figure 22B).

The data observed so far points to the U87.CD4 and U87.CD4.CXCR4 cell lines as excellent syngeneic models of differential CXCR4 expression, and are therefore expected to be far superior for the characterisation of novel antagonists and tracers for PET imaging than the A549 and HCT116 cell lines used in chapter 3.1. The previous use of unreliable methods to assess CXCR4 expression in these HCT116 and A549 cell lines was a confounding factor to the early positive

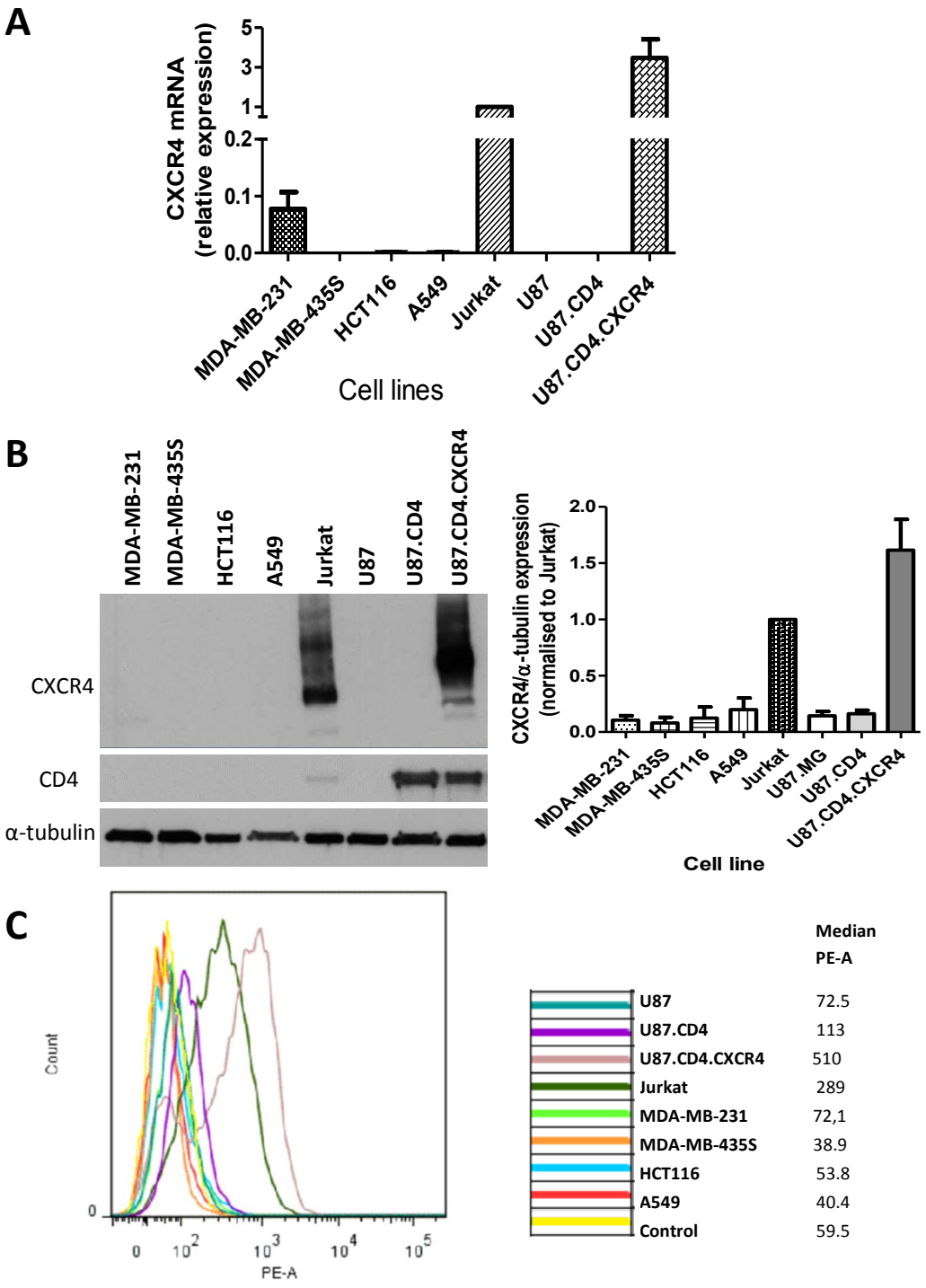

Figure 23. *In vitro* characterisation of CXCR4-overexpressing glioblastoma line

Comparison of CXCR4 expression in transfected U87 models against endogenous CXCR4 expression in panel of cancer cell lines by **A** qRT-PCR (showing expression values as relative to Jurkat CXCR4 mRNA ; n=3, error bars denotes SEM; refer to section 2.3), **B** by western blot of cell lines *in vitro* (example immunoblot and mean densitometric analysis, relative to Jurkat expression ; n=3, error bars show SEM; refer to section 2.4), and **C** analysis of cell lines by flow cytometry, showing average (n=3), refer to section 2.5. 'Control' refers to Jurkat cells stained with isotype control antibody.

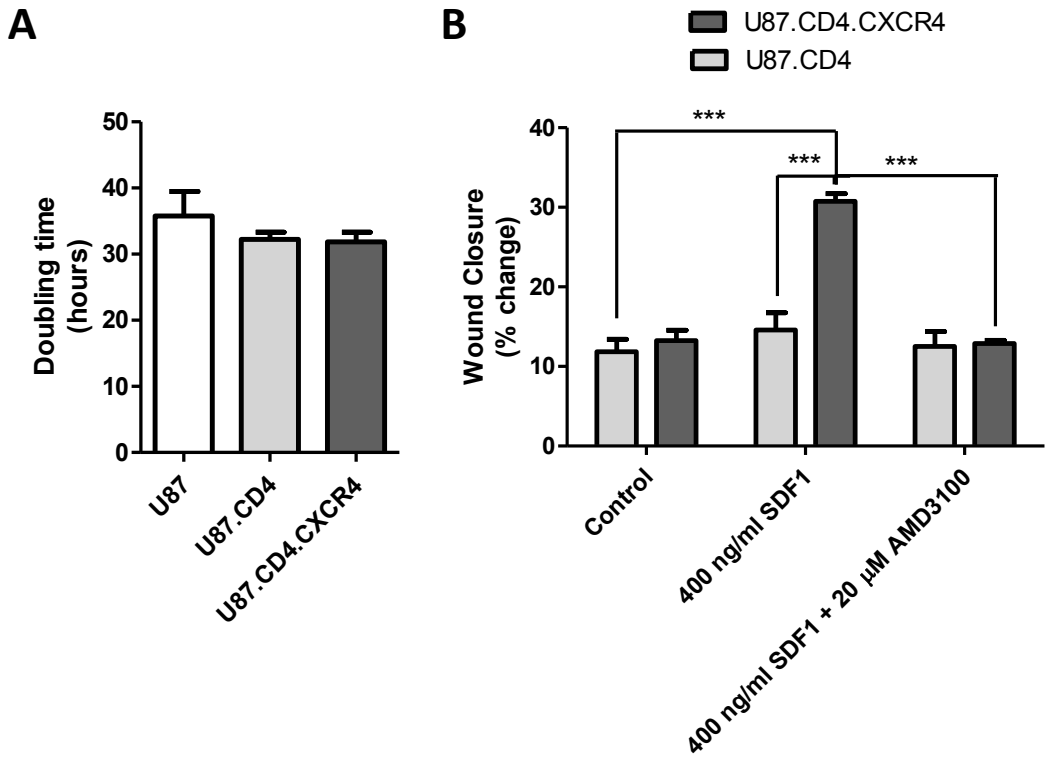

Figure 24. Effect of CXCR4 expression on CXCR4-dependent processes in glioblastoma *in vitro*

A Calculated doubling time of parental U87.MG, U87.CD4 and U87.CD4.CXCR4 cell lines *in vitro* (n=3 ; error bars show SEM). Refer to section2.8. **B** Effect of CXCR4 expression upon SDF1-induced wound closure in glioblastoma cells over 12 hours (n=3 ; P ≤ 0.001 ; error bars show SEM). Refer to section 2.9.

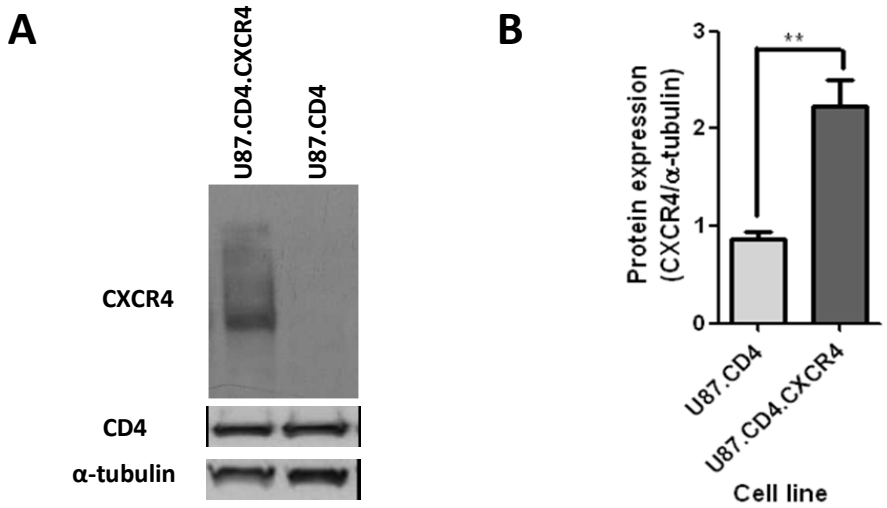

Figure 25. *In vivo* characterisation of U87.CD4 and U87.CD4.CXCR4 glioblastoma lines

A Representative image of homogenised snap-frozen tumour samples analysed by western blotting with CXCR4, CD4 and α-tubulin antibodies. **B** Densitometric analysis of CXCR4 expression in U87 glioblastoma tumours *in vivo* (n=3 ; error bars show SEM ; P ≤ 0.01). Refer to section 2.4ii and 2.4iii.

indications for the use of [^{18}F]CCIC7 as a CXCR4-specific tracer, with *in vitro* uptake experiments appearing to confirm the specificity of uptake into the supposedly higher CXCR4 expressing A549 cells (later disproved). However, [^{18}F]CCIC7 uptake was later judged to be nonspecific, as differential uptake into tumour cells was largely associated with differences in tumour cell size, rather than any true specificity for CXCR4. Furthermore, [^{18}F]CCIC7 was found to be extremely metabolically unstable *in vivo*, and therefore not suitable for further development using the newly characterised U87.CD4 and U87.CD4.CXCR4 glioblastoma models of low and high CXCR4 expression, respectively. It was therefore necessary to consider the characterisation of alternative novel CXCR4 antagonists, as described in the following chapters.

3.2 - Design of 14mer peptide CCIC16 and characterisation of effects of ion chelation and subsequent development of [^{68}Ga]CCIC16

3.21 - *Design of novel antagonist CCIC16*

In addition to the radiolabelling of the cyclic pentapeptide CCIC7, development was also sought with the well-characterised 14mer T140 derivative antagonist, TN14003. As reported in chapter 1.7, while some T140-derived PET tracers exhibited issues with non-specific binding on RBCs (Jacobson *et al.*, 2010), it was possible to avoid this disadvantage with the replacement of the interfering fluorobenzoyl group that introduced the radiolabel with chelating groups such as

1, 4, 7, 10-tetraazacyclododecane 1, 4, 7, 10-tetraacetic acid (DOTA) and 1, 4, 7-triazacyclononane 1, 4, 7-triacetic acid (NOTA) for the introduction of ^{64}Cu into TN14003. However, even with these improvements the uptake of the radiotracer in CXCR4-expressing tumours was low, suggesting the possibility for further optimisation (Jacobson *et al.*, 2012).

A number of further modifications to the structure of TN14003 tracer reported above were considered necessary. Firstly, for the reasons described previously, the ^{64}Cu radionuclide was exchanged for the more preferable ^{18}F or ^{68}Ga. Whilst DOTA or NOTA groups have been shown to be well-tolerated at the C-terminal of the 14-mer peptide (Jacobson *et al*., 2012), it is possible that a reduction in size of the conjugated chelating group may improve the affinity of the receptor, as a result of reduced steric hindrance. This suggestion is supported by the recently-reported crystal structure of CXCR4, which shows that both the N- and C-terminals of a T140-derived CXCR4 antagonist are buried within the 3D structure of CXCR4 (Wu *et al*., 2010), implying that the structures at these points may be important for binding affinity. It was therefore considered that direct conjugation of a 1, 4, 7-triazacyclononane 1, 4-diacetic acid (NODA or NO2A) group upon the C-terminus of the peptide antagonist might be suitable, as it is considerably smaller than the NOTA-Bn-thiourea chelating group used previously by Jacobson *et al*. (2005 ; figure 26B), and is also amenable to labelling with gallium-68 (Notni *et al.*, 2012) and aluminium fluoride-18 (McBride *et al*., 2012). It was hoped that these changes would result in a 14mer PET tracer

with an improved target-to-background ratio. The resulting peptide was designated CCIC16 (figure 26C).

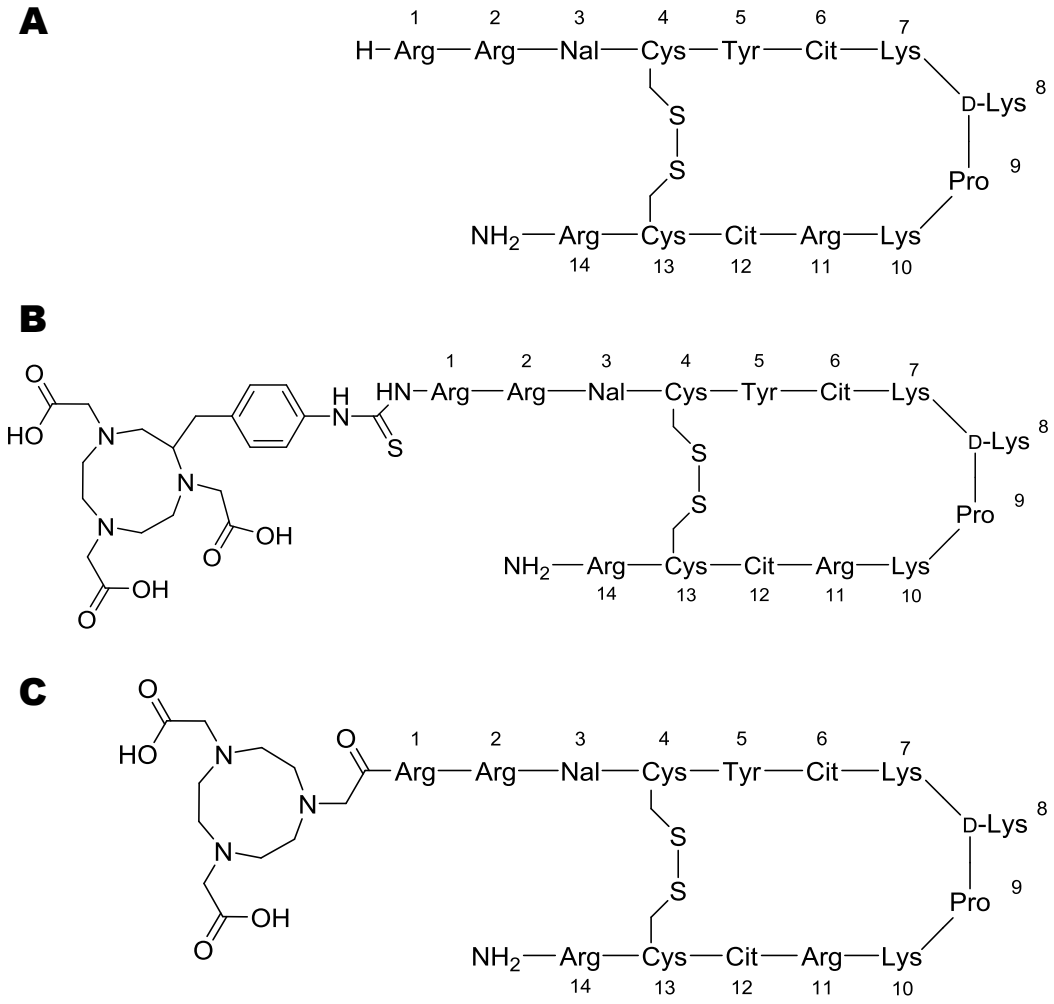

Figure 26. Evolution of TN14003 to NOTA-NFB-T140 to CCIC16.

A Structure of TN14003 **B** Structure of NOTA-NFB-T140 reported by (Jacobson *et al.*, 2012)
C Structure of CCIC16. Arginine (Arg) ; 2-Naphthylalanine (Nal) ; Cys (Cysteine) ; Tyr (Tyrosine) ; Citrulline (Cit) ; Lysine (Lys) ; Proline (Pro).

3.22 - *Assessment of CXCR4 antagonism by ion-chelated derivatives of CCIC16*

The newly synthesised CCIC16 was then labelled with a number of different metal cations that could potentially be used in nuclear imaging applications,

including Ga^{3+}, $[AlF]^{2+}$, Cu^{2+}, and In^{3+}. In order to assess their potential as novel antagonists, their ability to antagonise CXCR4 was investigated with competitive radioligand binding assays and migration assays. The potencies of these antagonists in these applications were compared against the commercially available T140 derivative known as TC14012 (Arg-Arg-Nal-Cys-Tyr-Cit-Lys-D-Cit-Pro-Tyr-Arg-Cit-Cys-Arg-NH_2). With the radioligand binding assay (refer to section 2.11i) it was seen that the affinities of the Ga^{3+}, $[AlF]^{2+}$, Cu^{2+} labelled CCIC16 antagonists were very similar to the affinity of the unlabelled CCIC16 antagonist, with mean IC_{50} values of 69-103 nM when competing for binding sites against 0.1 nM ^{125}I-SDF1. In contrast, the reference compound TC14012 and In-labelled CCIC16 showed higher affinity for the CXCR4 receptor, with IC_{50} values of 18.2 nM and 17.6 nM, respectively (figure 27A and table 6).

The compounds also showed an ability to inhibit CXCR4-mediated migration (refer to section 2.12), as Jurkat cells cultured in the presence of cation-labelled CCIC16 could prevent cell migration to transwell chambers containing 100 ng/ml SDF1 (Figure 27B). Similarly to the radioligand binding assay data, TC14012 again showed the greatest potency of the compounds assayed with an IC_{50} of 6.3 nM, while chelation with metal cations increased the antagonism shown by CCIC16 from 355.7 nM to values as low as 43.9 nM and 60.7 nM (as shown by AlF-CCIC16 and Ga-CCIC16, respectively). The high degree of antagonism shown by Ga-CCIC16 for CXCR4 (table 6) along with the benefits of ^{68}Ga as a PET

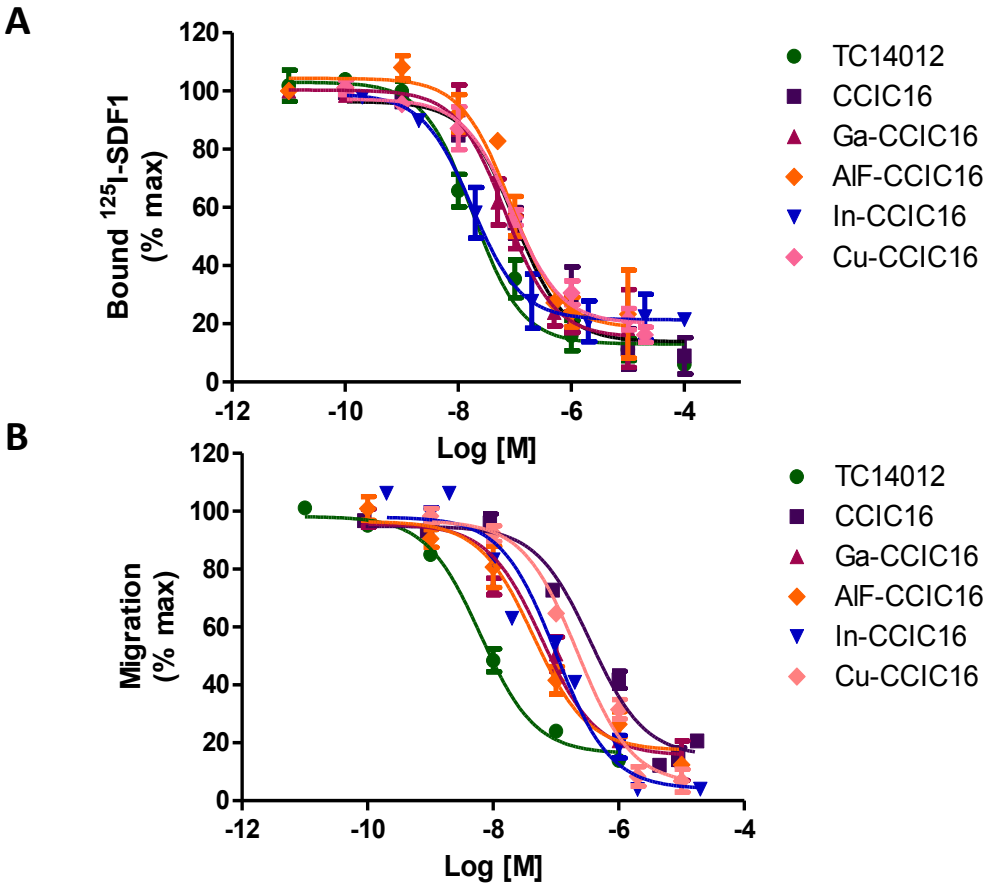

Figure 27. *In vitro* assessment of CCIC16 antagonism

A Inhibition of [^{125}I]SDF1α binding to U87.CD4.CXCR4 cells by indicated concentrations of antagonists. Curves shown are representative of at least 3 independent experiments, with error bars showing the SEM. Refer to section 2.11i. **B** Inhibition of CXCR4-mediated migration at 3 h in Jurkat cells. Curves shown are representative of at least 3 independent experiments, with error bars showing the SEM. Refer to section 2.12.

Table 6. Summary of the effects of ion chelation upon CCIC16 potency of CXCR4 binding and antagonism *in vitro*

Compound	Binding Assay (nM)	Migration Assay (nM)
TC14012	18.2	6.3
CCIC16	102.3	355.7
Ga-CCIC16	69.6	60.7
AlF-CCIC16	84.3	43.9
In-CCIC16	17.6	100.0
Cu-CCIC16	90.9	221.5

radionuclide as described in chapter 1.7 made ^{68}Ga-CCIC16 an obvious target for development as a PET tracer.

3.23 - *Investigation of specificity of [^{68}Ga]-CCIC16 for CXCR4*

In order to determine whether ^{68}Ga-CCIC16 could selectively label CXCR4-expressing cell lines, 0.74 MBq of the tracer was incubated with U87.CD4 and U87.CD4.CXCR4 cells for 60 minutes before measurement of bound radioactivity as described in section 2.13; it was found that ^{68}Ga-CCIC16 uptake was significantly higher in U87.CD4.CXCR4 cells than in the CXCR4-negative U87.CD4 cells by a mean of 3.1-fold. A 15 minute preincubation with 10 µM Ga-CCIC16 prevented this increased uptake in U87.CD4.CXCR4 cells, suggesting that uptake of radiotracer onto the cells was specific to CXCR4 expression (figure 28).

3.24 - *In vivo validation of [^{68}Ga]-CCIC16*

With evidence of specificity for CXCR4, it was decided to further assess the potential of [^{68}Ga]-CCIC16 as a CXCR4-targeting PET imaging tracer though *in vivo* imaging experiments as described in section 2.15i. To this end, BALB/c nu/nu mice bearing either CXCR4-negative U87.CD4 or CXCR4-positive U87.CD4.CXCR4 (n=6, 5, respectively) were injected with 3.7 MBq [^{68}Ga]CCIC16 at the commencement of a 60 minute dynamic PET/CT scan. As figure 29A and 29B show, there was a clear difference in radiotracer uptake between the two tumour types at 60 minutes. This occurred as a result of a time-dependent

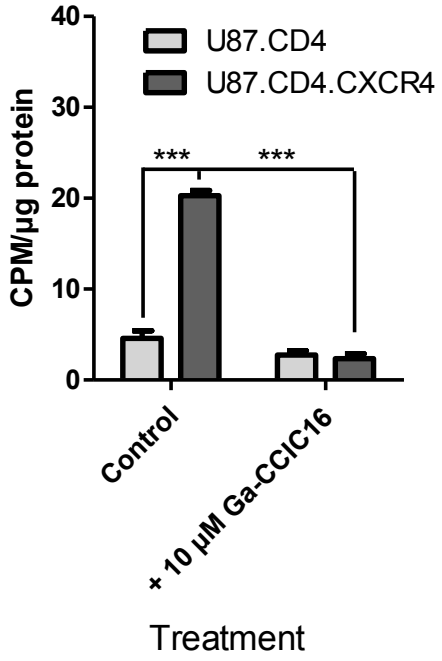

Figure 28. Uptake of [^{68}Ga]-CCIC16 *in vitro* following a 60 min incubation.

Uptake of 0.74 MBq ^{68}Ga]-CCIC16 in U87.CD4 and U87.CD4.CXCR4 cells. Figure shown is representative example of 3 independent experiments (*** signifies P≤0.001; error bars show SEM). Refer to section 2.13.

accumulation of radiotracer within the U87.CD4.CXCR4 tumours, whereas radiotracer accumulation within the CXCR4-negative U87.CD4 tumours steadily dropped following an initial peak at around 10 minutes post-injection (figure 29C). This curve shape is indicative of washout of [^{68}Ga]-CCIC16 from the U87.CD4 tumours, and is mirrored by tumour uptake in mice bearing U87.CD4.CXCR4 tumours that had been coinjected with 50 µg Ga-CCIC16 (>50-fold of injected radioactive dose; n=5), suggesting that the accumulation of radiotracer within the U87.CD4.CXCR4 tumours was specific to its increased CXCR4 expression. This was supported by the fact that the standardised uptake

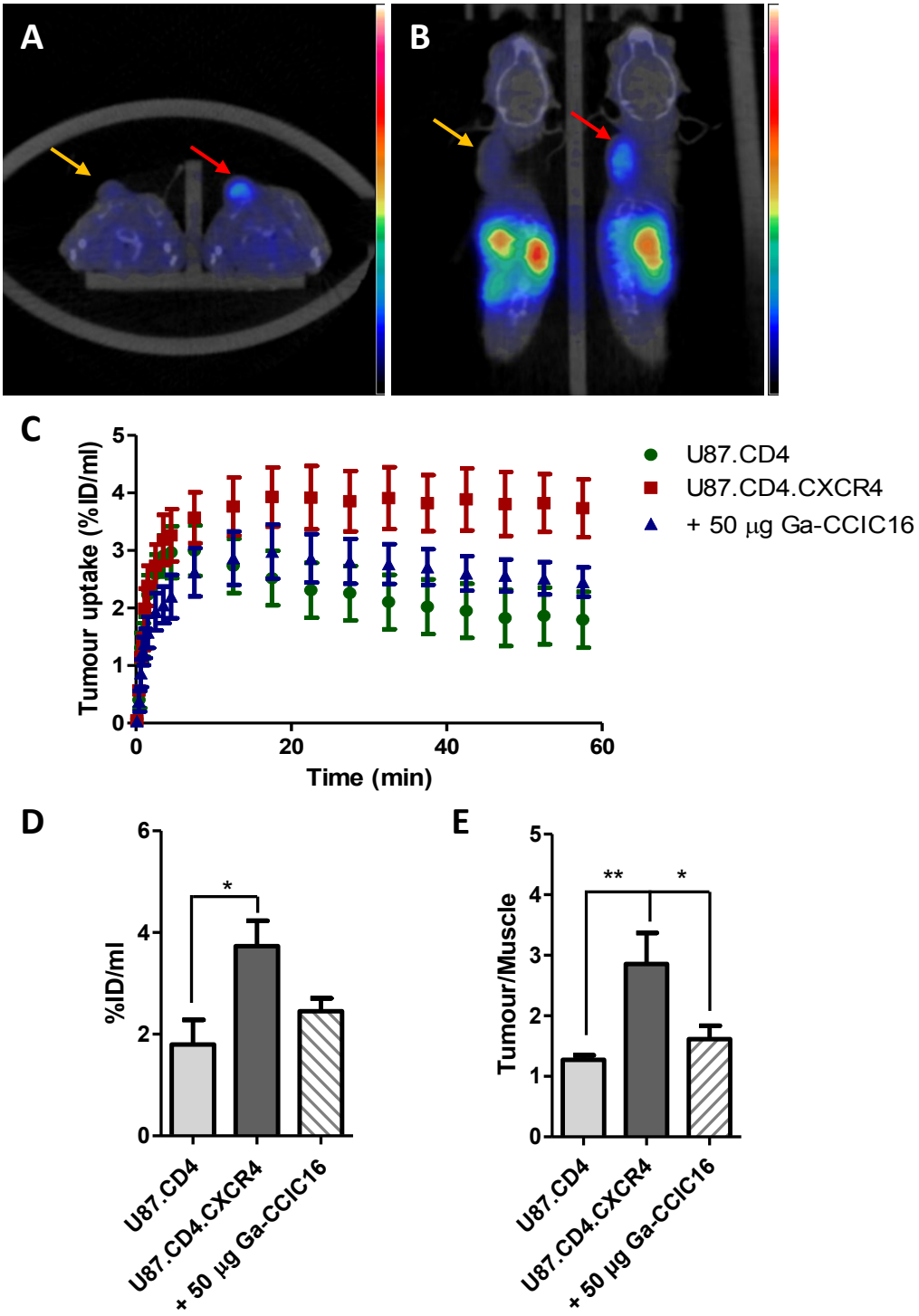

Figure 29. PET/CT imaging following a 3.7 MBq injection of [^{68}Ga]-CCIC16 in BALB/c nu/nu mice bearing U87.CD4 (yellow arrow) and U87.CD4.CXCR4 (red arrow) tumours, and U87.CD4.CXCR4 tumour-bearing mice that had been coinjected with 50 µg Ga-CCIC16 (n=6, 5, 5 respectively)

Representative **A** transverse and **B** sagittal merged PET/CT images of radiotracer at 60 minutes post-injection. **C** Time-activity curve of dynamic uptake of radioactivity in tumours over 60 mins. **D** Standardised uptake value at 60 minutes (SUV_{60}) and **E** tumour-to-muscle ratios of tumours. Error bars show SEM ; * signifies P≤0.05, ** signifies P≤P.01). Refer to section 2.15i.

value at 60 minutes (SUV_{60}) was significantly higher in U87.CD4.CXCR4 tumours than in the U87.CD4.CXCR4 tumours. Furthermore, the tumour-to-muscle ratios for the mice bearing these different tumour types were also significantly different, with the increase in this ratio within U87.CD4.CXCR4 tumours almost entirely blocked by the coinjection of the cold Ga-CCIC16 peptide.

The biodistribution of the radiotracer at 60 minutes (U87.CD4 tumour bearing n=3; U87.CD4.CXCR4 tumour bearing n=4) experiment conducted as described in section 2.15iii) within the mice was largely located within the liver, gallbladder, kidneys and urine (figure 30A and table 7), consistent with hepatic and urinary routes of excretion. Other sites of notable radiotracer uptake include the bone and spleen. The lack of significant reductions in tracer uptake within the bone and spleen following coinjection of 50 μg Ga-CCIC16 (n=5) suggest that the uptake in these areas may not have been CXCR4-specific, although CXCR4 expression has been reported in both these tissues (Shao *et al*., 2011, Federsppiel *et al*., 1993); alternatively, the sensitivity of the technique may not be high enough to discriminate the lower levels of expression likely associated with these tissues. Despite this possibility, it is apparent that [^{68}Ga]-CCIC16 allows the differentiation of tumours of high and low CXCR4 expression.

Given that peptidic compounds such as [^{68}Ga]-CCIC16 are notorious for poor bioavailability as a result of metabolism and clearance (Craik *et al*., 2013), it was

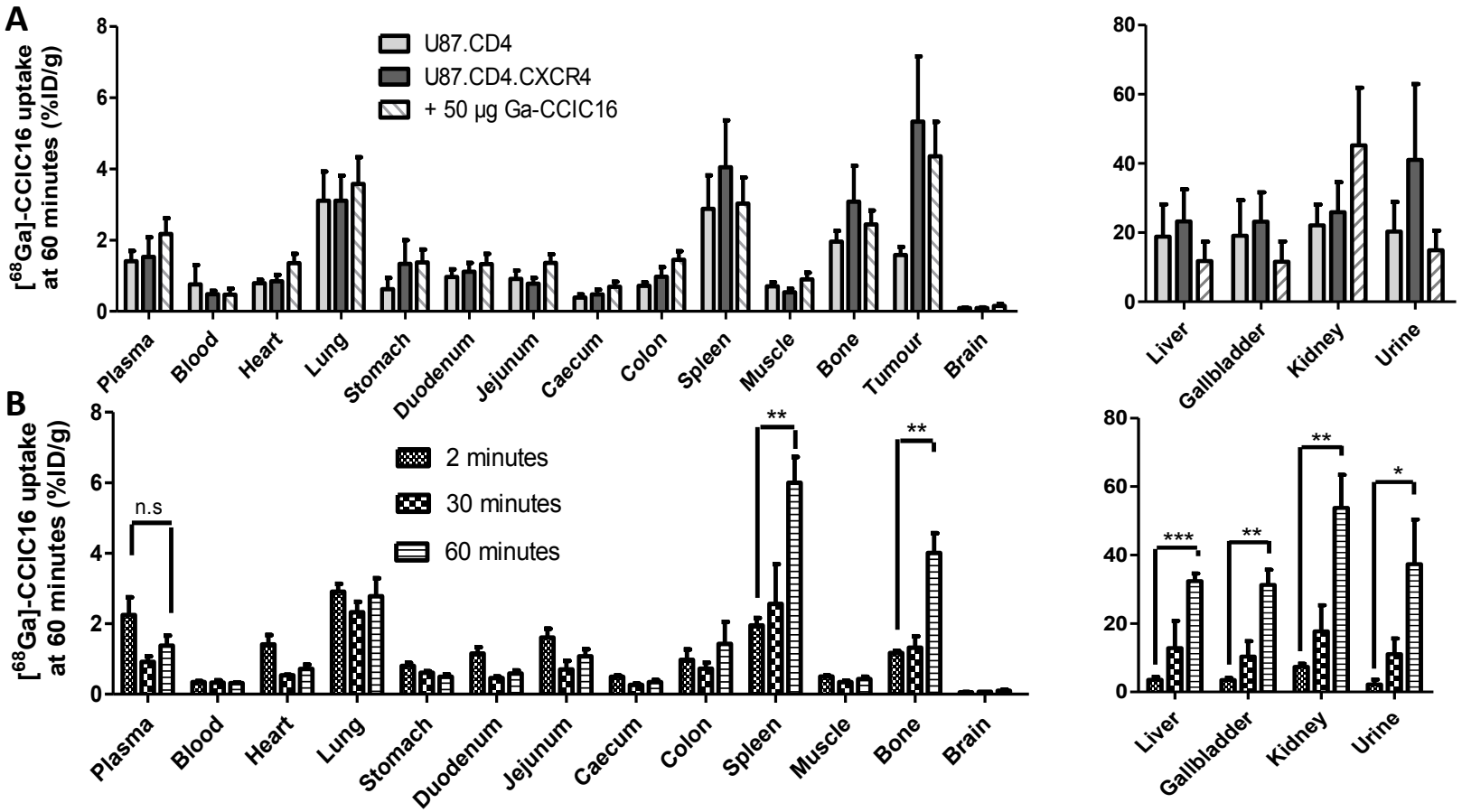

Figure 30. Biodistribution of [^{68}Ga]-CCIC16 A in BALB/c nu/nu mice bearing U87.CD4 or U87.CD4.CXCR4 tumours at 60 min post-injection, and blockade in U87.CD4.CXCR4-bearing mice by coinjection of 50 µg Ga-CCIC16 [n = 3, 4 and 5, respectively], and **B** in healthy BALB/c mice at 2 minutes, 30 minutes and 60 min post-injection (n=6, 4 and 4). Refer to section 2.15iii for protocol details.

Table 7. Biodistribution of 3.7 MBq [^{68}Ga]-CCIC16 at 60 minutes in BALB/c mice bearing U87.CD4 and U87.CD4.CXCR4 tumours, and in U87.CD4.CXCR4 tumour-bearing mice that had been coinjected with 50 µg Ga-CCIC16 (n=3, 4 and 5, respectively; refer to section 2.15iii)

	Biodistribution [^{68}Ga]-CCIC16 at 60 minutes (**%ID/g** ± SEM)	
Tissue	**No treatment**	**50 µg Ga-CCIC16**
Plasma	**1.467** ± 0.290	**2.174** ± 0.441
Blood	**0.617** ± 0.161	**0.467** ± 0.164
Heart	**0.817** ± 0.093	**1.351** ± 0.267
Lung	**3.104** ± 0.513	**3.573** ± 0.755
Liver	**21.034** ± 6.154	**11.799** ± 5.584
Gallbladder	**21.129** ± 6.221	**11.552** ± 5.848
Stomach	**0.977** ± 0.367	**1.375** ± 0.359
Duodenum	**1.037** ± 0.155	**1.325** ± 0.290
Jejunum	**0.840** ± 0.136	**1.362** ± 0.238
Caecum	**0.432** ± 0.075	**0.689** ± 0.140
Colon	**0.844** ± 0.139	**1.447** ± 0.243
Spleen	**3.462** ± 0.782	**3.027** ± 0.731
Kidney	**24.004** ± 4.920	**45.212** ± 16.688
Muscle	**0.619** ± 0.078	**0.899** ± 0.187
Bone	**2.518** ± 0.531	**2.443** ± 0.386
Brain	**0.093** ± 0.010	**0.149** ± 0.063
Urine	**30.667** ± 11.590	**66.298** ± 51.603
U87.CD4 tumour	**1.582** ± 0.228	
U87.CD4.CXCR4 tumour	**5.329** ± 1.836	**4.356** ± 0.970
U87.CD4 Tumour/Muscle	**2.373** ± 0.337	
U87.CD4.CXCR4 Tumour/Muscle	**9.502** ± 1.709	**4.839** ± 0.751
U87.CD4 Tumour/Plasma	**1.175** ± 0.118	
U87.CD4.CXCR4 Tumour/Plasma	**4.571** ± 1.525	**1.945** ± 0.259

decided to conduct time-course biodistribution and metabolism experiments (described in section 2.15iii and 2.16, respectively) in order to observe the clearance of [^{68}Ga]-CCIC16 over time, and to determine whether metabolism of the compound may play a significant role in the tracer's bioavailability. Non-tumour-bearing BALB/c subjects were injected with 7.4-11.1 MBq [^{68}Ga]-CCIC16 and sacrificed at 2, 30 and 60 minutes post-injection (n=6, 4, 4, respectively). It was seen that there were time-dependent increases in radiotracer accumulation

in the liver, gallbladder, kidneys and urine over the course of 60 minutes, with maximum accumulation in all these tissues at 60 minutes. In agreement with biodistribution studies at 60 minutes (figure 30A and table 7), time-dependent increases in tracer uptake were also observed in the bone and spleen (figure 30B). Tracer presence in plasma did not significantly decrease at 60 minutes, a considerable improvement in clearance characteristics as compared to [^{18}F]-CCIC7, which rapidly accumulated in the kidneys and liver (reaching maximal uptake in these tissues within a mere 5 minutes), resulting in a dramatic decline in radiotracer presence within the plasma within 30 minutes (figure 16).

Alongside the collection of biodistribution data for this experiment, tissues were also collected to assess the metabolism status of [^{68}Ga]-CCIC16 within these tissues at various time-points (n=3), as described in section 2.16. It was seen that the radiotracer was fairly serum-stable, with a mean 33% parent compound remaining in circulation at 15 minutes (figure 31 and table 8). However, a high proportion (>92%) of tracer within the urine had metabolised to more hydrophilic ^{68}Ga-containing metabolite fragments at every time-point tested from 2 minutes post-injection. Despite this, the relative abundance of unmetabolised tracer circulating in the plasma was very encouraging, as it suggests that the serum stability of the peptide was sufficient to allow the time-dependent uptake of [^{68}Ga]-CCIC16 observed in the imaging studies at 60 minutes (figure 28).

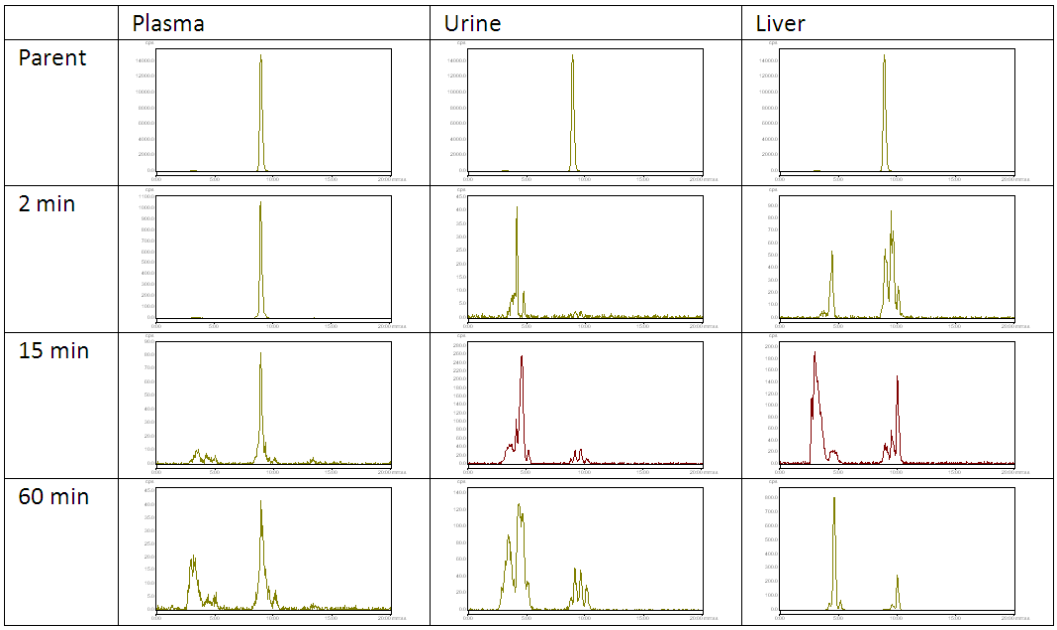

Figure 31. HPLC traces showing parent compound and metabolite peaks in liver and plasma extracts of BALB/c mice following 2, 15, and 60 minute inoculation of 7.4-11.1 MBq [^{68}Ga]-CCIC16 (n=3). Representative radiochromatograms of acetonitrile extracts from mouse plasma and homogenised liver samples at the indicated time points.

Table 8. *In vivo* metabolism of compound [^{68}Ga]-CCIC16 at selected time points, showing the percentage of [^{68}Ga]GaCCIC16 present in plasma, liver and urine extracts (n=3)

n=3	**Plasma**	**Urine**	**Liver**
2 mins	94 ± 7%	5 ± 4%	5 ± 2%
15 mins	43 ± 21%	6 ± 1%	3 ± 3%
60 mis	33 ± 12%	8 ± 1%	5 ± 4%

3.25 - *Use of [^{68}Ga]-CCIC16 to identify 17AAG-induced changes in CXCR4 expression*

Following the success of [^{68}Ga]-CCIC16 in identifying tumours of varying CXCR4 expression, it was considered whether the tracer could adapted for use as a non-invasive tool to detect response to treatment, in particular, the degradation of CXCR4 as a marker of response to HSP90 inhibitors. The following data shown is

the result of an investigation to determine whether [^{68}Ga]-CCIC16 could be used to noninvasively detect changes in CXCR4 expression induced by 17AAG, an HSP90 inhibitor. The first task was to confirm whether treatment of U87.CD4.CXCR4 cells with 17AAG (as described in section 2.17i) could result in the expected decrease in CXCR4 expression. As figure 32 shows, CXCR4 expression does indeed decrease markedly with increasing dose and duration of 17AAG treatment, to a maximum of 50% following 48 hours treatment with 500 nM 17AAG. In support of the involvement of HSP90 inhibition in the decrease of CXCR4 expression, the expression of HSP70 was also shown to be increased by incubation with 17AAG. HSP70 expression has been shown to be induced by HSP90 inhibition through withdrawal of HSP90-mediated suppression of heat shock factor 1 (HSF1)(Kim *et al.*, 1999). These findings confirm the ability of 24 and 48 hour treatments of 100-500 nM 17AAG to reduce functionality of HSP90 and the downregulation of CXCR4 protein expression, a client of HSP90.

With the above significant reduction in CXCR4 expression observed following 48 hours treatment, it was decided to assess the ability of [^{68}Ga]-CCIC16 to differentiate between U87.CD4.CXCR4 cells that were either treated with 100 nM 17AAG for 48 hours or treated only with the vehicle using an *in vitro* uptake assay (as described in section 2.17i). The 100 nM dose was chosen over the more effective 500 nM dose due to the considerably reduced viability of U87.CD4.CXCR4 cells following 48 hours treatment with 500 nM 17AAG. The 1.4-fold difference in CXCR4 expression between U87.CD4.CXCR4 cells treated with

100 nM 17AAG for 48 hours and untreated cells is considerably less than the 10-fold difference in expression between U87.CD4 and U87.CD4.CXCR4 cell models used in the previous uptake assay experiment (figure 28), so it was encouraging to observe that the difference in expression of the two groups could be detected in the form of a mean 1.6-fold reduction in [^{68}Ga]-CCIC16 uptake, which compares very favourably with differences in protein expression (figure 32). Uptake in both 17AAG-treated and untreated cells was reduced by preincubation with 10 µM cold Ga-CCIC16, confirming CXCR4-dependent uptake of [^{68}Ga]-CCIC16 in the cell lines.

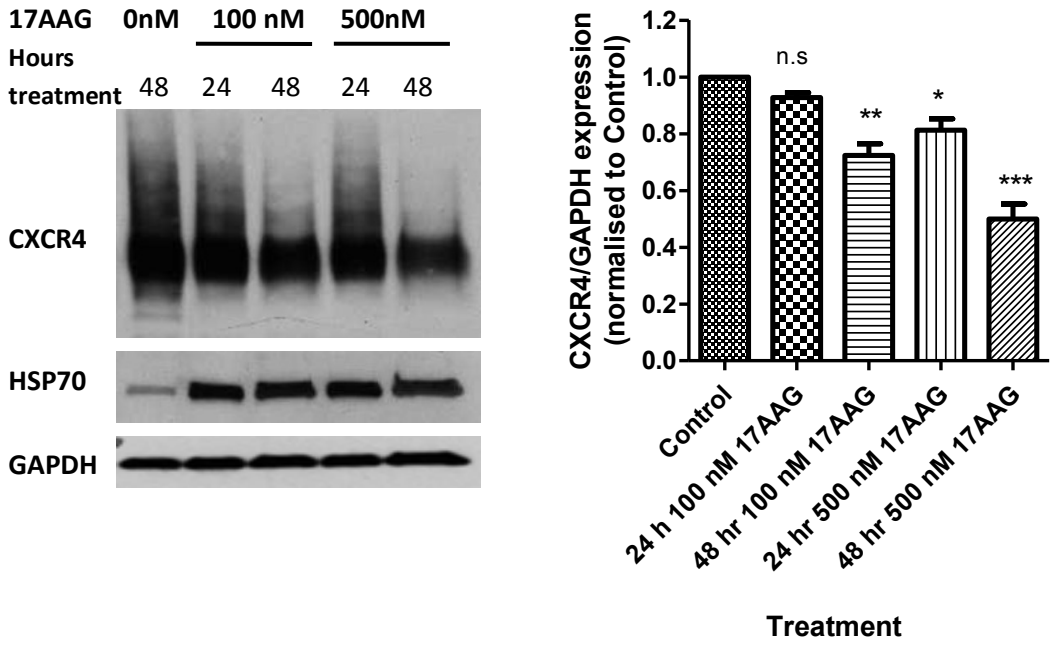

Figure 32. Effect of 17AAG treatment upon protein expression

Protein expression in U87.CD4.CXCR4 cells treated at the indicated concentration and length of time was determined by western blot. A Representative immunoblot showing expression of CXCR4, HSP70 and GAPDH. B Densitometric analysis of CXCR4 expression, normalised to GAPDH expression and to the control (n=3 ; error bars show SEM ; * signifies P≤0.05, ** signifies P≤0.01, *** signifies P≤0.001). Refer to section 2.17i.

As a result of the promising findings above, it was decided to further examine the ability of [^{68}Ga]-CCIC16 to detect 17AAG-induced changes in CXCR4 expression by beginning an *in vivo* experiment, where mice bearing U87.CD4.CXCR4 tumours were either treated with 80 mg/kg 17AAG or vehicle control daily for 48 hours prior to injection with 3.7 MBq [^{68}Ga]-CCIC16 (n=6, 5, respectively), as described in section 2.17ii. Unfortunately at this stage in the project there were no imaging facilities available due to the closure of the Biological Imaging Centre (BIC) at Imperial College London, and so the only *in vivo* investigations that could be performed were biodistribution experiments. Disappointingly, there was no difference in uptake of the radiotracer in the tumours of 17AAG-treated mice

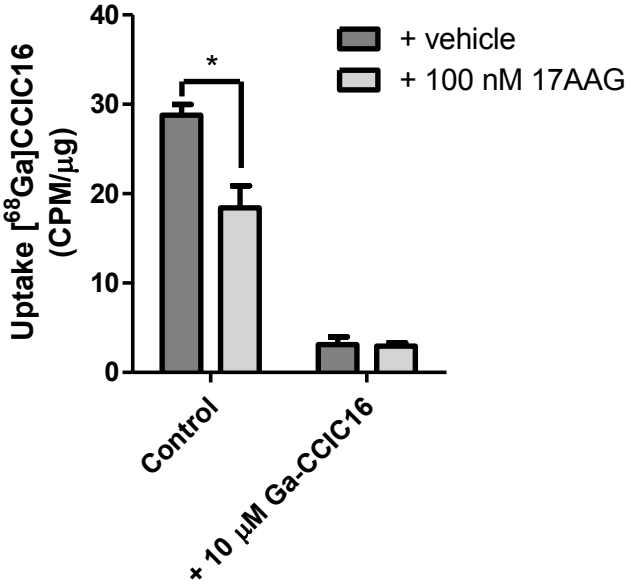

Figure 33. [^{68}Ga]-CCIC16 uptake in U87.CD4.CXCR4 cells either treated or untreated with 100 nM 17AAG for 48 hours.

Representative figure of three independent experiments. Error bars show SEM (* signifies P=0.05). Refer to section 2.17i.

(figure 34). There were also no notable differences in the spleen and bone of treated and untreated mice (table 9), which had been associated with time-dependent increases in [^{68}Ga]-CCIC16 uptake (figure 30B), possibly as a result of their endogenous CXCR4 expression.

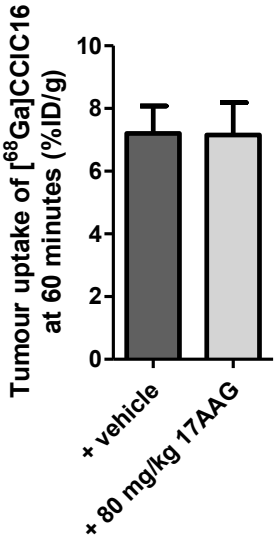

Figure 34. Uptake of [^{68}Ga]-CCIC16 at 60 minutes in U87.CD4.CXCR4 tumours of mice treated with either 80 mg/kg 17AAG daily for 48 hours or vehicle

Error bars show SEM (n=6, 5, respectively). Refer to section 2.17ii.

It was considered that the dose of 17AAG administered may not have been sufficient to result in CXCR4 degradation within the tumour, or alternatively that the reductions in CXCR4 expression associated with U87.CD4.CXCR4 tumour growth *in vivo* (figure 25) might have reduced the maximum fold-difference in CXCR4 expression achievable *in vivo*. Thus protein analysis of CXCR4 expression was carried out on the homogenised snap-frozen tumour samples by western blot (as described in section 2.17i and 2.4ii). At first glance it appeared that daily treatment with 80 mg/kg 17AAG for 48 hours resulted in an *increase* in CXCR4 expression in U87.CD4.CXCR4 tumours (figure 35A), rather than the expected

Table 9. Biodistribution of [^{68}Ga]-CCIC16 at 60 minutes in U87.CD4.CXCR4 tumour-bearing mice treated with either 80 mg/kg 17AAG daily for 48 hours or vehicle (n=6, 5, respectively)

	Biodistribution [^{68}Ga]CCIC16 at 60 minutes (**%ID/g** ± SEM)	
Tissue	**Vehicle**	**80 mg/kg 17AAG**
Plasma	**1.681** ± 0.366	**1.568** ± 0.247
Blood	**0.552** ± 0.101	**0.548** ± 0.072
Heart	**1.389** ± 0.175	**1.23** ± 0.154
Lung	**4.728** ± 0.554	**4.595** ± 0.492
Liver	**18.857** ± 2.758	**16.656** ± 1.402
Gallbladder	**25.488** ± 2.903	**22.022** ± 2.762
Stomach	**0.591** ± 0.164	**0.374** ± 0.081
Duodenum	**1.253** ± 0.160	**1.252** ± 0.149
Jejunum	**1.133** ± 0.202	**1.144** ± 0.133
Caecum	**0.954** ± 0.173	**0.743** ± 0.129
Colon	**1.456** ± 0.418	**1.271** ± 0.160
Spleen	**4.630** ± 0.688	**5.072** ± 0.547
Kidney	**36.884** ± 6.444	**39.378** ± 6.560
Muscle	**1.152** ± 0.276	**0.873** ± 0.122
Bone	**4.737** ± 0.649	**4.755** ± 0.997
Brain	**0.127** ± 0.015	**0.132** ± 0.018
Urine	**42.968** ± 11.611	**48.217** ± 8.681
U87.CD4.CXCR4 Tumour	**7.208** ± 0.874	**7.153** ± 1.037
U87.CD4.CXCR4 Tumour/Muscle	**7.194** ± 1.074	**8.522** ± 1.316
U87.CD4.CXCR4 Tumour/Plasma	**4.691** ± 0.653	**5.442** ±1.618

decrease, although this difference was determined to be nonsignificant following densitometric analysis (figure 35B). However, this unexpected mean 2-fold increase was seen in mice that had been treated in separate cohorts, and so had been treated and processed on separate occasions, which would appear to preclude the possibility of investigator error (for example confusion of the subject groups). Furthermore, this finding coincided with a statistically significant mean 3.5-fold increase in HSP70 expression, in line with expectations for HSP90 inhibition. The reason for the unexpected departure in CXCR4 expression *in vivo* as compared to that predicted by the *in vitro* data (figures 32

and 33) is currently unconfirmed; however potential reasons are discussed further in chapter 5.

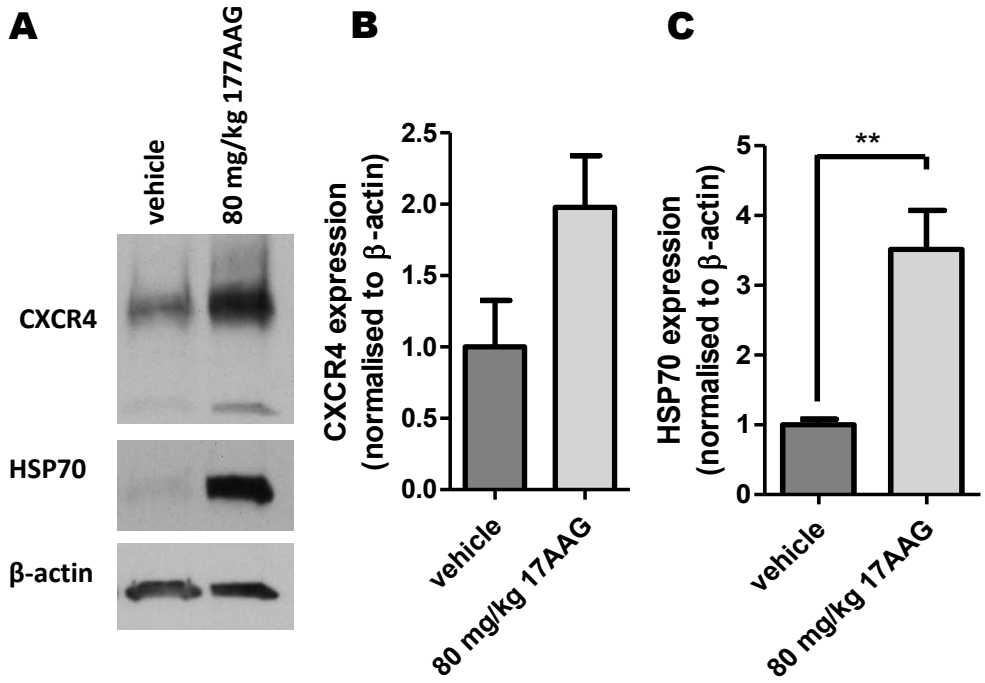

Figure 35. Assessment of the effect of 48 hours daily 80 mg/kg 17AAG treatment upon the expression of HSP90 targets CXCR4 and HSP70 in U87.CD4.CXCR4 tumours *in vivo*

A Representative western blot of homogenised snap-frozen tumour samples with CXCR4, HSP70 and β-actin antibodies. Densitometric analysis of **B** CXCR4 and **C** HSP70 expression in tumour samples, normalised to β-actin and mean expression in vehicle-treated samples. Error bars show SEM; (vehicle n=5, treated n=6); ** signifies P≤0.01.

While it is possible that with increased sample sizes that a significant difference in CXCR4 expression between the two groups of treated tumour samples might reach significance, the fact remains that [^{68}Ga]-CCIC16 was unable to differentiate between the tumours of treated and untreated subjects to *any* discernible degree (figure 33), let alone with the confidence of statistical significance. However, it is likely that insufficient difference in CXCR4 expression was the root cause of the tracer's failure in this investigation.

3.3- Design and structure-activity relationships of pentapeptide library, and characterisation of [^{18}F]CCIC15 and [^{18}F]CCIC30

3.31 - Design of pentapeptide library

As discussed in the introduction, tetra- and penta-peptide derivatives of T140 have previously been found to antagonise CXCR4 with a similar efficacy to T140, with cyclisation of pharmacophore enabling downsizing and a reduction in peptide character (Tanaka *et al.*, 2008). However, as chapter 3.1 shows, modification of the FC131 structure to include a PEG2-FB functional group which was designed to allow incorporation of ^{18}F into the pentapeptide structure resulted in a compound with lacklustre affinity for CXCR4, and extremely poor bioavailability. It was theorised that the poor pharmacokinetics of [^{18}F]CCIC7 *in vivo* may have occurred as a result of the increased size of the pentapeptide structure. The increased size of the compound may also account for the modest antagonism CCIC7 bore against CXCR4-directed migration *in vitro*; the affinity of the antagonist for the receptor was possibly reduced by the linker group, as the FC131 structure upon which CCIC7 was based shows extremely high potency in CXCR4 antagonism (Tanaka *et al*., 2008).

Alternative methods of incorporating radionuclides suitable for PET into pentapeptides were therefore investigated, with a particular focus on size reduction. It was decided that a fluorinated triazole (FTA) group would be an

Table 10. Structures of novel pentapeptide CXCR4 antagonist library

Name	Structure	Simplified structure
FC131	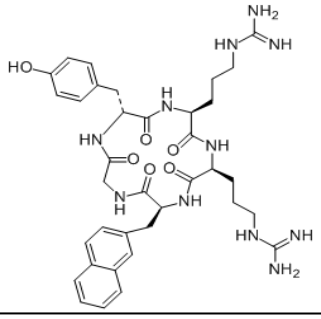	cyclo[tyr-arg-arg-nal-gly]
CCIC30	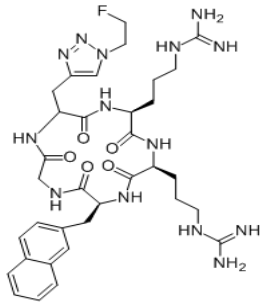	cyclo[FTA-arg-arg-nal-gly]
CCIC15	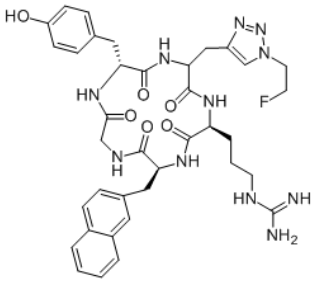	cyclo[tyr-FTA-arg-nal-gly]
CCIC29	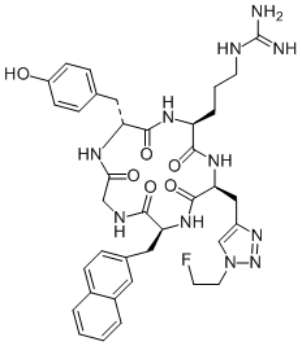	cyclo[tyr-arg-FTA-nal-gly]
CCIC36	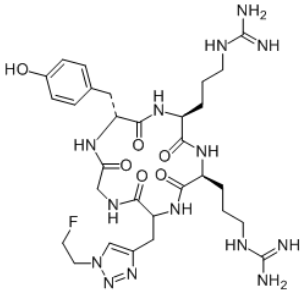	cyclo[tyr-arg-arg-FTA-gly]

appropriate conjugate, as it appeared to meet the desired criteria, both in terms of size and ease of radiolabelling. Furthermore, it rationalised that the best position of the FTA group should be determined, in order to optimise the affinity of the antagonist for CXCR4. Thus a small pentapeptide library was created for testing, comprised of novel antagonists CCIC15, CCIC29, CCIC30 and CCIC36 (see table 10).

3.32 - Assessment of CXCR4 antagonism, and modification of radioligand binding assay protocol

The first step in evaluating the above novel antagonist compounds for their potential as radiotracers was to assess their affinity for CXCR4. This proved to be more difficult than anticipated, as initial attempts to derive the half maximal inhibitory concentration (IC_{50}) of antagonists in a radioligand binding assay (as described in section 2.11i) resulted in values far higher than expected. For example, the antagonists CCIC29 and CCIC30 showed IC_{50} values of >50 µM and 5.6 µM, respectively (fig 36A), much greater than the values reported in the literature for the FC131 pentapeptide antagonist (5-150 nM (Tanaka *et al.*, 2008, Tamamura *et al.*, 2005c), on which their designs were based. Furthermore, when FC131 was purchased and investigated under the same assay conditions the IC_{50} value yielded by this protocol (method A, referred to in chapter 2.11i) was 18.9 ± 5.0 µM, over 120-fold higher than the expected value. This enormous discrepancy between the values from published literature and observed results suggested that the assay conditions for method A were not optimal, and that in

order to determine accurate IC_{50} values for the novel compounds an alternative method would have to be used.

As such, a number of different techniques were attempted with no success, until the implementation of a modified procedure (method B, described in chapter 2.11ii) which used a PBS-based buffer for the assay, with no added salts. Following this protocol, an IC_{50} of 600 nM was obtained for FC131, reflecting a 30-fold improvement on the previously used method. Subsequently, novel antagonists assayed using this method were found to show affinity for CXCR4, and were capable of competitively binding to CXCR4 in the presence of ^{125}I-SDF1. Most notably, the compounds CCIC15 and CCIC30 performed comparably to FC131, with IC50 values of 962 and 305 nM, respectively (figure 36B and table 11). In addition to the radioligand binding assay, the novel compounds were also assessed for CXCR4 antagonism using a transwell migration assay (according to the protocol described in 2.12), where their abilities to inhibit SDF1α-induced migration of Jurkat cells was determined (figure 36C). In this assay, FC131 inhibited migration with an IC50 value of 80 nM, far surpassing that of its nearest competitor, CCIC15. A complete overview of the IC50 values of the novel compounds in both the radioligand binding and migration assay is provided in table 11 (CCIC30 and CCIC36 was not tested due to a shortage of available compound), and enables a structure-activity relationship to be tentatively suggested. Substitution of the naphthylalanine with FTA at the C5 position

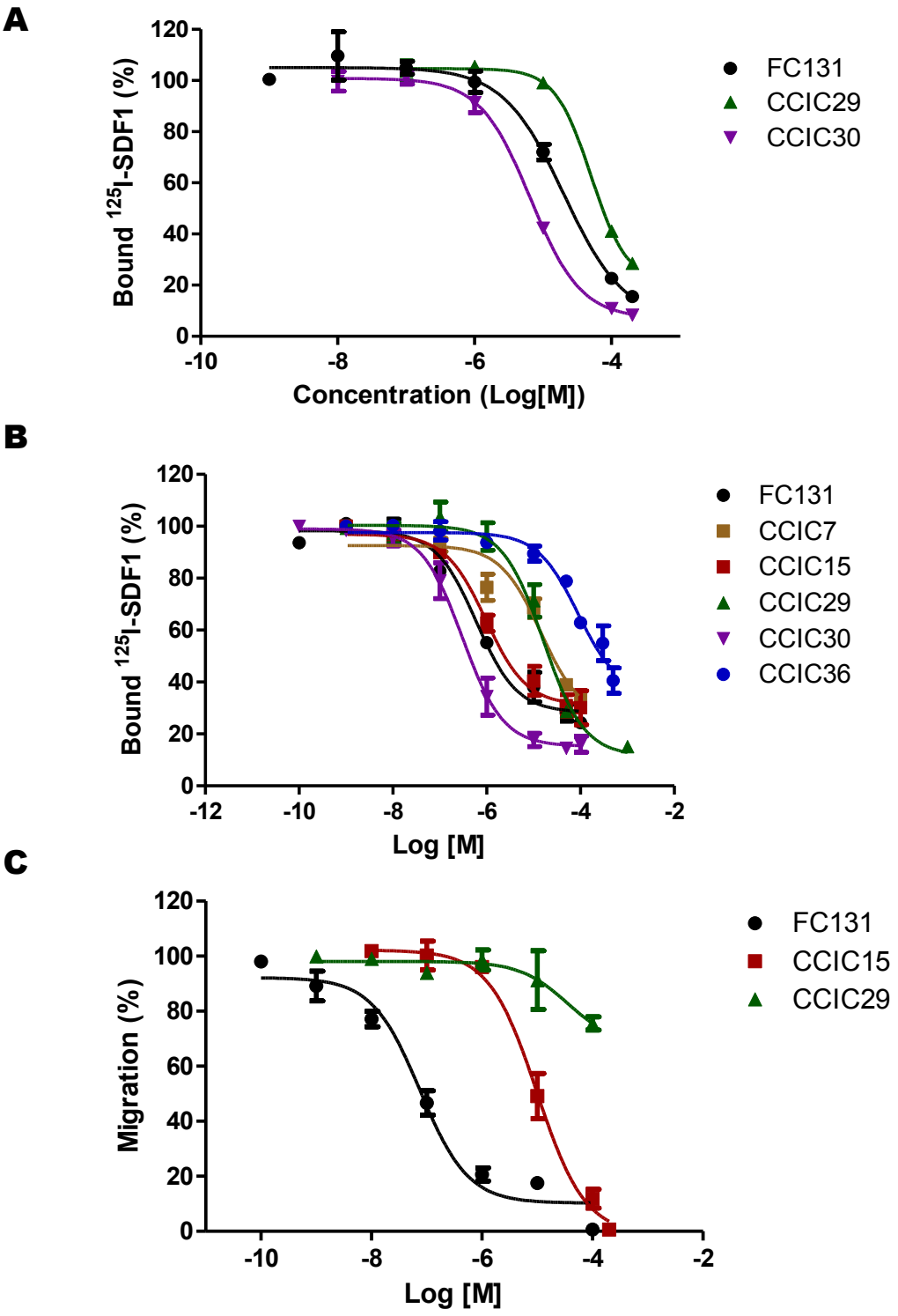

Figure 36. ***In vitro*** **characterisation of novel pentapeptide antagonists**

A Radioligand binding assay with FC131, CCIC29 and CCIC30 using method A (described in chapter 2.11i). **B** Radioligand binding assay with FC131 and other novel antagonists using improved method B (described in chapter 2.11ii). Note the apparent increase in potency of compounds shown compared to **A C** Inhibition of SDF1-mediated migration in Jurkat cells by FC131 and novel antagonists (refer to section 2.12). Curves shown are representative examples of 3 independent experiments, error bars show SEM.

Table 11. Summary of IC_{50} values for FC131 and novel pentapeptide compounds

Name	Structure	RBA IC_{50} (μM)	Migration assay IC_{50} (μM)
FC131	cyclo[tyr-arg-arg-nal-gly]	0.60	0.08
CCIC15	cyclo[tyr-FTA-arg-nal-gly]	0.96	9.93
CCIC29	cyclo[tyr-arg-FTA-nal-gly]	16.18	> 100
CCIC30	cyclo[FTA-arg-arg-nal-gly]	0.30	not tested
CCIC36	cyclo[tyr-arg-arg-FTA-gly]	> 100	not tested

Radioligand binding assay data refers to data collected using method B described in chapter 2.12ii. Migration assay data refers to data collected using protocol described in section 2.13. Compounds CCIC30 and CCIC36 were not tested in for their inhibition of migration due to a lack of available compound for the assay. N=3. Radioligand binding assay (RBA); Fluorotriazole (FTA).

resulted in the poorest affinity for CXCR4, whereas substitution at C2 or C5 (CCIC30 and CCIC15) showed the greatest potency in CXCR4 antagonism. It was therefore decided that these 2 compounds would be selected for further development as potential PET tracers by radiolabelling with ^{18}F. While the affinity of the ion-chelated CCIC16 T140 compound was higher than either CCIC15 or CCIC30, the potential for a more improved pharmacokinetic profile due to their cyclisation was anticipated, and so the novel compounds CCIC15 and CCIC30 were selected for further development as ^{18}F-radiolabelled PET tracers.

3.33 - Validation of [^{18}F]CCIC15 *in vitro* and *in vivo*

Following radiolabelling of [^{18}F]CCIC15, an initial experiment was required to determine the CXCR4 specificity of the radiotracer. To this end, the uptake of 0.37 MBq of [^{18}F]CCIC15 into U87.CD4 and U87.CD4. CXCR4 cell lines *in vitro* was investigated as described in section 2.13. As figure 37A shows, uptake of

[^{18}F]CCIC15 into U87.CD4.CXCR4 cells was on average 2-fold higher than in U87.CD4 cells at 60 minutes, suggesting CXCR4-dependent uptake. In confirmation, 15 minutes pre-incubation with 20 µM FC131 as a competitive inhibitor prevented this increase in uptake, confirming that uptake of [^{18}F]CCIC15 occurs in a CXCR4-specific manner.

Following this promising development, the potential of [^{18}F]CCIC15 was further investigated in its first *in vivo* experiment; unfortunately at this point in the programme there was an interruption in the use of imaging facilities following the closure of Biological Imaging Centre at Imperial College London, and the only *in vivo* studies that could take place at this time were biodistribution experiments. Biodistribution was conducted with U87.CD4.CXCR4 tumour-bearing mice at 60 minutes post-injection of 3.7 MBq [^{18}F]CCIC15 (n=3), as described in section 2.15iii. As can be seen in figure 37B, there was no detectable CXCR4-dependent uptake of [^{18}F]CCIC15 in the tumour, as there was no difference in tracer uptake within the tumour compared to muscle. The most notable sites of [^{18}F]CCIC15 accumulation were instead seen within the gallbladder, duodenum and urine of the animals, suggesting clearance of the tracer from the blood through hepatic and urinary routes of excretion. Given the lack of tumour uptake of [^{18}F]CCIC15, the *in vivo* experiments were curtailed in order to reduce the number of animal subjects used unnecessarily; it was considered possible that the potency of CCIC15 antagonism for CXCR4 may not have been sufficient to allow CXCR4-dependent uptake *in vivo*.

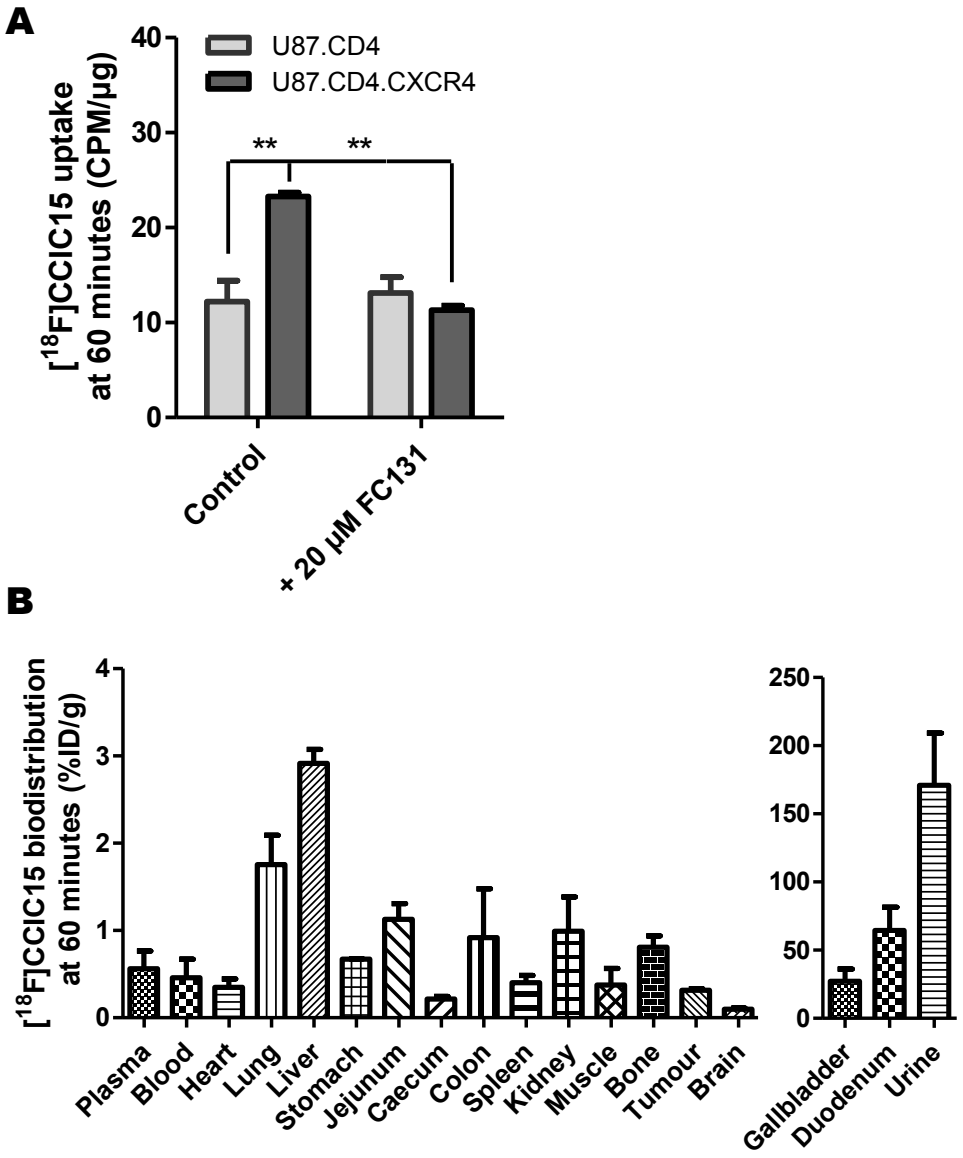

Figure 37. *In vitro* and *in vivo* uptake of [^{18}F]CCIC15 at 60 minutes

A Example of uptake of U87.CD4 and U87.CD4.CXCR4 cells with 0.37 MBq [^{18}F]CCIC15 at 60 minutes (n=3), as described in section 2.13. Cells were pre-treated for 15 mins with either 20 µM FC131 or inhibitor-naive media. **B** Biodistribution of 3.7 MBq [^{18}F]CCIC15 in BALB/c nu/nu mice bearing U87.CD4.CXCR4 tumours at 60 min post-injection (n=3) as described in 2.15iii. Error bars show SEM; ** signifies P≤0.01.

3.34 - Validation of [^{18}F]CCIC30 *in vitro* and *in vivo*

Given that CCIC30 had shown a higher affinity for CXCR4 than CCIC15, it was hoped that [^{18}F]CCIC30 might also show potential as a CXCR4-targeting

radiotracer. Indeed, the mean difference in tracer uptake at 60 minutes was 2-fold higher in U87.CD4 cells than in U87.CD4.CXCR4 cells *in vitro* (using the protocol described in section 2.13), the accumulation of which could be blocked by pre-treatment with 20 µM FC131 as a competitive inhibitor (figure 38), suggesting that uptake of [^{18}F]CCIC30 was specific to CXCR4 expression.

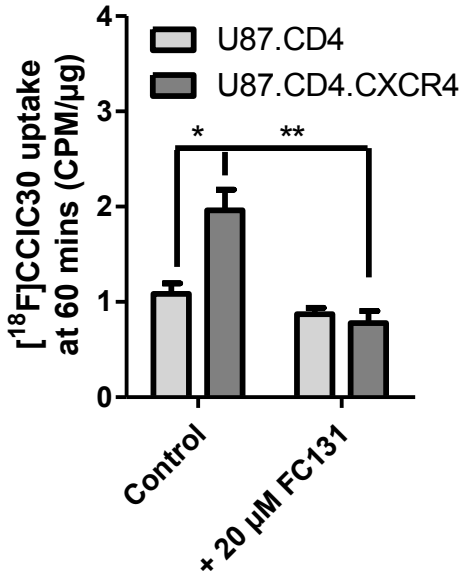

Figure 38. *In vitro* uptake of [^{18}F]CCIC30 at 60 minutes

U87.CD4 and U87.CD4.CXCR4 cells were incubated for 60 minutes with 0.37 MBq [^{18}F]CCIC30 following a 15 minute pre-treatment with either 20 µCi FC131 or untreated media, as dexribed in section 2.13. Figure shown is an example of 3 independent experiments. Error bars show SEM ; * signifies P≤0.05, ** signifies P≤0.01.

As a result of these promising *in vitro* findings, *in vivo* PET imaging experiments were planned (using the Genysis^4 benchtop scanner that was now available; refer to section 2.15ii for protocol; n =3). Initial experiments appeared to show a degree of promise, as the U87.CD4.CXCR4 tumour was visible against background uptake, especially at early time-points within the scan (figure 39).

Furthermore, biodistribution data (using the protocol described in section 2.15iii; n=3) showed a 3-fold difference in [^{18}F]CCIC30 uptake in the U87.CD4.CXCR4 tumour compared to the muscle, even at 60 minutes (figure 40). However, expansion of the experiment to include U87.CD4 tumour-bearing mice showed no difference in uptake between the two tumour groups at any time-point, and the time-activity curves (TACs) of radioactivity uptake in the tumour did not reflect the typical upward slope expected of TACs depicting radiotracer accumulation (such as seen for ^{68}Ga-CCIC16, figure 29C), but rather a downward slope from 5 minutes indicative of tracer washout. As with the results observed for [^{18}F]CCIC15, there was no significant difference in the biodistribution of [^{18}F]CCIC30 in U87.CD4 and U87.CD4.CXCR4 tumours at 60 minutes post-injection (figure 40). Biodistribution data for *in vivo* uptake of [^{18}F]CCIC30 also showed that the vast quantity of radioactivity was present within the urine, with additional sites of uptake at the liver and gallbladder, consistent with a predominantly urinary route of excretion.

It was initially considered that the reason for the this discouraging lack of CXCR4-dependent uptake in tumours might have been as a result of rapid tracer metabolism, in a similar manner to that seen for [^{18}F]CCIC7 (figure 31). Thus to rule out metabolism as a cause, a limited metabolism experiment was carried out at 2 time-points (n=1) in order to gain an insight into the stability of the compound *in vivo*. It was found that [^{18}F]CCIC30 was extremely stable in the plasma, liver, and urine samples of the mice tested (figure 41), with very little

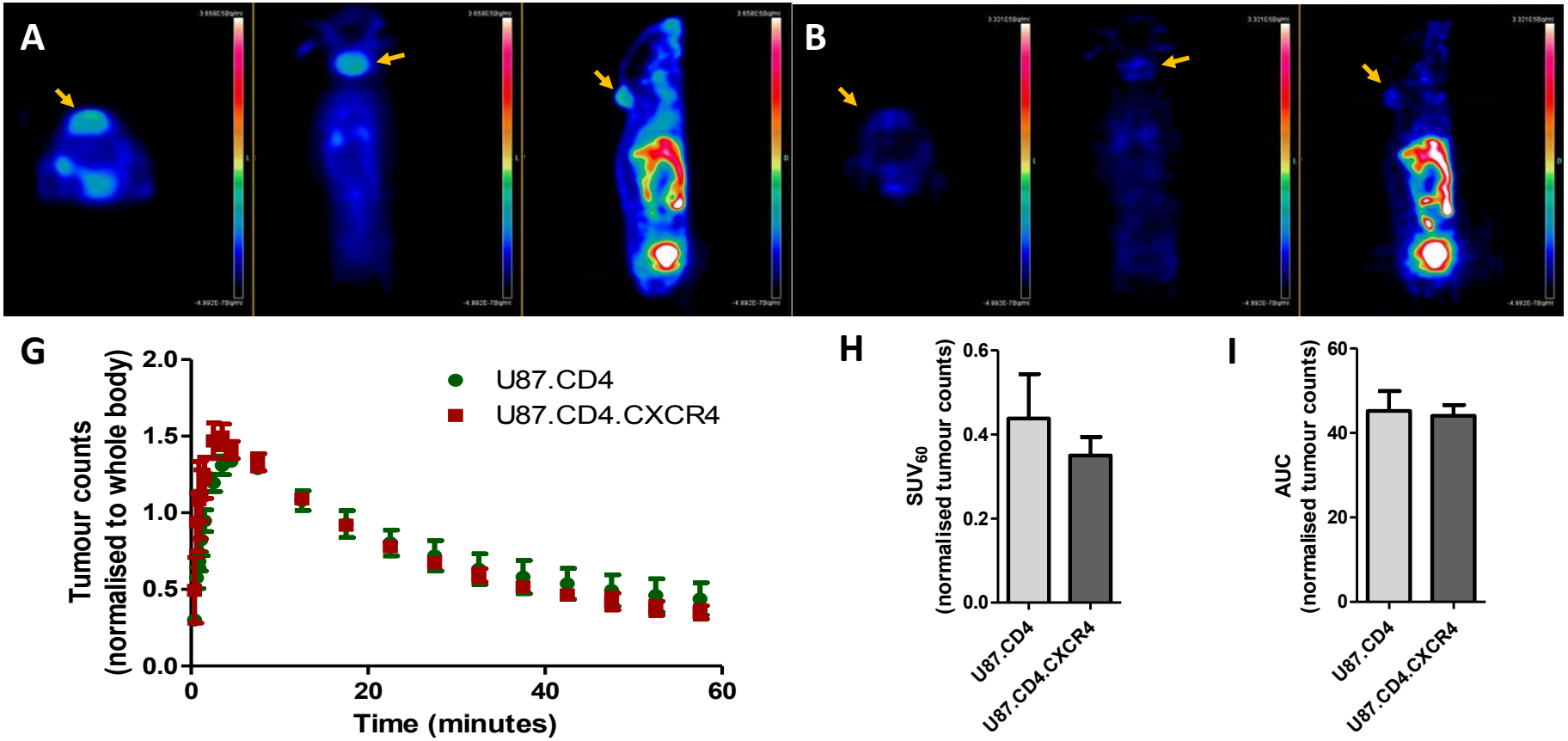

Figure 39. Dynamic PET imaging of 1.1 MBq [^{18}f]CCIC30 in U87.CD4 and U87.CD4.CXCR4 xenografts. Representative PET images in BALB/c nu/nu mouse bearing U87.CD4.CXCR4 tumour following 1.1 MBq [^{18}F]CCIC30 injection at **A** between 5 and 30 minutes and **B** at 60 minutes post-injection (refer to section 2.15ii). Transverse (left), coronal (middle) and sagittal (right) fields of view shown. Position of U87.CD4.CXCR4 tumour indicated by arrow. **G** Time-activity curve (TAC) of [^{18}F]CCIC30 uptake in tumours. **H** Standardised uptake value (SUV) at 60 minutes in tumours. **I** AUC values for tumours during 60 minute scan. Error bars show SEM (n=3).

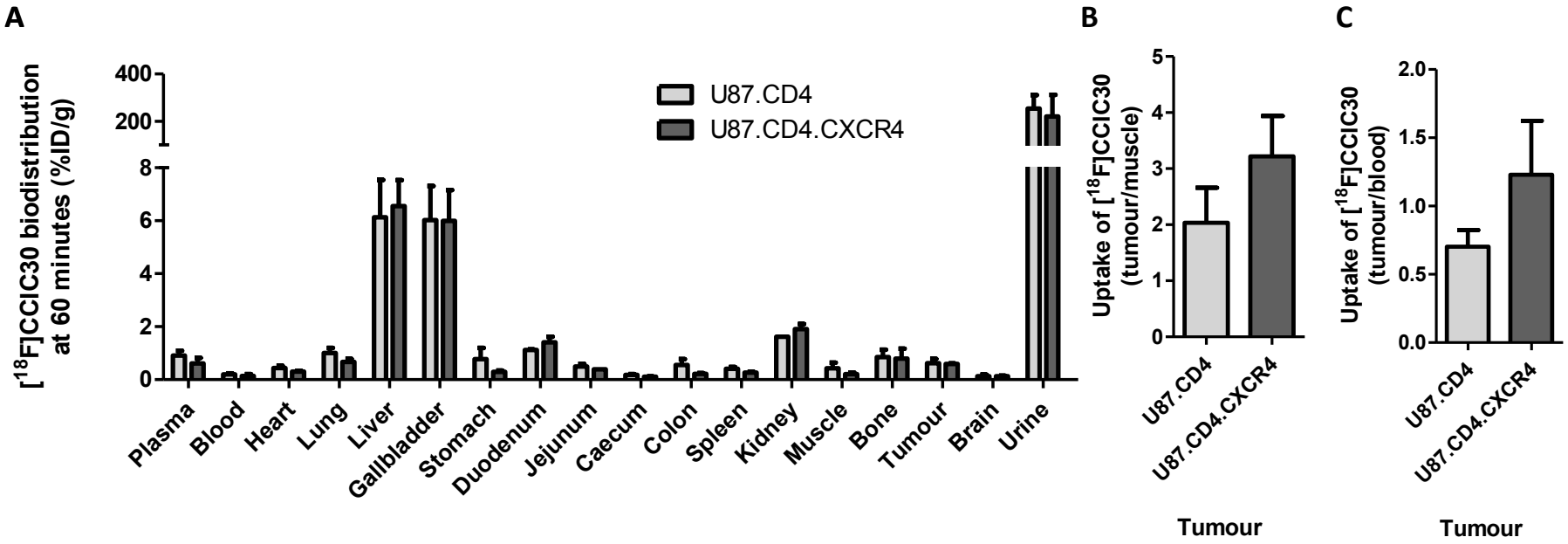

Figure 40. Biodistribution of 1.1MBq [^{18}F]CCIC30 in BALB/c nu/nu mice bearing U87.CD4 or U87.CD4.CXCR4 tumours at 60 min post-injection

A Tracer uptake in selected tissues **B** Tumour-to-muscle ratio and **C** tumour-to-blood ratio of U87.CD4 and U87.CD4.CXCR4 tumours, as calculated from biodistribution data. Error bars show SEM (n=3). Refer to section 2.15iii.

evidence of tracer metabolism within the plasma, liver or urine even as late as 60 minutes post-injection (92%, 88% and 85%, respectively); thus it seemed that [^{18}F]CCIC30 was considerably serum stable. Despite this, the tracer showed extremely poor pharmacokinetics due to rapid clearance from the blood to the urine, which likely affected the ability of the tracer to accumulate in CXCR4-expressing tumours.

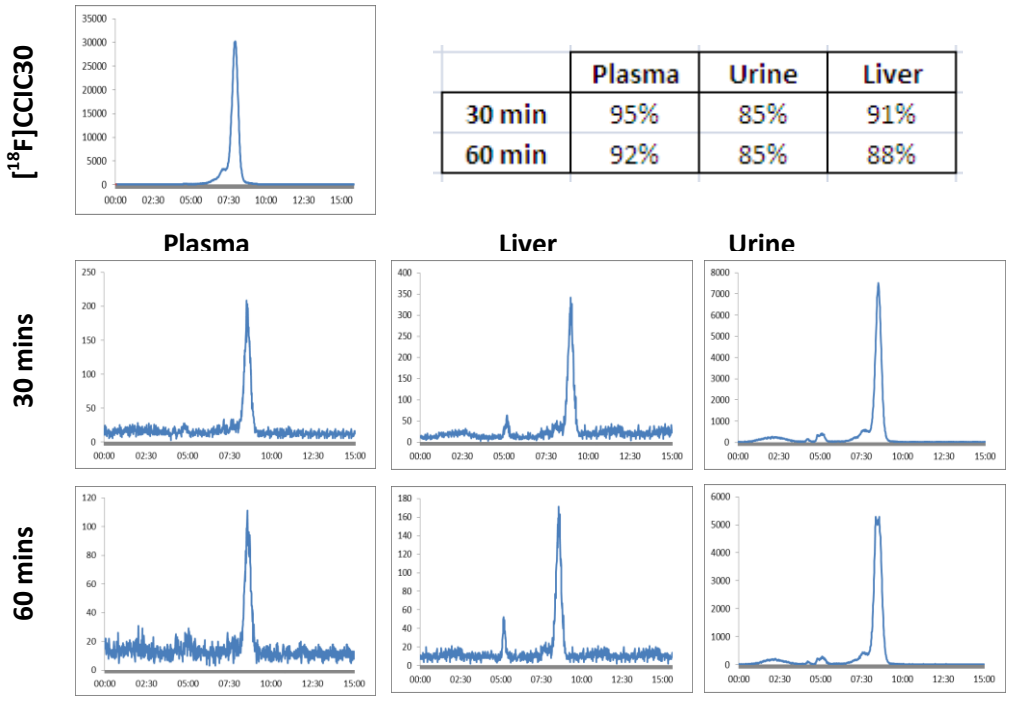

	Plasma	Urine	Liver
30 min	95%	85%	91%
60 min	92%	85%	88%

Figure 41. HPLC traces showing parent compound and metabolite peaks in liver and plasma extracts of BALB/c mice following 30 and 60 minute inoculation of 3.7 MBq [^{18}F]CCIC30. **R**adiochromatograms from acetonitrile extracts from mouse plasma and homogenised liver samples at the indicated time points (n=1). Refer to section 2.16.

3.35 - Overview of pentapeptide tracers [^{18}F]CCIC7, [^{18}F]CCIC15 and [^{18}F]CCIC30

None of the pentapeptide radiotracers investigated in this project (*i.e.* [^{18}F]CCIC7, [^{18}F]CCIC15 or [^{18}F]CCIC30), were successful in identifying CXCR4 expressing tumours *in vivo*. When the *in vivo* biodistribution data for the three novel pentapeptide tracers are compared (table 12 and 13; refer to section 2.15iii) it can be seen that despite their similarities in structure (as shown previously in figure 12 and table 10), the biodistribution of each tracer at 60 minutes were quite different. While the uptake of [^{18}F]CCIC7 was rapidly confined to the hepatic excretory pathway, hepatic uptake of [^{18}F]CCIC30 was comparatively low. [^{18}F]CCIC15 showed tracer uptake in the gallbladder and liver, but not the duodenum and jejunum as observed with [^{18}F]CCIC7, implying slower hepatic clearance. All tracers showed considerable renal/urinary excretion, yet no other to the same degree as [^{18}F]CCIC30, where uptake at 60 minutes was primarily confined. None of these tracers showed any appreciable uptake in endogenous sites of CXCR4 expression, such as the lung, spleen and bone.

Of [^{18}F]CCIC15 and [^{18}F]CCIC30, which were both assessed for their ability to identify U87 glioblastoma tumours of differing CXCR4 expression, neither showed high uptake in U87.CD4.CXCR4 tumours at 60 minutes. However, while [^{18}F]CCIC15 failed to accumulate in the tumour above background levels,

[^{18}F]CCIC30 fared slightly better, with a maximum 3.2-fold difference in uptake between U87.CD4.CXCR4 tumours and muscle (table 13). However, as was previously described, in U87.CD4 tumours the fold-difference was still 2-fold, and not significantly different. Thus it seems that what [^{18}F]CCIC30 uptake there was in the tumour was not specific to CXCR4 expression. Thus the investigation into the effectiveness of pentapeptide antagonists as PET tracers was, in this instance, extremely disappointing; suggested reasons for this lack of success are outlined in chapter 5.

Table 12. Biodistribution of [^{18}F]CCIC7, [^{18}F]CCIC15 and [^{18}F]CCIC30 in selected tissues of BALB/c nu/nu mice in vivo at 60 minutes post-injection (refer to section 2.15iii; n=4, 3 and 3, respectively)

	Mean biodistribution at 60 minutes (**%ID/g** ± SEM)		
	[^{18}F]CCIC7	**[^{18}F]CCIC15**	**[^{18}F]CCIC30**
Blood	**1.298** ± 0.573	**0.457** ± 0.214	**0.171** ± 0.053
Heart	**0.681** ± 0.164	**0.349** ± 0.096	**0.368** ± 0.053
Lung	**0.943** ± 0.208	**1.756** ± 0.336	**0.870** ± 0.138
Liver	**0.943** ± 0.208	**2.914** ± 0.161	**6.341** ± 0.776
Gallbladder	**7.923** ± 1.758	**27.193** ± 8.878	**6.007** ± 0.779
Stomach	**4.367** ± 1.988	**0.672** ± 0.002	**0.533** ± 0.220
Duodenum	**37.249** ± 11.970	**64.508** ± 17.050	**1.291** ± 0.138
Jejunum	**24.191** ± 15.444	**1.127** ± 0.180	**0.473** ± 0.069
Caecum	**0.373** ± 0.108	**0.215** ± 0.030	**0.147** ± 0.019
Colon	**0.329** ± 0.081	**0.917** ± 0.560	**0.380** ± 0.127
Spleen	**0.468** ± 0.125	**0.402** ± 0.082	**0.340** ± 0.043
Kidney	**3.413** ± 1.301	**0.990** ± 0.395	**1.839** ± 0.155
Muscle	**0.296** ± 0.118	**0.375** ± 0.188	**0.317** ± 0.111
Bone	**0.442** ± 0.153	**0.809** ± 0.127	**0.825** ± 0.207
Brain	**0.117** ± 0.0254	**0.097** ± 0.014	**0.132** ± 0.026
Urine	**57.490** ± 13.595	**170.956** ± 38.326	**236.819** ± 49.012

Table 13. Biodistribution of [^{18}F]CCIC15 and [^{18}F]CCIC30 in U87.CD4.CXCR4 tumour-bearing BALB/c nu/nu mice at 60 minutes post-injection (n=3). Refer to section 2.15iii.

	U87.CD4.CXCR4 tumour uptake ± SEM		
	(%ID/g)	**(Tumour/muscle)**	**(Tumour/Blood)**
[^{18}F]CCIC15	0.315 ± 0.018	1.155 ± 0.626	0.633 ± 0.199
[^{18}F]CCIC30	0.596 ± 0.012	3.219 ± 0.722	1.230 ± 0.395

3.4 - Modification of small molecular antagonists It1t and AMD3465

3.41 - Design of novel isothiourea antagonist library

While the [^{68}Ga]-CCIC16 tracer described in chapter 3.2 has enabled identification of CXCR4-expressing tumours *in vivo*, peptidic compounds such as CCIC16 bear a number of disadvantages against many non-peptide compounds. Such problems include a vulnerability to metabolism and low bioavailability (Craik *et al*., 2013). Cyclicisation to produce cyclic pentapeptides was hoped to reduce the extent of these inherent flaws, although as chapters 3.1 and 3.3 show, our own investigations into the development of such radiotracers were largely unsuccessful. Thus it was decided to look to alternative compound classes that might also show specificity for CXCR4, but without the drawbacks associated with peptides.

One potential group is the isothiourea CXCR4 antagonists (described in chapter 1.5), which have shown extremely high potency for CXCR4. Furthermore, very little in the way of development has been undertaken with these compounds, with only one main article reporting the structure-activity relationship of these derivatives (Thoma *et al*., 2008). There is therefore substantial grounds for hope that the current lead compound, It1t, may not yet be fully optimised, and therefore that the process of introducing functional groups for radiolabelling with ^{18}F might improve or maintain the potency of It1t for CXCR4. The development of ^{18}F-labelled It1t analogues might also be aided by the recent publication of the crystal structure of CXCR4 (Wu *et al*., 2010), with co-crystallisation of It1t, allowing determination of the likely binding sites. It1t interacts with CXCR4 at numerous sites within its structure, however one the most promising sites for functionalization is at one of the cyclohexane groups, which is less integral to CXCR4 binding than many other locations on the molecule (Wu *et al*., 2010).

Through utilisation of a number of different techniques, a compound library of It1t derivatives was designed (table 14), bearing functional groups that could allow radiolabelling with ^{18}F. A number of methods for the integration of a fluoride-containing group into the vicinity of this ring structure were attempted; One approach was the substitution of the cyclohexane group for an alternative ring structure, such as an ortho-, meta- or para-fluorophenyl group (giving rise to the compounds GG343, CCIC8 and GG345), or a piperidine-ethyl-fluoride ring

Table 14. Structure of novel It1t-derived analogues.

Name	Structure	Name	Structure	Name	Structure
It1t	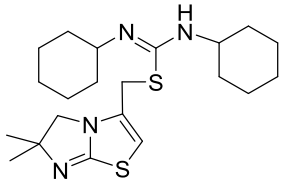	**GG345**	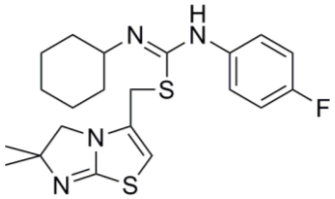	**GG337**	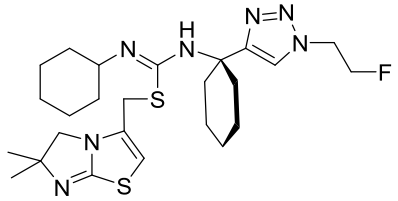
GG343	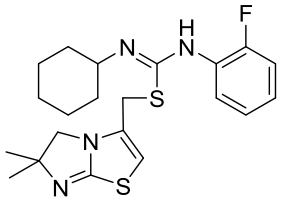	**GG366**	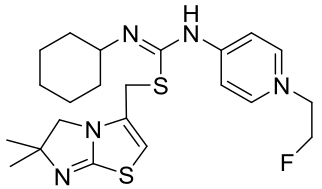	**GG338**	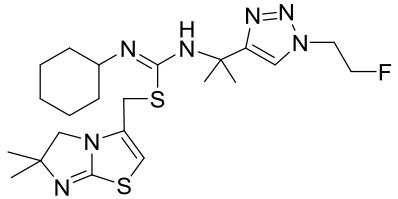
CCIC8	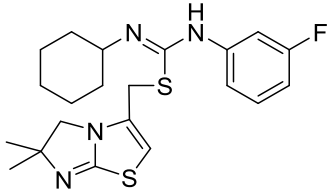	**CCIC27**	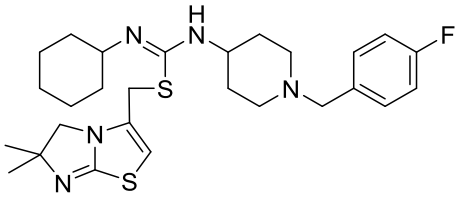	**GG248**	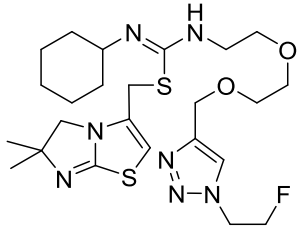

(giving rise to GG366). Other modifications included the substitution of cyclohexane for a piperidine-para-fluorobenzyl group (as is the case for CCIC27), or for ipso-cyclohexyl-triazol-ethyl-fluoride (creating GG337). More drastic alterations were made by the removal of the ring structure altogether, through substitution with isopropyl-triazol-ethyl-fluoride (such as in the case of GG338), or alternatively with PEG2-triazol-ethyl-fluoride, giving rise to GG248. This library represents a varied and experimental approach to optimisation of the functionalisation of It1t for use as a PET radiotracer.

3.42 - Assessment of novel isothiourea library antagonism of CXCR4

As with the pentapeptide compounds described in chapter 3.3, initial attempts to assess the affinity of It1t antagonists for CXCR4 were hampered by the unexpectedly high IC_{50} values yielded with the initial competitive radioligand binding assay protocol used (protocol A, see chapter 2.11i). Given that the expected IC_{50} value for the lead compound It1t was expected to be in the region of 8 nM (Thoma *et al*., 2008), an observed value of > 100 µM, over 12,000-fold higher than expected, gave considerable cause for concern (figure 42A). Fortunately, modification of the radioligand binding assay protocol to method B (described in chapter 2.11ii) resulted in a mean IC_{50} value of 1.5 nM being obtained (figure 42B), in line with expectations, and so the novel It1t-derived compounds displayed in table 14 were assessed using the same method. A considerable range in potencies was observed, from the nM- to the mM-scale; most notable among these were CCIC8, GG345 and 366, with IC_{50} values of 34.4

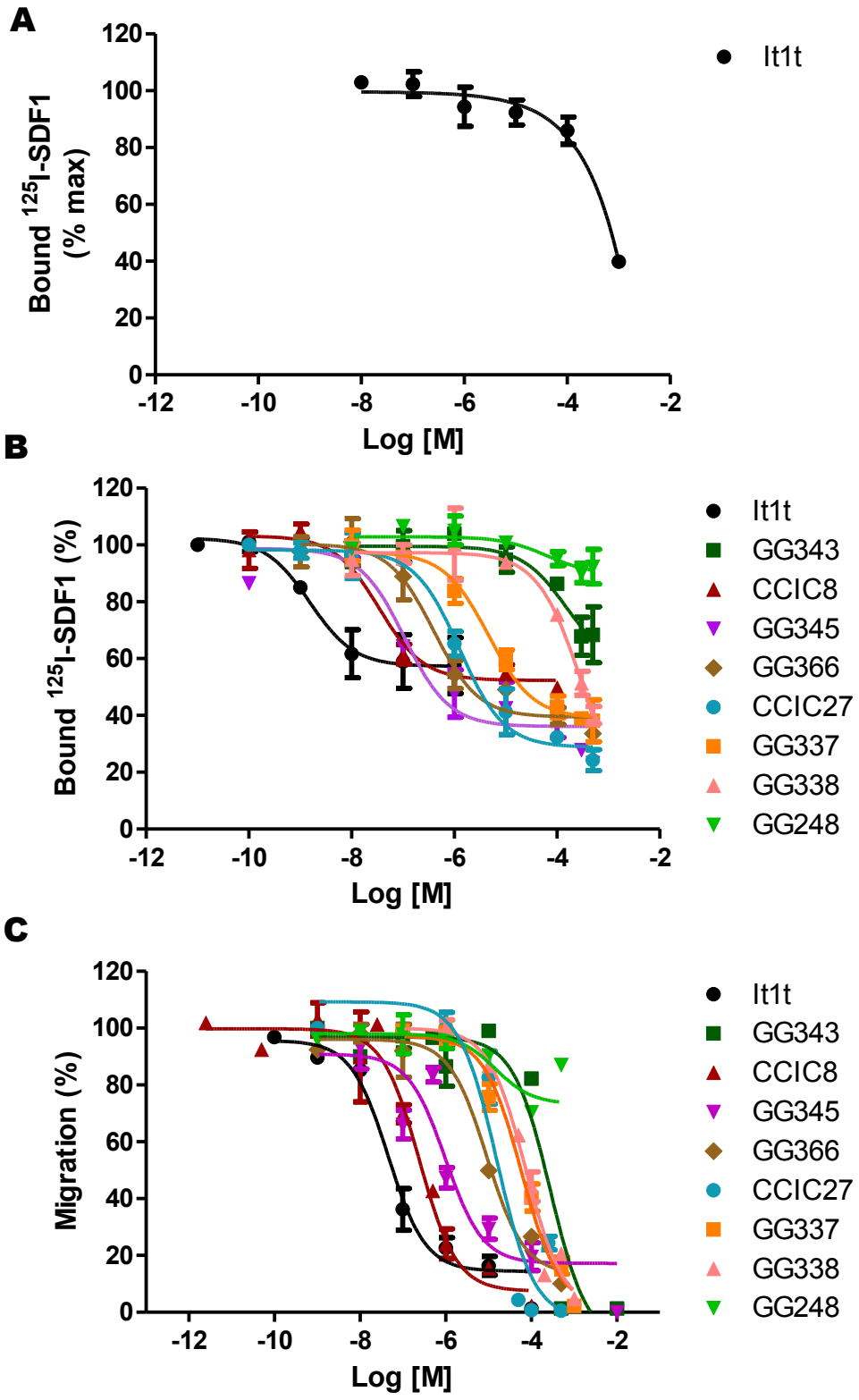

Figure 42. ***In vitro*** **assessment of isothiourea novel antagonist library for antagonism of CXCR4**

Inhibition of radioligand binding by novel antagonist using **A** protocol A (chapter 2.11i) and **B** protocol B (chapter 2.11ii). **C** Inhibition of Jurkat cell migration by novel antagonist compounds (refer to chapter 2.12). Curves shown are representative of at least 2 independent experiments, error bars show SEM.

Table 15. Comparative table of novel It1t analogue antagonism as judged by inhibition of radioligand binding and migration.

	Radioligand binding assay		Migration assay	
Compound	**IC_{50} (μM)**	**n**	**IC_{50} (μM)**	**n**
It1t	0.002	3	0.045	3
GG343	> 100	2	> 100	2
CCIC8	0.034	3	0.242	3
GG345	0.108	2	0.987	3
GG366	0.396	3	9.130	2
CCIC27	1.263	2	15.730	3
GG337	4.645	2	58.130	3
GG338	> 100	2	74.050	3
GG248	> 100	3	> 100	3

N refers to the number of independent experiments.

nM, 107.5 nM and 361.1 nM, respectively. Of low potency were CCIC27 and G337, with values of 1.3 μM and 4.6 μM, respectively, whereas GG343, GG338 and GG248 showed very little affinity for CXCR4 whatsoever (figure 42B and table 15).

Similar potencies were observed with the compounds' inhibition of SDF1-mediated migration in Jurkat cells (according to the protocol described in section 2.12), with the reference compound It1t showing the greatest antagonism at 45 nM, followed by the fluorobenzoylated CCIC8 and GG345 with 987.0 nM and 242.0 nM, respectively. Low potency was observed with GG366, CCIC27 and GG337 with 9.1 μM, 15.7 μM and 58.1 μM, respectively, and again, little to no antagonism by GG338, GG343 and GG248. The binding affinity of the

compounds to the CXCR4 receptor is therefore directly proportional to their ability to inhibit SDF1-induced migration. With the highest potencies for CXCR4 shown by the novel antagonists CCIC8 and GG345, these compounds would appear to show the greatest potential for radiolabelling with ^{18}F. Unfortunately there was insufficient time remaining on the project to make progress in this regard, although plans for future experiments are discussed in chapter 4.

3.43 - Functionalisation of cyclam AMD3465

In addition to the isothiourea-derived compounds, there are also many other small molecular categories of compounds that may be used to inhibit CXCR4-dependent signalling processes (outlined in chapter 3.3). Of these classes, the monocyclam AMD3465 has perhaps shown the most potential for use in PET imaging (De Silva *et al*., 2011), although the only method of functionalisation assessed so far is the chelation of ^{64}Cu within the cyclam core. It is possible that alternative approaches towards functionalisation might bear advantages; among the possible alterations to AMD3465 structure is the substitution of the pyridine ring for a dimethylamine fluorophenyl group, a novel compound named DB011 (figure 43). In contrast to the previously reported [^{64}Cu]AMD3465, the proposed radionuclide is a covalently bound ^{18}F, which bears a number of advantages over ^{64}Cu when used in PET imaging (as explained previously in chapter 1.5). Furthermore, the use of covalent bonding rather than chelation at the cyclam may help to promote specificity of the tracer, as transchelation of radionuclides

can be associated with nonspecific uptake into non-target organs (Tolmachev and Stone-Elander, 2010).

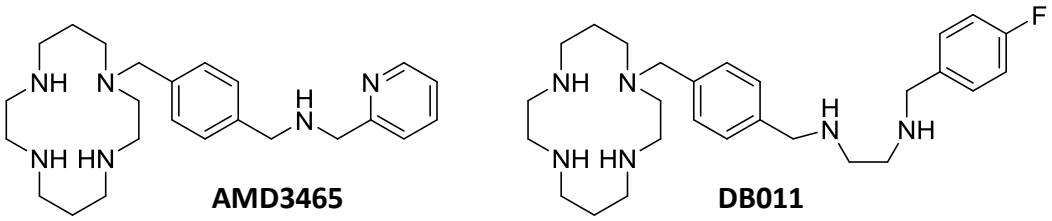

Figure 43. Structures of AMD3465 and novel derivative DB011

Assessment of AMD3465 and the derived DB011 using *in vitro* assays compared their respective potencies for the CXCR4 receptor through inhibition of ligand binding and subsequent migration. The results were promising, with very little difference in potency observed between the two compounds (see figure 44 and table 16), with half-maximal inhibitory concentrations observed at 89.8 and 111.3 nM, respectively (using the protocol described in section 2.11ii). IC_{50} values for the inhibition of SDF1-dorected migration (using the protocol described in 2.12) by AMD3465 and DB011 were similarly alike at 79.9 and 226.6 nM, respectively. These observations strongly suggest that the modification of AMD3465 to incorporate a fluoride atom in this manner should have little-to-no effect upon the affinity of the tracer for CXCR4, with respect to the unmodified AMD3465. The potency of DB011 for CXCR4 is therefore high, and would benefit from further development towards radiolabelling with the ^{18}F radionuclide. Unfortunately, there was insufficient time remaining to investigate

this more fully within the project, however the compound certainly shows promise for future investigations.

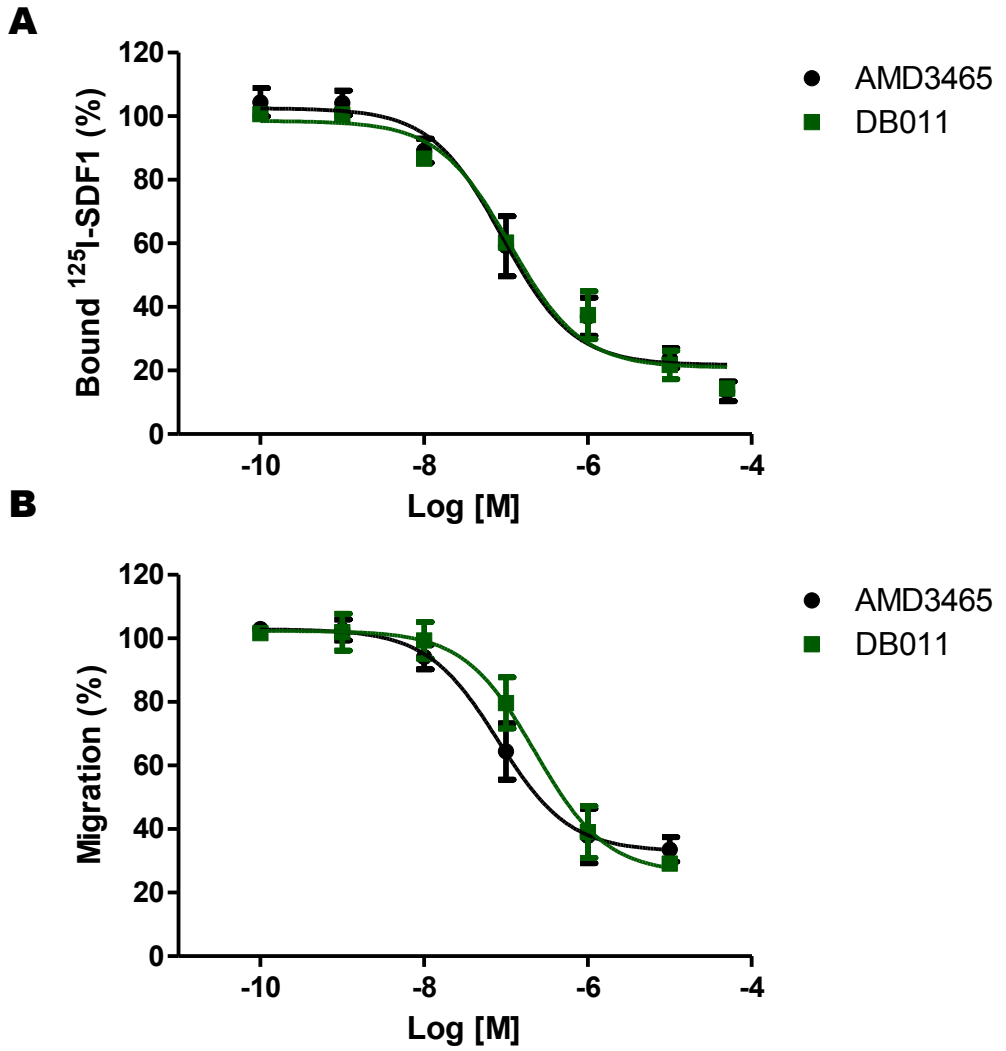

Figure 44. ***In vitro*** **antagonism of CXCR4 by AMD3465 and novel derivative DB011**

A Radioligand binding assay using protocol A (chapter 2.11ii). **B** Inhibition of SDF1-induced migration of Jurkat cells (refer to section 2.12). Curves shown are representative of at least 2 independent experiments, error bars show SEM.

Table 16. ***In vitro*** **antagonism of CXCR4 by AMD3465 and novel derivative DB011**

	Radioligand binding assay		Migration assay	
Compound	**IC_{50} (nM)**	**n**	**IC_{50} (nM)**	**n**
AMD3465	89.8	3	79.9	3
DB011	111.3	3	226.6	2

Chapter Four - Discussion

CXCR4 is a chemokine receptor that has been strongly implicated in the progression of cancer, and may be a potential biomarker of tumour aggressiveness and patient prognosis. The work presented here details the approaches made to functionalising a variety of classes of CXCR4 antagonist for use as novel PET tracers; these antagonist types included a T140 14mer peptide, numerous peptidomimetic cyclic pentapeptides, various isothioureas, and a monocyclam. At least one example of every group of novel antagonists showed potent antagonism of ligand binding and inhibited migration in CXCR4-expressing cellular models, highlighting their potential for use for *in vivo* imaging applications. Several of these candidates were assessed for their ability to successfully identify tumours of high CXCR4 expression *in vivo*. This aim was addressed most completely with the novel 14mer peptide tracer [^{68}Ga]-CCIC16, which enabled the identification of tumours expressing high levels of CXCR4 expression from those expressing lower levels of CXCR4. This achievement and several others will now be discussed, along with the challenges and potential solutions.

4.1 - On the assessment of CXCR4 expression, and cellular models

Initial attempts to validate the novel CXCR4-targeting radiotracer [^{18}F]CCIC7 were impeded by uncertainty regarding the suitability of HCT116 and A549 as cellular models of high and low CXCR4 expression, respectively. As outlined previously, it was rationalised that the antibody ab2074 was likely subject to a degree of nonspecific binding, as predictions of differential CXCR4 expression in HCT116 and A549 cells were not supported by qRT-PCR or flow cytometric analysis. In contrast, data collected by western blot using the UMB2 clone anti-CXCR4 antibody used in subsequent experiments showed considerably improved agreement with these alternative methods of CXCR4 expression analysis. Furthermore, observations of the increased expression in U87.CD4.CXCR4 compared to U87.CD4 cells predicted by the UMB2 clone antibody were supported by increased *in vitro* uptake of the novel radiotracers [^{68}Ga]-CCIC16, [^{18}F]CCIC15 and [^{18}F]CCIC30. These observations point to UMB2 as the most suitable antibody for the assessment of CXCR4 expression, and thus that the conclusions derived from its use are correct (*i.e.* that the isogenic U87.CD4 and U87.CD4.CXCR4 cell lines represent low and high CXCR4 expression, respectively).

Antibodies to GPCRs such as CXCR4 are notoriously unreliable, resulting in cross-reactivity against related GPCR family members (Michel *et al.*, 2009). More

specifically, there is evidence that many antibodies to CXCR4 used in published studies are far from optimal, with cross-reactivity against its closest family member, CXCR7, as well as the observation of unexpected cellular localisation patterns, suggesting non-specificity and leading to erroneous conclusions (Fischer *et al*., 2008). However, in this same publication, Fischer *et al* postulated that the UMB2 clone antibody to CXCR4 was highly specific, in contrast to the other antibodies assessed, strongly supporting this study's favourable assessment of its validity.

As such, the results presented in this study appear to confirm that the U87.CD4.CXCR4 cell line reliably expresses at least 5-fold more CXCR4 than the isogenic U87.CD4 cell line, and higher expression even than Jurkat cells, a known expresser of CXCR4 (Hesselgesser *et al*., 1998). This is in accordance with previous reports of the cell lines' expression profiles (Endres *et al*., 1996, Nimmagadda *et al*., 2010). This finding, in combination with the observation that U87.CD.CXCR4 cells also exhibit significantly more effective wound-closure than the CXCR4-negative cell line, confirms that a biologically functional CXCR4 receptor is overexpressed and therefore that the cell lines are appropriate models of differential CXCR4 expression for the development of CXCR4-specific radiotracers.

4.2 - [^{68}Ga]-CCIC16 validation and HSP90 inhibition

Of all the novel antagonists assessed within this study for use in PET imaging, the NO2A-conjugated TN14003 analogue CCIC16 was the most characterised, showing potent inhibition of radioligand binding as well as SDF1-directed migration. Like many other described CXCR4 antagonists, cationic chelation resulted in an increased affinity of CCIC16 for CXCR4 (Demmer *et al*., 2011, Gourni *et al*., 2011, Hennrich *et al*., 2012, Gerlach *et al*., 2003). This phenomenon may be explained by the interaction of the metal cations with key amino residues of CXCR4 that mediate ligand binding. Mutational analysis of CXCR4 has identified Asp^{262} as being exclusively responsible for the increase in CXCR4 binding potency observed as a result of cation chelation to AMD3100 (Gerlach *et al*., 2003). Furthermore, analysis of the crystal structure of CXCR4 when co-crystallised with the peptide antagonist CVX15 has resulted in the identification of a number of interactions between CVX15 and CXCR4 (Wu *et al*., 2010); as the 16-mer CVX15 shares many characteristics with the 14-mer antagonist CCIC16, the proposed interactions of a metal ion-chelated CCIC16 with CXCR4 are outlined in figure 44. It is possible that the cation is able to interact with the electronegative aspartate residues of CXCR4, such as either Asp^{187} or Asp^{262}, enabling higher affinity binding of the cation-chelated CCIC16 than the unchelated peptide. Future work involving co-crystallisation or mutational analysis could confirm the veracity of this hypothesis.

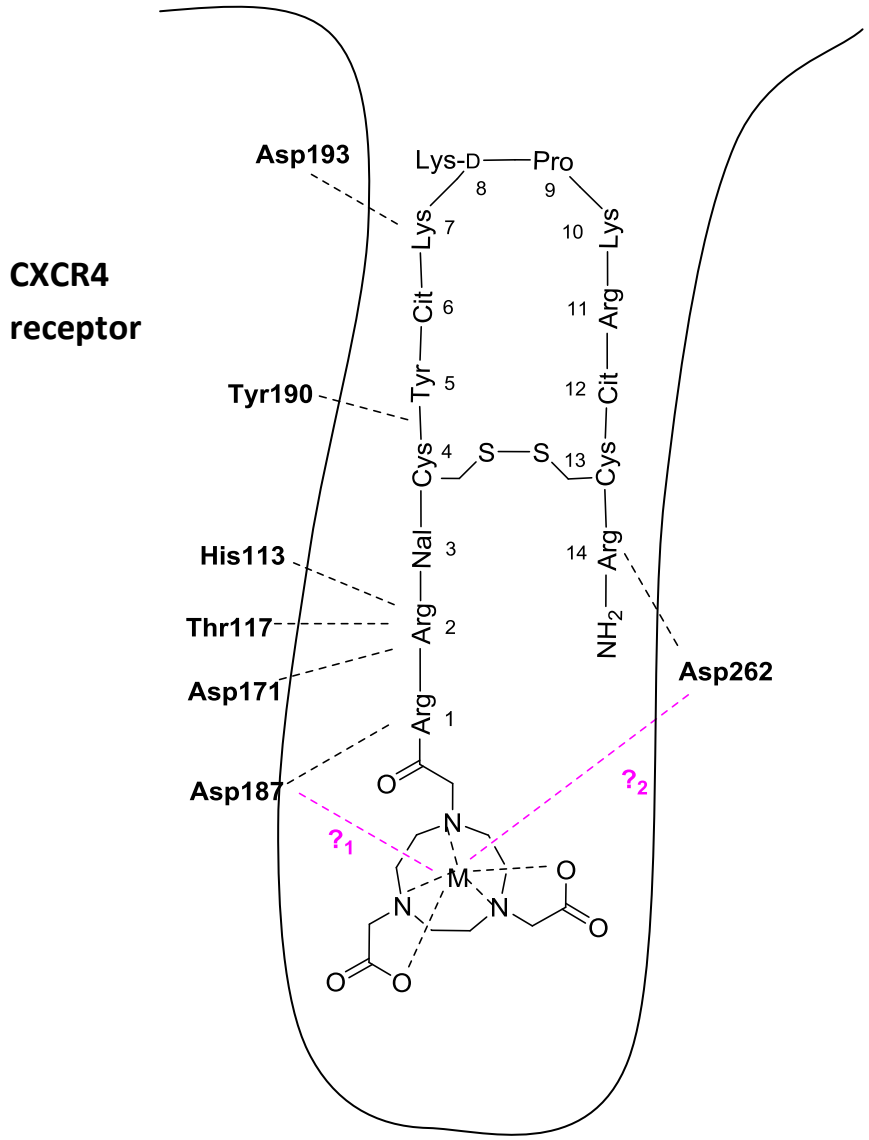

Figure 45. Proposed interactions of metal-chelated CCIC16 with CXCR4

Interactions shown by dashed lines. Suggested hypothetical interactions between chelated cation (M) and CXCR4 shown in magenta ($?_1$ and $?_2$). Adapted from (Wu *et al.*, 2010) and (Gerlach *et al.*, 2003).

The observation that Ga-CCIC16 reliably inhibited CXCR4 binding and function at low concentrations identified it as a candidate for radiolabelling, following which it was found that [^{68}Ga]-CCIC16 bound to *in vitro* cultures of U87 glioblastoma cells in a CXCR4-specific manner. Further investigation *in vivo* showed that tracer uptake in U87.CD4.CXCR4 tumours was 2.1-fold higher than in U87.CD4 tumours,

closely reflecting the mean difference in CXCR4 expression between *in vivo* tumour samples, supporting the stance that uptake is specific to CXCR4 expression levels. The discrepancy in CXCR4 expression fold-differences of the *in vitro* cultures versus the same cell lines growing as tumours *in vivo* is likely to be as a result of a number of factors; primarily that the maintenance of transgene expression is likely to be adversely affected by the lack of G418 selection pressure *in vivo* (Kaufman *et al.*, 2008). In addition, CXCR4 expression could be introduced to tumours via other cellular components of the tumour, such as infiltrating immunocytes which are widely acknowledged to express CXCR4 (Sica *et al.*, 2006); this could account for the CXCR4 expression observed in U87.CD4 tumours *in vivo*, where no *in vitro* expression had been noted.

The potential of [^{68}Ga]-CCIC16 as a radiotracer for the PET imaging of CXCR4-expressing tumours was further highlighted by signal-to-background uptake values and stability in systemic circulation *in vivo* that enabled an improved biodistribution of [^{68}Ga]-CCIC16 in comparison to the previously assessed [^{18}F]CCIC7. Also of note is the time-dependent accumulation of radiotracer in the bone and spleen, where CXCR4 has previously been reported to be expressed (Shao *et al*., 2011, Federsppiel *et al*., 1993), suggesting the potential for CXCR4-dependent uptake in other tissues. The above information paints a picture of [^{68}Ga]-CCIC16 as a CXCR4-specific PET radiotracer, with a high affinity for CXCR4 and potency of subsequent signalling-mechanisms.

Despite these features, [^{68}Ga]-CCIC16 exhibits a number of limitations in comparison to previously developed radiotracers targeting CXCR4. For example, overall tracer uptake in CXCR4-expressing tumours is low at 3.7%ID/ml, considerably lower than the 12-102%ID/g range reported for some of the ^{64}Cu-labelled small-molecular antagonists (Nimmagadda *et al.*, 2010, Weiss *et al.*, 2011, De Silva *et al.*, 2011). However, ^{68}Ga can be considered a more desirable radionuclide due to its high proportion of radioactivity decay by positron emission as well the ability for rapid radiolabelling in the absence of cyclotron facilities, as the radionuclide is produced instead using cost-effective Germanium-Gallium generators.

Furthermore, in contrast to many T140-derived analogues that have been functionalised for use in PET imaging (Jacobson *et al.*, 2010, Jacobson *et al.*, 2011), there was no evidence of high red blood cell uptake interfering with the ability of the radiotracer's ability to accumulate in CXCR4-expressing tumours, which considerably simplifies the process of image interpretation. The only other reported radiotracers for CXCR4 that have been labelled with ^{68}Ga show comparable levels of tumour uptake to [^{68}Ga]-CCIC16, and yet they have not validated their results in tumours of low CXCR4 expression (Demmer *et al.*, 2011, Gourni *et al.*, 2011), so conclusions of their specificity to CXCR4 cannot be confidently made. The data presented with respect to [^{68}Ga]-CCIC16 therefore succeeded in the primary aim of the project, which was to develop potent antagonists to CXCR4 which could be used as a PET tracer for the detection of

CXCR4 in cancer, and represents a competitive addition to the current range of available radiotracers for the detection of CXCR4 expression in cancer.

While [^{68}Ga]-CCIC16 proved adept at identifying U87.CD4.CXCR4 tumours from U87.CD4 tumours, the use of the tracer to attempt to noninvasively identify a 17AAG-induced reduction in CXCR4 expression *in vivo* failed for a number of reasons. Firstly, 48 hours daily treatment 80 mg/kg 17AAG resulted in an entirely unexpected 2-fold *increase* in CXCR4 expression, rather than a decrease. Secondly, this increase in CXCR4 expression was variable between tumour samples, and so the increase observed was not statistically significant. It is not likely that the inability to observe a reduction in CXCR4 expression was as a result of unsatisfactory HSP90 inhibition, as treatment was marked by a clear increase in HSP70 expression. The dose and formulation used is also equivalent to that which has been administered in previous published studies to induce significant reductions in HSP90 client proteins (Rodrigues *et al.*, 2012, Bagatell *et al.*, 2000). Thus the lack of observed reduction in CXCR4 expression is not thought to be related to the dosing formulation or regimens.

Given that the CXCR4 protein expressed by U87.CD4.CXCR4 cells is the product of transfection with a cDNA sequence to CXCR4 rather than endogenous CXCR4 protein (Bjorndal *et al*., 1997), it is possible that high turnover of CXCR4 expression where CXCR4 expression is driven by a promoter may mask CXCR4

degradation as a result of HSP90 inhibition by 17AAG. In support of this suggestion, it has previously been reported that cells overexpressing transgenic CXCR4 was less susceptible to indirect HSP90 inhibition by histone deacetylase inhibitors than cells which expressed CXCR4 endogenously (Mandawat *et al.*, 2010). It is therefore possible that the U87.CD4.CXCR4 cell line was an unsuitable cellular model for the assessment of 17AAG-induced reductions in CXCR4 expression. Future work using a tumorigenic cell line of high endogenous expression may better illuminate the potential of [^{68}Ga]-CCIC16 in identifying changes in CXCR4 expression in response to treatment. The tracer may also be suitable for further investigation in alternative applications. For example, increases in CXCR4 expression has been described in tumours developing resistance to various cancer therapies (Singh *et al.*, 2010, Kioi *et al.*, 2010, Dubrovska *et al.*, 2012b); as a result, CXCR4 antagonism is being investigated as a sensitiser to therapy. With this in mind, tracers targeting CXCR4 such as [^{68}Ga]-CCIC16 might be capable of identifying tumours that are developing resistance, and therefore indicating situations where CXCR4-targeted therapy may be worthwhile pursuing.

4.3 - IC50 determination of cyclic pentapeptide antagonists, and structure-activity relationships

The cyclopentapeptide CCIC7 (cyclo[tyr-fluorobenzyl hydroxy arg-arg-nal-gly]) was designed with reference to previous observations that the arg^2 of FC131

(cyclo[tyr-arg-arg-nal-gly]) was less important to the structure-activity relationship of lead compound FC131 than other amino residues (Tamamura *et al.,* 2005a). However, inhibition of CXCR4-directed migration by the inhibitor was not potent, with its half-maximal concentration for the inhibition of migration higher than 10 µM. *In vivo*, tumour uptake of [^{18}F]CCIC7 was hampered by poor pharmacokinetics at 60 minutes as well as rapid metabolism into more hydrophilic metabolites; even at 5 minutes post-injection the plasma-circulating tracer was widely present in a metabolised form, suggesting that the compound was extremely metabolically unstable. In the light of the overall failure of CCIC7 to adequately target CXCR4, the structure of the current lead compound FC131 was revisited in order to develop the novel antagonists CCIC15, CCIC29, CCIC30, and CCIC36. In developing these compounds, the assumption that arg^2 represented the most favourable site for functionalisation was discarded, as CCIC7 failed to show the high potency for CXCR4 and the *in vivo* stability required for use as a PET tracer.

Assessment of the structure-activity affinity of the novel cyclopentapeptide antagonists for CXCR4 was impeded by the lack of consistency shown by the radioligand binding assay method A (referred to in chapter 2.11i) between CXCR4 antagonists of different structural classes. While the small-molecular cyclam AMD3100 and T140-derived TC14012 inhibited radioligand binding with high potency, reference compounds for other classes of CXCR4 antagonist exhibited half-maximal inhibition of SDF1 binding at concentrations hundreds or

even thousands of fold higher than expected from published studies (including FC131, representing cyclic pentapeptides (Inokuchi *et al.*, 2011, Ueda *et al.*, 2008), and It1t, representing isothioureas (Thoma *et al.*, 2008). There appeared no obvious reason for the problems; the protocol was based upon a previously reported method (Jacobson *et al.*, 2012), and was consistent with many recommendations for good practice in radioligand binding assays (Bylund and Toews, 1993).

After considerable optimisation by trial and error, an alternative protocol was settled upon (method B, chapter 2.11ii), and showed a considerable improvement in the observed IC_{50} values of pentapeptide- and isothiourea-derived CXCR4 antagonists. While an observed IC_{50} of 600 nM for FC131 is 5-fold higher than has been previously reported in a radioligand binding assay (Inokuchi *et al.*, 2011), it is worthwhile bearing in mind that with differences in method and in cell line that some discrepancies are to be expected. Nonetheless, the measurement obtained using the new protocol B reflects at least a 30-fold reduction in observed IC_{50} value for FC131 within the project, and is likely to represent a more accurate estimation of its affinity for CXCR4. The precise reason for the discrepancy in measured half-maximal concentrations is not confidently known, however monovalent and divalent cations have been associated in some cases with changes in agonist affinity (Tsai and Lefkowitz, 1978, Reith and Coffey, 1993). Any changes in SDF1 radioligand binding at CXCR4

would ultimately have secondary effects upon the perceived potency of the antagonist being assessed.

Using the radioligand binding assay method B, it was found that CCIC30 (cyclo[tyr-FTA-arg-nal-gly]) was the most potent of the novel pentapeptide library investigated in this report. This is consistent with the findings of a recently published review, which finds that the Tyr^{1} is a relatively dispensible component of the pharmacophore (Mungalpara *et al.*, 2013). The fluorotriazole functional group of CCIC30 is very electronegative, and may allow hydrogen bonding to Tyr^{45} of CXCR4, where the hydroxyl group Tyr^{1} of FC131 would ordinarily interact (Yoshikawa *et al.*, 2012) - see figure 45 for proposed interactions of FC131 with CXCR4. The electronegativity of the fluorotriazole may also help to explain the reasonably potent affinity of CCIC15 (cyclo[tyr-FTA-arg-nal-gly]) for CXCR4; FC131's polar Arg^{2} residue is likely well-served by replacement with FTA and may help to preserve interactions with CXCR4. Arg^{3}-fluorotriazole substitution to create a relatively ineffectual CCIC29 (cyclo[tyr-arg-FTA-nal-gly]) is consistent with the suggested indispensibility of Arg^{3} as an anchor to CXCR4 (Tamamura *et al*., 2002). Conversely, the least potent of the pentapeptide library assayed, CCIC36 (cyclo[tyr-arg-arg-FTA-gly]), replaced the hydrophobic naphthylalanine residue with charged FTA, which likely prevents the proposed pi-stacking arrangement of His^{203} with the aromatic ring (Mungalpara *et al*., 2013).

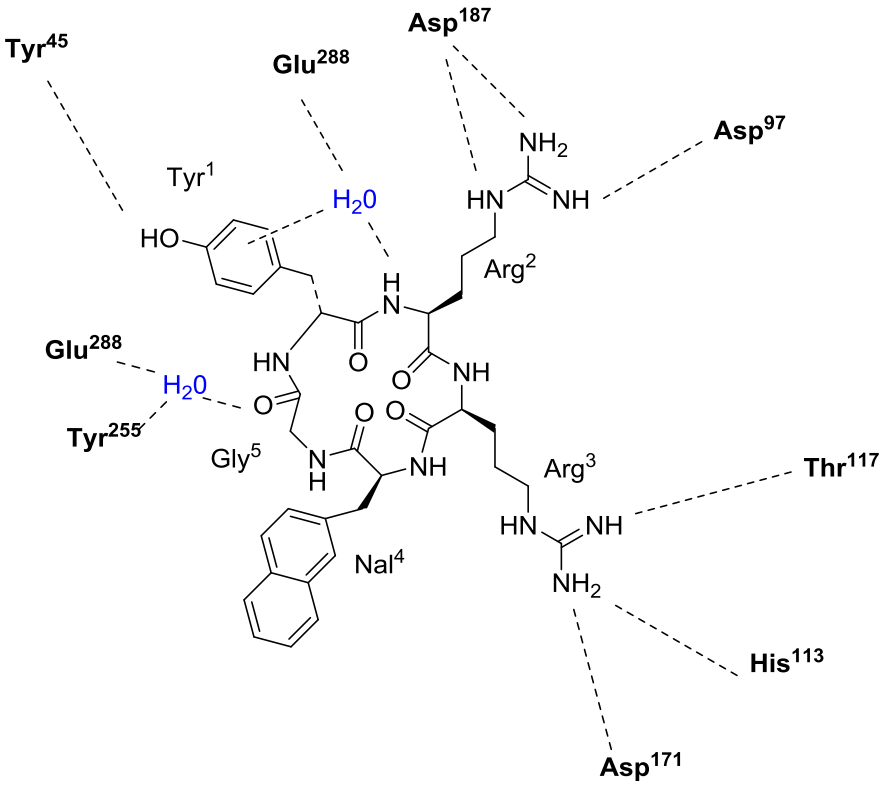

Figure 46. Proposed interactions of pentapeptide antagonist FC131 with CXCR4

Interactions shown as dashed line. Bold amino groups reflect binding positions of CXCR4 receptor structure. H_20 in blue denotes water molecules indicated by crystal structure. Adapted from docking experiments (Yoshikawa *et al*., 2012).

With the structure-activity relationship of cyclic pentapeptides elucidated, further development of a compound more suitable for use as a PET radiotracer can be considered. While glycine has not been substituted within this project, and glycine does not form part of the pharmacophore of T140, previous research has shown that the steric arrangement of glycine in cyclopentapeptides is vital for the preservation of affinity for CXCR4, and has so far only successfully been replaced with D-alanine (Ueda *et al.*, 2007). For this reason, functionalisation at this residue is unlikely to yield satisfactory results. With all these findings in mind it can be seen that the structure of FC131 does not allow

much scope for functionalisation without compromising potency for CXCR4; although numerous studies have systematically substituted amino residues, few approach the potency of FC131. However, substitution of key residues in the peptide backbone with isosteric amidine groups has been shown to drastically improve the inhibitory capabilities of pentapeptide antagonists (Inokuchi *et al*., 2011). In this investigation, CCIC30 has been shown to inhibit radioligand binding at lower concentrations than FC131, and so reflects a useful stepping stone towards derivitisation of pentapeptides as a radiotracer. Future progress with the pentapeptide class of CXCR4 antagonists may potentially come from exploring the use of isosteric peptidomimetic bonds in CCIC30-related derivatives.

Future work in the development of pentapeptide radiotracers should involve steps to improve the poor *in vivo* pharmacokinetics which were observed with tracers [^{18}F]CCIC7, [^{18}F]CCIC15 and [^{18}F]CCIC30, leading to poor tracer uptake at CXCR4-expressing tumour. Peptide drugs are notorious for proteolytic instability, and so further investigation into the biostability of cyclic pentapeptide antagonists with human liver microsomes would be a useful and clinically relevant approach for the precise determination of locations susceptible to degradation (Asha and Vidyavathi, 2010). While the terminal amino residues of many 14-mer T140 derivatives are marked by their vulnerability to degradation by the liver (Tamamura *et al.*, 2003), it is not currently clear whether pentapeptide derivatives are similarly affected. [^{18}F]CCIC7 was subject to

extremely rapid metabolism *in vivo* that precipitated the poor tumour uptake of radiotracer at 60 minutes; further analysis to confirm whether degradation occurs at the pentapeptide backbone or the amino acid side chains is necessary.

In contrast, [^{18}F]CCIC30 was found to be metabolically stable, and yet was rapidly cleared from circulation via the kidneys. Renal clearance is complex and therefore can be difficult to predict, however a number of drug qualities are associated with rapid clearance rates, including hydrophilicity and ionic state. [^{18}F]CCIC30 exhibited a LogD of -2.30, and the presence of positively charged arginine residues may contribute to a physiochemical phenotype that is prone to secretion at the proximal tubule, perhaps by the organic cation transporter (OCT) (Feng *et al.*, 2010). The possibility of this could be investigated by competition with cimetidine in a drug-drug interaction (DDI) study. Positive identification of elimination via the transporter would initiate a redesign of the compound to reduce the potency of the antagonist as a substrate.

4.4 - Potential of small molecular inhibitors of CXCR4

While the development of novel small molecular CXCR4 antagonists based on isothiourea and monocyclam compounds progressed only a small distance before the end of the project, it is possible to begin to make tentative conclusions regarding the structure-activity relationships of the isothioureas.

The greatest potential for CXCR4 antagonism appears to be shown by those compounds with the least modifications to the structure of the lead compound, It1t; the highest potential is indicated within CCIC8 and GG345 – compounds almost identical to It1t except for the substitution of one of the cyclohexane rings for a fluorophenyl ring. An exception to this apparent rule is GG343, an almost entirely inactive fluorobenzoylated derivative of It1t that was fluorinated at the adjacent ring carbon to the thiourea linking group, rather than the more medial placement of the fluorine within CCIC8 and GG345 (table 14). This vast difference in potency for CXCR4 with only very minor differences in structure may possibly be explained with reference to the interactions between It1t and CXCR4; as shown in figure 46, it can be seen that for It1t the nearby urea forms a hydrogen bond with Asp^{97} of CXCR4. The presence of an electronegative fluorine atom at the adjacent carbon of the benzene ring may prevent the protonation of the urea group and hence formation of the hydrogen bond between the urea and the hydroxyl group of the aspartate residue.

In contrast, with the exception of GG343, by far the least potent compounds assayed were GG338 and GG248, which are notable for the fact that both of these compounds are missing the second ring group that is typical of It1t and the other novel antagonists assayed. This strongly suggests that the presence of a ring structure (whether cyclohexane or benzene-derived) is vital to the potency of these compounds for CXCR4. In the case of GG248, it is possible that the presence of electronegative oxygen and nitrogen atoms might interfere with the

formation of hydrophobic interactions that would otherwise form between the ring structure of the It1t analogues and the arginine 183 and isoleucine 185 of the CXCR4 receptor (refer to figure 46). With GG338, the ring structure responsible for these hydrophic interactions is simply absent. Alternatively, it may be that the reduced rigidity of these non-cyclic functional groups may impede interaction of the It1t analogues at the binding site of CXCR4. The explanations above are to some degree supported by the compounds GG366, CCIC27 and GG337, which show a more moderate affinity for CXCR4 than the more potent It1t, CCIC8 and GG345 compounds. It is possible that larger molecular size causes steric hindrance, and higher electronegativity within the functional groups may reduce the hydrophobic interactions that aid the binding of isothioureas to the CXCR4 binding pocket.

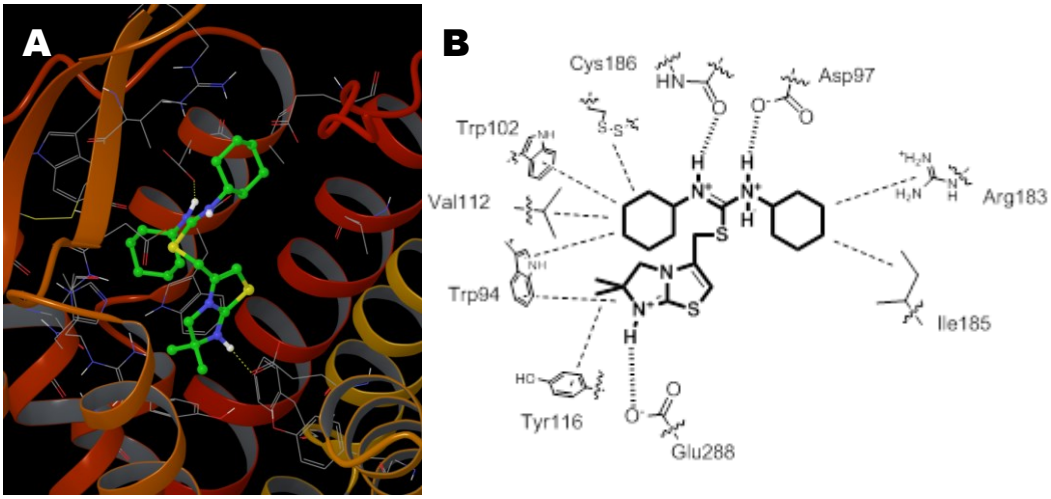

Figure 47. Conclusions on the interactions between It1t and CXCR4, as determined by co-crystallisation

Derived from information reported in (Wu *et al.*, 2010). **A** Molecular modelling as illustrated by Schrödinger software; hydrogen bonds depicted with yellow dotted lines. **B** Diagrammatic representation of It1t-CXCR4 interactions; thin dashed line denote hydrophobic interactions, thick dashed lines denote salt bridges and hydrogen bonds. Figures reproduced with permission (George, 2013).

With the observation that CCIC8 and GG345 showed the highest potency for CXCR4, and therefore the greatest chance of successful development into a PET imaging radiotracer, the next step in the development process would therefore be the [^{18}F] radiolabelling of the compounds, however as of yet this step has not been completed. A reason for the lack of development in this regard is that the synthetic process that would enable the radiolabelling of these compounds has only very recently been described (Lee *et al.*, 2012) and the use of such a novel approach therefore required considerable optimisation, and could not be achieved by the associated radiochemists in time for the project's completion. However, the effort in perfecting this approach would likely be well-spent, as the compounds show a considerable degree of promise in terms of potency for CXCR4. Despite the limited progress of the current developments of the isothiourea compounds at present, the investigation discussed here reflects a considerable advancement in the development of the compounds for PET imaging, as to date there no published research exploring the functionalization of isothiourea compounds for radiolabelling.

Lastly, substitution of the AMD3465 pyridine ring for a dimethylamine fluorophenyl group created the novel monocyclam antagonist DB011, which showed a potency very similar to that of AMD3465 in both radioligand binding and migration experiments, showing that derivatives of AMD3465 can potentially be radiolabelled with ^{18}F whilst retaining a high degree of affinity for CXCR4. Radiolabelled [^{18}F]DB011 shows considerable promise for development

as a radiotracer, as the most successful novel CXCR4-targeting radiotracer so far was also derived from AMD3465, and showed highest uptake of all measured tissues in CXCR4-expressing tumours with an exceptionally high target-to-background ratio (De Silva *et al.*, 2011). If similar characteristics were to be shown by [^{18}F]DB011 in future developments this would reflect an extremely competitive addition to the current repertoire of CXCR4-specific radiotracers, as the tracer could be expected to bear a number of advantages over the previously described [^{64}Cu]AMD3465: Firstly, the use of the more desirable ^{18}F would allow images with a greater degree of resolution and with a lower dose of ionising radiation to the patient. Secondly, the incorporation of the radionuclide through covalent conjugation rather than chelation prevents the occurrence of radionuclide transchelation from the CXCR4 antagonist, reducing the likelihood of nonspecific uptake of radioactivity in non-target tissues (Boswell *et al.*, 2004).

One characteristic that both the novel isothiourea and AMD3465 derivative antagonists share is that they are small molecular compounds; that it to say that they are not in any way peptidic in nature. Small molecular compounds such as these have a significant advantage over non-peptidic drugs in that they show a higher degree of 'druglikeness' - the collective observation that many approved drugs share the same 5 characteristics, known as the Lipinski rule of 5 (Leeson, 2012). These include the preferences for a molecular weight of less than 500, a LogP value of less than 5, and less than 5 electron donating groups, or 10 electron accepting groups. Furthermore, as non-peptidic compounds, there is

potential for high bioavailability of the compounds in vivo due to a reduced vulnerability to metabolism, as shown by previous studies (Thoma *et al.*, 2008). It is useful to note that the lead compounds It1t and AMD3465 pass all of these criteria (along with the most potent novel antagonist derivatives, CCIC8, GG345 and DB011), whereas the compounds T140 and FC131 fail on one or more counts (table 17). This indicates that the small molecular CXCR4 antagonists may show improved characteristics *in vivo*, and may therefore be more effective than the peptidic CXCR4-targeting radiotracers developed thus far.

Table 17. Comparative table of example CXCR4 antagonists adherence to the 'Rule of 5'

Compound	< 500 kDa ?	< 5 EDG ?	< 10 EAG ?	LogP < 5 ?
T140	×	×	×	✓
FC131	×	×	✓	✓
It1t	✓	✓	✓	✓
AMD3465	✓	✓	✓	✓

kDa (kiloDaltons) ; EDG (electron-donating groups) ; EAG (electron-accepting groups) ; LogP (Log partition coefficient) ; ✓ signifies compound has passed the indicated criterion, × signifies compound has failed indicated criterion.

The most potent small molecular antagonists, CCIC8, GG345 and DB011, clearly show potential and would therefore benefit from further research, including but not necessarily limited to their radiosynthesis, assessment with *in vitro* uptake assay, and imaging, biodistribution and metabolism experiments *in vivo*. These experiments would go some way toward determination of their suitability as CXCR4-specific radiotracers for the detection of cancer.

4.5 - Conclusions

The emergence of CXCR4 as a biomarker for disease progression in cancer precedes the necessary development of diagnostic tools for its detection *in vivo*. Positron emission tomography with a sensitive radiolabelled probe specific to CXCR4 protein would enable rapid noninvasive assessment of the tumour which could be applicable to a physician's judgement of patient prognosis and subsequent treatment options. The present study has explored modifications to a wide range of available antagonists to CXCR4 to determine their suitability as radiotracers of CXCR4 expression.

Most notably, [^{68}Ga]-CCIC16, a novel radiolabelled derivative of the 14mer antagonist T140, was found to be a potent inhibitor of SDF1 binding and migration in CXCR4 expressing cell lines, and could accumulate in tumours in a CXCR4-specific manner, with further evidence of tracer uptake in tissues of high CXCR4 expression, including the spleen and bone. [^{68}Ga]-CCIC16 uptake showed a favourable target-to-background ratio, and sufficient serum stability to enable imaging of the tracer uptake at 60 minutes post-injection. In contrast to many previously reported CXCR4-targeting PET radiotracers in development, the identification of CXCR4-positive tumours [^{68}Ga]-CCIC16 was not dependent upon blockade of non-specific binding by unlabelled antagonist. The tracer also takes advantage of several convenient properties of the ^{68}Ga radionuclide, including a favourably short half-life, with a high rate of radioactive decay by positron

emission, as well as a relatively inexpensive and accessible mode of generation. [^{68}Ga]-CCIC16 therefore represents an original contribution to the field of CXCR4 molecular imaging.

An additional aim of the present study was to determine whether changes in CXCR4 expression induced by HSP90 inhibition could be detected using a novel radiotracer. An HSP90 inhibitor, 17AAG, was shown to downregulate CXCR4 expression in treated cells *in vitro*, which could be identified by the radiotracer [^{68}Ga]-CCIC16. Unfortunately, the tracer did not identify untreated from treated tumours *in vivo*, possibly as a result of high receptor turnover by promoter-driven expression in U87.CD4.CXCR4 cells, masking the effects of CXCR4 protein degradation. Future work inhibiting HSP90 function in tumours derived from cells expressing CXCR4 endogenously would enable the limitations of this study to be overcome, and to confirm whether [^{68}Ga]-CCIC16 detection of CXCR4 expression could be used to identify response to HSP90-inhibiting therapy.

The present study also investigated functionalisation of the potent pentapeptide CXCR4 antagonist, FC131, with limited degrees of success. Substitution of Arg^{2} with a fluorobenzyl PEG2 linker to create CCIC7 considerably reduced the affinity of the pentapeptide for CXCR4, and *in vivo* assessment of the radiolabelled [^{18}F]CCIC7 was hampered by extremely rapid metabolic degradation of the tracer. In a different approach, the effect of substituting a fluorotriazole

functional group in various positions of the pentapeptide structure was investigated, and found to be extremely well-tolerated at Tyr^1 (giving rise to CCIC30), and moderately so at Arg^2 (resulting in CCIC15). However, *in vivo* assessment of [^{18}F]CCIC30 and [^{18}F]CCIC15 showed that neither radiotracer could identify tumours of varying CXCR4 expression; in contrast to [^{18}F]CCIC7, [^{18}F]CCIC30 was found to be metabolically very stable, with low systemic presence as a result of extremely rapid kidney clearance. The work described represents a continuation of developments to optimise pentapeptide antagonists for use as radiotracers, and suggests future work to improve pharmacokinetics *in vivo*, including comprehensive analysis of metabolic stability and renal clearance.

Lastly, the project explored the functionalisation of a number of potent small molecular antagonists of CXCR4, including the monocyclam AMD3465 and isothiourea It1t. Substitution of the AMD3465 pyridine ring for a dimethyl fluorophenyl group gave rise to the monocyclam compound DB011, while functionalisation of the isothiourea It1t by substitution of the cyclohexane group with meta- and para-fluorophenyl groups yielded CCIC8 and GG345, respectively; all three of these novel antagonists showed excellent affinity for CXCR4. While not yet fully developed, the compounds DB011, CCIC8 and GG345 are ideal candiadates for further investigation as ^{18}F-labelled radiotracers for CXCR4 expression, and their development so far represents advances in understanding of small molecular structure-activity relationships with CXCR4,

and is the first reported attempt to functionalise the little-explored isothiourea-derived antagonists as radiotracers. Small molecular antagonists such as isothiourea and monocyclams show considerable potential as radiotracers as they show increased druglikeness compared to either the 14mer peptide or cyclopentapeptide antagonists of CXCR4, and may therefore show improved *in vivo* characteristics.

The findings discussed in this report confirm CXCR4 expression as a viable target for the molecular imaging of cancer, and presents novel information on the structure-activity relationships of a wide variety of antagonists with CXCR4. With further development, novel tracers to CXCR4 such as [^{68}Ga]-CCIC16 may enable selective imaging of primary tumours prone to progession and metastases, and tumours showing signs of resistance to therapy.

Publications

1. Ola Åberg, Federica Pisaneschi, Graham Smith, Quang-Dé Nguyen, Elizabeth Stevens and Eric O. Aboagye (2012). ^{18}F-labelling of a cyclic pentapeptide inhibitor of the chemokine receptor CXCR4. *Journal of Fluorine Chemistry*, volume 135, pages 200-206.

2. Guillaume P.C. George, Federica Pisaneschi, Elizabeth Stevens, Quang-Dé Nguyen, Ola Åberg, Alan C. Spivey, and Eric O. Aboagye (2013). Scavenging strategy for specific activity improvement: application to a new CXCR4-specific cyclopentapeptide positron emission tomography tracer. *Journal of Labelled Compounds and Radiopharmaceuticals*, volume 56, issue 13, pages 679-685.

3. Guillaume P.C. George, Elizabeth Stevens, Ola Åberg, Quang-Dé Nguyen, Federica Pisaneschi, Alan C. Spivey and Eric O. Aboagye (2013). Preclinical evaluation of a CXCR4-specific 68Ga-labelled TN14003 derivative for cancer PET imaging. *Bioorganic and Medicinal Chemistry*, volume 22, issue 2, pages 796-803.

References

Office for National Statistics (2008). Cancer National Statistics Online [Online]. . Available: http://www.statistics.gov.uk/cci/nugget.asp?id=915 [Accessed 25/06/2011 2011].

Adams, K. E., Ke, S., Kwon, S., Liang, F., Fan, Z., Lu, Y., Hirschi, K., Mawad, M. E., Barry, M. A. & Sevick-Muraca, E. M. 2007. Comparison of visible and near-infrared wavelength-excitable fluorescent dyes for molecular imaging of cancer. *J Biomed Opt,* 12**,** 024017.

Ahsan, A., Ramanand, S. G., Whitehead, C., Hiniker, S. M., Rehemtulla, A., Pratt, W. B., Jolly, S., Gouveia, C., Truong, K., Van Waes, C., Ray, D., Lawrence, T. S. & Nyati, M. K. 2012. Wild-type EGFR is stabilized by direct interaction with HSP90 in cancer cells and tumors. *Neoplasia,* 14**,** 670-7.

Alberti, C. 2012. From molecular imaging in preclinical/clinical oncology to theranostic applications in targeted tumor therapy. *Eur Rev Med Pharmacol Sci,* 16**,** 1925-33.

Anderson, C. J. & Welch, M. J. 1999. Radiometal-labeled agents (non-technetium) for diagnostic imaging. *Chem Rev,* 99**,** 2219-34.

Appaiah, H., Bhat-Nakshatri, P., Mehta, R., Thorat, M., Badve, S. & Nakshatri, H. 2010. ITF2 is a target of CXCR4 in MDA-MB-231 breast cancer cells and is associated with reduced survival in estrogen receptor-negative breast cancer. *Cancer Biol Ther,* 10**,** 600-14.

Ara, T., Nakamura, Y., Egawa, T., Sugiyama, T., Abe, K., Kishimoto, T., Matsui, Y. & Nagasawa, T. 2003. Impaired colonization of the gonads by primordial germ cells in mice lacking a chemokine, stromal cell-derived factor-1 (SDF-1). *Proc Natl Acad Sci U S A,* 100**,** 5319-23.

Arora, S., Bhardwaj, A., Singh, S., Srivastava, S. K., Mcclellan, S., Nirodi, C. S., Piazza, G. A., Grizzle, W. E., Owen, L. B. & Singh, A. P. 2013. An undesired effect of chemotherapy: gemcitabine promotes pancreatic cancer cell invasiveness through reactive oxygen species-dependent, nuclear factor kappaB- and hypoxia-inducible factor 1alpha-mediated up-regulation of CXCR4. *J Biol Chem,* 288**,** 21197-207.

Asha, S. & Vidyavathi, M. 2010. Role of human liver microsomes in in vitro metabolism of drugs-a review. *Appl Biochem Biotechnol,* 160**,** 1699-722.

Ashley, R. L., Antoniazzi, A. Q., Anthony, R. V. & Hansen, T. R. 2011. The chemokine receptor CXCR4 and its ligand CXCL12 are activated during implantation and placentation in sheep. *Reprod Biol Endocrinol,* 9**,** 148.

Bachelder, R. E., Wendt, M. A. & Mercurio, A. M. 2002. Vascular endothelial growth factor promotes breast carcinoma invasion in an autocrine manner by regulating the chemokine receptor CXCR4. *Cancer Res,* 62**,** 7203-6.

Bagatell, R., Paine-Murrieta, G. D., Taylor, C. W., Pulcini, E. J., Akinaga, S., Benjamin, I. J. & Whitesell, L. 2000. Induction of a heat shock factor 1-dependent stress response alters the cytotoxic activity of hsp90-binding agents. *Clin Cancer Res,* 6**,** 3312-8.

Balabanian, K., Lagane, B., Infantino, S., Chow, K. Y., Harriague, J., Moepps, B., Arenzana-Seisdedos, F., Thelen, M. & Bachelerie, F. 2005a. The chemokine SDF-1/CXCL12 binds to and signals through the orphan receptor RDC1 in T lymphocytes. *J Biol Chem,* 280**,** 35760-6.

Balabanian, K., Lagane, B., Pablos, J. L., Laurent, L., Planchenault, T., Verola, O., Lebbe, C., Kerob, D., Dupuy, A., Hermine, O., Nicolas, J. F., Latger-Cannard, V., Bensoussan, D., Bordigoni, P., Baleux, F., Le Deist, F., Virelizier, J. L., Arenzana-Seisdedos, F. & Bachelerie, F. 2005b. WHIM syndromes with different genetic anomalies are accounted for by impaired CXCR4 desensitization to CXCL12. *Blood,* 105**,** 2449-57.

Barretina, J., Junca, J., Llano, A., Gutierrez, A., Flores, A., Blanco, J., Clotet, B. & Este, J. A. 2003. CXCR4 and SDF-1 expression in B-cell chronic lymphocytic leukemia and stage of the disease. *Ann Hematol,* 82**,** 500-5.

Bartolome, R. A., Ferreiro, S., Miquilena-Colina, M. E., Martinez-Prats, L., Soto-Montenegro, M. L., Garcia-Bernal, D., Vaquero, J. J., Agami, R., Delgado, R., Desco, M., Sanchez-Mateos, P. & Teixido, J. 2009. The chemokine receptor CXCR4 and the metalloproteinase MT1-MMP are mutually required during melanoma metastasis to lungs. *Am J Pathol,* 174**,** 602-12.

Becaud, J., Mu, L., Karramkam, M., Schubiger, P. A., Ametamey, S. M., Graham, K., Stellfeld, T., Lehmann, L., Borkowski, S., Berndorff, D., Dinkelborg, L., Srinivasan, A., Smits, R. & Koksch, B. 2009. Direct one-step 18F-labeling of peptides via nucleophilic aromatic substitution. *Bioconjug Chem,* 20**,** 2254-61.

Beider, K., Nagler, A., Wald, O., Franitza, S., Dagan-Berger, M., Wald, H., Giladi, H., Brocke, S., Hanna, J., Mandelboim, O., Darash-Yahana, M., Galun, E. & Peled, A. 2003. Involvement of CXCR4 and IL-2 in the homing and retention of human NK and NK T cells to the bone marrow and spleen of NOD/SCID mice. *Blood,* 102**,** 1951-8.

Bernhagen, J., Krohn, R., Lue, H., Gregory, J. L., Zernecke, A., Koenen, R. R., Dewor, M., Georgiev, I., Schober, A., Leng, L., Kooistra, T., Fingerle-Rowson, G., Ghezzi, P., Kleemann, R., Mccoll, S. R., Bucala, R., Hickey, M. J. & Weber, C. 2007. MIF is a noncognate ligand of CXC chemokine receptors in inflammatory and atherogenic cell recruitment. *Nat Med,* 13**,** 587-96.

Bjorndal, A., Deng, H., Jansson, M., Fiore, J. R., Colognesi, C., Karlsson, A., Albert, J., Scarlatti, G., Littman, D. R. & Fenyo, E. M. 1997. Coreceptor usage of primary

human immunodeficiency virus type 1 isolates varies according to biological phenotype. *J Virol,* 71**,** 7478-87.

Blom, E., Langstrom, B. & Velikyan, I. 2009. 68Ga-labeling of biotin analogues and their characterization. *Bioconjug Chem,* 20**,** 1146-51.

Bodart, V., Anastassov, V., Darkes, M. C., Idzan, S. R., Labrecque, J., Lau, G., Mosi, R. M., Neff, K. S., Nelson, K. L., Ruzek, M. C., Patel, K., Santucci, Z., Scarborough, R., Wong, R. S., Bridger, G. J., Macfarland, R. T. & Fricker, S. P. 2009. Pharmacology of AMD3465: a small molecule antagonist of the chemokine receptor CXCR4. *Biochem Pharmacol,* 78**,** 993-1000.

Boswell, C. A., Sun, X., Niu, W., Weisman, G. R., Wong, E. H., Rheingold, A. L. & Anderson, C. J. 2004. Comparative in vivo stability of copper-64-labeled cross-bridged and conventional tetraazamacrocyclic complexes. *J Med Chem,* 47**,** 1465-74.

Brattain, M. G., Fine, W. D., Khaled, F. M., Thompson, J. & Brattain, D. E. 1981. Heterogeneity of malignant cells from a human colonic carcinoma. *Cancer Res,* 41**,** 1751-6.

Breeman, W. A. & Verbruggen, A. M. 2007. The 68Ge/ 68Ga generator has high potential, but when can we use 68Ga-labelled tracers in clinical routine? *Eur J Nucl Med Mol Imaging,* 34**,** 978-81.

Bridger, G. J., Skerlj, R. T., Hernandez-Abad, P. E., Bogucki, D. E., Wang, Z., Zhou, Y., Nan, S., Boehringer, E. M., Wilson, T., Crawford, J., Metz, M., Hatse, S., Princen, K., De Clercq, E. & Schols, D. 2010. Synthesis and structure-activity relationships of azamacrocyclic C-X-C chemokine receptor 4 antagonists: analogues containing a single azamacrocyclic ring are potent inhibitors of T-cell tropic (X4) HIV-1 replication. *J Med Chem,* 53**,** 1250-60.

Buckle, T., Kuil, J., Van Den Berg, N. S., Bunschoten, A., Lamb, H. J., Yuan, H., Josephson, L., Jonkers, J., Borowsky, A. D. & Van Leeuwen, F. W. 2013. Use of a single hybrid imaging agent for integration of target validation with in vivo and ex vivo imaging of mouse tumor lesions resembling human DCIS. *PLoS One,* 8**,** e48324.

Burdon, P. C., Martin, C. & Rankin, S. M. 2008. Migration across the sinusoidal endothelium regulates neutrophil mobilization in response to ELR + CXC chemokines. *Br J Haematol,* 142**,** 100-8.

Burke, B. P., Clemente, G. S. & Archibald, S. J. 2014. Recent advances in chelator design and labelling methodology for Ga radiopharmaceuticals. *J Labelled Comp Radiopharm*.

Bylund, D. B. & Toews, M. L. 1993. Radioligand binding methods: practical guide and tips. *Am J Physiol,* 265**,** L421-9.

Bzyl, J., Palmowski, M., Rix, A., Arns, S., Hyvelin, J. M., Pochon, S., Ehling, J., Schrading, S., Kiessling, F. & Lederle, W. 2013. The high angiogenic activity in very early

breast cancer enables reliable imaging with VEGFR2-targeted microbubbles (BR55). *Eur Radiol,* 23**,** 468-75.

Cabioglu, N., Yazici, M. S., Arun, B., Broglio, K. R., Hortobagyi, G. N., Price, J. E. & Sahin, A. 2005. CCR7 and CXCR4 as novel biomarkers predicting axillary lymph node metastasis in T-1 breast cancer. *Clinical Cancer Research,* 11**,** 5686-5693.

Ceradini, D. J., Kulkarni, A. R., Callaghan, M. J., Tepper, O. M., Bastidas, N., Kleinman, M. E., Capla, J. M., Galiano, R. D., Levine, J. P. & Gurtner, G. C. 2004. Progenitor cell trafficking is regulated by hypoxic gradients through HIF-1 induction of SDF-1. *Nat Med,* 10**,** 858-64.

Chambers, A. F. 2009. MDA-MB-435 and M14 cell lines: identical but not M14 melanoma? *Cancer Res,* 69**,** 5292-3.

Chen, F., Yu, Y., Qian, J., Wang, Y., Cheng, B., Dimitropoulou, C., Patel, V., Chadli, A., Rudic, R. D., Stepp, D. W., Catravas, J. D. & Fulton, D. J. 2012. Opposing actions of heat shock protein 90 and 70 regulate nicotinamide adenine dinucleotide phosphate oxidase stability and reactive oxygen species production. *Arterioscler Thromb Vasc Biol,* 32**,** 2989-99.

Cianfrocca, M. & Gradishar, W. 2009. New molecular classifications of breast cancer. *CA Cancer J Clin,* 59**,** 303-13.

Clarke, E. T. & Martell, A. E. 1991. Stabilities of the Fe(Iii), Ga(Iii) and in(Iii) Chelates of N,N',N''-Triazacyclononanetriacetic Acid. *Inorganica Chimica Acta,* 181**,** 273-280.

Craik, D. J., Fairlie, D. P., Liras, S. & Price, D. 2013. The future of peptide-based drugs. *Chem Biol Drug Des,* 81**,** 136-47.

Curtis, C., Shah, S. P., Chin, S. F., Turashvili, G., Rueda, O. M., Dunning, M. J., Speed, D., Lynch, A. G., Samarajiwa, S., Yuan, Y., Graf, S., Ha, G., Haffari, G., Bashashati, A., Russell, R., Mckinney, S., Caldas, C., Aparicio, S., Brenton, J. D., Ellis, I., Huntsman, D., Pinder, S., Purushotham, A., Murphy, L., Bardwell, H., Ding, Z., Jones, L., Liu, B., Papatheodorou, I., Sammut, S. J., Wishart, G., Chia, S., Gelmon, K., Speers, C., Watson, P., Blamey, R., Green, A., Macmillan, D., Rakha, E., Gillett, C., Grigoriadis, A., Di Rinaldis, E., Tutt, A., Parisien, M., Troup, S., Chan, D., Fielding, C., Maia, A. T., Mcguire, S., Osborne, M., Sayalero, S. M., Spiteri, I., Hadfield, J., Bell, L., Chow, K., Gale, N., Kovalik, M., Ng, Y., Prentice, L., Tavare, S., Markowetz, F., Langerod, A., Provenzano, E. & Borresen-Dale, A. L. 2012. The genomic and transcriptomic architecture of 2,000 breast tumours reveals novel subgroups. *Nature*.

Dakappagari, N., Neely, L., Tangri, S., Lundgren, K., Hipolito, L., Estrellado, A., Burrows, F. & Zhang, H. 2010. An investigation into the potential use of serum Hsp70 as a novel tumour biomarker for Hsp90 inhibitors. *Biomarkers,* 15**,** 31-8.

Dale, D. C., Bolyard, A. A., Kelley, M. L., Westrup, E. C., Makaryan, V., Aprikyan, A., Wood, B. & Hsu, F. J. 2011. The CXCR4 antagonist plerixafor is a potential therapy for myelokathexis, WHIM syndrome. *Blood,* 118**,** 4963-6.

Darash-Yahana, M., Pikarsky, E., Abramovitch, R., Zeira, E., Pal, B., Karplus, R., Beider, K., Avniel, S., Kasem, S., Galun, E. & Peled, A. 2004. Role of high expression levels of CXCR4 in tumor growth, vascularization, and metastasis. *FASEB J,* 18**,** 1240-2.

De Palma, M. & Hanahan, D. 2012. The biology of personalized cancer medicine: Facing individual complexities underlying hallmark capabilities. *Mol Oncol,* 6**,** 111-27.

De Silva, R. A., Peyre, K., Pullambhatla, M., Fox, J. J., Pomper, M. G. & Nimmagadda, S. 2011. Imaging CXCR4 expression in human cancer xenografts: evaluation of monocyclam 64Cu-AMD3465. *J Nucl Med,* 52**,** 986-93.

Dean, B., Pavey, G. & Opeskin, K. 1997. [3H]raclopride binding to brain tissue from subjects with schizophrenia: methodological aspects. *Neuropharmacology,* 36**,** 779-86.

Deguchi, Y. & Kehrl, J. H. 1993. High level expression of the homeobox gene HB24 in a human T-cell line confers the ability to form tumors in nude mice. *Cancer Res,* 53**,** 373-7.

Demmer, O., Dijkgraaf, I., Schumacher, U., Marinelli, L., Cosconati, S., Gourni, E., Wester, H. J. & Kessler, H. 2011. Design, synthesis, and functionalization of dimeric peptides targeting chemokine receptor CXCR4. *J Med Chem,* 54**,** 7648-62.

Devalaraja, M. N. & Richmond, A. 1999. Multiple chemotactic factors: fine control or redundancy? *Trends Pharmacol Sci,* 20**,** 151-6.

Devine, S. M., Flomenberg, N., Vesole, D. H., Liesveld, J., Weisdorf, D., Badel, K., Calandra, G. & Dipersio, J. F. 2004. Rapid mobilization of CD34+ cells following administration of the CXCR4 antagonist AMD3100 to patients with multiple myeloma and non-Hodgkin's lymphoma. *J Clin Oncol,* 22**,** 1095-102.

Ding, Y. S., Shiue, C. Y., Fowler, J. S., Wolf, A. P. & Plenevaux, A. 1990. No-Carrier-Added (Nca) Aryl [F-18] Fluorides Via the Nucleophilic Aromatic-Substitution of Electron-Rich Aromatic Rings. *Journal of Fluorine Chemistry,* 48**,** 189-205.

Doitsidou, M., Reichman-Fried, M., Stebler, J., Koprunner, M., Dorries, J., Meyer, D., Esguerra, C. V., Leung, T. & Raz, E. 2002. Guidance of primordial germ cell migration by the chemokine SDF-1. *Cell,* 111**,** 647-59.

Dubeykovskaya, Z., Dubeykovskiy, A., Solal-Cohen, J. & Wang, T. C. 2009. Secreted trefoil factor 2 activates the CXCR4 receptor in epithelial and lymphocytic cancer cell lines. *J Biol Chem,* 284**,** 3650-62.

Dubrovska, A., Elliott, J., Salamone, R. J., Telegeev, G. D., Stakhovsky, A. E., Schepotin, I. B., Yan, F., Wang, Y., Bouchez, L. C., Kularatne, S. A., Watson, J., Trussell, C.,

Reddy, V. A., Cho, C. Y. & Schultz, P. G. 2012a. CXCR4 expression in prostate cancer progenitor cells. *PLoS One,* 7**,** e31226.

Dubrovska, A., Hartung, A., Bouchez, L. C., Walker, J. R., Reddy, V. A., Cho, C. Y. & Schultz, P. G. 2012b. CXCR4 activation maintains a stem cell population in tamoxifen-resistant breast cancer cells through AhR signalling. *Br J Cancer,* 107**,** 43-52.

Duda, D. G., Kozin, S. V., Kirkpatrick, N. D., Xu, L., Fukumura, D. & Jain, R. K. 2011. CXCL12 (SDF1alpha)-CXCR4/CXCR7 pathway inhibition: an emerging sensitizer for anticancer therapies? *Clin Cancer Res,* 17**,** 2074-80.

Eash, K. J., Greenbaum, A. M., Gopalan, P. K. & Link, D. C. 2010. CXCR2 and CXCR4 antagonistically regulate neutrophil trafficking from murine bone marrow. *J Clin Invest,* 120**,** 2423-31.

Eash, K. J., Means, J. M., White, D. W. & Link, D. C. 2009. CXCR4 is a key regulator of neutrophil release from the bone marrow under basal and stress granulopoiesis conditions. *Blood,* 113**,** 4711-9.

Ebos, J. M., Lee, C. R., Christensen, J. G., Mutsaers, A. J. & Kerbel, R. S. 2007. Multiple circulating proangiogenic factors induced by sunitinib malate are tumor-independent and correlate with antitumor efficacy. *Proc Natl Acad Sci U S A,* 104**,** 17069-74.

Eisenhardt, A., Frey, U., Tack, M., Rosskopf, D., Lummen, G., Rubben, H. & Siffert, W. 2005. Expression analysis and potential functional role of the CXCR4 chemokine receptor in bladder cancer. *Eur Urol,* 47**,** 111-7.

Ellison, G., Klinowska, T., Westwood, R. F., Docter, E., French, T. & Fox, J. C. 2002. Further evidence to support the melanocytic origin of MDA-MB-435. *Mol Pathol,* 55**,** 294-9.

Endres, M. J., Clapham, P. R., Marsh, M., Ahuja, M., Turner, J. D., Mcknight, A., Thomas, J. F., Stoebenau-Haggarty, B., Choe, S., Vance, P. J., Wells, T. N., Power, C. A., Sutterwala, S. S., Doms, R. W., Landau, N. R. & Hoxie, J. A. 1996. CD4-independent infection by HIV-2 is mediated by fusin/CXCR4. *Cell,* 87**,** 745-56.

Engelhardt, E. L., Schneider, R. F., Seeholzer, S. H., Stobbe, C. C. & Chapman, J. D. 2002. The synthesis and radiolabeling of 2-nitroimidazole derivatives of cyclam and their preclinical evaluation as positive markers of tumor hypoxia. *Journal of Nuclear Medicine,* 43**,** 837-850.

Ermondi, G., Lorenti, M. & Caron, G. 2004. Contribution of ionization and lipophilicity to drug binding to albumin: A preliminary step toward biodistribution prediction. *Journal of Medicinal Chemistry,* 47**,** 3949-3961.

Federsppiel, B., Melhado, I. G., Duncan, A. M., Delaney, A., Schappert, K., Clark-Lewis, I. & Jirik, F. R. 1993. Molecular cloning of the cDNA and chromosomal localization

of the gene for a putative seven-transmembrane segment (7-TMS) receptor isolated from human spleen. *Genomics,* 16**,** 707-12.

Feng, B., Laperle, J. L., Chang, G. & Varma, M. V. 2010. Renal clearance in drug discovery and development: molecular descriptors, drug transporters and disease state. *Expert Opin Drug Metab Toxicol,* 6**,** 939-52.

Feng, Y., Broder, C. C., Kennedy, P. E. & Berger, E. A. 1996. HIV-1 entry cofactor: functional cDNA cloning of a seven-transmembrane, G protein-coupled receptor. *Science,* 272**,** 872-7.

Fischer, T., Nagel, F., Jacobs, S., Stumm, R. & Schulz, S. 2008. Reassessment of CXCR4 chemokine receptor expression in human normal and neoplastic tissues using the novel rabbit monoclonal antibody UMB-2. *PLoS One,* 3**,** e4069.

Fricker, S. P., Anastassov, V., Cox, J., Darkes, M. C., Grujic, O., Idzan, S. R., Labrecque, J., Lau, G., Mosi, R. M., Nelson, K. L., Qin, L., Santucci, Z. & Wong, R. S. 2006. Characterization of the molecular pharmacology of AMD3100: a specific antagonist of the G-protein coupled chemokine receptor, CXCR4. *Biochem Pharmacol,* 72**,** 588-96.

Fu, J., Koul, D., Yao, J., Wang, S., Yuan, Y., Colman, H., Sulman, E. P., Lang, F. F. & Yung, W. K. 2013. Novel HSP90 inhibitor NVP-HSP990 targets cell-cycle regulators to ablate Olig2-positive glioma tumor-initiating cells. *Cancer Res,* 73**,** 3062-74.

Fujii, N., Oishi, S., Hiramatsu, K., Araki, T., Ueda, S., Tamamura, H., Otaka, A., Kusano, S., Terakubo, S., Nakashima, H., Broach, J. A., Trent, J. O., Wang, Z. X. & Peiper, S. C. 2003. Molecular-size reduction of a potent CXCR4-chemokine antagonist using orthogonal combination of conformation- and sequence-based libraries. *Angew Chem Int Ed Engl,* 42**,** 3251-3.

Genzyme. 2008. *European Commission Approves Genzyme's Mozobil* [Online]. Available: http://www.genzyme.com/corp/media/GENZ%20PR-080509.asp.

George, G. P. C. 2013. Design and synthesis of CXCR4-specific tracers for positron emission tomography. . *PhD thesis. Imperial College London.*

Geraldes, C. F. & Laurent, S. 2009. Classification and basic properties of contrast agents for magnetic resonance imaging. *Contrast Media Mol Imaging,* 4**,** 1-23.

Gerlach, L. O., Jakobsen, J. S., Jensen, K. P., Rosenkilde, M. R., Skerlj, R. T., Ryde, U., Bridger, G. J. & Schwartz, T. W. 2003. Metal ion enhanced binding of AMD3100 to Asp262 in the CXCR4 receptor. *Biochemistry,* 42**,** 710-7.

Glaser, M. & Arstad, E. 2007. "Click labeling" with 2-[18f]fluoroethylazide for positron emission tomography. *Bioconjug Chem,* 18**,** 989-93.

Gourni, E., Demmer, O., Schottelius, M., D'alessandria, C., Schulz, S., Dijkgraaf, I., Schumacher, U., Schwaiger, M., Kessler, H. & Wester, H. J. 2011. PET of CXCR4

expression by a (68)Ga-labeled highly specific targeted contrast agent. *J Nucl Med,* 52**,** 1803-10.

Guleng, B., Tateishi, K., Ohta, M., Kanai, F., Jazag, A., Ijichi, H., Tanaka, Y., Washida, M., Morikane, K., Fukushima, Y., Yamori, T., Tsuruo, T., Kawabe, T., Miyagishi, M., Taira, K., Sata, M. & Omata, M. 2005. Blockade of the stromal cell-derived factor-1/CXCR4 axis attenuates in vivo tumor growth by inhibiting angiogenesis in a vascular endothelial growth factor-independent manner. *Cancer Res,* 65**,** 5864-71.

Gulino, A. V., Moratto, D., Sozzani, S., Cavadini, P., Otero, K., Tassone, L., Imberti, L., Pirovano, S., Notarangelo, L. D., Soresina, R., Mazzolari, E., Nelson, D. L. & Badolato, R. 2004. Altered leukocyte response to CXCL12 in patients with warts hypogammaglobulinemia, infections, myelokathexis (WHIM) syndrome. *Blood,* 104**,** 444-52.

Guo, W., Reigan, P., Siegel, D. & Ross, D. 2008. Enzymatic reduction and glutathione conjugation of benzoquinone ansamycin heat shock protein 90 inhibitors: relevance for toxicity and mechanism of action. *Drug Metab Dispos,* 36**,** 2050-7.

Hanahan, D. & Weinberg, R. A. 2011. Hallmarks of cancer: the next generation. *Cell,* 144**,** 646-74.

Hanaoka, H., Mukai, T., Tamamura, H., Mori, T., Ishino, S., Ogawa, K., Iida, Y., Doi, R., Fujii, N. & Saji, H. 2006. Development of a 111In-labeled peptide derivative targeting a chemokine receptor, CXCR4, for imaging tumors. *Nucl Med Biol,* 33**,** 489-94.

Hartimath, S. V., Domanska, U. M., Walenkamp, A. M., Rudi, A. J. O. D. & De Vries, E. F. 2013. [(9)(9)mTc]O(2)-AMD3100 as a SPECT tracer for CXCR4 receptor imaging. *Nucl Med Biol,* 40**,** 507-17.

Hatse, S., Princen, K., Bridger, G., De Clercq, E. & Schols, D. 2002. Chemokine receptor inhibition by AMD3100 is strictly confined to CXCR4. *FEBS Lett,* 527**,** 255-62.

Hendrix, C. W., Collier, A. C., Lederman, M. M., Schols, D., Pollard, R. B., Brown, S., Jackson, J. B., Coombs, R. W., Glesby, M. J., Flexner, C. W., Bridger, G. J., Badel, K., Macfarland, R. T., Henson, G. W. & Calandra, G. 2004. Safety, pharmacokinetics, and antiviral activity of AMD3100, a selective CXCR4 receptor inhibitor, in HIV-1 infection. *J Acquir Immune Defic Syndr,* 37**,** 1253-62.

Hennrich, U., Seyler, L., Schafer, M., Bauder-Wust, U., Eisenhut, M., Semmler, W. & Bauerle, T. 2012. Synthesis and in vitro evaluation of 68Ga-DOTA-4-FBn-TN14003, a novel tracer for the imaging of CXCR4 expression. *Bioorg Med Chem,* 20**,** 1502-10.

Hernandez, P. A., Gorlin, R. J., Lukens, J. N., Taniuchi, S., Bohinjec, J., Francois, F., Klotman, M. E. & Diaz, G. A. 2003. Mutations in the chemokine receptor gene CXCR4 are associated with WHIM syndrome, a combined immunodeficiency disease. *Nat Genet,* 34**,** 70-4.

Hesselgesser, J., Liang, M., Hoxie, J., Greenberg, M., Brass, L. F., Orsini, M. J., Taub, D. & Horuk, R. 1998. Identification and characterization of the CXCR4 chemokine receptor in human T cell lines: ligand binding, biological activity, and HIV-1 infectivity. *J Immunol,* 160**,** 877-83.

Higgins, L. J. & Pomper, M. G. 2011. The evolution of imaging in cancer: current state and future challenges. *Semin Oncol,* 38**,** 3-15.

Hongo, K., Tsuno, N. H., Kawai, K., Sasaki, K., Kaneko, M., Hiyoshi, M., Murono, K., Tada, N., Nirei, T., Sunami, E., Takahashi, K., Nagawa, H., Kitayama, J. & Watanabe, T. 2013. Hypoxia enhances colon cancer migration and invasion through promotion of epithelial-mesenchymal transition. *J Surg Res,* 182**,** 75-84.

Hord, J. D., Whitlock, J. A., Gay, J. C. & Lukens, J. N. 1997. Clinical features of myelokathexis and treatment with hematopoietic cytokines: a case report of two patients and review of the literature. *J Pediatr Hematol Oncol,* 19**,** 443-8.

Inokuchi, E., Oishi, S., Kubo, T., Ohno, H., Shimura, K., Matsuoka, M. & Fujii, N. 2011. Potent CXCR4 Antagonists Containing Amidine Type Peptide Bond Isosteres. *Acs Medicinal Chemistry Letters,* 2**,** 477-480.

Jacobson, O., Weiss, I. D., Kiesewetter, D. O., Farber, J. M. & Chen, X. 2010. PET of tumor CXCR4 expression with 4-18F-T140. *J Nucl Med,* 51**,** 1796-804.

Jacobson, O., Weiss, I. D., Szajek, L., Farber, J. M. & Kiesewetter, D. O. 2009. 64Cu-AMD3100--a novel imaging agent for targeting chemokine receptor CXCR4. *Bioorg Med Chem,* 17**,** 1486-93.

Jacobson, O., Weiss, I. D., Szajek, L. P., Niu, G., Ma, Y., Kiesewetter, D. O., Farber, J. M. & Chen, X. 2011. PET imaging of CXCR4 using copper-64 labeled peptide antagonist. *Theranostics,* 1**,** 251-262.

Jacobson, O., Weiss, I. D., Szajek, L. P., Niu, G., Ma, Y., Kiesewetter, D. O., Peled, A., Eden, H. S., Farber, J. M. & Chen, X. 2012. Improvement of CXCR4 tracer specificity for PET imaging. *J Control Release,* 157**,** 216-23.

Jelinski, M., Hamacher, K. & Coenen, H. H. 2002. C-Terminal F-18-fluoroethylamidation exemplified on [Gly-OH9] oxytocin. *Journal of Labelled Compounds & Radiopharmaceuticals,* 45**,** 217-229.

Jiang, Y. P., Wu, X. H., Shi, B., Wu, W. X. & Yin, G. R. 2006. Expression of chemokine CXCL12 and its receptor CXCR4 in human epithelial ovarian cancer: an independent prognostic factor for tumor progression. *Gynecol Oncol,* 103**,** 226-33.

Jinquan, T., Jacobi, H. H., Jing, C., Reimert, C. M., Quan, S., Dissing, S., Poulsen, L. K. & Skov, P. S. 2000. Chemokine stromal cell-derived factor 1alpha activates basophils by means of CXCR4. *J Allergy Clin Immunol,* 106**,** 313-20.

Johnson, B. D., Schumacher, R. J., Ross, E. D. & Toft, D. O. 1998. Hop modulates Hsp70/Hsp90 interactions in protein folding. *J Biol Chem,* 273**,** 3679-86.

Jung, Y., Kim, J. K., Shiozawa, Y., Wang, J., Mishra, A., Joseph, J., Berry, J. E., Mcgee, S., Lee, E., Sun, H., Jin, T., Zhang, H., Dai, J., Krebsbach, P. H., Keller, E. T., Pienta, K. J. & Taichman, R. S. 2013. Recruitment of mesenchymal stem cells into prostate tumours promotes metastasis. *Nat Commun,* 4**,** 1795.

Kabashima, K., Shiraishi, N., Sugita, K., Mori, T., Onoue, A., Kobayashi, M., Sakabe, J., Yoshiki, R., Tamamura, H., Fujii, N., Inaba, K. & Tokura, Y. 2007. CXCL12-CXCR4 engagement is required for migration of cutaneous dendritic cells. *Am J Pathol,* 171**,** 1249-57.

Kanelakis, K. C., Shewach, D. S. & Pratt, W. B. 2002. Nucleotide binding states of hsp70 and hsp90 during sequential steps in the process of glucocorticoid receptor.hsp90 heterocomplex assembly. *J Biol Chem,* 277**,** 33698-703.

Kaufman, W. L., Kocman, I., Agrawal, V., Rahn, H. P., Besser, D. & Gossen, M. 2008. Homogeneity and persistence of transgene expression by omitting antibiotic selection in cell line isolation. *Nucleic Acids Res,* 36**,** e111.

Kawai, T. & Malech, H. L. 2009. WHIM syndrome: congenital immune deficiency disease. *Curr Opin Hematol,* 16**,** 20-6.

Kim, H. K., De La Luz Sierra, M., Williams, C. K., Gulino, A. V. & Tosato, G. 2006. G-CSF down-regulation of CXCR4 expression identified as a mechanism for mobilization of myeloid cells. *Blood,* 108**,** 812-20.

Kim, H. R., Kang, H. S. & Kim, H. D. 1999. Geldanamycin induces heat shock protein expression through activation of HSF1 in K562 erythroleukemic cells. *IUBMB Life,* 48**,** 429-33.

Kim, J., Takeuchi, H., Lam, S. T., Turner, R. R., Wang, H. J., Kuo, C., Foshag, L., Bilchik, A. J. & Hoon, D. S. 2005. Chemokine receptor CXCR4 expression in colorectal cancer patients increases the risk for recurrence and for poor survival. *J Clin Oncol,* 23**,** 2744-53.

Kioi, M., Vogel, H., Schultz, G., Hoffman, R. M., Harsh, G. R. & Brown, J. M. 2010. Inhibition of vasculogenesis, but not angiogenesis, prevents the recurrence of glioblastoma after irradiation in mice. *J Clin Invest,* 120**,** 694-705.

Kitaori, T., Ito, H., Schwarz, E. M., Tsutsumi, R., Yoshitomi, H., Oishi, S., Nakano, M., Fujii, N., Nagasawa, T. & Nakamura, T. 2009. Stromal cell-derived factor 1/CXCR4 signaling is critical for the recruitment of mesenchymal stem cells to the fracture site during skeletal repair in a mouse model. *Arthritis Rheum,* 60**,** 813-23.

Kohler, R. E., Comerford, I., Townley, S., Haylock-Jacobs, S., Clark-Lewis, I. & Mccoll, S. R. 2008. Antagonism of the chemokine receptors CXCR3 and CXCR4 reduces the

pathology of experimental autoimmune encephalomyelitis. *Brain Pathol,* 18**,** 504-16.

Kojima, Y., Acar, A., Eaton, E. N., Mellody, K. T., Scheel, C., Ben-Porath, I., Onder, T. T., Wang, Z. C., Richardson, A. L., Weinberg, R. A. & Orimo, A. 2010. Autocrine TGF-beta and stromal cell-derived factor-1 (SDF-1) signaling drives the evolution of tumor-promoting mammary stromal myofibroblasts. *Proc Natl Acad Sci U S A,* 107**,** 20009-14.

Kolligs, F. T., Nieman, M. T., Winer, I., Hu, G., Van Mater, D., Feng, Y., Smith, I. M., Wu, R., Zhai, Y., Cho, K. R. & Fearon, E. R. 2002. ITF-2, a downstream target of the Wnt/TCF pathway, is activated in human cancers with beta-catenin defects and promotes neoplastic transformation. *Cancer Cell,* 1**,** 145-55.

Kuil, J., Buckle, T., Oldenburg, J., Yuan, H., Borowsky, A. D., Josephson, L. & Van Leeuwen, F. W. 2011a. Hybrid peptide dendrimers for imaging of chemokine receptor 4 (CXCR4) expression. *Mol Pharm,* 8**,** 2444-53.

Kuil, J., Buckle, T., Yuan, H., Van Den Berg, N. S., Oishi, S., Fujii, N., Josephson, L. & Van Leeuwen, F. W. 2011b. Synthesis and evaluation of a bimodal CXCR4 antagonistic peptide. *Bioconjug Chem,* 22**,** 859-64.

Laforest, R. & Liu, X. 2008. Image quality with non-standard nuclides in PET. *Quarterly Journal of Nuclear Medicine and Molecular Imaging,* 52**,** 151-158.

Laruelle, M., Slifstein, M. & Huang, Y. 2003. Relationships between radiotracer properties and image quality in molecular imaging of the brain with positron emission tomography. *Mol Imaging Biol,* 5**,** 363-75.

Laverdiere, C., Hoang, B. H., Yang, R., Sowers, R., Qin, J., Meyers, P. A., Huvos, A. G., Healey, J. H. & Gorlick, R. 2005. Messenger RNA expression levels of CXCR4 correlate with metastatic behavior and outcome in patients with osteosarcoma. *Clin Cancer Res,* 11**,** 2561-7.

Leary, S. E. & Olson, J. M. 2012. The molecular classification of medulloblastoma: driving the next generation clinical trials. *Curr Opin Pediatr,* 24**,** 33-9.

Lee, E., Hooker, J. M. & Ritter, T. 2012. Nickel-mediated oxidative fluorination for PET with aqueous [18F] fluoride. *J Am Chem Soc,* 134**,** 17456-8.

Leeson, P. 2012. Drug discovery: Chemical beauty contest. *Nature,* 481**,** 455-6.

Levesque, J. P., Liu, F., Simmons, P. J., Betsuyaku, T., Senior, R. M., Pham, C. & Link, D. C. 2004. Characterization of hematopoietic progenitor mobilization in protease-deficient mice. *Blood,* 104**,** 65-72.

Levoye, A., Balabanian, K., Baleux, F., Bachelerie, F. & Lagane, B. 2009. CXCR7 heterodimerizes with CXCR4 and regulates CXCL12-mediated G protein signaling. *Blood,* 113**,** 6085-93.

Li, D., Marchenko, N. D., Schulz, R., Fischer, V., Velasco-Hernandez, T., Talos, F. & Moll, U. M. 2011. Functional inactivation of endogenous MDM2 and CHIP by HSP90 causes aberrant stabilization of mutant p53 in human cancer cells. *Mol Cancer Res,* 9**,** 577-88.

Li, J., Chaudhary, A., Chmura, S. J., Pelizzari, C., Rajh, T., Wietholt, C., Kurtoglu, M. & Aydogan, B. 2010a. A novel functional CT contrast agent for molecular imaging of cancer. *Phys Med Biol,* 55**,** 4389-97.

Li, J., Jiang, K., Qiu, X., Li, M., Hao, Q., Wei, L., Zhang, W., Chen, B. & Xin, X. 2013. Overexpression of CXCR4 is significantly associated with cisplatin-based chemotherapy resistance and can be a prognostic factor in epithelial ovarian cancer. *BMB Rep*.

Li, M., Yu, J., Li, Y., Li, D., Yan, D. & Ruan, Q. 2010b. CXCR4+ progenitors derived from bone mesenchymal stem cells differentiate into endothelial cells capable of vascular repair after arterial injury. *Cell Reprogram,* 12**,** 405-15.

Li, Z., Graf, N., Herrmann, K., Junger, A., Aichler, M., Feuchtinger, A., Baumgart, A., Walch, A., Peschel, C., Schwaiger, M., Buck, A., Keller, U. & Dechow, T. 2012. FLT-PET is superior to FDG-PET for very early response prediction in NPM-ALK-positive lymphoma treated with targeted therapy. *Cancer Res,* 72**,** 5014-24.

Liang, Z., Brooks, J., Willard, M., Liang, K., Yoon, Y., Kang, S. & Shim, H. 2007a. CXCR4/CXCL12 axis promotes VEGF-mediated tumor angiogenesis through Akt signaling pathway. *Biochem Biophys Res Commun,* 359**,** 716-22.

Liang, Z., Wu, H., Reddy, S., Zhu, A., Wang, S., Blevins, D., Yoon, Y., Zhang, Y. & Shim, H. 2007b. Blockade of invasion and metastasis of breast cancer cells via targeting CXCR4 with an artificial microRNA. *Biochem Biophys Res Commun,* 363**,** 542-6.

Liang, Z., Wu, T., Lou, H., Yu, X., Taichman, R. S., Lau, S. K., Nie, S., Umbreit, J. & Shim, H. 2004. Inhibition of breast cancer metastasis by selective synthetic polypeptide against CXCR4. *Cancer Res,* 64**,** 4302-8.

Liang, Z., Yoon, Y., Votaw, J., Goodman, M. M., Williams, L. & Shim, H. 2005. Silencing of CXCR4 blocks breast cancer metastasis. *Cancer Res,* 65**,** 967-71.

Liang, Z., Zhan, W., Zhu, A., Yoon, Y., Lin, S., Sasaki, M., Klapproth, J. M., Yang, H., Grossniklaus, H. E., Xu, J., Rojas, M., Voll, R. J., Goodman, M. M., Arrendale, R. F., Liu, J., Yun, C. C., Snyder, J. P., Liotta, D. C. & Shim, H. 2012. Development of a unique small molecule modulator of CXCR4. *PLoS One,* 7**,** e34038.

Libura, J., Drukala, J., Majka, M., Tomescu, O., Navenot, J. M., Kucia, M., Marquez, L., Peiper, S. C., Barr, F. G., Janowska-Wieczorek, A. & Ratajczak, M. Z. 2002. CXCR4-SDF-1 signaling is active in rhabdomyosarcoma cells and regulates locomotion, chemotaxis, and adhesion. *Blood,* 100**,** 2597-606.

Lieber, M., Smith, B., Szakal, A., Nelson-Rees, W. & Todaro, G. 1976. A continuous tumor-cell line from a human lung carcinoma with properties of type II alveolar epithelial cells. *Int J Cancer,* 17**,** 62-70.

Ling, X., Spaeth, E., Chen, Y., Shi, Y., Zhang, W., Schober, W., Hail, N., Jr., Konopleva, M. & Andreeff, M. 2013. The CXCR4 antagonist AMD3465 regulates oncogenic signaling and invasiveness in vitro and prevents breast cancer growth and metastasis in vivo. *PLoS One,* 8**,** e58426.

Ludwig, J. A. & Weinstein, J. N. 2005. Biomarkers in cancer staging, prognosis and treatment selection. *Nat Rev Cancer,* 5**,** 845-56.

Ma, W. F., Du, J., Fu, L. P., Fang, R., Chen, H. Y. & Cai, S. H. 2009. Phenotypic knockout of CXCR4 by a novel recombinant protein TAT/54R/KDEL inhibits tumors metastasis. *Mol Cancer Res,* 7**,** 1613-21.

Machulla, H. J., Blocher, A., Kuntzsch, M., Piert, M., Wei, R. & Grierson, J. R. 2000. Simplified labeling approach for synthesizing 3 '-deoxy-3 '-[F-18]fluorothymidine ([F-18]FLT). *Journal of Radioanalytical and Nuclear Chemistry,* 243**,** 843-846.

Maeda, H., Wu, J., Sawa, T., Matsumura, Y. & Hori, K. 2000. Tumor vascular permeability and the EPR effect in macromolecular therapeutics: a review. *J Control Release,* 65**,** 271-84.

Mandawat, A., Fiskus, W., Buckley, K. M., Robbins, K., Rao, R., Balusu, R., Navenot, J. M., Wang, Z. X., Ustun, C., Chong, D. G., Atadja, P., Fujii, N., Peiper, S. C. & Bhalla, K. 2010. Pan-histone deacetylase inhibitor panobinostat depletes CXCR4 levels and signaling and exerts synergistic antimyeloid activity in combination with CXCR4 antagonists. *Blood,* 116**,** 5306-15.

Mankoff, D. A. 2008. Molecular Imaging as a Tool for Transplating Breast Cancer Science. *Breast Cancer Research,* 10**,** S1-S3.

Mankoff, D. A., Link, J. M., Linden, H. M., Sundararajan, L. & Krohn, K. A. 2008. Tumor receptor imaging. *Journal of Nuclear Medicine,* 49**,** 149s-163s.

Marchesi, F., Monti, P., Leone, B. E., Zerbi, A., Vecchi, A., Piemonti, L., Mantovani, A. & Allavena, P. 2004. Increased survival, proliferation, and migration in metastatic human pancreatic tumor cells expressing functional CXCR4. *Cancer Res,* 64**,** 8420-7.

Maroni, P., Bendinelli, P., Matteucci, E. & Desiderio, M. A. 2007. HGF induces CXCR4 and CXCL12-mediated tumor invasion through Ets1 and NF-kappaB. *Carcinogenesis,* 28**,** 267-79.

Martin, C., Burdon, P. C., Bridger, G., Gutierrez-Ramos, J. C., Williams, T. J. & Rankin, S. M. 2003. Chemokines acting via CXCR2 and CXCR4 control the release of neutrophils from the bone marrow and their return following senescence. *Immunity,* 19**,** 583-93.

Mcbride, W. J., D'souza, C. A., Sharkey, R. M. & Goldenberg, D. M. 2012. The radiolabeling of proteins by the [18F]AlF method. *Appl Radiat Isot,* 70**,** 200-4.

Mccandless, E. E., Piccio, L., Woerner, B. M., Schmidt, R. E., Rubin, J. B., Cross, A. H. & Klein, R. S. 2008. Pathological expression of CXCL12 at the blood-brain barrier correlates with severity of multiple sclerosis. *Am J Pathol,* 172**,** 799-808.

Mcdermott, D. H., Liu, Q., Ulrick, J., Kwatemaa, N., Anaya-O'brien, S., Penzak, S. R., Filho, J. O., Priel, D. A., Kelly, C., Garofalo, M., Littel, P., Marquesen, M. M., Hilligoss, D., Decastro, R., Fleisher, T. A., Kuhns, D. B., Malech, H. L. & Murphy, P. M. 2011. The CXCR4 antagonist plerixafor corrects panleukopenia in patients with WHIM syndrome. *Blood,* 118**,** 4957-62.

Meyer, U. A. 1996. Overview of enzymes of drug metabolism. *Journal of Pharmacokinetics and Biopharmaceutics,* 24**,** 449-459.

Michel, M. C., Wieland, T. & Tsujimoto, G. 2009. How reliable are G-protein-coupled receptor antibodies? *Naunyn Schmiedebergs Arch Pharmacol,* 379**,** 385-8.

Misra, P., Lebeche, D., Ly, H., Schwarzkopf, M., Diaz, G., Hajjar, R. J., Schecter, A. D. & Frangioni, J. V. 2008. Quantitation of CXCR4 expression in myocardial infarction using 99mTc-labeled SDF-1alpha. *J Nucl Med,* 49**,** 963-9.

Miyanishi, N., Suzuki, Y., Simizu, S., Kuwabara, Y., Banno, K. & Umezawa, K. 2010. Involvement of autocrine CXCL12/CXCR4 system in the regulation of ovarian carcinoma cell invasion. *Biochem Biophys Res Commun,* 403**,** 154-9.

Mizuno, N., Niwa, T., Yotsumoto, Y. & Sugiyama, Y. 2003. Impact of drug transporter studies on drug discovery and development. *Pharmacological Reviews,* 55**,** 425-461.

Modi, S., Stopeck, A., Linden, H., Solit, D., Chandarlapaty, S., Rosen, N., D'andrea, G., Dickler, M., Moynahan, M. E., Sugarman, S., Ma, W., Patil, S., Norton, L., Hannah, A. L. & Hudis, C. 2011. HSP90 inhibition is effective in breast cancer: a phase II trial of tanespimycin (17-AAG) plus trastuzumab in patients with HER2-positive metastatic breast cancer progressing on trastuzumab. *Clin Cancer Res,* 17**,** 5132-9.

Modi, S., Stopeck, A. T., Gordon, M. S., Mendelson, D., Solit, D. B., Bagatell, R., Ma, W., Wheler, J., Rosen, N., Norton, L., Cropp, G. F., Johnson, R. G., Hannah, A. L. & Hudis, C. A. 2007. Combination of trastuzumab and tanespimycin (17-AAG, KOS-953) is safe and active in trastuzumab-refractory HER-2 overexpressing breast cancer: a phase I dose-escalation study. *J Clin Oncol,* 25**,** 5410-7.

Morishima, Y., Kanelakis, K. C., Murphy, P. J., Lowe, E. R., Jenkins, G. J., Osawa, Y., Sunahara, R. K. & Pratt, W. B. 2003. The hsp90 cochaperone p23 is the limiting component of the multiprotein hsp90/hsp70-based chaperone system in vivo where it acts to stabilize the client protein: hsp90 complex. *J Biol Chem,* 278**,** 48754-63.

Muller, A., Homey, B., Soto, H., Ge, N., Catron, D., Buchanan, M. E., Mcclanahan, T., Murphy, E., Yuan, W., Wagner, S. N., Barrera, J. L., Mohar, A., Verastegui, E. & Zlotnik, A. 2001. Involvement of chemokine receptors in breast cancer metastasis. *Nature,* 410**,** 50-6.

Mungalpara, J., Zachariassen, Z. G., Thiele, S., Rosenkilde, M. M. & Vabeno, J. 2013. Structure-activity relationship studies of the aromatic positions in cyclopentapeptide CXCR4 antagonists. *Org Biomol Chem*.

Murakami, J., Li, T. S., Ueda, K., Tanaka, T. & Hamano, K. 2009a. Inhibition of accelerated tumor growth by blocking the recruitment of mobilized endothelial progenitor cells after chemotherapy. *Int J Cancer,* 124**,** 1685-92.

Murakami, T., Kumakura, S., Yamazaki, T., Tanaka, R., Hamatake, M., Okuma, K., Huang, W., Toma, J., Komano, J., Yanaka, M., Tanaka, Y. & Yamamoto, N. 2009b. The novel CXCR4 antagonist KRH-3955 is an orally bioavailable and extremely potent inhibitor of human immunodeficiency virus type 1 infection: comparative studies with AMD3100. *Antimicrob Agents Chemother,* 53**,** 2940-8.

Murphy, P. M. 2002. International Union of Pharmacology. XXX. Update on Chemokine Receptor Nomenclature. *Pharmacological Reviews,* 54**,** 227-229.

Nagengast, W. B., De Korte, M. A., Oude Munnink, T. H., Timmer-Bosscha, H., Den Dunnen, W. F., Hollema, H., De Jong, J. R., Jensen, M. R., Quadt, C., Garcia-Echeverria, C., Van Dongen, G. A., Lub-De Hooge, M. N., Schroder, C. P. & De Vries, E. G. 2010. 89Zr-bevacizumab PET of early antiangiogenic tumor response to treatment with HSP90 inhibitor NVP-AUY922. *J Nucl Med,* 51**,** 761-7.

Nakashima, H., Masuda, M., Murakami, T., Koyanagi, Y., Matsumoto, A., Fujii, N. & Yamamoto, N. 1992. Anti-human immunodeficiency virus activity of a novel synthetic peptide, T22 ([Tyr-5,12, Lys-7]polyphemusin II): a possible inhibitor of virus-cell fusion. *Antimicrob Agents Chemother,* 36**,** 1249-55.

Nanki, T., Hayashida, K., El-Gabalawy, H. S., Suson, S., Shi, K., Girschick, H. J., Yavuz, S. & Lipsky, P. E. 2000. Stromal cell-derived factor-1-CXC chemokine receptor 4 interactions play a central role in CD4+ T cell accumulation in rheumatoid arthritis synovium. *J Immunol,* 165**,** 6590-8.

Neckers, L. & Workman, P. 2012. Hsp90 molecular chaperone inhibitors: are we there yet? *Clin Cancer Res,* 18**,** 64-76.

Nimmagadda, S., Pullambhatla, M. & Pomper, M. G. 2009. Immunoimaging of CXCR4 expression in brain tumor xenografts using SPECT/CT. *J Nucl Med,* 50**,** 1124-30.

Nimmagadda, S., Pullambhatla, M., Stone, K., Green, G., Bhujwalla, Z. M. & Pomper, M. G. 2010. Molecular imaging of CXCR4 receptor expression in human cancer xenografts with [64Cu]AMD3100 positron emission tomography. *Cancer Res,* 70**,** 3935-44.

Niu, G., Cai, W., Chen, K. & Chen, X. 2008. Non-invasive PET imaging of EGFR degradation induced by a heat shock protein 90 inhibitor. *Mol Imaging Biol,* 10**,** 99-106.

Niu, G., Li, Z., Cao, Q. & Chen, X. 2009. Monitoring therapeutic response of human ovarian cancer to 17-DMAG by noninvasive PET imaging with (64)Cu-DOTA-trastuzumab. *Eur J Nucl Med Mol Imaging,* 36**,** 1510-9.

Notni, J., Pohle, K. & Wester, H. J. 2012. Comparative gallium-68 labeling of TRAP-, NOTA-, and DOTA-peptides: practical consequences for the future of gallium-68-PET. *EJNMMI Res,* 2**,** 28.

O'boyle, G., Swidenbank, I., Marshall, H., Barker, C. E., Armstrong, J., White, S. A., Fricker, S. P., Plummer, R., Wright, M. & Lovat, P. E. 2013. Inhibition of CXCR4-CXCL12 chemotaxis in melanoma by AMD11070. *Br J Cancer,* 108**,** 1634-40.

Oh, J. R., Byun, B. H., Hong, S. P., Chong, A., Kim, J., Yoo, S. W., Kang, S. R., Kim, D. Y., Song, H. C., Bom, H. S. & Min, J. J. 2011. Comparison of (1)(3)(1)I whole-body imaging, (1)(3)(1)I SPECT/CT, and (1)(8)F-FDG PET/CT in the detection of metastatic thyroid cancer. *Eur J Nucl Med Mol Imaging,* 38**,** 1459-68.

Oude Munnink, T. H., De Vries, E. G., Vedelaar, S. R., Timmer-Bosscha, H., Schroder, C. P., Brouwers, A. H. & Lub-De Hooge, M. N. 2012. Lapatinib and 17AAG reduce 89Zr-trastuzumab-F(ab')2 uptake in SKBR3 tumor xenografts. *Mol Pharm,* 9**,** 2995-3002.

Pan, F., Ma, S., Cao, W., Liu, H., Chen, F., Chen, X. & Shi, R. 2013. SDF-1alpha upregulation of MMP-2 is mediated by p38 MAPK signaling in pancreatic cancer cell lines. *Mol Biol Rep,* 40**,** 4139-46.

Parameswaran, R., Yu, M., Lim, M., Groffen, J. & Heisterkamp, N. 2011. Combination of drug therapy in acute lymphoblastic leukemia with a CXCR4 antagonist. *Leukemia,* 25**,** 1314-23.

Peng, H. M., Morishima, Y., Clapp, K. M., Lau, M., Pratt, W. B. & Osawa, Y. 2009. Dynamic cycling with Hsp90 stabilizes neuronal nitric oxide synthase through calmodulin-dependent inhibition of ubiquitination. *Biochemistry,* 48**,** 8483-90.

Pettersson, S., Perez-Nueno, V. I., Mena, M. P., Clotet, B., Este, J. A., Borrell, J. I. & Teixido, J. 2010. Novel monocyclam derivatives as HIV entry inhibitors: Design, synthesis, anti-HIV evaluation, and their interaction with the CXCR4 co-receptor. *ChemMedChem,* 5**,** 1272-81.

Petty, J. M., Sueblinvong, V., Lenox, C. C., Jones, C. C., Cosgrove, G. P., Cool, C. D., Rai, P. R., Brown, K. K., Weiss, D. J., Poynter, M. E. & Suratt, B. T. 2007. Pulmonary stromal-derived factor-1 expression and effect on neutrophil recruitment during acute lung injury. *J Immunol,* 178**,** 8148-57.

Phillips, R. J., Burdick, M. D., Lutz, M., Belperio, J. A., Keane, M. P. & Strieter, R. M. 2003. The stromal derived factor-1/CXCL12-CXC chemokine receptor 4 biological axis

in non-small cell lung cancer metastases. *Am J Respir Crit Care Med,* 167**,** 1676-86.

Pike, V. W. 2009. PET radiotracers: crossing the blood-brain barrier and surviving metabolism. *Trends in Pharmacological Sciences,* 30**,** 431-440.

Poethko, T., Schottelius, M., Thumshim, G., Hersel, U., Herz, M., Henriksen, G., Kessler, H., Schwaiger, M. & Wester, H. J. 2004a. Two-step methodology for high-yield routine radiohalogenation of peptides: (18)F-labeled RGD and octreotide analogs. *Journal of Nuclear Medicine,* 45**,** 892-902.

Poethko, T., Schottelius, M., Thumshirn, G., Herz, M., Haubner, R., Henriksen, G., Kessler, H., Schwaiger, M. & Wester, H. J. 2004b. Chemoselective pre-conjugate radiohalogenation of unprotected mono- and multimeric peptides via oxime formation. *Radiochimica Acta,* 92**,** 317-327.

Pratt, W. B., Morishima, Y., Peng, H. M. & Osawa, Y. 2010. Proposal for a role of the Hsp90/Hsp70-based chaperone machinery in making triage decisions when proteins undergo oxidative and toxic damage. *Exp Biol Med (Maywood),* 235**,** 278-89.

Rahmim, A. & Zaidi, H. 2008. PET versus SPECT: strengths, limitations and challenges. *Nucl Med Commun,* 29**,** 193-207.

Ramakrishnan, M., Mathur, S. R. & Mukhopadhyay, A. 2013. Fusion derived epithelial cancer cells express hematopoietic markers and contribute to stem cell and migratory phenotype in ovarian carcinoma. *Cancer Res*.

Ratajczak, M. Z., Kucia, M., Reca, R., Majka, M., Janowska-Wieczorek, A. & Ratajczak, J. 2004. Stem cell plasticity revisited: CXCR4-positive cells expressing mRNA for early muscle, liver and neural cells 'hide out' in the bone marrow. *Leukemia,* 18**,** 29-40.

Redondo-Munoz, J., Escobar-Diaz, E., Samaniego, R., Terol, M. J., Garcia-Marco, J. A. & Garcia-Pardo, A. 2006. MMP-9 in B-cell chronic lymphocytic leukemia is up-regulated by alpha4beta1 integrin or CXCR4 engagement via distinct signaling pathways, localizes to podosomes, and is involved in cell invasion and migration. *Blood,* 108**,** 3143-51.

Rehman, A. O. & Wang, C. Y. 2009. CXCL12/SDF-1 alpha activates NF-kappaB and promotes oral cancer invasion through the Carma3/Bcl10/Malt1 complex. *Int J Oral Sci,* 1**,** 105-18.

Reith, M. E. & Coffey, L. L. 1993. Cationic and anionic requirements for the binding of 2 beta-carbomethoxy-3 beta-(4-fluorophenyl)[3H]tropane to the dopamine uptake carrier. *J Neurochem,* 61**,** 167-77.

Rimland, J., Xin, W., Sweetnam, P., Saijoh, K., Nestler, E. J. & Duman, R. S. 1991. Sequence and expression of a neuropeptide Y receptor cDNA. *Mol Pharmacol,* 40**,** 869-75.

Rodrigues, L. M., Chung, Y. L., Al Saffar, N. M., Sharp, S. Y., Jackson, L. E., Banerji, U., Stubbs, M., Leach, M. O., Griffiths, J. R. & Workman, P. 2012. Effects of HSP90 inhibitor 17-allylamino-17-demethoxygeldanamycin (17-AAG) on NEU/HER2 overexpressing mammary tumours in MMTV-NEU-NT mice monitored by Magnetic Resonance Spectroscopy. *BMC Res Notes,* 5**,** 250.

Roe, S. M., Prodromou, C., O'brien, R., Ladbury, J. E., Piper, P. W. & Pearl, L. H. 1999. Structural basis for inhibition of the Hsp90 molecular chaperone by the antitumor antibiotics radicicol and geldanamycin. *J Med Chem,* 42**,** 260-6.

Rosen, O., Sharon, M., Quadt-Akabayov, S. R. & Anglister, J. 2006. Molecular switch for alternative conformations of the HIV-1 V3 region: implications for phenotype conversion. *Proc Natl Acad Sci U S A,* 103**,** 13950-5.

Rosenkilde, M. M., Gerlach, L. O., Hatse, S., Skerlj, R. T., Schols, D., Bridger, G. J. & Schwartz, T. W. 2007. Molecular mechanism of action of monocyclam versus bicyclam non-peptide antagonists in the CXCR4 chemokine receptor. *J Biol Chem,* 282**,** 27354-65.

Russell, H. V., Hicks, J., Okcu, M. F. & Nuchtern, J. G. 2004. CXCR4 expression in neuroblastoma primary tumors is associated with clinical presentation of bone and bone marrow metastases. *J Pediatr Surg,* 39**,** 1506-11.

Salzwedel, K. & Berger, E. A. 2000. Cooperative subunit interactions within the oligomeric envelope glycoprotein of HIV-1: functional complementation of specific defects in gp120 and gp41. *Proc Natl Acad Sci U S A,* 97**,** 12794-9.

Samuni, A. & Goldstein, S. 2012. Redox properties and thiol reactivity of geldanamycin and its analogues in aqueous solutions. *J Phys Chem B,* 116**,** 6404-10.

Sanchez-Crespo, A., Andreo, P. & Larsson, S. A. 2004. Positron flight in human tissues and its influence on PET image spatial resolution. *Eur J Nucl Med Mol Imaging,* 31**,** 44-51.

Sasaki, K., Natsugoe, S., Ishigami, S., Matsumoto, M., Okumura, H., Setoyama, T., Uchikado, Y., Kita, Y., Tamotsu, K., Sakurai, T., Owaki, T. & Aikou, T. 2008. Expression of CXCL12 and its receptor CXCR4 correlates with lymph node metastasis in submucosal esophageal cancer. *J Surg Oncol,* 97**,** 433-8.

Scala, S., Giuliano, P., Ascierto, P. A., Ierano, C., Franco, R., Napolitano, M., Ottaiano, A., Lombardi, M. L., Luongo, M., Simeone, E., Castiglia, D., Mauro, F., De Michele, I., Calemma, R., Botti, G., Caraco, C., Nicoletti, G., Satriano, R. A. & Castello, G. 2006. Human melanoma metastases express functional CXCR4. *Clin Cancer Res,* 12**,** 2427-33.

Schioppa, T., Uranchimeg, B., Saccani, A., Biswas, S. K., Doni, A., Rapisarda, A., Bernasconi, S., Saccani, S., Nebuloni, M., Vago, L., Mantovani, A., Melillo, G. & Sica, A. 2003. Regulation of the chemokine receptor CXCR4 by hypoxia. *J Exp Med,* 198**,** 1391-402.

Schmid, B. C., Rudas, M., Rezniczek, G. A., Leodolter, S. & Zeillinger, R. 2004. CXCR4 is expressed in ductal carcinoma in situ of the breast and in atypical ductal hyperplasia. *Breast Cancer Res Treat,* 84**,** 247-50.

Schulte, T. W., Akinaga, S., Soga, S., Sullivan, W., Stensgard, B., Toft, D. & Neckers, L. M. 1998. Antibiotic radicicol binds to the N-terminal domain of Hsp90 and shares important biologic activities with geldanamycin. *Cell Stress Chaperones,* 3**,** 100-8.

Schwartz, V., Lue, H., Kraemer, S., Korbiel, J., Krohn, R., Ohl, K., Bucala, R., Weber, C. & Bernhagen, J. 2009. A functional heteromeric MIF receptor formed by CD74 and CXCR4. *FEBS Lett,* 583**,** 2749-57.

Scotton, C. J., Wilson, J. L., Scott, K., Stamp, G., Wilbanks, G. D., Fricker, S., Bridger, G. & Balkwill, F. R. 2002. Multiple actions of the chemokine CXCL12 on epithelial tumor cells in human ovarian cancer. *Cancer Res,* 62**,** 5930-8.

Sehgal, A., Keener, C., Boynton, A. L., Warrick, J. & Murphy, G. P. 1998. CXCR-4, a chemokine receptor, is overexpressed in and required for proliferation of glioblastoma tumor cells. *J Surg Oncol,* 69**,** 99-104.

Shaked, Y., Henke, E., Roodhart, J. M., Mancuso, P., Langenberg, M. H., Colleoni, M., Daenen, L. G., Man, S., Xu, P., Emmenegger, U., Tang, T., Zhu, Z., Witte, L., Strieter, R. M., Bertolini, F., Voest, E. E., Benezra, R. & Kerbel, R. S. 2008. Rapid chemotherapy-induced acute endothelial progenitor cell mobilization: implications for antiangiogenic drugs as chemosensitizing agents. *Cancer Cell,* 14**,** 263-73.

Shao, H., Xu, Q., Wu, Q., Ma, Q., Salgueiro, L., Wang, J., Eton, D., Webster, K. A. & Yu, H. 2011. Defective CXCR4 expression in aged bone marrow cells impairs vascular regeneration. *J Cell Mol Med,* 15**,** 2046-56.

Sica, A., Schioppa, T., Mantovani, A. & Allavena, P. 2006. Tumour-associated macrophages are a distinct M2 polarised population promoting tumour progression: potential targets of anti-cancer therapy. *Eur J Cancer,* 42**,** 717-27.

Siciliano, M. J., Barker, P. E. & Cailleau, R. 1979. Mutually exclusive genetic signatures of human breast tumor cell lines with a common chromosomal marker. *Cancer Res,* 39**,** 919-22.

Singh, A. P., Arora, S., Bhardwaj, A., Srivastava, S. K., Kadakia, M. P., Wang, B., Grizzle, W. E., Owen, L. B. & Singh, S. 2012. CXCL12/CXCR4 Protein Signaling Axis Induces Sonic Hedgehog Expression in Pancreatic Cancer Cells via Extracellular Regulated Kinase- and Akt Kinase-mediated Activation of Nuclear Factor kappa B IMPLICATIONS FOR BIDIRECTIONAL TUMOR-STROMAL INTERACTIONS. *Journal of Biological Chemistry,* 287**,** 39115-39124.

Singh, S., Srivastava, S. K., Bhardwaj, A., Owen, L. B. & Singh, A. P. 2010. CXCL12-CXCR4 signalling axis confers gemcitabine resistance to pancreatic cancer cells: a novel target for therapy. *Br J Cancer,* 103**,** 1671-9.

Sjodahl, G., Lauss, M., Lovgren, K., Chebil, G., Gudjonsson, S., Veerla, S., Patschan, O., Aine, M., Ferno, M., Ringner, M., Mansson, W., Liedberg, F., Lindgren, D. & Hoglund, M. 2012. A molecular taxonomy for urothelial carcinoma. *Clin Cancer Res*.

Skerlj, R. T., Bridger, G. J., Kaller, A., Mceachern, E. J., Crawford, J. B., Zhou, Y., Atsma, B., Langille, J., Nan, S., Veale, D., Wilson, T., Harwig, C., Hatse, S., Princen, K., De Clercq, E. & Schols, D. 2010. Discovery of novel small molecule orally bioavailable C-X-C chemokine receptor 4 antagonists that are potent inhibitors of T-tropic (X4) HIV-1 replication. *J Med Chem,* 53**,** 3376-88.

Skotland, T. 2012. Molecular imaging: challenges of bringing imaging of intracellular targets into common clinical use. *Contrast Media Mol Imaging,* 7**,** 1-6.

Smith-Jones, P. M., Solit, D., Afroze, F., Rosen, N. & Larson, S. M. 2006. Early tumor response to Hsp90 therapy using HER2 PET: comparison with 18F-FDG PET. *J Nucl Med,* 47**,** 793-6.

Smith, M. C., Luker, K. E., Garbow, J. R., Prior, J. L., Jackson, E., Piwnica-Worms, D. & Luker, G. D. 2004. CXCR4 regulates growth of both primary and metastatic breast cancer. *Cancer Res,* 64**,** 8604-12.

Sotsios, Y., Whittaker, G. C., Westwick, J. & Ward, S. G. 1999. The CXC chemokine stromal cell-derived factor activates a Gi-coupled phosphoinositide 3-kinase in T lymphocytes. *J Immunol,* 163**,** 5954-63.

Stankiewicz, M., Nikolay, R., Rybin, V. & Mayer, M. P. 2010. CHIP participates in protein triage decisions by preferentially ubiquitinating Hsp70-bound substrates. *FEBS J,* 277**,** 3353-67.

Stone, N. D., Dunaway, S. B., Flexner, C., Tierney, C., Calandra, G. B., Becker, S., Cao, Y. J., Wiggins, I. P., Conley, J., Macfarland, R. T., Park, J. G., Lalama, C., Snyder, S., Kallungal, B., Klingman, K. L. & Hendrix, C. W. 2007. Multiple-dose escalation study of the safety, pharmacokinetics, and biologic activity of oral AMD070, a selective CXCR4 receptor inhibitor, in human subjects. *Antimicrob Agents Chemother,* 51**,** 2351-8.

Strieter, R. M., Polverini, P. J., Kunkel, S. L., Arenberg, D. A., Burdick, M. D., Kasper, J., Dzuiba, J., Van Damme, J., Walz, A., Marriott, D. & *Et Al*. 1995. The functional role of the ELR motif in CXC chemokine-mediated angiogenesis. *J Biol Chem,* 270**,** 27348-57.

Sugiura, G., Kuhn, H., Sauter, M., Haberkorn, U. & Mier, W. 2014. Radiolabeling strategies for tumor-targeting proteinaceous drugs. *Molecules,* 19**,** 2135-65.

Sun, Y., Cheng, Z., Ma, L. & Pei, G. 2002. Beta-arrestin2 is critically involved in CXCR4-mediated chemotaxis, and this is mediated by its enhancement of p38 MAPK activation. *J Biol Chem,* 277**,** 49212-9.

Sun, Y. X., Wang, J., Shelburne, C. E., Lopatin, D. E., Chinnaiyan, A. M., Rubin, M. A., Pienta, K. J. & Taichman, R. S. 2003. Expression of CXCR4 and CXCL12 (SDF-1) in human prostate cancers (PCa) in vivo. *J Cell Biochem,* 89**,** 462-73.

Supko, J. G., Hickman, R. L., Grever, M. R. & Malspeis, L. 1995. Preclinical pharmacologic evaluation of geldanamycin as an antitumor agent. *Cancer Chemother Pharmacol,* 36**,** 305-15.

Suratt, B. T., Petty, J. M., Young, S. K., Malcolm, K. C., Lieber, J. G., Nick, J. A., Gonzalo, J. A., Henson, P. M. & Worthen, G. S. 2004. Role of the CXCR4/SDF-1 chemokine axis in circulating neutrophil homeostasis. *Blood,* 104**,** 565-71.

Tachibana, K., Hirota, S., Iizasa, H., Yoshida, H., Kawabata, K., Kataoka, Y., Kitamura, Y., Matsushima, K., Yoshida, N., Nishikawa, S., Kishimoto, T. & Nagasawa, T. 1998. The chemokine receptor CXCR4 is essential for vascularization of the gastrointestinal tract. *Nature,* 393**,** 591-4.

Tamamura, H., Araki, T., Ueda, S., Wang, Z., Oishi, S., Esaka, A., Trent, J. O., Nakashima, H., Yamamoto, N., Peiper, S. C., Otaka, A. & Fujii, N. 2005a. Identification of novel low molecular weight CXCR4 antagonists by structural tuning of cyclic tetrapeptide scaffolds. *J Med Chem,* 48**,** 3280-9.

Tamamura, H., Esaka, A., Ogawa, T., Araki, T., Ueda, S., Wang, Z., Trent, J. O., Tsutsumi, H., Masuno, H., Nakashima, H., Yamamoto, N., Peiper, S. C., Otaka, A. & Fujii, N. 2005b. Structure-activity relationship studies on CXCR4 antagonists having cyclic pentapeptide scaffolds. *Org Biomol Chem,* 3**,** 4392-4.

Tamamura, H., Fujisawa, M., Hiramatsu, K., Mizumoto, M., Nakashima, H., Yamamoto, N., Otaka, A. & Fujii, N. 2004. Identification of a CXCR4 antagonist, a T140 analog, as an anti-rheumatoid arthritis agent. *FEBS Lett,* 569**,** 99-104.

Tamamura, H., Hiramatsu, K., Mizumoto, M., Ueda, S., Kusano, S., Terakubo, S., Akamatsu, M., Yamamoto, N., Trent, J. O., Wang, Z., Peiper, S. C., Nakashima, H., Otaka, A. & Fujii, N. 2003. Enhancement of the T140-based pharmacophores leads to the development of more potent and bio-stable CXCR4 antagonists. *Org Biomol Chem,* 1**,** 3663-9.

Tamamura, H., Hiramatsu, K., Ueda, S., Wang, Z., Kusano, S., Terakubo, S., Trent, J. O., Peiper, S. C., Yamamoto, N., Nakashima, H., Otaka, A. & Fujii, N. 2005c. Stereoselective synthesis of [L-Arg-L/D-3-(2-naphthyl)alanine]-type (E)-alkene dipeptide isosteres and its application to the synthesis and biological evaluation of pseudopeptide analogues of the CXCR4 antagonist FC131. *J Med Chem,* 48**,** 380-91.

Tamamura, H., Omagari, A., Hiramatsu, K., Gotoh, K., Kanamoto, T., Xu, Y., Kodama, E., Matsuoka, M., Hattori, T., Yamamoto, N., Nakashima, H., Otaka, A. & Fujii, N. 2001. Development of specific CXCR4 inhibitors possessing high selectivity indexes as well as complete stability in serum based on an anti-HIV peptide T140. *Bioorg Med Chem Lett,* 11**,** 1897-902.

Tamamura, H., Omagari, A., Hiramatsu, K., Oishi, S., Habashita, H., Kanamoto, T., Gotoh, K., Yamamoto, N., Nakashima, H., Otaka, A. & Fujii, N. 2002. Certification of the critical importance of L-3-(2-naphthyl)alanine at position 3 of a specific CXCR4 inhibitor, T140, leads to an exploratory performance of its downsizing study. *Bioorg Med Chem,* 10**,** 1417-26.

Tamamura, H., Xu, Y., Hattori, T., Zhang, X., Arakaki, R., Kanbara, K., Omagari, A., Otaka, A., Ibuka, T., Yamamoto, N., Nakashima, H. & Fujii, N. 1998. A low-molecular-weight inhibitor against the chemokine receptor CXCR4: a strong anti-HIV peptide T140. *Biochem Biophys Res Commun,* 253**,** 877-82.

Tanaka, T., Nomura, W., Narumi, T., Esaka, A., Oishi, S., Ohashi, N., Itotani, K., Evans, B. J., Wang, Z. X., Peiper, S. C., Fujii, N. & Tamamura, H. 2009. Structure-activity relationship study on artificial CXCR4 ligands possessing the cyclic pentapeptide scaffold: the exploration of amino acid residues of pentapeptides by substitutions of several aromatic amino acids. *Org Biomol Chem,* 7**,** 3805-9.

Tanaka, T., Tsutsumi, H., Nomura, W., Tanabe, Y., Ohashi, N., Esaka, A., Ochiai, C., Sato, J., Itotani, K., Murakami, T., Ohba, K., Yamamoto, N., Fujii, N. & Tamamura, H. 2008. Structure-activity relationship study of CXCR4 antagonists bearing the cyclic pentapeptide scaffold: identification of the new pharmacophore. *Organic & Biomolecular Chemistry,* 6**,** 4374-4377.

Tang, C. H., Tan, T. W., Fu, W. M. & Yang, R. S. 2008a. Involvement of matrix metalloproteinase-9 in stromal cell-derived factor-1/CXCR4 pathway of lung cancer metastasis. *Carcinogenesis,* 29**,** 35-43.

Tang, G., Zeng, W. B., Yu, M. X. & Kabalka, G. 2008b. Facile synthesis of N-succinimidyl 4-[(18)F]fluorobenzoate ([(18)F]SFB) for protein labeling. *Journal of Labelled Compounds & Radiopharmaceuticals,* 51**,** 68-71.

Tarantola, G., Zito, F. & Gerundini, P. 2003. PET instrumentation and reconstruction algorithms in whole-body applications. *J Nucl Med,* 44**,** 756-69.

Tekgunduz, E., Altuntas, F., Sivgin, S., Aki, S. Z., Donmez, A., Topcuoglu, P., Yildirim, R., Baysal, N. A., Ayyildiz, E., Yuksel, M. K., Sari, I., Tombuloglu, M., Unal, A. & Ilhan, O. 2012. Plerixafor use in patients with previous mobilization failure: A multicenter experience. *Transfus Apher Sci,* 47**,** 77-80.

Terada, N., Hamazaki, T., Oka, M., Hoki, M., Mastalerz, D. M., Nakano, Y., Meyer, E. M., Morel, L., Petersen, B. E. & Scott, E. W. 2002. Bone marrow cells adopt the phenotype of other cells by spontaneous cell fusion. *Nature,* 416**,** 542-5.

Thariani, R., Veenstra, D. L., Carlson, J. J., Garrison, L. P. & Ramsey, S. 2012. Paying for personalized care: Cancer biomarkers and comparative effectiveness. *Mol Oncol,* 6**,** 260-6.

Thoma, G., Streiff, M. B., Kovarik, J., Glickman, F., Wagner, T., Beerli, C. & Zerwes, H. G. 2008. Orally bioavailable isothioureas block function of the chemokine receptor CXCR4 in vitro and in vivo. *J Med Chem,* 51**,** 7915-20.

Tolmachev, V. & Stone-Elander, S. 2010. Radiolabelled proteins for positron emission tomography: Pros and cons of labelling methods. *Biochim Biophys Acta,* 1800**,** 487-510.

Tomasi, G. & Aboagye, E. O. 2013. Introduction to the analysis of PET data in oncology. *J Pharmacokinet Pharmacodyn,* 40**,** 419-36.

Tsai, B. S. & Lefkowitz, R. J. 1978. Agonist-specific effects of monovalent and divalent cations on adenylate cyclase-coupled alpha adrenergic receptors in rabbit platelets. *Mol Pharmacol,* 14**,** 540-8.

Tsukada, H., Sato, K., Fukumoto, D. & Kakiuchi, T. 2006. Evaluation of D-isomers of O-F-18-fluoromethyl, O-F-18-fluoroethyl and O-F-18-fluoropropyl tyrosine as tumour imaging agents in mice. *European Journal of Nuclear Medicine and Molecular Imaging,* 33**,** 1017-1024.

Ueda, S., Kato, M., Inuki, S., Ohno, H., Evans, B., Wang, Z. X., Peiper, S. C., Izumi, K., Kodama, E., Matsuoka, M., Nagasawa, H., Oishi, S. & Fujii, N. 2008. Identification of novel non-peptide CXCR4 antagonists by ligand-based design approach. *Bioorg Med Chem Lett,* 18**,** 4124-9.

Ueda, S., Oishi, S., Wang, Z. X., Araki, T., Tamamura, H., Cluzeau, J., Ohno, H., Kusano, S., Nakashima, H., Trent, J. O., Peiper, S. C. & Fujii, N. 2007. Structure-activity relationships of cyclic peptide-based chemokine receptor CXCR4 antagonists: disclosing the importance of side-chain and backbone functionalities. *J Med Chem,* 50**,** 192-8.

Us Food and Drug Administration (Fda). 2008. *FDA Approves Drug that Boosts Stem Cell Yield for Bone Marrow Transplants* [Online]. Available: http://www.fda.gov/NewsEvents/Newsroom/PressAnnouncements/2008/ucm116995.htm [Accessed 09/05/2011 2011].

Velikyan, I., Maecke, H. & Langstrom, B. 2008. Convenient preparation of 68Ga-based PET-radiopharmaceuticals at room temperature. *Bioconjug Chem,* 19**,** 569-73.

Verel, I., Visser, G. W. M., Boerman, O. C., Van Eerd, J. E. M., Finn, R., Boellaard, R., Vosjan, M. J. W. D., Walsum, M. S. V., Snow, G. B. & Van Dongen, G. a. M. S. 2003. Long-lived positron emitters zirconium-89 and iodine-124 for scouting of therapeutic radioimmunoconjugates with PET. *Cancer Biotherapy and Radiopharmaceuticals,* 18**,** 655-661.

Vila-Coro, A. J., Rodriguez-Frade, J. M., Martin De Ana, A., Moreno-Ortiz, M. C., Martinez, A. C. & Mellado, M. 1999. The chemokine SDF-1alpha triggers CXCR4 receptor dimerization and activates the JAK/STAT pathway. *FASEB J,* 13**,** 1699-710.

Vogel, C. & Marcotte, E. M. 2012. Insights into the regulation of protein abundance from proteomic and transcriptomic analyses. *Nat Rev Genet,* 13**,** 227-32.

Wang, J., Dai, J., Jung, Y., Wei, C. L., Wang, Y., Havens, A. M., Hogg, P. J., Keller, E. T., Pienta, K. J., Nor, J. E., Wang, C. Y. & Taichman, R. S. 2007. A glycolytic mechanism regulating an angiogenic switch in prostate cancer. *Cancer Res,* 67**,** 149-59.

Wang, Y., Cui, L., Gonsiorek, W., Min, S. H., Anilkumar, G., Rosenblum, S., Kozlowski, J., Lundell, D., Fine, J. S. & Grant, E. P. 2009. CCR2 and CXCR4 regulate peripheral blood monocyte pharmacodynamics and link to efficacy in experimental autoimmune encephalomyelitis. *J Inflamm (Lond),* 6**,** 32.

Weiss, I. D., Jacobson, O., Kiesewetter, D. O., Jacobus, J. P., Szajek, L. P., Chen, X. & Farber, J. M. 2011. Positron Emission Tomography Imaging of Tumors Expressing the Human Chemokine Receptor CXCR4 in Mice with the Use of (64)Cu-AMD3100. *Mol Imaging Biol*.

Wendt, M. K., Cooper, A. N. & Dwinell, M. B. 2008. Epigenetic silencing of CXCL12 increases the metastatic potential of mammary carcinoma cells. *Oncogene,* 27**,** 1461-71.

Wong, D. & Korz, W. 2008. Translating an Antagonist of Chemokine Receptor CXCR4: from bench to bedside. *Clin Cancer Res,* 14**,** 7975-80.

Workman, P., Aboagye, E. O., Balkwill, F., Balmain, A., Bruder, G., Chaplin, D. J., Double, J. A., Everitt, J., Farningham, D. A., Glennie, M. J., Kelland, L. R., Robinson, V., Stratford, I. J., Tozer, G. M., Watson, S., Wedge, S. R. & Eccles, S. A. 2010. Guidelines for the welfare and use of animals in cancer research. *Br J Cancer,* 102**,** 1555-77.

Wu, B., Chien, E. Y., Mol, C. D., Fenalti, G., Liu, W., Katritch, V., Abagyan, R., Brooun, A., Wells, P., Bi, F. C., Hamel, D. J., Kuhn, P., Handel, T. M., Cherezov, V. & Stevens, R. C. 2010. Structures of the CXCR4 chemokine GPCR with small-molecule and cyclic peptide antagonists. *Science,* 330**,** 1066-71.

Www.Clinicaltrials.Gov. 2013. *NCT01339039: Plerixafor (AMD3100) and Bevacizumab for Recurrent High-Grade Glioma* [Online]. Available: http://clinicaltrials.gov/ct2/show/NCT01339039 [Accessed 31/05/2013.

Xia, X. M., Wang, F. Y., Zhou, J., Hu, K. F., Li, S. W. & Zou, B. B. 2011. CXCR4 antagonist AMD3100 modulates claudin expression and intestinal barrier function in experimental colitis. *PLoS One,* 6**,** e27282.

Xu, L., Duda, D. G., Di Tomaso, E., Ancukiewicz, M., Chung, D. C., Lauwers, G. Y., Samuel, R., Shellito, P., Czito, B. G., Lin, P. C., Poleski, M., Bentley, R., Clark, J. W., Willett, C. G. & Jain, R. K. 2009. Direct evidence that bevacizumab, an anti-VEGF antibody, up-regulates SDF1alpha, CXCR4, CXCL6, and neuropilin 1 in tumors from patients with rectal cancer. *Cancer Res,* 69**,** 7905-10.

Yamazaki, S., Nguyen, L., Vekich, S., Shen, Z., Yin, M. J., Mehta, P. P., Kung, P. P. & Vicini, P. 2011. Pharmacokinetic-pharmacodynamic modeling of biomarker response and tumor growth inhibition to an orally available heat shock protein 90

inhibitor in a human tumor xenograft mouse model. *J Pharmacol Exp Ther,* 338**,** 964-73.

Yang, Z. Q., Geng, X., Solit, D., Pratilas, C. A., Rosen, N. & Danishefsky, S. J. 2004. New efficient synthesis of resorcinylic macrolides via ynolides: establishment of cyclopropradicicol as synthetically feasible preclinical anticancer agent based on Hsp90 as the target. *J Am Chem Soc,* 126**,** 7881-9.

Yoon, Y., Liang, Z., Zhang, X., Choe, M., Zhu, A., Cho, H. T., Shin, D. M., Goodman, M. M., Chen, Z. G. & Shim, H. 2007. CXC chemokine receptor-4 antagonist blocks both growth of primary tumor and metastasis of head and neck cancer in xenograft mouse models. *Cancer Res,* 67**,** 7518-24.

Yoshikawa, Y., Kobayashi, K., Oishi, S., Fujii, N. & Furuya, T. 2012. Molecular modeling study of cyclic pentapeptide CXCR4 antagonists: new insight into CXCR4-FC131 interactions. *Bioorg Med Chem Lett,* 22**,** 2146-50.

Young, J. C. & Hartl, F. U. 2000. Polypeptide release by Hsp90 involves ATP hydrolysis and is enhanced by the co-chaperone p23. *EMBO J,* 19**,** 5930-40.

Yu, T., Wu, Y., Helman, J. I., Wen, Y., Wang, C. & Li, L. 2011. CXCR4 promotes oral squamous cell carcinoma migration and invasion through inducing expression of MMP-9 and MMP-13 via the ERK signaling pathway. *Mol Cancer Res,* 9**,** 161-72.

Yu, X., Chen, D., Zhang, Y., Wu, X., Huang, Z., Zhou, H. & Zhang, Z. 2012. Overexpression of CXCR4 in mesenchymal stem cells promotes migration, neuroprotection and angiogenesis in a rat model of stroke. *J Neurol Sci,* 316**,** 141-9.

Zanzonico, P. 2004. Positron emission tomography: a review of basic principles, scanner design and performance, and current systems. *Semin Nucl Med,* 34**,** 87-111.

Zhan, W., Liang, Z., Zhu, A., Kurtkaya, S., Shim, H., Snyder, J. P. & Liotta, D. C. 2007. Discovery of small molecule CXCR4 antagonists. *J Med Chem,* 50**,** 5655-64.

Zhang, J., Tian, J., Li, T., Guo, H. & Shen, L. 2010. 99mTc-AMD3100: A novel potential receptor-targeting radiopharmaceutical for tumor imaging. *Chinese Chemical Letters,* 21**,** 461-463.

Zhang, W. B., Navenot, J. M., Haribabu, B., Tamamura, H., Hiramatu, K., Omagari, A., Pei, G., Manfredi, J. P., Fujii, N., Broach, J. R. & Peiper, S. C. 2002. A point mutation that confers constitutive activity to CXCR4 reveals that T140 is an inverse agonist and that AMD3100 and ALX40-4C are weak partial agonists. *J Biol Chem,* 277**,** 24515-21.

Zhang, X. X., Sun, Z., Guo, J., Wang, Z., Wu, C., Niu, G., Ma, Y., Kiesewetter, D. O. & Chen, X. 2013. Comparison of F-labeled CXCR4 antagonist peptides for PET imaging of CXCR4 expression. *Mol Imaging Biol*.

Zhu, A., Zhan, W., Liang, Z., Yoon, Y., Yang, H., Grossniklaus, H. E., Xu, J., Rojas, M., Lockwood, M., Snyder, J. P., Liotta, D. C. & Shim, H. 2010. Dipyrimidine amines:

a novel class of chemokine receptor type 4 antagonists with high specificity. *J Med Chem,* 53**,** 8556-68.

Zhu, A. X., Sahani, D. V., Duda, D. G., Di Tomaso, E., Ancukiewicz, M., Catalano, O. A., Sindhwani, V., Blaszkowsky, L. S., Yoon, S. S., Lahdenranta, J., Bhargava, P., Meyerhardt, J., Clark, J. W., Kwak, E. L., Hezel, A. F., Miksad, R., Abrams, T. A., Enzinger, P. C., Fuchs, C. S., Ryan, D. P. & Jain, R. K. 2009. Efficacy, safety, and potential biomarkers of sunitinib monotherapy in advanced hepatocellular carcinoma: a phase II study. *J Clin Oncol,* 27**,** 3027-35.

Zlotnik, A. & Yoshie, O. 2000. Chemokines: a new classification system and their role in immunity. *Immunity,* 12**,** 121-7.

Zou, Y. R., Kottmann, A. H., Kuroda, M., Taniuchi, I. & Littman, D. R. 1998. Function of the chemokine receptor CXCR4 in haematopoiesis and in cerebellar development. *Nature,* 393**,** 595-9.

Zubair, A. & Frieri, M. 2013. Role of nuclear factor-kB in breast and colorectal cancer. *Curr Allergy Asthma Rep,* 13**,** 44-9.

Zuccarello, D., Ferlin, A., Garolla, A., Menegazzo, M., Perilli, L., Ambrosini, G. & Foresta, C. 2011. How the human spermatozoa sense the oocyte: a new role of SDF1-CXCR4 signalling. *Int J Androl,* 34**,** e554-65.

Appendix

Appendix One – Summary of included copyrighted works and proof of permission to re-use

Page Number	Type of work: text, figure, map, etc.	Source work	Copyright holder & year	Work out of copyright	Permission to re-use	Permission requested	permission refused	Orphan work
Page 204	figure	Guillaume George (2013). Design and synthesis of CXCR4-specific tracers for positron emission tomography, PhD thesis, Imperial College London	© 2013 Guillaume George		✓			

From: guetzo@gmail.com [guetzo@gmail.com] on behalf of Guillaume George [g.george09@imperial.ac.uk]
Sent: 30 May 2014 03:46
To: Stevens, Elizabeth
Subject: Re: permission to reproduce It1t figure

You are obviously most welcome to use it for your thesis.

Congrats :)

G

On 29/05/2014, Stevens, Elizabeth <e.stevens09@imperial.ac.uk> wrote:
> Hey Guillaume,
> I'm about to submit my thesis (finally), and I just realised I need to show
> proof of permission for the figure you said I could use from your thesis
> (shown below). I was wondering if you could write back giving permission,
> and then I would include the email in the appendix at the end?
>
>
>
>
> [image]
>
>
> Thanks,
>
> Liz
>
>